Water Use of Forests in the Netherlands

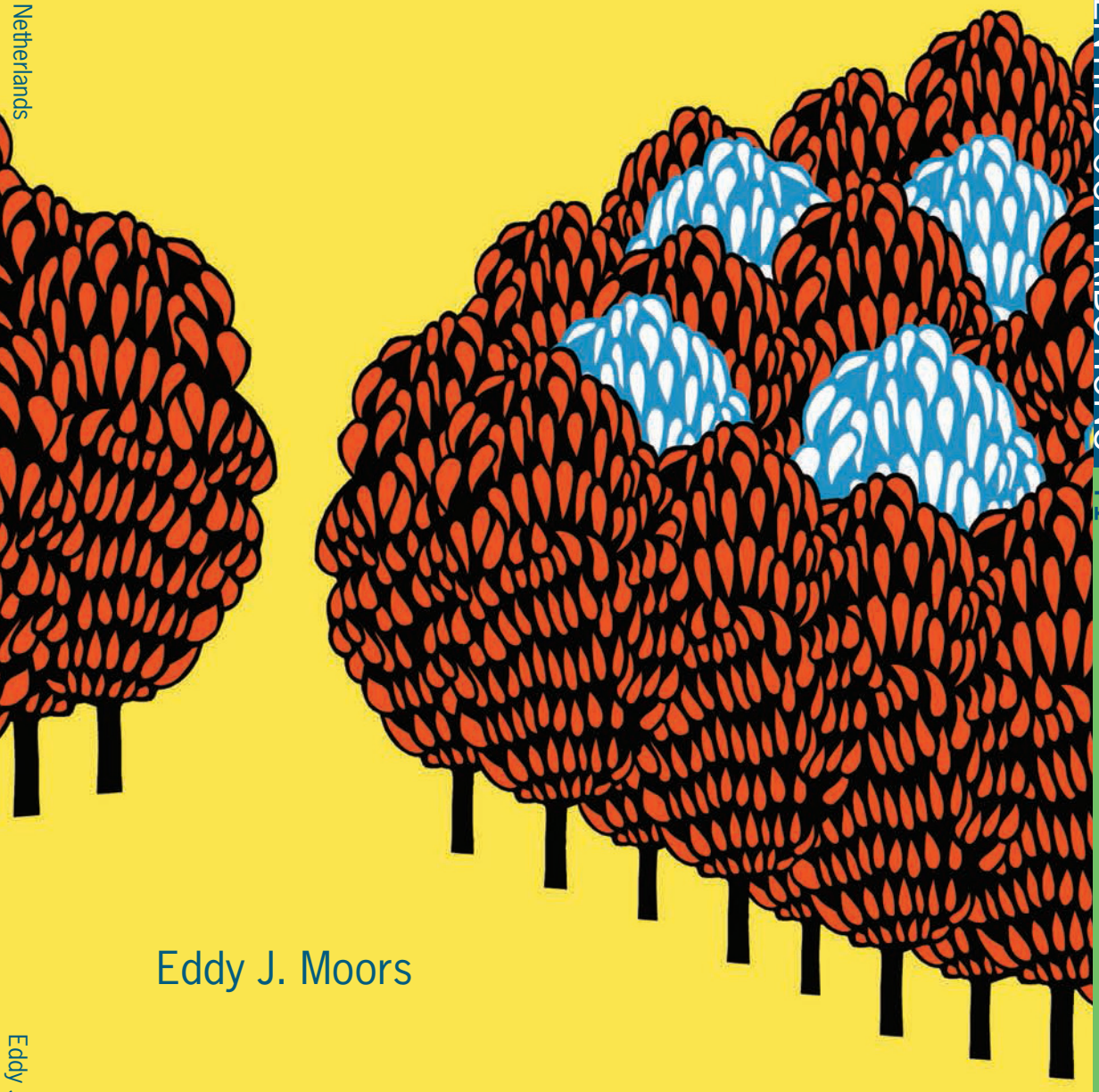

Eddy J. Moors

VU UNIVERSITY AMSTERDAM

ALTERRA WAGENINGEN UR

ALTERRA SCIENTIFIC CONTRIBUTIONS 41

Water Use of Forests in the Netherlands

Eddy J. Moors

Water Use of Forests in the Netherlands

MISSION: Alterra is the main centre of expertise on rural areas and water management in the Netherlands. It was founded 1 January 2000. Alterra combines a huge range of expertise on rural areas and their sustainable use, including aspects such as water, wildlife, forests, the environment, soils, landscape, climate and recreation, as well as various other aspects relevant to the development and management of the environment we live in. Alterra engages in strategic and applied research to support design processes, policymaking and management at the local, national and international level. This includes not only innovative, interdisciplinary research on complex problems relating to rural areas, but also the production of readily applicable knowledge and expertise enabling rapid and adequate solutions to practical problems.
The many themes of Alterra's research effort include relations between cities and their surrounding countryside, multiple use of rural areas, economy and ecology, integrated water management, sustainable agricultural systems, planning for the future, expert systems and modelling, biodiversity, landscape planning and landscape perception, integrated forest management, geo-information and remote sensing, spatial planning of leisure activities, habitat creation in marine and estuarine waters, green belt development and ecological webs, and pollution risk assessment.
Alterra is part of Wageningen University & Research centre (Wageningen UR).

VRIJE UNIVERSITEIT

Water Use of Forests in the Netherlands

ACADEMISCH PROEFSCHRIFT

ter verkrijging van de graad Doctor aan
de Vrije Universiteit Amsterdam,
op gezag van de rector magnificus
prof.dr. L.M. Bouter,
in het openbaar te verdedigen
ten overstaan van de promotiecommissie
van de faculteit der Aard- en Levenswetenschappen
op dinsdag 22 mei 2012 om 15.45 uur
in de aula van de universiteit,
De Boelelaan 1105

door

Eduardus Johannes Moors

geboren te Dakar, Senegal

promotoren: prof.dr. A.J. Dolman
prof.dr. R.A. Feddes

Leescommissie: Prof. Dr. R.J.M. Ceulemans
Dr. J.H. Gash
Prof. Dr. P. Kabat
Prof. Dr. Ir. R. Uijlenhoet
Dr. M.J. Waterloo

"*Why am I standing in the middle of nowhere, standing here with nothing to do?*"
(free after Caro Emerald)

Cover page: Artist impression by Almas Pieters (www.gestikt.nl).

The research presented in this publication was conducted at Alterra in Wageningen and Vrije Universiteit Amsterdam, the Netherlands.

Moors, Eddy J.
Water Use of Forests in the Netherlands, PhD-thesis Vrije Universiteit Amsterdam, the Netherlands. 290 p.

Moors, Eddy J.
Water Use of Forests in the Netherlands, Alterra Scientific Contributions 41, Alterra, part of Wageningen UR, the Netherlands. 290 p.
ISBN 978-90-327-0398-1

Abstract

Forests are complex ecosystems with a large variability in the horizontal as well as in the vertical space. To study the dissimilarities in water use for different forest types, the water and energy balance of five forest stands in the Netherlands were observed during periods varying from two years to more than 15 years. The main tree species of the stands were: Scots pine, poplar, oak, larch and at one site a mixture of pine, birch, beech and oak.

Two conditions were distinguished for the analysis of the driving processes of the evaporation rate: dry and wet. Under dry conditions the opening and closing of the stomatal conductance was the main process controlling the evaporation rate. The drivers controlling the opening and closing were different between tree species and for undergrowth and tree species. Overall the most important driver was the vapour pressure deficit. The inclusion of temperature did not improve the optimization results and it is advised not to include temperature as a driver to simulate the stomatal conductance for the present climatic conditions in the Netherlands. The contribution of the undergrowth varied with time between 5% and 100% during the year. The smallest contribution of the undergrowth to the total evaporation appeared in the middle of the summer. The highest contribution appeared in spring and autumn.

To improve the feedback of water stress by lowering groundwater tables during prolonged periods of drought a conceptual model is introduced incorporating two separate soil water signals. The model has a default feedback based on the water content at the deepest roots, and a site specific feedback through the soil water content of the surface layer containing 80 to 90% of all roots. The default feedback is based on data of multiple forest stands over Europe.

Under wet conditions it is shown that the evaporation at the end of the shower and just after the shower is much larger than often assumed. In most models this

underestimation of the evaporation rate of intercepted water is compensated by an under estimation of the water storage capacity of the leaves. The evaporation rate under wet conditions is better simulated by taking into account the vertical variation in the surface roughness lengths for heat and momentum.

Keywords: Forest, undergrowth, hydrology, evaporation, interception, drought, root water uptake.

Preface

So how did I get involved in writing this thesis? In most cases decisions largely depend on opportunities and contacts coming together. In my case I would like to acknowledge Reinder Feddes, who phoned me on a Saturday evening and introduced me to Han Dolman. Han was then looking for staff to work on the project "Hydrology of forests and forested areas in the Netherlands" (*Forest Hydrology Project*). This project was the starting point for my research and this thesis. Reinder Feddes together with Jon Wieringa became my promoters and Han Dolman my daily advisor. After Jon Wieringa retired, Han Dolman became my promoter together with Reinder Feddes. I want to express my gratitude to my team of promoters. Both Han Dolman en Reinder Feddes have been especially supportive and instrumental not only in starting up this study, but also in finally getting it finished. Han and Reinder, thank you very much!

The study started with the *Forest Hydrology Project* that was initiated in 1994 by the Ministry of Agriculture, Nature and Food Quality of the Netherlands and implemented by the The Winand Staring Centre (this later became Alterra-Wageningen UR). Financially this project was made possible not only by the Ministry of Agriculture, Nature and Food Quality, but also by VEWIN, "Staatsbosbeheer", "Natuurmonumenten"and "Unie van Landschappen". Wim Zeeman played a crucial role in mobilizing all these partners. The data collected for this project are the basis for the present thesis. Representatives of the organizations financially supporting the project as well as a number of representatives from scientific organization were member of the advisory board of the project.

I would like to thank the members of the advisory board of the *Forest Hydrology Project* for their feedback and advice during the first years 1994-1998 of this study:

- ir. J.M. Brand (directie Natuur, Ministerie van Landbouw, Natuurbeheer en Visserij);

- ir. G. van Tol (IKC, Natuur);
- dr. ir. W. Bouten (Universiteit van Amsterdam);
- Prof. A.W.L. Veen (Rijksuniversiteit van Groningen);
- ir. H.K.A. Rotermundt (NUON, representing VEWIN);
- ir. W.P.C. Zeeman (Staatsbosbeheer);
- ir. K. Voetberg (Natuurmonumenten);
- ir. H. Massop (Unie van Landschappen);
- J. Deurloo (Waterschap Regge en Dinkel).

To enlarge the number of forest types included in this study, an additional site, i.e. the Edesebos site, was added. The team of the Winand Staring Centre collecting the data at this site was lead by Marja Ogink-Hendriks from 1988-1990. After the end of the forest hydrology project, all sites except the Loobos site were dismantled.

In 1996 after the CO_2-flux measurements were started in the pine forest of Loobos, the Loobos site became part of the international flux database FLUXNET (www.fluxnet.ornl.gov). At the moment the Loobos site is world wide one of the sites with the longest record of evaporation, sensible heat and CO_2 flux data. This international collaboration was made possible with financial support of national and international projects, such as:

- Research program on Climate Change of Wageningen UR (Min. of Agriculture, Nature and Food Quality, NL);
- Integrated observations and modelling of greenhouse gas budgets at the ecosystem level in the Netherlands (Climate for Spatial Planning, NL);
- EuroFlux (DG Research, EU);
- CarboEurope (DG Research, EU);
- GHG-Europe (DG Research, EU).

Before the measurements for the *Forest Hydrology Project* could start, sites had to be selected. Together with Han Dolman we spent hours of driving around the country looking for the ultimate site with an almost unlimited fetch, i.e. the same forest type as far as the eye reaches. Finding such a site was not an easy task. By the time we thought we had found an excellent location, we often discovered that

without knowing we had crossed the border and were either in Belgium or Germany. Nevertheless, we managed to find a set of sites that fulfilled our purposes.

Many thanks I want to express also to the staff of the organizations managing the forests such as “Staatsbosbeheer”, “Natuurmonumenten” and “Unie van Landschappen”. They not only provided access to the sites, but also shared their knowledge and helped us with typical field work such as pulling Landrovers out of the mud and setting up fences to keep the wild ponies away.

Together with Jan Elbers, Han Dolman and Wim Snijders the measurement set-up was designed and measurement towers up to a height of 27 m were erected at each of the four sites. Especially Jan’s expertise in designing and constructing automatic measurement set-ups was very helpful. Jan and Wim were also heavily involved in the maintenance of the sites, equipment calibration, data quality checking, and all other work that is needed to maintain a number of continuous monitoring sites at remote locations. Special moments were the visits during Christmas together with Jan when the forests were very quiet and covered with snow.

Later Wilma Jans joined our group. Wilma together with Santi Sabaté was also responsible for the sapflow measurements collected at the Loobos site and used for validation purposes.

Of course it was impossible to collect and process all the data used in this thesis by myself. Fortunately, a large number of people were willing to contribute in numerous ways and by doing this enabled me to write this thesis.

Mark Ashby was one of the persons with whom the SWAPS model was developed. A number of the concepts as are used in this thesis were implemented in this model. The people working on the unsaturated zone model SWAP also deserve my thanks as the soil water flow of the SWAPS model is based on the concepts of the SWAP model. I would also like to thank Niall Hanan for his work on the sparse canopy light interception scheme for the SWAPS model. The Bankenbos site was much closer to Groningen than to Wageningen. Therefore, I am thankful that Henk de Groot, Jan van de Burg and Peter van Breugel were willing to assist us in the maintenance of this site. Marja Ogink-Hendriks (data collection and analysis of the Edesebos site), Marlies Hamaker (leaf area analysis of all needles), Erik van der Elzen (design electrical circuits), Gerard Veldman (soil sample analysis), Han te Beest (installation of the discharge structures and groundwater observation tubes), Lara Prihodko (reading groundwater levels of the observing tubes), Iwan Supit (proof reading a part of my thesis), Obbe Tuinenburg (LaTeX problem solver), Almas Pieters (cover design) and my two paranymphs Wies Nijman-Moors and Saskia Werners. I am aware that there are people whom I did not mention here, but I want you to be assured that I have much appreciated all your help.

During the years that passed since the start of my thesis a large number of people

in- and outside of Wageningen were always showing interest, providing moral support and willing to help if needed. Just to name a few: Pavel Kabat, Cor Jacobs, Bart Kruijt, Ronald Hutjes, Herbert ter Maat, Saskia Werners, Judith Klostermann, Annemarie Groot, Philip Hamaker, Catharien Terwisscha van Scheltinga, Laurens Ganzeveld, Petra Stolk, Jeroen Veraart, Nies Springer, Gerard Oosterbaan, Wim Cofino, and all other members of the groups I have had these years the privilege to work with, i.e. Water Atmosphere and Substances, Land Atmosphere Interactions, Earth System Sciences & Climate Change. Also the contacts with the national and international Flux-community was highly appreciated during these years.

An absence of four months made possible by Alterra, allowed me to make significant progress towards finishing my thesis. This time was spent in Amsterdam and I am very grateful for the hospitality of the people at the Eco-hydrology Group of "Vrije Universiteit van Amsterdam". Special thanks goes to Maarten Waterloo, Michiel van der Molen and Margriet Groenendijk for their warm welcome and the great opportunities not only to discuss scientific issues, but also to solve technical problems using analysis- and word processing software.

The work of the reading committee is at the end of a thesis. I thank all members of the reading committee for their time and comments.

Finally I would like to thank all my family and especially my parents Wim, Gerda, Frits and Ellen for their continuous support throughout my thesis.

Although the data collection was done as part of my work at Alterra, the analyses and writing was done mostly in the evenings, weekends and holidays. Niek, Céline and last but not least Franciska many many thanks for your help, support and your patience during all those years.

Eddy J. Moors
Opheusden, February 2012

Contents

Chapter 1

Introduction

1.1 Groundwater management in The Netherlands

In the beginning of the 1900's, inundations occurred regularly in The Netherlands. These inundations were mainly caused by a too small discharge capacity. To improve this situation the Land Consolidation Act of 1955 was put in place. This act stimulated measures to improve drainage and to accelerate discharge of water, leading to intensification of the surface and subsurface drainage system in combination with an enlargement of the drainage capacity of the surface water system. This improvement of the drainage system was one of the main causes of the lowering of the groundwater table at the second half of the 1950's and the first half of the 1960's (Rolf, 1989). Other causes of the lowering of the groundwater table were (Dufour, 2000):

- Increase in groundwater abstractions for drinking water and agriculture,
- Increase in evapotranspiration by higher crop yields per hectare and afforestation, and
- Decrease of the groundwater recharge by increased urbanization leading to an increase in impermeable paved area.

The lowering of the groundwater table created areas in which the connection between the ecosystems at the surface and the groundwater table disappeared. To reduce the area with desiccated natural ecosystems a regulation was implemented by the Dutch government in 1995. In this regulation a goal was set for the year 2000 to reduce the desiccated natural ecosystems area with at least 25% as compared to the reference year 1985. To realize this goal, the groundwater table needed to be increased to the desired level. To achieve an increase in the groundwater table, a number of compensating measures were proposed. Besides these measures aimed at reducing the groundwater extraction, also measures were proposed to reduce the discharge of ditches and brooks by impediment of drainage, promotion of meandering and allowing for more vegetation growth in the ditches as well as measures to increase groundwater recharge.

1.2 Deforestation increases groundwater recharge?

If afforestation did cause a decrease in the groundwater table, would deforestation then not increase the groundwater table? With this in mind water managers and foresters started to look at forest in a different perspective.

Most forested areas in the Netherlands are important infiltration regions for groundwater bodies. To increase the amount of available groundwater proposals were made to convert the predominantly dark and dense coniferous forests to deciduous forests or even deforest complete areas and replant them with vegetation of lower canopy height, i.e. heather (Stuurgroep-Grondwaterbeheer-Midden-Nederland, 1992). This discussion was stimulated by published reports that indicated high interception losses for forest (Evers et al., 1991). The main forest type studied at that time was Douglas fir because the main interest was to study acid rain and dry deposition. Douglas fir is among the trees with the highest leaf area index (up to $L_{AI} = 11$ m^2m^{-2}) and the highest water storage capacity (2.5 mm). Characteristics that are leading to high levels of deposition. According to common use, the benefits and effects were translated directly into economic values. Water supply companies became interested and were willing to compensate forest owners for changing the tree species from coniferous with a high interception storage to a land cover with a presumed much lower water loss, such as deciduous forest or grassland. The financial feasibility of such a change in vegetation depends primarily on the difference in volume of rechargeable water from the different types of tree species and secondary on the economic value of the tree species harvested (Filius and Roosenschoon, 1993). From the point of view of hydrologists and meteorologists this raised the question which eventually led to the present PhD thesis:

"What is the difference in water use between different tree species in the Netherlands?".

These developments are particularly important in the sandy areas of the Netherlands. In the lower parts of the Netherlands with mainly clay soils combined with relatively high water tables other developments brought about additional questions. Here organizations responsible for the management of large forested areas were confronted with increasing costs. On the one hand due to increasing taxes of the water boards and on the other hand due to increasing costs of compulsory maintenance of the ditches. Reducing these costs would be possible if the dimensions of the required water works could be reduced without increasing the discharge, especially the peak discharge of these areas. This became even more important in view of the goals set by the government to increase the area of forested land. First primarily for recreation and nature development, later also as a possibility to sequester CO_2. The total area of forest in the Netherlands is estimated in 2005 on 360.000 ha, i.e. 10% of the total

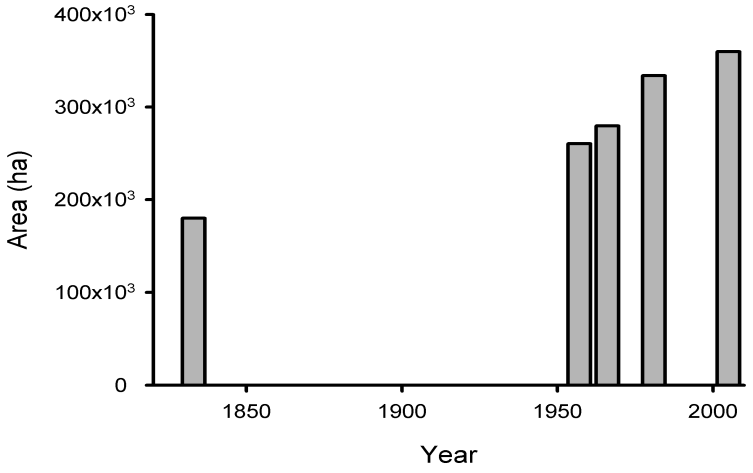

Figure 1.1: *Changes in forested area in the Netherlands (based on Dirkse et al., 2006).*

land surface. Figure 1.1 shows the increase in forested area in the Netherlands; a doubling compared to 1833 (MFV-Bos, 2006).

Even with this areal increase, forest in the Netherlands is still strongly dispersed; there are only a few extended forested areas and many small isolated plots. About half of the forest is mixed forest, the main mono species forest type is coniferous forest (32% in 2005, Dirkse et al., 2006). The last decades the average age of the forest has increased. Due to this ongoing land use change, two questions emerged:

- "Does a forested catchment have lower (peak) discharges than catchments with other land-use?"

- "Does a decrease in the number of maintained ditches of a forested catchment increase the (peak) discharge?"

A positive answer to the first and a negative to the second question would make it possible to reduce the dimensions of the infrastructural works required in a catchment that is to be afforested.

Later, after the high river levels of 1993 and 1995 and after the occasional flooding in some parts of the Netherlands became more and more serious, the possible effects of a climate change became more evident. This caused a growing interest in the possibility to retain water in forested catchments to decrease the peak discharge

during high water periods and to put even more weight on the required knowledge of the storage and discharge properties of forests.

These problems were combined into the following three leading questions for this study:

- "What are the main processes controlling the magnitude of the different components of the water balance of forested areas in the Netherlands?";
- "What are the controlling parameters of these processes and are they related to tree species?";
- "Will this knowledge be of added value to predict effects of different tree species on the water balance?".

The before mentioned problems and the associated questions were reason for the Ministry of Agriculture, Nature and Food Quality of the Netherlands to initiate in 1994 a study on the management of water resources of forests in the Netherlands. The study was executed by the Winand Staring Centre (which later became part of Alterra-Wageningen UR) and named "Hydrology of forests and forested areas in the Netherlands". The data collected for this project are the basis for the present thesis. This dataset was extended with financial support and a number of datasets of other projects.

1.3 The forest hydrology project 1994-1998

The increased number of stakeholders in demand for water, the decreasing volume of high quality water and the scarcity of land causes more and more demand for accurate and often small scale hydrological management strategies to comply to the needs of all stakeholders. This will only be possible if all the terms in the water balance can be estimated at a high level of certainty. The component of the water balance that is generally considered as a loss is evaporation. Hydrologists normally estimate evaporation losses as the residue of the water balance. This causes all errors of estimate of the other components of the water balance to accumulate in the estimated evaporation.

An alternative is to measure the change in soil water, either by (micro-)lysimeters or soil water sensors using for example the TDR-technique (Time Domain Reflectometry). The main disadvantage of these methods is the small measuring volume ($\pm 0.2 \cdot 10^{-3}$ m^3) and thus the problem to upscale the measurements to a larger area.

Other alternatives are methods that depend on micro-meteorological techniques. For these methods the energy balance together with measurements of gradients of

temperature, humidity and wind speed (e.g. the Bowen-ratio method) can determine the evaporation rate. Or, alternatively, high frequency measurements of wind speed and humidity and the fact that the vertical wind speed and scalars such as temperature and humidity are correlated can be used to determine the evaporation rate directly (e.g. the eddy-correlation method). Both types of methods have the benefit that they integrate over a relatively large area ($\approx$0.04-1 km^2) depending on the atmospheric stability and the height of the sensors above the forest. The main disadvantage of the Bowen-ratio is the fact that this method derives the amount of energy available for evaporation as the residue of the energy balance. This implies that all other components of the energy balance should be measured accurately. Here the same problem arises as mentioned earlier for the water balance. The most important drawback of the eddy-correlation method is the uncertainty associated with the time averaging and frequency response corrections.

In this study on nearly all sites the eddy-correlation method is used as it has shown to give reliable results (e.g. Aubinet et al., 2000; Moncrieff et al., 1997). It does not need additional measurements of other components of the energy balance, and the equipment has a low power consumption. This last quality was important as all sites were remote and main power was not available.

1.4 Research objectives and site selection

To answer the three leading questions as identified above the following research topics will be addressed in this thesis:

- Determine representative parameter sets to model the water use of the main forest types in the Netherlands;
- Quantify the effect of forest on the water balance.

The study areas were selected to represent the main forest types in the Netherlands. It was taken into account that the results of intensive studies on Douglas fir (*Pseudotsuga menziessii*) in the centre of The Netherlands (Bosveld, 1999) and on oak (*Querqus robur*) at the coast (Dolman, 1988) were already available or would come available in due course. With this in mind four forest types were selected: the main forest type in the Netherlands i.e. Scots pine (*Pinus sylvestrus*), an alternative to coniferous forest without needles in winter i.e. larch (*Larix kaempiferi*), a fast growing forest that was thought to be used in afforestation plans for parts in the west of the Netherlands with mainly clay and peat soils and a high groundwater table i.e. poplar (*Populus "Robusta"*) and a mixed forest consisting of different deciduous and coniferous trees and also with trees in different age classes. The last site was

selected because it was considered to be the forest of the future and it was expected that the same management would be used in the future in naturally managed forest. Although these four forests compose the main study area, data of one additional forest was added: an American oak (*Querqus rubra*) forest. This American oak forest was subject of an earlier study (Ogink-Hendriks, 1995). The site was interesting as it complemented the other sites being a deciduous forest on a sandy soil with a deep groundwater table.

These sites with their different forest types spread over a relatively small spatial area, making climate differences relatively small, together with an almost identical measurement set-up provided a unique opportunity to address the above mentioned research topics.

1.5 Outline of the thesis

The evaporation of a forest consists of two major components: interception loss and transpiration. Throughout this thesis distinction will be made between evaporation of a wet forest, i.e. interception loss and the evaporation of a dry forest, i.e. transpiration and soil evaporation. In general soil evaporation is relatively small under dry conditions, but the evaporation of the undergrowth may be substantial. How substantial the contribution of the undergrowth to the total evaporation is, is part of this study.

One of the possible changes in climate are shifts in precipitation and temperature distribution combined with a rise in CO_2 concentration causing more severe periods of droughts (e.g. Davi et al., 2006; Kruijt et al., 2008; Baldocchi and Xu, 2007). The impact of these on the water balance in general will among others depend on the water use of forests. Two main characteristics determine the water use of vegetated surfaces: the stomata and the root system. The loss of water is regulated by the stomatal closure and the availability of water for transpiration is determined by the root water uptake. It has been shown that vegetation and especially trees are able to extract water from deep layers enabling them to survive periods of drought (e.g. Rambal, 1984; Talsma and Gardner, 1986). As it is expected that climate change will come with prolonged periods without rain (Christensen et al., 2007), in this study special attention is paid to derive parametrizations for water stress. For areas like the lower parts of The Netherlands, the connection between the root zone and the groundwater table often determines the quality of the natural vegetation cover. Prolonged desiccation because of the cessation of connection between groundwater and root zone may have serious consequences for such ecosystems.

The theory and equations governing the water and energy flow of a forested plot are introduced in Chapter 2 “Theory of forest evaporation”. These equations also

form the basis for the parametrizations of a numerical model. The concepts behind these equations will be evaluated to determine possible conceptual improvements to simulate the effects of different forest types on the water balance.

To assure practical applicability of the findings, field data are a prerequisite. For this thesis an extensive amount of data have been collected at five different forest sites in the Netherlands. A detailed description including most of the parameters representing the characteristics of the vegetation and the soil at these sites is provided in Chapter 3 "Characteristics of the research sites". The measurement set-up including a discussion on the associated uncertainties is given in Chapter 4 "Hydrometeorological measurements at the sites".

Chapter 5 "Quality control of the flux measurements" discusses the quality of the measurements of the latent and sensible heat flux under dry and wet conditions. As the fetch conditions of the site determine the location and the magnitude of the contribution of the sources upwind of the flux sensor, an estimation is made of the length of the fetch. The footprint of the flux measurements together with the quality assessment of the measurements are also discussed in Chapter 5.

The behaviour of ecosystems in relation to their environment is often explained and projected into the future by the use of models. To test if such models and their parametrizations are adequate, the models should be fed by data series that cover the widest possible data space. In most cases an extensive enough data space is only obtained by collecting long term data series. For this study the records varied from 2 to more than 10 years. However, as it is almost impossible to obtain continuous series of measured data, methods to derive data to fill the gaps in the series are explored in Chapter 6 "Gap filling to generate continuous datasets".

Chapter 7 "Dry canopy evaporation" describes the variation in parameter values determining the transpiration rate for five typical forests in the Netherlands and the contribution of the undergrowth for two of these forest stands. The main objective in Chapter 7 is to improve our understanding of the processes determining the transpiration rate of forest, with special attention to the differences between stands with different tree species and the contribution of the undergrowth. The evaporation rate is measured using different methods: eddy correlation and Bowen ratio (see Chapter 4). As an independent check on the model performance sap flow measurements done at the Loobos site will be used. In view of the increasing periods of prolonged droughts, special attention will paid to the root water uptake and the parametrization of water stress. For the two sites with more abundant undergrowth an attempt will be made to separate the evaporation rate of the undergrowth and the trees. To explain the variation in evaporation between years and the variation between sites the Jarvis-Stewart parametrization using a sparse canopy single and dual source model will be optimized for different periods. Besides giving insight in

the variation of these parameters, it will also enable us to investigate the uncertainty in the parameter values based on relatively short measurement periods.

The precipitation input to a catchment is of paramount importance in obtaining a good prediction of the run-off. In forested catchments the throughfall rate determines the net precipitation input to the system. The throughfall amount is the gross precipitation minus the interception loss, which is defined here as the amount of precipitation intercepted by the (vegetated) surface and directly evaporated without reaching the soil. In Chapter 8 "Wet canopy evaporation" the parameters determining the water holding characteristics of that vegetation, i.e. the storage capacity C and the evaporation rate E_i will be explored. The discussion on the correct parametrization of E_i is a long standing one. In Chapter 8 we will try to answer the intriguing question originating from the discussion by Gash et al. (1999) is: "Is there a relation between the canopy cover and the ratio of the surface roughness lengths of momentum and heat z_{0M}/z_{0H} and does this ratio change during showers?". In this Chapter attention will also be paid to dependency of the storage capacity C on variables such as leaf area and wind speed and how these relations may change with season over the year.

To provide the answers to the three main research questions of this thesis, the findings of the earlier chapters will be integrated in Chapter 9 "Epilogue". A short note will describe how the techniques used in this thesis may support the knowledge water managers may need for e.g. extreme dry conditions. The thesis ends with suggestions how to improve the derivation of the actual evaporation rate of forests in the Netherlands and suggestions for further research on this topic.

To facilitate the reader, in the chapters where comparison of tree species is important, the main tree species of this study are set in italics. Most data used for this research are available on-line: www.climateXchange.nl (see "verdamping - boshydrologie project", or select the sites by their name).

Chapter 2

Theory of forest evaporation

2.1 Introduction

The analysis in this thesis is primarily concerned with the vertical transport of water and the energy balance. Effects of lateral exchanges of water and energy will be discussed only briefly. In the following sections the concepts to measure and analyse the one-dimensional interaction of water and energy between soil, vegetation and atmosphere are discussed.

2.2 Water balance of forests

2.2.1 Water balance above the soil surface

The rate of net precipitation P_{net} (m s^{-1}) reaching the soil surface is determined by the gross precipitation rate P (m s^{-1}), the change in time t (s) of the water storage $\mathrm{d}C/\mathrm{d}t$(m s^{-1}) and the evaporation rate E_i/ρ_w (m s^{-1}) of water intercepted by the vegetation above the soil surface, with ρ_w (kg m^{-3}) being the density of water. Hence the water balance equation above the surface can be written as:

$$P_{net} = P - \frac{\mathrm{d}C}{\mathrm{d}t} - \frac{E_i}{\rho_w} \tag{2.1}$$

P_{net} may be determined as the sum of the throughfall rate T_f (m s^{-1}) and stemflow rate S_f (m s^{-1}), i.e.:

$$P_{net} = T_f + S_f \tag{2.2}$$

Throughfall may consist of free throughfall, i.e. precipitation directly falling on the soil, and of drip, i.e. precipitation first falling on the vegetation before reaching the soil. Hence, the change in storage rate of intercepted water $\mathrm{d}C$ may be expressed as:

$$\frac{\mathrm{d}C}{\mathrm{d}t} = P - \frac{E_i}{\rho_w} - T_f - S_f \tag{2.3}$$

where T_f may be replaced by the total of the rate of canopy drip D (m s^{-1}) and the free throughfall:

$$T_f = (1 - c_{veg})P + D \tag{2.4}$$

where c_{veg} (-) is the fraction of canopy cover.

2.2.2 Water balance below the soil surface

The conservation equation of water for a unit volume of soil is:

$$\frac{\partial \theta}{\partial t} = -\frac{\partial q}{\partial z} - S_{roots} - S_E \tag{2.5}$$

where θ (m^{3}m^{-3}) denotes the volumetric soil water content, q (m s^{-1}) denotes the water flow rate, z (m) depth, S_{roots} (m^3 m^{-3} s^{-1}) represents the sink term for root water uptake and S_E (m^3 m^{-3} s^{-1}) the sink term for latent heat. The second sink term takes into account the evaporation (as well as condensation) that will be generated in deeper soil layers and will pass the soil surface as a vapour flux. This second sink term is for densely vegetated surfaces and relatively humid conditions relatively small. Therefore in this study, S_E will be considered to be negligible for forests in the Netherlands.

In the soil, water flow may be described by the Darcy flow equation:

$$q = -k(\psi)\frac{\partial(\psi + \rho_w g z)}{g \partial \rho_w z} \tag{2.6}$$

where $k(\psi)$ denotes the hydraulic conductivity (m s^{-1}), ρ_w the density of water (kg m^{-3}), g the gravitational acceleration (m s^{-2}), ψ the soil water pressure (Pa) and z the elevation head (m). Combining the Darcy flow equation with the conservation equation leads to the Richard equation for one-dimensional vertical transient soil water flow:

$$\frac{\partial \theta}{\partial t} = \frac{\partial}{\partial z}\left[k(\psi)(\frac{1}{g}\frac{\partial \psi}{\partial \rho_w z} + 1)\right] - S_{roots} \tag{2.7}$$

where θ and k are functions of ψ for which in this thesis the parametric descriptions as given by Van Genuchten (1980) have been used. The soil water retention curve is given by:

$$\theta(\psi) = \theta_r + \frac{\theta_s - \theta_r}{\left(1 + \left|g^{-1}\rho_w^{-1}\alpha\psi\right|^n\right)^{-m}} \tag{2.8}$$

and the hydraulic conductivity curve by:

$$k(\psi) = k_s \frac{\left[\left(1 + \left|g^{-1}\rho_w^{-1}\alpha\psi\right|^n\right)^m - \left|g^{-1}\rho_w^{-1}\alpha\psi\right|^{n-1}\right]^2}{\left(1 + \left|g^{-1}\rho_w^{-1}\alpha\psi\right|^n\right)^{m(l+2)}} \tag{2.9}$$

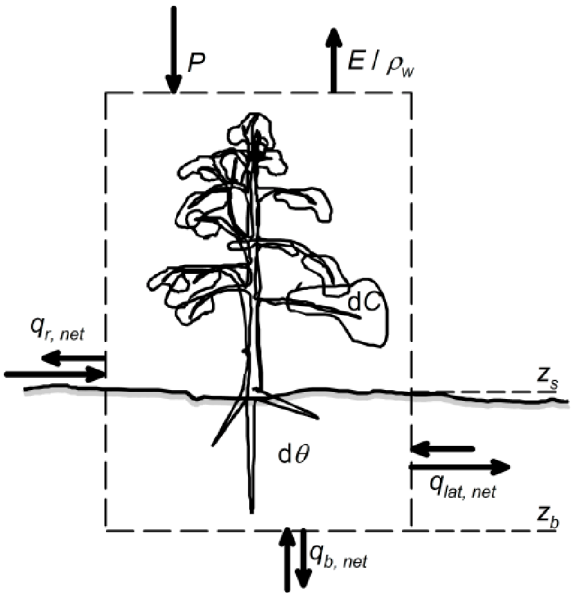

Figure 2.1: *Schematic view of the water balance components of a forest.*

where θ_s (m^3m^{-3}) and θ_r (m^3m^{-3}) are the saturated ($\psi = 0$) and residual volumetric soil water contents, α (m^{-1}), n (-), $m = 1 - n^{-1}$ (-) and l (-) are soil specific parameters, and k_s (m s^{-1}) the saturated hydraulic conductivity.

Combining Eqs. 2.3 and 2.5 and taking into account the lateral and vertical flows over the borders of a unit volume, allows to describe the water balance of a unit volume for a forest over a certain period of time (see Fig. 2.1) as:

$$P = \frac{E}{\rho_w} + q_{r,net} + q_{b,net} + q_{lat,net} + \frac{\mathrm{d}C}{\mathrm{d}t} + \frac{\mathrm{d}\int_{z_s}^{z_b} \theta \mathrm{d}z}{\mathrm{d}t} \tag{2.10}$$

where $q_{r,net}$ (m s^{-1}) the net surface runoff, $q_{b,net}$ (m s^{-1}) the net discharge rate at the bottom out of the soil column, $q_{lat,net}$ (m s^{-1}) the net flow rate of the incoming and outgoing lateral soil water, which may change with depth, z the depth in the soil (m) with the subscripts s and b indicating respectively the surface and the bottom boundary of the soil profile. The evaporation flux E (kg $m^{-2}s^{-1}$) may consist of evaporation of intercepted precipitation directly from the vegetation or from the litter layer as well as transpiration of the vegetation and soil evaporation.

2.3 The energy balance

2.3.1 Radiation balance

The rate of evaporation of forest depends to a large extent on the amount of energy available to the system. For natural surfaces such as forests, the main energy source is the sun.

Net radiation flux density R_{net} (W m^{-2}) is the balance between upward and downward flux densities of short and long wave radiation:

$$R_{net} = (1 - a_s)R_s + R_l^{down} - R_l^{up} \tag{2.11}$$

where a_s denotes the albedo of the surface, R_s the short-wave (0.3-3 μm) radiation flux density (W m^{-2}) and R_l the downward and upward flux densities of long-wave (3-100 μm) radiation (W m^{-2}). The upward longwave radiation R_l^{up} reads as:

$$R_l^{up} = \varepsilon_s \sigma T_s^4 + \alpha_l R_l^{down} \tag{2.12}$$

where ε_s denotes the emissivity of the surface, σ ($= 5.67 \cdot 10^{-8}$ W m^{-2} K^{-4}) is the Stefan Boltzmann constant, T_s the surface temperature (K) and α_l the reflectivity of the surface for the long-wave radiation. For a natural surface (i.e. an opaque non-black body) $\alpha_l = 1 - \xi_l$, and as for the same radiation the absorptivity ξ_l equals the emissivity, α_l is either replaced by $1 - \varepsilon_s$ or is ignored.

2.3.2 Energy storage fluxes in air and vegetation

The change in energy storage J (W m^{-2}) for a volume extending from the surface to the reference level over a unit area can be separated into three terms (Thom et al., 1975):

$$J = J_H + J_E + J_{veg} \tag{2.13}$$

where J_H denotes the change in storage of sensible heat in the air, J_E the latent heat storage in the air and J_{veg} the change in heat stored in the vegetation within the stand. They are respectively described as:

$$J_H = \int_0^{z_{ref}} \rho_a c_p \frac{\partial T}{\partial t} dz \tag{2.14}$$

$$J_E = \int_0^{z_{ref}} \rho_a \frac{\partial \varkappa}{\partial t} dz \tag{2.15}$$

$$J_{veg} = \int_0^{z_{ref}} \rho_a c_{veg} \frac{\partial T_{veg}}{\partial t} dz \tag{2.16}$$

where z_{ref} is the reference level (m), ρ_a the density of the air (kg m^{-3}), c$_p$ the specific heat of the air (J kg^{-1} K^{-1}), T the air temperature (K), $\varkappa$ the specific humidity of the air (kg kg^{-1}), t the time (s) and z the height (m). The subscript veg refers to the density ρ_{veg} (kg m^{-3}), the specific heat c$_{veg}$ (J kg^{-1} K^{-1}) and the temperature T_{veg} (K) of the vegetation. On a daily basis the energy storage is considered to be negligible. However, for shorter periods, especially when pronounced changes in temperature and humidity occur, storage fluxes may reach values up to 100 W m^{-2}.

2.3.3 Soil heat flux density

The heat flux density by conduction in a homogeneous medium may be expressed as:

$$G = -k_T \frac{\partial T}{\partial z} \tag{2.17}$$

where k_T denotes the thermal conductivity (W m^{-1} K^{-1}). In soil k_T is an effective thermal conductivity and is a weighted average of the individual soil constituents (De Vries, 1963). To account for the convective transport of heat in soil the effective thermal conductivity is replaced by an apparent thermal conductivity now relating temperature gradients to total soil heat flux densities including both conductive and convective transport of heat. Combining Eq. 2.17 with the conservation equation yields:

$$\frac{\partial}{\partial z}(k'_T \frac{\partial T}{\partial z}) = -\frac{\partial G}{\partial z} - S_E \tag{2.18}$$

where k'_T is the apparent thermal conductivity (W m^{-1} K^{-1}), G the soil heat flux induced by convection and conduction and S_E the sink of heat because of vaporisation. As mentioned before, in a moderate climate with relatively wet soils this sink is small and will therefore be neglected in this study.

2.3.4 Energy balance of a forest

The latent heat flux density λE (W m^{-2}) couples the water balance in eq. 2.10 with the energy balance equation:

$$\lambda E = R_{net} - H - G + F_{lat} - J - \mu F_A \tag{2.19}$$

where λ denotes the latent heat of vaporisation (J kg^{-1}), H the sensible heat flux density (W m^{-2}), F_{lat} the lateral advective energy flux density (W m^{-2}), μF_A the flux density of the energy absorbed by the vegetation for net photosynthesis (W m^{-2}). Here $\mu \approx 0.422$ J μmol $(CO_2)^{-1}$ and denotes the solar energy stored in the bonds of carbohydrate created by photosynthesis, F_A (μmol CO$_2$ m^{-2} s^{-1}). For forests at mid latitudes, the term μF_A of the energy balance is often less than 2% of R_{net}.

2.4 Turbulent fluxes of momentum, latent and sensible heat

2.4.1 Turbulent fluxes based on Reynolds averaging

The atmospheric flux densities of latent heat λE, sensible heat H and momentum τ can be defined in terms of the turbulent components of the wind velocities, heat and moisture. Using Reynolds averaging, the velocity components u, v and w (m s^{-1}) and the scalars potential temperature Θ (K) and the specific humidity of the air $\varkappa$ (kg kg^{-1}) can be separated in a mean component denoted by an overbar and a turbulent component denoted by a prime. The velocity components u, v and w are defined along the x, y and z axes respectively, with z being taken positive upwards. If we define the direction of the mean flow along the x axis then $\overline{v} = \overline{w} = 0$. Mean flux across a plane implies correlation between the wind component normal to that plane and the entity in question (Kaimal and Finnigan, 1994).

Assuming a flat horizontal plane, the covariance between the vertical wind velocity and an entity gives a direct measure of the flux density across the plane:

$$\lambda E = \lambda \rho_a \overline{w' \varkappa'} \tag{2.20}$$

$$H = \rho_a c_p \overline{w' \Theta'} \tag{2.21}$$

$$\tau = -\rho_a \overline{u' w'} \tag{2.22}$$

where τ denotes the momentum flux or shear stress (kg m^{-1} s^{-2}). The minus sign is introduced because momentum is absorbed at the surface and acts as a sink. It should be noted that τ is defined positively downwards, this in contrast to λE and H which are defined positively upwards

2.4.2 Turbulent fluxes based on gradients

In analogy to molecular diffusion the fluxes may also be parametrized in terms of time averaged vertical gradients of wind speed, heat and moisture and eddy-diffusion coefficients:

$$\lambda E = -\rho_a \lambda K_E \frac{\partial \overline{\varkappa}}{\partial z} \tag{2.23}$$

$$H = -\rho_a c_p K_H \frac{\partial \overline{\Theta}}{\partial z} \tag{2.24}$$

$$\tau = \rho_a K_M \frac{\partial \overline{u}}{\partial z} \tag{2.25}$$

where K_E, K_H and K_M ($m^2\ s^{-1}$) are turbulent exchange coefficients for moisture, heat and momentum. These coefficients depend on height and on the non-dimensional similarity functions ϕ:

$$K_X = \kappa z u_* \phi_X^{-1} \tag{2.26}$$

where the subscript X denotes E, H or M, κ (-) the von Karman constant and $u_* = \sqrt{\tau \rho_a^{-1}}$ ($m\ s^{-1}$) the friction velocity. These functions are determined experimentally for a flat surface and are generally assumed to be universally applicable (Dyer, 1974):

$$\phi_E = \phi_H = \begin{cases} (1+16|\zeta|)^{-1/2} & -2 \le \zeta \le 0 \\ 1+5\zeta & 0 \le \zeta \le 1 \end{cases} \tag{2.27}$$

$$\phi_M = \begin{cases} (1+16|\zeta|)^{-1/4} & -2 \le \zeta \le 0 \\ 1+5\zeta & 0 \le \zeta \le 1 \end{cases} \tag{2.28}$$

where $\zeta = \frac{z}{L}$ is a stability parameter with z the height (m) and L the Monin-Obukhov scaling length (m). When the atmosphere is unstable $\zeta < 0$, when stable $\zeta > 0$. The Monin-Obukhov scaling length can be expressed as:

$$L = -\frac{u_*^3 \overline{\Theta}}{g\kappa(\overline{w'\Theta'})} \tag{2.29}$$

where g denotes the acceleration of gravity ($m\ s^{-2}$). For a tall vegetation such as forest the displacement height d (m) is introduced. d is such that under near neutral conditions and assuming a logarithmic wind profile $\overline{u} = 0$ at a height $d + z_{0M}$, where z_{0M} is the roughness length for momentum (m). The stability parameter ζ now becomes $\frac{z-d}{L}$.

Integrating ϕ_M over the wind profile between $d + z_{0M}$ and the reference height z_{ref} yields the total contribution of atmospheric stability to the momentum flux, ψ_M. For unstable conditions the formulation as given by Paulson (1970) has been applied in this study. For the stable case the formulation as given by Van Ulden and Holtslag (1985) has been applied:

$$\psi_M(\zeta) = \begin{cases} 2\ln(\frac{1+x}{2}) + \ln(\frac{1+x^2}{2}) - 2\arctan(x) + \frac{\pi}{2}, & -2 \le \zeta \le 0 \\ -(0.7\zeta + 0.75(\zeta - \frac{5}{0.35})\exp(-0.35\zeta) + 0.75\frac{5}{0.35}), & 0 \le \zeta \le 1 \end{cases} \tag{2.30}$$

where x is defined as:

$$x = (1 - 16\zeta)^{0.25} \tag{2.31}$$

2.4.3 Turbulent transport using eddy diffusivities "K-theory"

It has been shown that the K-theory concept of eddy diffusivities to describe the turbulent transport in and above the canopy has shortcomings. As noted by Corrsin

(1974) the K-theory is only applicable if the length scale of the eddies maintaining the turbulent flux is much smaller than the length scale over which the mean gradients change. In forest canopies this condition is not always met, as eddies within a forest canopy may have a length scale similar to the tree height, while the change in mean gradient can be less than the tree height (Denmead and Bradley, 1985).

The best evidence for the failure of the K-theory is the existence of counter gradient fluxes within the trunk space, indicating negative eddy diffusivities, together with positive fluxes above the canopy (Denmead and Bradley, 1985). Raupach (1989) used a Lagrangian model as an alternative for the K-theory based models. Katul et al. (1997) showed that the modelled CO_2 fluxes using the inverse approach of the Lagrangian model represent the eddy-correlation measured fluxes in the canopy better than the K-theory derived fluxes. This finding is at apparent variance with those of Van den Hurk and McNaughton (1995) and Dolman and Wallace (1991), who found only a small difference between the fluxes of the two models. For most applications in forest hydrology, especially for predictive purposes, the K-theory is still considered the most practical concept (e.g. Shuttleworth, 2007).

2.5 Evaporation of a "dry" forest

When the surface of the vegetation of a forest with a full canopy cover is dry, the transpiration process is by far the largest contributor to the total evaporation.

The main drivers of the transpiration process are the available energy, i.e. radiation and the specific humidity deficit. The actual amount of water evaporated depends on both the root water uptake and the extend the leaves open or close their stomata. Depending on the structure of the leaves, there may also be some water loss through the cuticula, bypassing the stomata. However, in moderate climatic conditions such as in the Netherlands this water loss is minor as compared to the overall transpiration rate.

The opening and closing of the stomata is a physiological process combining photosynthesis and transpiration. The model concepts for these processes were all developed in the 1970's and the 1980's (e.g. Jarvis, 1976; Cowan, 1977; Ball, 1987; Farquhar et al., 1980. All of these models use semi-empirical relationships. Until now it has not been possible to develop a general theory for these semi-empirical relationships as a function of climate, that is able to explain the differences in parameter values between sites and species.

In this study the emphasis is on the evaporation process under wet and dry conditions and the photosynthesis process will not be taken into account. To use a single concept to model the evaporation rate for both conditions, the Penman-Monteith equation has been chosen. As all known functions for the stomatal closure are based

on empirical relationships with site specific parameters, the classical empirical approach of Jarvis (1976) will be used for the analysis of the stomata behaviour of a dry canopy.

2.5.1 "*Big leaf*" model

To describe the resistance to diffusion of water vapour and heat of the plant surface at z_1 to the reference level at z_{ref}, the profile gradient relations may be rewritten in analogy to electrical circuits:

$$H = -\rho_a c_p \frac{\overline{\Theta}(z_{ref}) - \overline{\Theta}(z_1)}{r_{aH}} \tag{2.32}$$

$$\lambda E = -\rho_a \lambda \frac{\overline{\varkappa}(z_{ref}) - \overline{\varkappa}(z_1)}{r_{aE}} \tag{2.33}$$

where r_{aH} denotes the aerodynamic resistance for heat (s m^{-1}) and r_{aE} the aerodynamic resistance for vapour (s m^{-1}) respectively. The resistances are the reciprocals of the eddy diffusivities integrated over the height between the surface and the reference level. Often the assumptions are made that the leaves are isothermal and the air in the sub-stomatal cavities of the leaves is saturated. With these assumptions the resistance of the transfer of water vapour from the sub-stomatal cavities to the leaf surface is described by a canopy resistance r_s:

$$r_s = \frac{E}{\rho_a \left[\overline{\varkappa}(z_1) - \overline{\varkappa_s}(\overline{\Theta}(z_1))\right]} \tag{2.34}$$

where $\overline{\varkappa_s}(\overline{\Theta}(z_1))$ is the saturated specific humidity (kg kg^{-1}) at the temperature of the surface at height z_1.

Combination of the above resistance equations for H and λE with the energy balance equation leads to the well known Penman-Monteith equation and (Penman, 1948 and Monteith, 1965). To derive the Penman-Monteith equation it is needed to assume that all sinks and sources of water vapour and heat are at the same level, and Δ is introduced, i.e. the change of the saturated vapour pressure e_s (hPa) with T. This equation is the basis for the "big leaf "model and has the advantage that all variables are measured at the same level:

$$\lambda E = \frac{\Delta_\varkappa A + \rho_a \mathrm{c}_p \varkappa_D r_{aH}^{-1}}{\Delta_\varkappa + \mathrm{c}_p(1 + r_s r_{aH}^{-1})\lambda^{-1}} \tag{2.35}$$

where A (W m^{-2}) denotes the energy available for conversion into H and λE and $\varkappa_D = \overline{\varkappa_s}(\overline{\Theta}) - \overline{\varkappa}$ is the specific humidity deficit (kg kg^{-1}). The gradient of the

saturated specific humidity versus the temperature curve (kg kg^{-1} K^{-1}) is given as:

$$\Delta_\varkappa = \frac{d\varkappa_s}{d\Theta} \tag{2.36}$$

The aerodynamic resistance r_{aH} represents the transport resistance encountered by moisture and heat moving from the source (in most cases the leaf) to the reference level. The surface resistance r_s for a forest mainly reflects the physiological response of the canopy to vapour transport to the surface.

2.5.2 Aerodynamic resistance

Often r_{aH} is replaced by the resistance for momentum transport r_{aM}, which is defined as:

$$r_{aM} = \frac{u}{u_*^2}$$

Under neutral conditions r_{aM} can be calculated by:

$$r_{aM} = \frac{1}{\kappa u_*} \ln\left(\frac{z_{ref} - d}{z_{0M}}\right) = \frac{1}{\kappa^2 u}\left[\ln\left(\frac{z_{ref} - d}{z_{0M}}\right)\right]^2 \tag{2.37}$$

For non-neutral condition a stability correction is added:

$$r_{aM} = \frac{1}{\kappa u_*}\left[\ln\left(\frac{z_{ref} - d}{z_{0M}}\right) - \psi_M\left(\frac{z_{ref} - d}{L}\right)\right] \tag{2.38}$$

It should be noted that the stability correction for the roughness length has been left out, as this term is generally negligible in comparison to the other terms. In the case of the transport of a scalar like heat or vapour, there is an added boundary layer resistance that in contrast to momentum accounts for the lack of pressure effects on the exchange of vapour and heat:

$$r_{bH} = \frac{1}{\kappa u_*}\left[\ln\left(\frac{z_{0M}}{z_{0H}}\right) + \psi_M\left(\frac{z_{ref} - d}{L}\right) - \psi_H\left(\frac{z_{ref} - d}{L}\right)\right] \tag{2.39}$$

Eq. 2.39 leads to the aerodynamic resistance for heat (and vapour):

$$r_{aH} = r_{aM} + r_{bH} \tag{2.40}$$

which under neutral conditions is given by:

$$r_{aH} = \frac{u}{u_*^2} + \frac{1}{\kappa u_*} \ln\left(\frac{z_{0M}}{z_{0H}}\right) \tag{2.41}$$

and under non-neutral conditions by:

$$r_{aH} = \frac{1}{\kappa u_*}\left[\ln\left(\frac{z_{ref} - d}{z_{0M}}\right) - \psi_H\left(\frac{z_{ref} - d}{L}\right) + \ln\left(\frac{z_{0M}}{z_{0H}}\right)\right] \tag{2.42}$$

or:

$$r_{aH} = \frac{u}{u_*^2} + \frac{1}{\kappa u_*}\left[\ln\left(\frac{z_{0M}}{z_{0H}}\right) + \psi_M\left(\frac{z_{ref}-d}{L}\right) - \psi_H\left(\frac{z_{ref}-d}{L}\right)\right] \tag{2.43}$$

where z_{0H} denotes the roughness length for heat and ψ_H the stability function for heat. As the stability functions ψ_M and ψ_H are not very sensitive to the exact value of the displacement height d and also play a minor role under wet conditions (i.e. $<$ 2% difference), Eq. 2.43 primarily depends on the estimation of the ratio of z_{0H} and z_{0M} and the correct measurement of u and u_*.

The roughness lengths z_{0M} and z_{0H} are theoretical properties, which cannot be measured directly. However, if T_s and H are known, r_{aH} can be derived from:

$$r_{aH} = \rho_a c_p \frac{\Theta_s - \Theta(z_{ref})}{H} \tag{2.44}$$

where Θ_s is an (effective) potential surface temperature. With Eq. 2.44 and Eq. 2.42 z_{0H} may then be calculated by (Blyth and Dolman, 1995):

$$z_{0H} = \frac{z_{ref}-d}{\exp\left[r_{aH}\kappa u_* + \psi_H\left(\frac{z_{ref}-d}{L}\right)\right]} \tag{2.45}$$

2.5.3 Stomatal conductance

The response of stomata to stress is controlled by a complex set of biomechanical feedbacks to among others radiation, leaf water potential, ambient water vapour and carbon dioxide levels. However as these feedback mechanisms vary between vegetation species and locations, there is still no universal applicable concept available (e.g. Domec et al., 2009; Leuning et al., 2008; McLaren et al., 2008; Woodruff et al., 2007). Two main concepts in parametrizing the effect of stomatal closure on the transpiration rate exist. The first stems from a mainly hydrological point of view, which basically reduces the maximum possible evaporation rate based on the available water in the root zone (see e.g. Feddes et al., 2001). The second concept is based on plant physiological relationships. These relationships describe the opening and closure of the stomata as being influenced by a number of environmental drivers. In some of these relationships the feedbacks on the closure of the stomata is enhanced by enzymatic reactions (e.g. Lösch and Schulze, 1994; Dewar, 2002 or Buckley, 2005).

There are a number of methods to parametrize the stomatal conductance g_s (m s^{-1}). According to Jarvis (1976), the stomatal conductance is a function of solar radiation, specific humidity deficit, temperature, leaf water potential and ambient CO_2 concentration. Jarvis described the relation between g_s and these variables in a synergistic model, where the maximum stomatal conductance $g_{s,\max}$ (m s^{-1}) is

reduced by stress functions. These stress functions are assumed to act independently. At present the discussion on the feedbacks of elevated concentrations of ambient CO_2 concentration on the stomatal conductance is ongoing. Fig 8.3 by Jarvis (1980) suggests that the reaction of the relative stomatal conductance to changes in ambient CO_2 is limited at least for Scots pine. This is in line with the review by Medlyn et al. (2001) who concluded that conifers have a less pronounced decrease in stomatal conductance than broad-leaved species. Nevertheless, whether elevated CO_2 will either reduce stomatal frequency in the field, or increase the leaf area, is still a point of discussion (e.g. Kouwenberg et al., 2003). Additional complications are the non-univocal outcome of some of the FACE sites (e.g. Calfapietra et al., 2010). Because of these uncertainties we do not include a parametrization for the ambient CO_2 concentration as suggested by e.g. Jarvis (1976) but will follow Stewart (1977). Stewart (1977) modified this model to enable the derivation of g_s from λE measured above the forest using the Penman-Monteith equation. The Jarvis-Stewart model for g_s is given by:

$$g_s = g_{s,\max} \frac{L_{AI}}{L_{AI\,\max}} \mathrm{f}(R_s^{down})\ \mathrm{f}(T_a)\ \mathrm{f}(e_D)\ \mathrm{f}(\theta_D) \tag{2.46}$$

where L_{AI} is the leaf area index and $L_{AI\,\max}$ the maximum leaf area index, $\mathrm{f}(R_s^{down})$ is a function of R_s^{down}, $\mathrm{f}(T_a)$ is a function of T_a, $\mathrm{f}(e_D)$ is a function of e_D, and $\mathrm{f}(\theta_D)$ is a function of θ_D. As these functions describe reductions with respect to $g_{s,\max}$, the functions take values between 0 and 1. The functions as used by different authors, do not always take the same form. The mathematical formulation of such a function may have an impact on the parameter values of the other functions (see Ogink-Hendriks, 1995), which puts a constraint on the comparison of parameters obtained from different equations. Furthermore the Jarvis-Stewart model is empirical, so parameter values are specific for species and sites. As Jarvis (1976) pointed out that, for proper parameter estimation it is important that the variables adequately fill the variable space, i.e. all combinations of variable values occur. However, under field conditions this may not be true. T_a and V_{PD}, for example, are often correlated and in some cases (e.g. Wright, 1996) regression results may be improved by removing the explicit dependency on T_a.

For the response to R_s^{down} the following function will be used:

$$\mathrm{f}(R_s) = \frac{R_s^{down}(R_{s,\max}^{down} + \mathrm{a}_R)}{R_{s,\max}^{down}(R_s^{down} + \mathrm{a}_R)} \tag{2.47}$$

where a_R is a constant and the maximum short wave radiation is set to $R_{s,\max}^{down} = 1000$ Wm^{-2}. The temperature response function to be used is taken as:

$$\mathrm{f}(T) = \frac{(T - T_{\min})}{(\mathrm{a}_T - T_{\min})} \left\{ \frac{(T_{\max} - T)}{(T_{\max} - \mathrm{a}_T)} \right\}^{\frac{(T_{\max} - \mathrm{a}_T)}{(\mathrm{a}_T - T_{\min})}} \tag{2.48}$$

where a_T (^{0}C) is a constant, $T_{\min}$ is set to 0 ^{0}C and $T_{\max}$ to 32 ^{0}C. The vapour pressure deficit function to be used is:

$$f(e_D) = e^{-a_{e_D}(e_D - c_{e_D})} \tag{2.49}$$

where a_{e_D} (hPa^{-1}) and c_{e_D} (hPa) are constants. Stress caused by limited water availability is the most complicating factor, among others because of the difficulty to measuring root distributions and θ. Therefore, spatial variability in θ and changes in time of the root distribution with depth, carry a relatively high uncertainty. In general a relatively simple approach may be used, which reduces to some extend the effect of spatial variability in soil water. Therefore, θ will be scaled by:

$$S = \frac{\theta - \theta_r}{\theta_s - \theta_r} \tag{2.50}$$

where S (-) denotes the relative saturation. In this case soil water deficit is defined as $\theta_D = 1 - S$. θ_s at each depth will be determined as the maximum θ during the winter period after the internal drainage rate returned to a negligible value. For θ_r the minimum value measured will be used. The degree of saturation over the root zone will be calculated as the average of the measurements of θ at each depth weighted by the thickness of the soil layer between the sensors.

To model the stomatal response on soil water stress, a function similar to that of the vapour pressure deficit will be used:

$$f(\theta_D) = e^{-a_{\theta_D}(\theta_D - c_{\theta_D})} \tag{2.51}$$

where a_{θ_D} (m^{-3}m^3) and c_{θ_D} (m^{3}m^{-3}) are constants.

2.5.4 Root water uptake

Water flows along a water potential gradient. Therefore water will flow to the roots if the roots have a lower water potential than the soil. The root water uptake can be represented as a sink term that is added to the vertical water flow (see Eq. 2.7). The flow rate towards the roots depends on the hydraulic conductivity of the soil and the path length. Root water uptake is in general described by either a microscopic or a macroscopic approach (Feddes et al., 2001).

The *microscopic* approach is based on radial flow towards individual roots. The integral over the root zone of the individual roots describes the entire root system (see e.g. Jackson et al., 2000). The *macroscopic* approach represents the rooting system as a single root. Because the microscopic approach requires detailed root information that is in general not readily available at most sites, the macroscopic approach is used in this study.

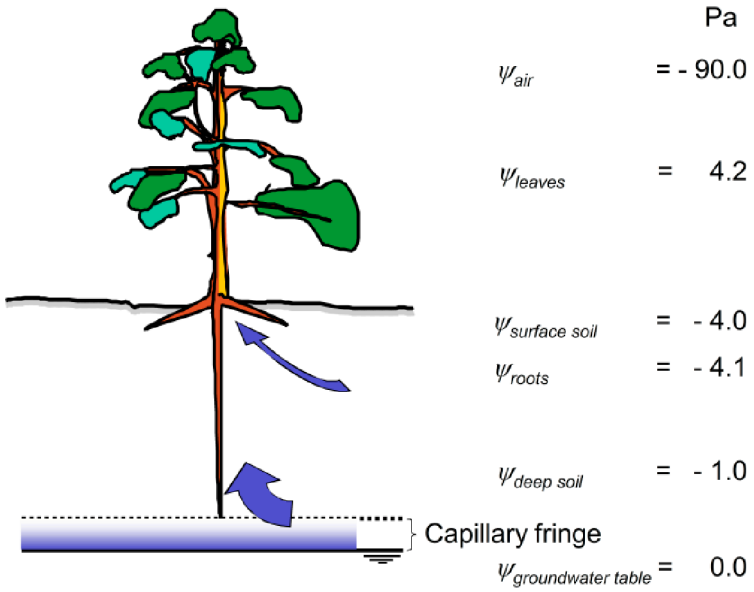

Figure 2.2: *Movement of soil water as driven by soil water pressure and root water pressure and leaf water pressure (free after Chapin et al., 2002). Also depicted is the capillary fringe of which deep roots tap water especially under dry conditions.*

The macroscopic approach is often used in hydrological models running on a daily time step. In these models the actual evaporation rate is based on a water stress function and the available soil water in the root zone. The water stress may be described by a function as proposed by Feddes (1978). This root water stress function can be extended for saline conditions (e.g. Shalhevet et al., 1976).

In the present study the actual evaporation rate is based on Eq. 2.35 and the feedback of the soil water stress on g_s is described by Eq. 2.51. This evaporation demand is distributed over the soil profile by weighting the root extraction at a given depth proportionally to the root density and available soil water. The latter is determined by specifying limiting pressures for the root uptake of water, and as such represents a decoupling of root uptake from the surface conductance model. The root water uptake is distributed over the soil profile assuming energy conservation. As a consequence the root water uptake, from soil layers with high soil water availability and high root density will be larger, than the root water uptake of soil layers with less available water and lower root densities (see Fig. 2.2).

For most forests root distribution can be split into two parts: the upper part with a high root density and the lower part with a low root density often existing of tap roots only (e.g. Dawson, 1996). Because of the high root density in the upper

layer it is assumed that, during daytime periods of high evaporation demand, all available soil water in this layer will be under high water demand by the roots. This water demand creates large differences in soil water pressure ψ over a relatively short distance in the soil aggregate. Redistribution of soil water at night (among others by "hydraulic lift for some species"as reported by Ludwig et al., 2003; Caldwell et al., 1998; Dawson, 1996) will largely eliminate differences in ψ. The redistribution of soil water allows for an efficient use of available water of a relatively thin layer at the top of the soil profile over a large area. In the deeper soil layers, where only a few roots are present, the distance between the root surface and soil water sources is much larger. Hence it will take more time to reach equilibrium of ψ in this soil layer after depletion during daytime by root abstraction. The soil water pressure and the hydraulic conductivity of the soil will play a major role in the transport of water from the moist zones towards the drier zones close to the roots in this deeper layer (see e.g. Feddes et al., 2001).

2.5.5 "*Dual source*" model for two vegetation layers

The vegetation of a forest is not always a well mixed ensemble of leaves. In such cases the vegetation of the forest is often better represented by two separate layers, i.e. trees and understorey. This representation can either be because the canopy of the trees is not completely closed above a closed layer of undergrowth, or because the trees are standing wide apart, with distinct patches of vegetation with a limited height in between.

The contribution of the two vegetation layers can be simulated using a sparse canopy model (Shuttleworth and Wallace, 1985; Dolman, 1993, Verhoef and Allen, 2000). This model assumes that the contributions of the latent heat flux of the two sources can be added up:

$$\lambda E = \alpha \lambda E_{Low} + \beta \lambda E_{Up} \tag{2.52}$$

where α and β are coefficients determining the weighted contribution of the two layers indicated by the subscripts Up and Low.

In the case of two layers one above the other, both layers have equal weight, i.e. $\alpha = \beta = 1$ (Fig. 2.3A). In the case of two distinct layers next to each other, i.e. two distinct vegetation patches, their total weight is one, i.e. $\alpha + \beta = 1$ (Fig. 2.3B). For the sites in this study the version with the two layers on top of each other i.e. $\alpha = \beta = 1$, will be used.

The model uses separate energy balances for each layer. The layers are coupled by the in-canopy vapour pressure deficit e_{D0} (hPa), defined as:

$$e_{D0} = e_D + \frac{\Delta_e A - (\Delta_e + \gamma)\lambda E}{\rho c_p} r_{aM} \tag{2.53}$$

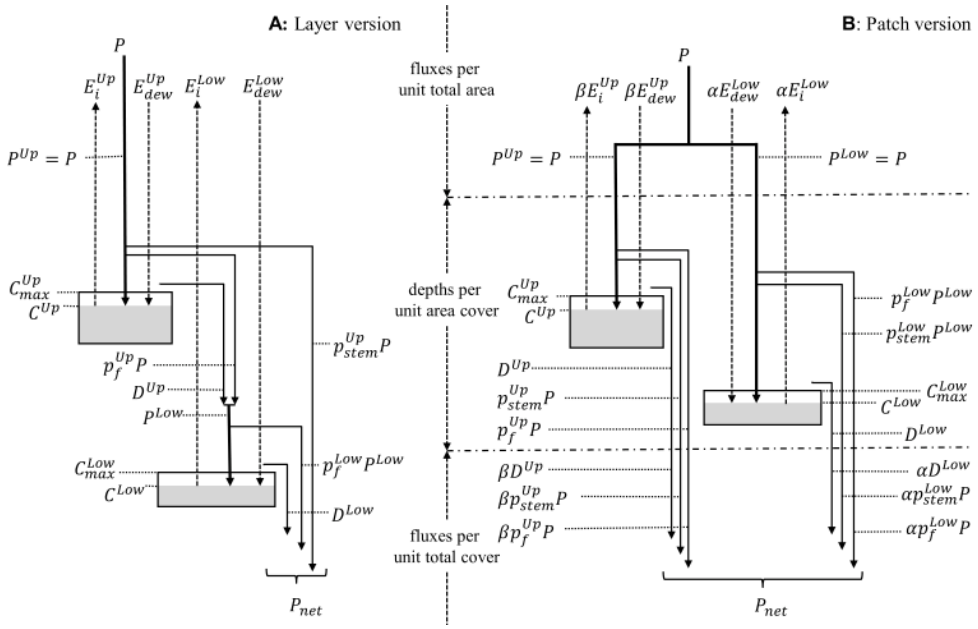

Figure 2.3: *Treatment of the water balance components for the layer version (left panel A) and the patch version (right panel B) of the two layer model with water present on the layers. (adjusted from Ashby et al., 1996). In the depicted configuration the lower layer represents vegetation or soil litter. See also Eq. 2.52.*

To describe the turbulent transfer within the canopy, K-theory will be used. The aerodynamic resistance r_{aM} to turbulent transfer of the total vegetation cover is the height integration of the reciprocal of the eddy diffusivity. In case of the two layer model this integration is composed of two parts. The first part is the resistance in the vegetation layer integrated from $d_M^{Up} + z_{0M}^{Up}$ to the height of the upper layer h_{Up}. The second part of r_{aM} is the resistance above the vegetation layer integrated from the height of the upper layer h_{Up} to the reference height z_{ref}. For the first part, $z < h_{Up}$, the eddy diffusivity K_z ($\mathrm{m^2 s^{-1}}$) is:

$$K_z = K_h^{Up} \exp\left[-\eta\left(1 - \frac{z}{h_{Up}}\right)\right] \tag{2.54}$$

where η is the eddy decay coefficient and K_h^{Up} is the eddy diffusivity at the height of the upper layer h_{Up}. For the second part, above the vegetation layer, $z > h_{Up}$, K_z is given by:

$$K_z = ku_* (z - d_M) \tag{2.55}$$

The integrated form of r_{aM} becomes then:

$$r_{aM} = \frac{1}{ku_*}\left\{\ln\left(\frac{z_{ref}-d_M}{h_{Up}-d_M}\right) - \Psi_{H'}\right\} + \frac{h_{up}}{nK_h^{Up}}\left\{\exp\left[\eta\left(1-\frac{z_{0M}^{Up}+d_M^{Up}}{h_{Up}}\right)\right]-1\right\} \tag{2.56}$$

where

$$\Psi_{H'} = \Psi_H(\frac{z_{ref}-d_M}{L}) - \Psi_H(\frac{h_{Up}-d_M}{L}) \tag{2.57}$$

The eddy diffusivity above the canopy, K_h^{Up} follows from Eq. 2.55. In contrast to the "big leaf" model the excess resistance of vapour and heat transport adjacent to the vegetation is explicitly modelled using a boundary layer resistance r_b. The surface resistance of the upper layer is defined by:

$$r_s^{Up} = \left[\frac{\Delta_e(A_{Up}) + \frac{\rho c_p e_{D0}}{r_b^{Up}}}{\lambda E_{Up}\gamma} - \frac{\Delta_e}{\gamma} - 1\right] r_b^{Up} \tag{2.58}$$

For the lower layer:

$$r_s^{Low} = \left[\frac{\Delta_e(A_{Low}) + \frac{\rho c_p e_{D0}}{(r_a^{Low}+r_b^{Low})}}{\lambda E_{Low}\gamma} - \frac{\Delta_e}{\gamma} - 1\right](r_a^{Low}+r_b^{Low}) \tag{2.59}$$

The boundary layer resistance is defined as:

$$r_b^{Up/Low} = 100\frac{\eta}{2L_{AI}{}^{Up/Low}\left[1-\exp(-\frac{\eta}{2})\right]}\sqrt{\frac{L_c^{Up/Low}}{u_{Up/Low}}} \tag{2.60}$$

where $L_c^{Up/Low}$ is the characteristic length scale (m) of the upper or lower vegetation layer and $u_{Up/Low}$ the wind speed at the height of the tree canopy and the understorey respectively. Assuming exponential decay of the momentum transport in the canopy, the aerodynamic resistance for the lower layer is given by:

$$r_a^{Low} = \frac{h_{Up}\exp(\eta)}{\eta K_h^{Up}}\left[\exp\left(-\eta\frac{z_{0M}^{Low}+d_M^{Low}}{h_{Up}}\right) - \exp\left(-\eta\frac{z_{0M}^{Up}+d_M^{Up}}{h_{Up}}\right)\right] \tag{2.61}$$

2.6 Evaporation of a "wet" forest

At mid latitudes evaporation is the largest component of the water balance especially in summer. The uncertainty associated with the measurement and modelling of evaporation of forests for time steps of a day or less is sometimes as high as 100%. This is in particular the case during wet conditions.

The two most important constituents determining the magnitude of the interception loss are the amount of water on the vegetation and the rate at which this amount evaporates. Both entities are difficult to obtain by direct measurement in the field and are thus often derived in the laboratory or indirectly.

2.6.1 Interception storage

To determine the storage capacity of the vegetation Aston (1979) used weighting of tree samples (or more specific tree branches) before and after wetting by a rainfall simulator in a laboratory. Bouten et al. (1991) used microwave transmission to measure the amount of water on the leaves in the field. In contrast to these direct observations, the more common method is to plot the throughfall (or alternatively the interception loss) against the precipitation as measured above the canopy. The saturation storage capacity is then derived as the negative intercept of the line, with a slope of one passing through the upper most points assuming no evaporation loss for these points (Leyton et al., 1967). Klaassen et al. (1998) discussed some of these methods based on the same principle. The direct measurements in general provide high values for the storage capacity, which is caused by the fact that these measurements are executed under laboratory conditions and thus are not representative for the field. Hence, although these studies can help us to better understand the processes involved, it is difficult to use these measurements for interception models like those of Rutter et al. (1971) or Gash (1979) as these models need parameters representing average field conditions. However, also methods based indirectly on field measurements have their drawbacks; e.g. the uncertainty in the method of Leyton et al. (1967) because of the sensitivity to the selection of the data points used. The number of data points that can be used in the analysis depends on the number of events (i.e. showers or rainy days) with minimal or no evaporation. Often there are only a limited number of such events available and it is difficult to determine if the assumption of negligible evaporation is really applicable under these conditions. In these cases the uncertainty in the derived parameter values is relatively high. Ignoring other possible errors the uncertainty may amount up to at least half the size of the lowest resolution i.e. 0.1 or 0.2 mm for the tipping bucket gauges used.

2.6.2 Evaporation rate under wet conditions

At present there are techniques available to measure the evaporation rate directly such as the Bowen-ratio and the eddy-correlation or -covariance technique. However, under wet conditions measurement of the vapour pressure (essential in both techniques) is prone to errors, which makes these techniques less suitable. A solution to bypass this problem is to use H being measured with an eddy-correlation system.

The evaporation rate is then derived as the residue of the energy balance (e.g. Gash et al., 1999) or Van der Tol et al., 2003). These measurements suggest a substantial overestimation of values based on either regression analysis or the Penman-Monteith equation using $r_s = 0$ s m^{-1} (e.g. Mizutani and Ikeda, 1994 or Lankreijer et al., 1999).

2.6.3 Interception loss as a fraction of P

The most simple estimate of interception loss is interception expressed as a fraction of rainfall on an annual basis. However, the interception loss depends strongly on the capacity of the vegetation to retain water on its surface. Also the magnitude of this storage capacity is thought to be linearly dependent on the leaf area. As the interception loss depends on the leaf area, the interception loss as a fraction of the precipitation also changes with the seasons (see e.g. Gerrits et al., 2010). These seasonal changes however, are not necessarily always observed. For example Trimble and Weitzman (1954) found for a 50 year old mixed hardwood forest $E_i = 0.2P$ (mm) both during winter and summer.

Later Dolman (1987) reported similar numbers for an oak forest in The Netherlands. He attributed the low fraction during the foliated season to two attacks from the leaf roller moth Tortrix viridana reducing L_{AI} from 4.2 to 2.0.

Calder (1990) found that the effect of thinning on the interception loss of a spruce forest in England was much less then could be expected on a ratio basis. He attributed this phenomena to an increased ventilation and a reduced aerodynamic resistance of the remaining canopy.

Teklehaimanot et al. (1991) studied the relation between tree spacing and interception loss for one tree species: Sitka spruce. They found a significant relationship between the number of trees and percentage of throughfall (%); $T_f/P = 254.88 N_{tree}^{-0.19}$ ($R^2 = 0.98$) where N_{tree} denotes the tree density. However, their relationship is of questionable use for most mature forest, because it is very sensitive at low tree densities i.e. producing results with a high uncertainty.

From this short review it may be clear that it is not only the leaf area that determines the range of interception losses, but other factors also play a role. Crockford and Richardson (2000) reached similar conclusions based on a review of interception as a percentage of precipitation. They concluded that it is difficult to derive universal relationships on the percentage of interception loss for a particular forest and climate.

2.6.4 Interception loss as a function of storm intensity

Horton (1919) derived a series of empirical relationships in estimating interception per storm event. Assuming an exponential increase of interception as rainfall increases,

the interception loss E_i (mm) may be written as:

$$E_i = a\left[1 - \exp^{(-bP)}\right] \tag{2.62}$$

where P (mm) is the amount of precipitation of the storm. In Horton's original model the two parameters were replaced by one, by defining b as the reciprocal value of a. The parameter a represents the maximum interception loss and was defined by Horton as:

$$a = C_{max} + Et_P \tag{2.63}$$

where C_{max} (mm) is the storage capacity, E (mm h^{-1}) the wet canopy evaporation rate and t_P the duration of the shower (h). Sometimes Et_P is multiplied by the ratio of the evaporating surface to the projected area, i.e. the leaf area index of vegetated surfaces. Models of this type can also be applied to daily values of precipitation.

Hall and Harding (1993) and Calder (1990) used the two parameter model with daily values and obtained satisfactory results for coniferous forest in Britain. Calder considered b a fitting parameter and did give no physical explanation for the parameter.

2.6.5 Interception loss based on physical concepts

During a short time step the evaporation rate of intercepted water is difficult to measure in the field and only a few studies are available that succeeded in obtaining reliable observations (e.g. Stewart, 1977). Hence virtually all estimates of evaporation of intercepted water are based on interception models being calibrated and validated against gross precipitation, stem flow and throughfall measurements. Some models make a distinction between the canopy and the stem (Rutter et al., 1975), while others subdivide the canopy into multiple layers (e.g. Sellers and Lockwood, 1981). Besides these physically based models, also stochastic models have been developed (Calder, 1986).

Rutter et al. (1971) formulated one well known physical model. Their model is based on a running water budget for the canopy and trunk. The evaporation rate was calculated by means of the Penman-Monteith equation (see Eq. 2.35) with $r_c = 0$ mm s^{-1}. Rutter et al. (1975) found on a monthly basis satisfactory agreement between simulated and observed interception loss for Douglas fir, Corsican Pine, Norway Spruce and Hornbeam, i.e. within 10% of the observed interception loss. However, they underestimated the interception loss of Oak by 20% of the observed total loss. The authors ascribed this feature to a possible low estimation of the roughness length z_{0M} in both leafy and leafless periods. Using slightly different models but based on the same concept, many other authors obtained, for seasonal

Figure 2.4: *Picture on the left shows a thin layer of water covering the entire surface of the leaves during a light shower. Picture in the middle shows droplets of rain distributed on the leaf surface. Picture on the right shows needle leaves with droplets at their tips.*

to yearly averages, similar good results for different forest types (e.g. Gash et al., 1995; Lankreijer et al., 1999; Pypker et al., 2005). However, at shorter time steps and primarily for low intensity showers, less good results were obtained (e.g. van Dijk and Bruijnzeel, 2001b).

A common concept used in interception modelling is to consider the interception storage as a layer of water completely covering the vegetation. In reality this situation occurs only at either very low rainfall rates or in the presence of fog.

Under most rainfall conditions the leaves will be covered by drops of water (Fig. 2.4). When needles are present nearly all water is accumulated at the tips which function as drip points.

Butler (1985) and Butler (1986) studied the energy balance of water drops at a leaf surface and concluded that the conduction of heat from leaf tissue to drops will significantly increase the evaporation rate of leaf surface water. He also concludes that as the exposed surface area of drops is 30% of the leaf surface, the evaporation rate is also about 30% of a totally wet surface, not including the heat conduction mentioned before.

In a similar way Bosveld and Bouten (2003) presented a single layer model which allows for energy exchange between a wet and a dry surface fraction by conduction and for a prescribed degree of stomatal blocking. They conclude that for a dense Douglas fir forest, most of the transpiration reduction originates from energy competition and micro-climate influence. The remaining reduction was explained by assuming that during maximum canopy storage one third of the stomata are blocked by water.

This energy partitioning between different locations within the canopy appears to be somewhat similar to the findings of Shuttleworth (1978). The latter presented a multi-layer model written in analytically continuous form, which can be applied to conditions with large-scale variation in surface wetness. An essential part of the model is that there is a wet part and a dry part of the canopy, each having a specific T_s.

2.6.6 Effect roughness length for momentum and heat on E_i

Sellers and Lockwood (1981) used a multi-layer model and showed that the Rutter model underestimated the interception loss for low precipitation rates. They primarily attributed this feature to the assumption of Rutter et al. (1971) that during periods when the canopy is not saturated, the interception evaporation is proportional to the ratio of the actual amount of water on the canopy over the maximum amount.

Later it was shown by Lankreijer et al. (1993) that for two different sites an analytical form of the Rutter model (Gash, 1979) gave an overestimation of the interception loss. They showed that a much better result could be obtained by introducing an extra resistance for heat and vapour transport in the aerodynamic resistance.

Gash et al. (1995) however, obtained for the same sites similar good results as Lankreijer et al. (1993) by introducing a sparse canopy in his original model using only the resistance for momentum. Good results for sparse pine and eucalyptus forests in Portugal were also obtained by Valente et al. (1997) using the aerodynamic resistance for momentum flux and the earlier mentioned sparse canopy concept as applied to the Rutter and the Gash model. In addition Gash et al. (1999) obtained poor model performance for the sparse pine forest when the estimated aerodynamic resistance included an empirical relationship between the roughness lengths for heat/vapour and momentum derived previously for dry conditions.

Hormann et al. (1996) also used the original Gash model and improved his simulation results by introducing a wind speed dependent canopy storage. Linsley et al. (1982) stated that as wind speed increases the interception storage capacity is reduced, but the rate of evaporation however increased. They concluded that during a long storm high wind speeds tend to augment total interception while decreasing it for a short storm.

2.6.7 Methods to derive interception loss and canopy storage

There are different ways to derive interception loss and canopy storage from experimental data. The following section discusses the methods used in this thesis.

For showers saturating the canopy (assuming there is no drip before saturation) interception loss E_i (mm) can be expressed as:

$$E_i = \int_0^t E \mathrm{d}t + C \tag{2.64}$$

where t (h^{-1}) is the total duration of the shower, E (mm h^{-1}) the evaporation rate

and C (mm) the amount of water on the canopy when rainfall and throughfall have stopped. It should be noted that the term canopy includes leaves, twigs and branches.

Based on Eq. 2.64 Gash (1979) developed an analytical model, later improved by Gash et al. (1995) introducing the so called "sparse canopy" concept. This concept has proven to give accurate estimates of interception losses especially on seasonally and yearly basis provided locally calibrated parameters are used (e.g. Lankreijer et al., 1999; Pypker et al., 2005). Although this model is event-based, the parameters used have the same physical meaning as those used by the short time step model of Rutter et al. (1971). Assumptions used in the Gash model are: stem flow is diverted to the trunks only after the canopy has become saturated; rainfall is represented by a series of discrete events separated by periods long enough to allow the canopy to completely dry; meteorological conditions are constant throughout an event; there is no drip from the canopy during the wetting-up phase; evaporation from partially wet canopies is linearly related to the evaporation from saturated canopies. Generally the assumption is made of one event per day i.e allowing the use of daily data.

The threshold value required to saturate the canopy P' is given by:

$$P' = -\frac{\overline{P}C_c}{\overline{E_c}} \ln\left[1 - \frac{\overline{E_c}}{\overline{P}}\right] \tag{2.65}$$

where the storage capacity of the canopy equals $C_c = C/c_{veg}$ (mm) and the evaporation rate per unit canopy cover c_{veg} (-) is $\overline{E_c} = \overline{E}/c_{veg}$, with $\overline{E}$ (mm h^{-1}) being the average evaporation and $\overline{P}$ (mm h^{-1}) the average precipitation rate during the event.

The Gash model describes E_i on "event basis" by:

$$\begin{aligned} E_i &= c_{veg}P && \text{for } P \leq P' \\ E_i &= c_{veg}\left[(P' - C_c) + \tfrac{\overline{E_c}}{\overline{P}}(P - P') + C_c\right] && \text{for } P > P' \end{aligned} \tag{2.66}$$

where Eq. 2.66 is based on the underlying assumption that all evaporation takes place at the same point in the canopy and that stem flow S_f is negligible. See Appendix A for the stem flow observations at four of the forest sites of this study.

In general E is calculated using the Penman-Monteith equation (see Eq. 2.35), where r_s is set to zero. The aerodynamic resistance r_{aH} represents the transport resistance encountered by moisture and heat moving from the source (in most cases the leaf) to the reference level (see Eq. 2.43). r_{aH} can be derived from Eq. 2.42 if the potential surface temperature Θ_s is known.

Direct measurement of Θ_s is complicated. To obtain a first estimate however, the outgoing long wave radiation R_l^{up} can be used. Following Bosveld (1999) the emissivity ε_s for the forest is assumed to be close to 1. Often the aerodynamic

resistance for momentum r_{aM} is assumed to be equal to r_{aH}. r_{aM} can be calculated for each individual time step using a fixed optimised value for d being based on friction velocity u_* and wind profile measurements under near neutral conditions.

A convenient way to express the ratio between the aerodynamic resistance for heat and momentum is the von Karman constant k times the reciprocal of the Stanton number B:

$$kB^{-1} = \ln(\frac{z_{0M}}{z_{0H}}) + \psi_M \left(\frac{z_{ref} - d}{L}\right) - \psi_H \left(\frac{z_{ref} - d}{L}\right) \tag{2.67}$$

The stability corrections in Eq. 2.67 only have effect for the unstable cases and are often not taken into account (Verma et al., 1986).

To derive an estimate of the values of the parameters C, $\overline{E}$ and the free throughfall coefficient p_f two methods are used. The most common method is by Leyton et al. (1967), using P, T_f and S_f either based on showers or daily data, the latter under the assumption of one shower per day. From the same input data estimates may be derived for $p_f = 1 - c_{veg}$ and for the ratio $\overline{E}/\overline{P}$.

As an alternative the storage capacity C_c has been derived by inverting the Gash model for conditions when the canopy is saturated (Gash et al., 1995):

$$C_c = \frac{\frac{\overline{E_c}}{\overline{P}} \left(E_i - c_{veg} \frac{\overline{E_c}}{\overline{P}} P\right)}{c_{veg} \left(\frac{\overline{E_c}}{\overline{P}} - 1\right) \ln\left[1 - \frac{\overline{E_c}}{\overline{P}}\right]} \tag{2.68}$$

The advantage of this approach is that the derived parameter values will implicitly inherit the model concept and hence provide the best estimate. To avoid cross correlation between parameters, as many independent measurements as possible will be used, i.e. estimates of c_{veg} will be based on the LAI-2000 and anascope measurements in combination with photographs of the canopy. The average evaporation rate has been based on λE derived as the residual of the energy balance. C_c has been derived by optimizing E_i in Eq. 2.68.

In most climate models C is estimated by multiplying L_{AI} with a constant factor i.e. approximately 0.15 for broad-leaved and 0.2 - 0.3 for needle-leaved trees (see e.g. Luxmoore, 1983; Watanabe and Mizutani, 1994; Wilson et al., 2001). The review presented by van Dijk and Bruijnzeel (2001b) shows the high variability of this number due to the method used to derive C (e.g. the data of Lankreijer et al., 1999) as well as the variability due to other factors than the L_{AI}, e.g. roughness of the leaves (Waterloo, 1994). In both cases the variation in C per L_{AI} is as high as 100%.

The direct measurement in the field of C is complicated and has been performed only in a few studies for a limited period (Calder, 1986 and Bouten et al., 1991).

These studies showed relatively high values for C in contrast to most other studies using indirect methods. The more widely used indirect method is the method of Leyton et al. (1967) (see e.g. the overviews by Deguchi et al., 2006; van Dijk and Bruijnzeel, 2001b). There is however some doubt about what these values physically represent.

Chapter 3

Characteristics of the research sites

3.1 Introduction

In this Chapter static or slowly changing site characteristics are described. Measurements have been taken at 5 different locations, i.e. Bankenbos, Edesebos, Fleditebos, Kampina and Loobos (see Fig. 3.1).

The measurements at the locations Bankenbos, Fleditebos and Loobos started towards the end of 1994 and the beginning of 1995, at the Kampina site early 1996. The main goal was to establish water balances and parameter sets characterizing the water and energy balances of different types of forests in the Netherlands. The instrumentation at these sites was almost identical.

The data at the Edesebos site were collected in the framework of the "Forest and Water"project of the Research committee on Water management of Nature, Forest

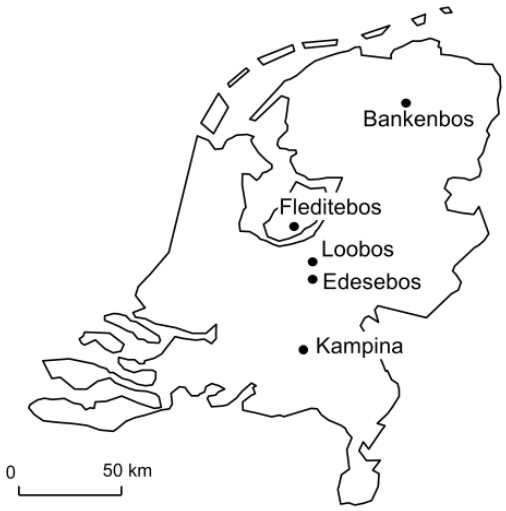

Figure 3.1: *Location of the sites.*

and Landscape. To establish the water balance of this forest 3 campaigns in 1988, 1989 and 1990 were executed (Hendriks et al., 1990).

3.2 Methods being used

Almost all forests in the Netherlands are man-made. As a consequence the tree species found are reflecting the ideas in forest management at the time of planting. The choice of the tree specie to be planted is often a combination of the management objective (e.g. wood for construction, paper production, nature reserve) and the expected growth characteristics based on the soil type and the hydrological regime at the location. The undergrowth of the forest grows naturally and depends on soil type and the hydrological regime in combination with the quality of the litter of the trees. Hence each forest stand is a unique combination of vegetation, i.e. trees and undergrowth, soil type and hydrological regime. In the Netherlands, with its flat topography, the depth of the groundwater table together with the hydraulic characteristics of the soil determine the hydrological regime of a location and hence, the amount of water available for root uptake of the vegetation.

3.2.1 Vegetation characteristics

Vegetation characteristics such as tree density N_{tree}, tree diameter at breast height D_{BH}, tree height z_{tree}, lowest level of the canopy z_{can} and canopy diameter D_{can}, were measured every one or two years.

Tree height z_{tree} as presented in this chapter represents the average z_{tree} of all trees in the stand. For z_{tree} to be used in conjunction with the reference height z_{ref} of the meteorological measurements, the heights as observed from the tower should be used. Differences between these two heights are caused by differences in topography as is the case at the Loobos site.

The fraction of the canopy cover $c_{veg}$was estimated at all sites but the Edesebos site by using the measurements of the LAI-2000 (Li-Cor) sensor (see Fig. 3.2). To check the accuracy of these estimates simultaneously measurements with the LAI-2000 sensor were made and pictures were taken using a digital camera above all 36 throughfall buckets at each site. The average c_{veg} of both methods differed less than 4% of the total coverage at all occasions. At the Edesebos site c_{veg} was measured using an anascope similar to the one applied by Ford (1976). At 380 points distributed over an area of 400 m^2 surrounding the tower the anascope was used to detect the canopy cover.

The Leaf Area Index L_{AI} was measured at the Loobos site by destructive sampling. At all other sites L_{AI} was measured using leaf litter fall trays or optical sensors,

Figure 3.2: *Employment of the LAI-2000 sensor below the canopy to measure the leaf area.*

i.e. LAI-2000 (Li-Cor).

To derive L_{AI} from the leaf litter fall, the leaf area was measured from sub samples.

For the needle leaves 10 sub samples of 100 needles each were taken of each sample. For the broad leaves the leaf area of 10% of each sample was measured. After that the leaves were dried for one week and weighed. The dry weights were used to calculate the maximum L_{AI}.

From 1996 onward L_{AI} measurements were made using two LAI-2000 (Li-Cor) simultaneously. Typically measurements were made every two weeks in the growing season, otherwise every month. At each site one instrument was mounted on top of the scaffolding tower and one employed along transects including 70 to 100 measurement points with a 3 m spacing below the canopy. Care was taken for each set of measurements to measure as much as possible under the same conditions. Points were chosen to prevent tree stems from obstructing the view. Under overcast conditions measurements were made above the head of the operator. Under sunny conditions the operator was blocked out by using a cap covering 45^0 of the surface of the sensor lens. No significant differences could be detected between the two methods of operation.

The measurements made with the LAI-2000 sensor were calibrated by comparing the measurements with the results from the litter trays or with the results from the destructive sampling. For this calibration it was assumed that the LAI-2000 instrument measures the Vegetation Area Index V_{AI} and that during the leafless periods these measurements represent the Wood Area Index W_{AI}. L_{AI} was then obtained by the relationship:

$$L_{AI} = V_{AI} - W_{AI} \tag{3.1}$$

3.2.2 Soil physical characteristics

To obtain the soil water characteristics $\theta(\psi)$ and $k(\psi)$ as defined by the Eqs. 2.7 and 2.9, undisturbed soil samples were taken in duplicate at different depths and analysed in the laboratory. To determine the water retention characteristics the evaporation method of Wind (1968), Boels et al. (1978) and Wendroth et al. (1993) was used. For the clay soil at Fleditebos additional measurements of θ were performed using a membrane press (at $\psi = +\ 0.5$ MPa and $\psi = +\ 1$ MPa). Also a measurement of θ at $\psi = 0.01$ MPa was made in a room at constant T and $\varkappa_r$ of 50% (personal communication Veerman, 1998). To reduce the uncertainty of the evaporation method in the wet range for the determination of the $k(\psi)$ characteristics, the results of the evaporation method were combined with those of the drip infiltrometer.

The soil fractions were derived in the laboratory and based on mixtures of 10 samples at each location and depth. The clay fraction has been defined as the mineral parts up to 2 μm, the sand fraction consisting of the mineral parts between 2 and 2000 μm and thus includes the silt fraction.

Figure 3.3: *Larch stand at the Bankenbos site showing the litter trays and the scaffolding tower. Low resolution picture taken with one of the first digital camera's.*

3.3 Bankenbos

This site (53°1′21″N – 6°24′32″E) being located close to the town of Veenhuizen is covered by a 100% Japanese larch (*Larix Kaempferi*) stand.

The area of the Bankenbos site was 250 m by 900 m, with the greatest length being oriented in SW to NE direction. The stand was located at the edge of a larger forest system containing other tree species, such as oak. At the west side the stand is connected to a cut over bog being covered by purple moor grass (*Molinia Carulea*). To obtain the best fetch for the prevailing SW wind direction, the measurement tower was placed in the NE corner of the stand. The shortest distance from the tower to the bog was 200 m. Fig. 3.4 shows the main land use around the flux tower.

The larch trees had an average height z_{tree} of 22 m and a tree density N_{tree} of 300 stems ha^{-1}. There was a very sparse undergrowth of purple moor grass. Table 3.1 summarizes the different parameters characterizing the vegetation of the Bankenbos site.

In 1995 and 1996 L_{AI} was measured using 5 leaf litter fall trays of 1 m^2 each. The V_{AI} measurements made with the LAI-2000 were converted into L_{AI} using Eq.

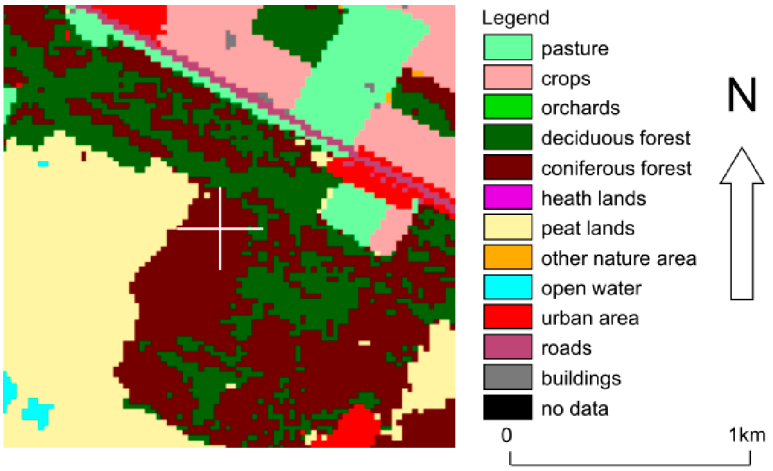

Figure 3.4: *Different types of land use in an area of 2 x 2 km surrounding the Bankenbos site as classified in the land use database LGN.*

Table 3.1: *Vegetation characteristics near the tower at the Bankenbos site. All values are average values for the stand. The standard deviation if available is also provided. The tree heights z_{tree} are given at the start as well as at the end of the observation period. All other characteristics have been averaged over this observation period.*

Site	Bankenbos	Stand. dev.
Tree species	Larch	
Undergrowth	Purple moor grass	
Planting year	±1930	
Observation period	1995-1997	
Tree density, N_{tree}	300 tree ha^{-1}	
Tree height, z_{tree}	22.0-23.4 m	± 1.5 m
D_{BH}	0.29 m	±0.04 m
Crown radius	3.31 m	
Projected crown area	35 m^{2}tree^{-1}	±11 m^{2}tree^{-1}
Crown base, z_{can}	14.7 m	±1.5 m
L_{AI}tree, maximum	1.8 m^{2}m^{-2}	
L_{AI}undergrowth, maximum	<1.0 m^{2}m^{-2}	
Canopy cover fraction, c_{veg}, maximum	0.6	
Canopy cover fraction, c_{veg}, minimum	0.4	
Rooting depth, z_{root}, 90% of all roots	0.3 m	
Rooting depth, z_{root}, maximum	0.7 m	

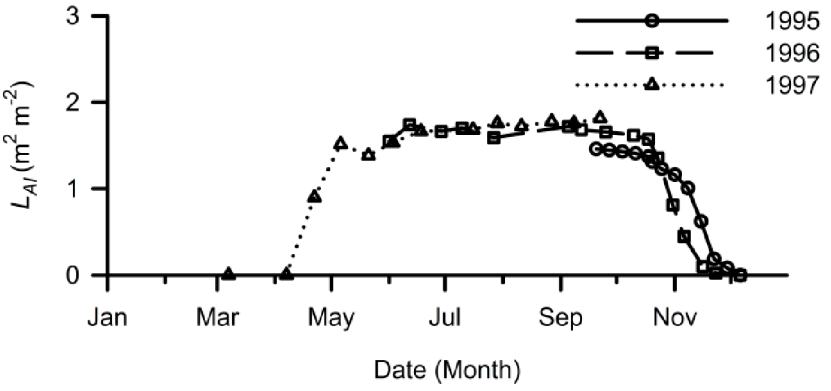

Figure 3.5: *Leaf Area Index (L_{AI}) of the larch stand at the Bankenbos site for the different years.*

3.1. Based on the V_{AI} measurements made during the leafless period, the $W_{AI}$for the larch trees was estimated as 0.92 m^2 m^{-2}. Comparison of the resulting values with the L_{AI} values from the litter trays yielded a correction factor of 1.89. This calibration factor was used to correct the LAI-2000 measurements for the other years. The thus derived L_{AI} was lower than the values reported by Breuer et al. (2003), i.e. most likely because of the much higher stand density and younger age class of the stand reported by Breuer et al. (2003). The L_{AI}-values compared well with the values reported by Ohta et al. (2008) for a larch stand of comparable tree density. Chason et al. (1991) found for an oak-hickory stand that the LAI-2000 underestimated L_{AI} using a litter trap by 45%. This underestimation is comparable with our results, i.e. an underestimation of 47% of L_{AI} in comparison with the litter traps was found. In Fig. 3.5 the projected one-sided L_{AI} for the different years is depicted.

Most of the roots were found in the first 0.3 m, with some roots occurring at 0.7 m depth.

The soil consists of a 1 m layer of fine loamy sand on top of a loam layer. The photograph of the soil profile at the Bankenbos site in Fig. 3.6 clearly shows the upper soil layer with a high fraction of organic matter and the slightly grey bottom layer containing some loam.

The volume fractions of sand X_q, clay X_c and organic material X_o as well as the soil density ρ for different depths are given in Table 3.2. Table 3.3 shows the hydraulic characteristics of the soil at different depths. The layer of sand decreases from 1.5 m at the west side to 0.5 m at the east side of the stand.

During the observing period the groundwater level varied between 0.82 cm and 2.43 cm below the surface. The average groundwater table depth during the observing

Figure 3.6: *The soil profile at the Bankenbos site showing the accumulated organic matter on top of the mineral soil. The length of the tape in the picture is 1.2 m.*

Table 3.2: *Volume fractions of sand X_q, clay X_c and organic material X_o and the densities ρ at the Bankenbos site.*

Depth (m)	X_q (m^3m^{-3})	X_c (m^3m^{-3})	X_o (m^3m^{-3})	ρ_{sample} (kg m^{-3})
0-0.30	0.41	0.01	0.05	1260
0.55-0.70	0.64	0.01	0.02	1650
0.60-0.90	0.65	0.02	0.01	1760

period was 1.7 m below the soil surface. At the east side of the stand there is a ditch with a depth of 1.9 m.

Under dry conditions the relatively high groundwater table may provide an additional source of water for the roots to tap into. Under wet conditions the low permeability of the loam layer sometimes creates a perched groundwater table close to the surface. Under these conditions the tree roots may suffer from oxygen shortage. During the period of observation of our study a perched groundwater table only occurred during winter and early spring and as such did not influence the physiology of the trees.

Table 3.3: *The soil hydraulic parameters obtained by fitting $\psi(\theta)$ and $k(\psi)$ to respectively Eqs. 2.7 and 2.9 at the Bankenbos site. The last column shows the hydraulic conductivity k_s as determined separately for a saturated sample. The second sample at 0.90 -0.98 m depth consisted mainly of loam. The depth is given below the top of the mineral layer.*

Depth	θ_r	θ_s	α	n	m	l	k_s	
								sat. sample
(m)	(-)	(-)	(cm^{-1})	(-)	(-)	(-)	(cm d^{-1})	(cm d^{-1})
0.10-0.18	0.01	0.53	0.0147	1.651	0.394	0.000	11.479	127.0
0.32-0.40	0.01	0.40	0.0190	1.869	0.465	0.000	19.956	123.0
0.56-0.64	0.01	0.33	0.0179	2.882	0.653	0.000	18.260	248.0
0.90-0.98	0.01	0.31	0.0175	2.181	0.542	0.000	10.558	48.0
0.90-0.98	0.01	0.32	0.0366	1.154	0.133	-3.751	59.144	-

Figure 3.7: *View through the oak canopy on the tower at the Edesebos site*

3.4 Edesebos

The Edesebos site was located near the town of Ede (52°02′19″N – 5°45′06″E) being covered for more than 90% by red oak (*Quercus rubra*), Fig. 3.7.

The area of the oak stand amounts to 16 ha and is surrounded by coniferous forest.

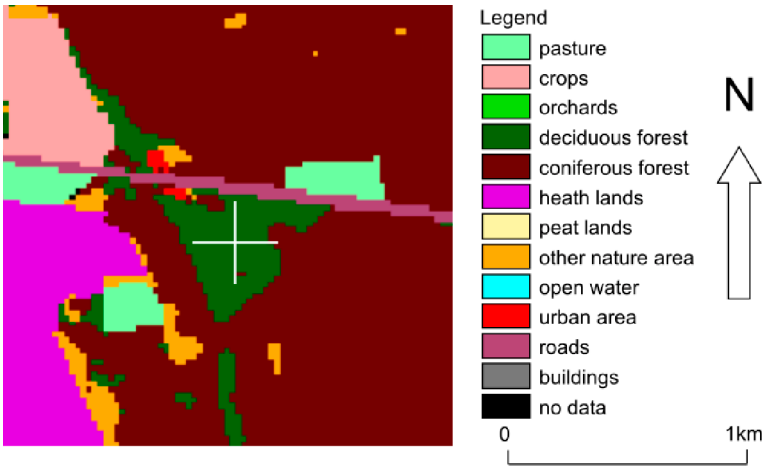

Figure 3.8: *Different types of land use in an area of 2 x 2 km surrounding the Edesebos site as classified in the land use database LGN.*

The sparse undergrowth is regrowth of cut red oak. Fig 3.8 shows the main land use in the surroundings of the flux tower. The length of the fetch is somewhat limited, i.e. $\pm$ 300 m. However, it is not expected that this limited fetch will have a major effect on the daytime flux during the growing season. Especially as the surrounding coniferous forest will cause only a small change in surface roughness.

The average tree height was 17.1 and 17.4 m in 1988 and 1989 respectively. Other tree species found at the site were birch (*Betula spec.*) and Douglas fir (*Pseudotsuga menziesii*). The tree density amounted to 600 stems ha^{-1}.

Table 3.4 summarizes the different parameters characterizing the vegetation of the Edesebos site.

For the Edesebos location L_{AI} was measured using 9 leaf litter trays in combination with photographs taken with a fish-eye lens. The seasonal trend is depicted in Fig. 3.9.

At the Edesebos site detailed measurements of the root distribution were made. Along a trench excavated between 2 trees all roots were counted. The fine roots, i.e. roots with a diameter < 1 mm, follow an exponential distribution with depth (see Fig. 3.10). Most roots, i.e. 90% was found in the upper 0.65 m of the soil. Some roots however, were found at 1.6 m depth.

The soil is a loamy sand with a deep groundwater table depth being at approximately 5 m below the soil surface (Hendriks et al., 1990). The top 0.7 m of the soil consists of loamy fine sand, ρ = 1100 - 1300 kg m^{-3}. Below this horizon the loam fraction decreases and ρ increases to 1600 kg m^{-3}. The deeper soil layer consists of

Table 3.4: *Vegetation characteristics near the tower of the Edesebos site. All values are average values for the stand. As the original tree characteristic data were not available, only a limited number of variables is shown. The tree heights z_{tree} are given at the start as well as at the end of the observation period. All other characteristics have been averaged over this observation period.*

Site	Edesebos
Tree species	Oak
Undergrowth	Bare soil and some regrowth of oak
Planting year	1944
Observation period	1988-1990
Tree density, N_{tree}	600 tree ha^{-1}
Tree height, z_{tree}	17.1-17.4 m
L_{AI}tree, maximum	4.9 m^2m^{-2}
L_{AI}under, maximum	<1.0 m^2m^{-2}
Canopy cover fraction, c_{veg}, maximum	0.69
Canopy cover fraction, c_{veg}, minimum	0.2
Rooting depth, z_{root}, 90% of all roots	0.65 m
Rooting depth, z_{root}, maximum	1.6 m

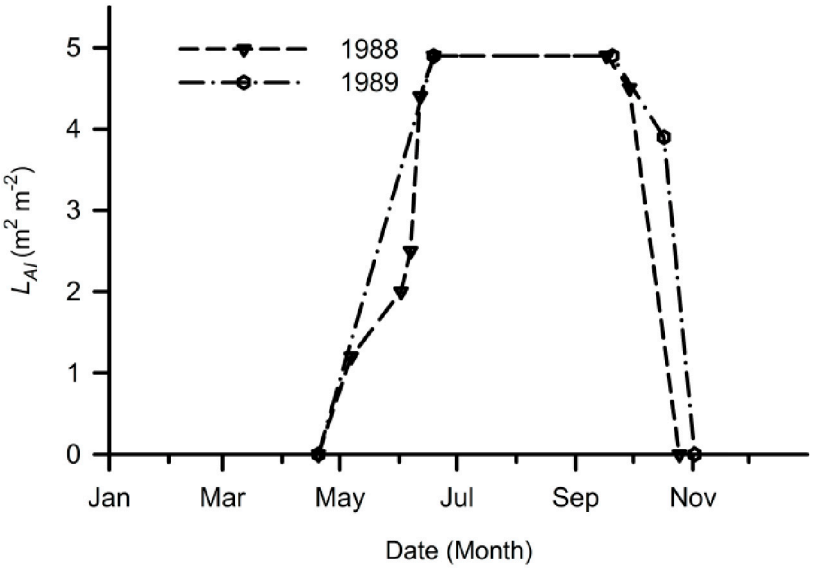

Figure 3.9: *Leaf Area Index (L_{AI}) of the oak stand at the Edesebos site for different years.*

sand with some bands of fine gravel. The volume fractions of sand X_q, clay X_c and organic material X_o as well as the soil densities ρ for different depths are presented

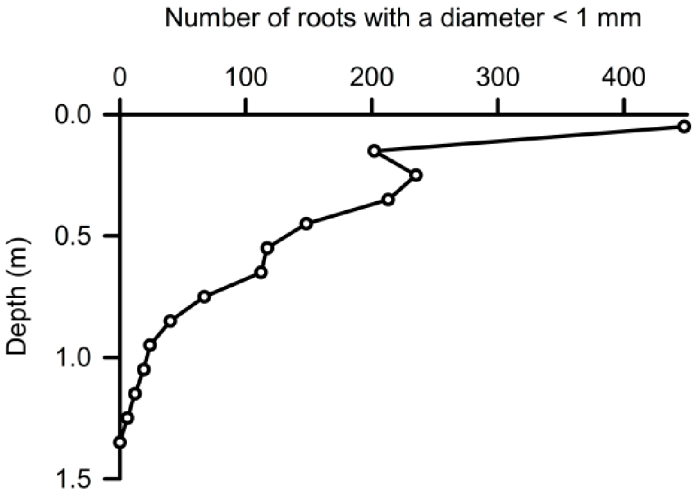

Figure 3.10: *Fine root (diameter < 1 mm) distribution of the oak stand at the Edesebos site.*

Table 3.5: *Volume fractions of sand X_q, clay X_c and organic material X_o and the densities ρ at the Edesebos site. Remarks: [1]) Litter layer. [2]) Values are estimated.*

Depth (m)	X_q (m^3m^{-3})	X_c (m^3m^{-3})	X_o (m^3m^{-3})	ρ_{sample} (kg m^{-3})
-0.05-0[1]	0.07	0.0	0.12	400
0-0.70[2]	0.55	0.01	0.02	1200
0.70-1.60[2]	0.60	0.01	0.02	1600

in Table 3.5. Table 3.6 shows the hydraulic characteristics of the soil at different depths.

Table 3.6: *The soil hydraulic parameters obtained by fitting $\psi(\theta)$ and $k(\psi)$ to respectively Eqs. 2.7 and 2.9 at the Edesebos site. The depth is given below the top of the mineral layer. The first row shows data from the litter layer on top of the mineral layer.*

Depth (m)	θ_r (-)	θ_s (-)	α (cm^{-1})	n (-)	m (-)	l (-)	k_s (cm d^{-1})
-0.05-0.0	0.000	0.62	0.022	1.616	0.500	5.662	300.0
0.11-0.19	0.001	0.49	0.040	1.459	0.500	1.385	200.0
0.33-0.41	0.001	0.41	0.028	1.555	1.211	1.211	200.0
0.51-0.59	0.001	0.35	0.032	1.598	0.500	0.978	200.0
0.96-1.04	0.010	0.33	0.141	1.593	0.372	-0.158	80.0

The groundwater table raised by 0.9 m from 5.5 m below the soil surface in January 1988 to 4.6 m in December 1988. During 1989 the groundwater table remained at this level for most of the year and only started to drop towards the end of 1989. The groundwater table lowered at the same rate in 1990. At the end of 1990 the groundwater table was at 5.2 m below the soil surface.

With these low groundwater tables (the highest level was at 4.6 m depth), it is unlikely that the trees will be able to use the groundwater reservoir to sustain evaporation during dry periods.

Figure 3.11: *Poplar stand at the Fleditebos site with stinging nettle and grass as main undergrowth. Also visible is a part of the trough to measure the throughfall. Low resolution picture taken with one of the first digital camera's.*

3.5 Fleditebos

This site was located in a poplar (*Populus*) stand (52°19′06″N – 5°27′12″E) near Zeewolde on a land reclamation area. The average elevation of the stand is NAP – 3.5 m.

The measuring tower was located almost in the middle between the two ditches draining the area. In a radius of 500 m around the tower almost 80% was covered with poplar with the dominant clone *Populus Robusta*. Of the total area approximately 5% was in use as grassland, open water or roads. Other tree species found near the site were ash (*Fraxinus esp.*), oak (*Quercus rubra*), sycamore (*Acer pseudoplatanus*) and beech (*Fagus sylvatica*). The site was surrounded by other similar stands of mainly poplar trees with similar height.

Fig. 3.12 shows the main land use in the surroundings of the flux tower.

Table 3.7 summarizes the different parameters characterizing the vegetation of the Fleditebos site.

The poplar trees were planted in 1985. The trees were set every 4.5 m in rows with

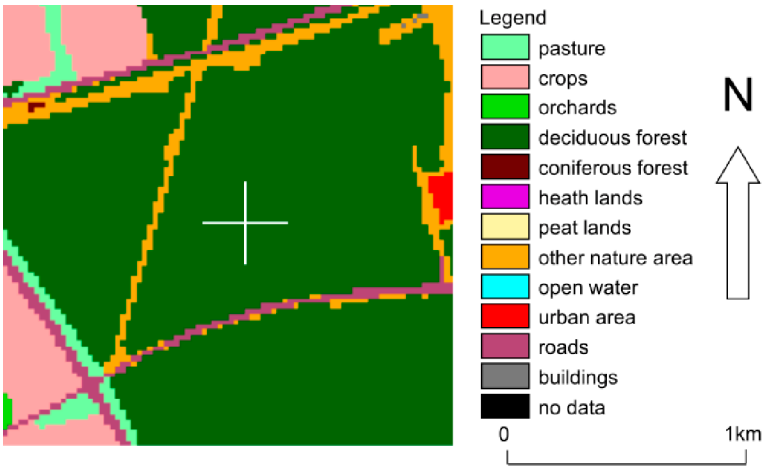

Figure 3.12: *Different types of land use in an area of 2 x 2 km surrounding the Fleditebos site as classified in the land use database LGN.*

Table 3.7: *Vegetation characteristics near the tower at the Fleditebos site. All values are average values for the stand. The standard deviation if available is also provided. The tree heights z_{tree} are given at the start as well as at the end of the observation period. All other characteristics have been averaged over this observation period.*

Site	Fleditebos	Stand. dev.
Tree species	Poplar	
Undergrowth	Stinging nettle, cleavers, grass	
Planting date	1985	
Observation period	1995-1998	
Tree density, N_{tree}	440 tree ha^{-1}	
Tree height, z_{tree}	16.2-18.7 m	$\pm$ 0.5 m
D_{BH}	0.24 m	$\pm$0.02 m
Crown radius	2.57 m	
Projected crown area	20 $m^2 tree^{-1}$	$\pm$4 $m^2 tree^{-1}$
Crown base	8.7 m	$\pm$0.8 m
L_{AI}tree, max.	3.7 $m^2 m^{-2}$	0.01 $m^2 m^{-2}$
L_{AI}under, max.	4.0 $m^2 m^{-2}$	
Canopy cover fraction, c_{veg}, maximum	0.8	
Canopy cover fraction, c_{veg}, minimum	0.2	
Rooting depth, z_{root},90% of all roots	0.6 m	
Rooting depth, z_{root},maximum	1.8 m	

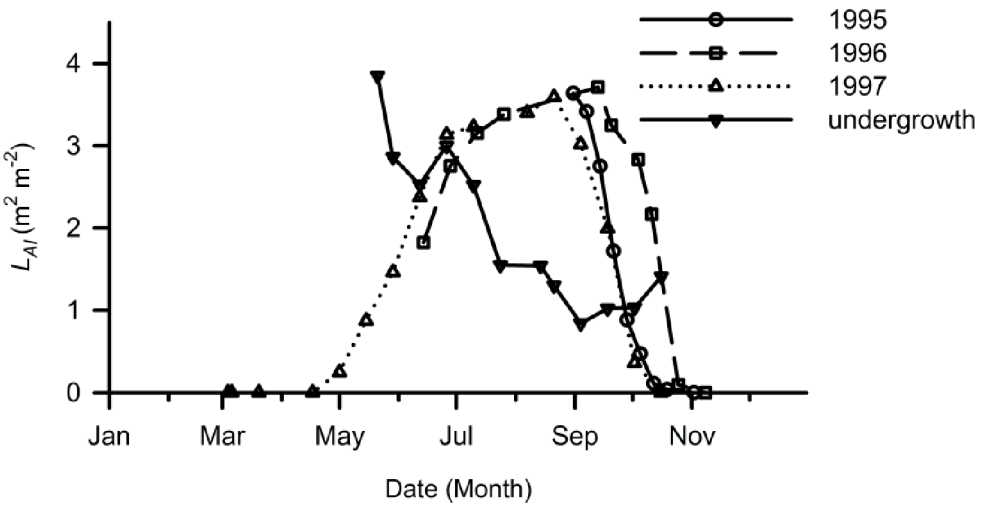

Figure 3.13: *Leaf Area Index (L_{AI}) of the trees and the undergrowth at the poplar stand of the Fleditebos site for different years.*

a distance of 5 m. Poplar is a fast growing species: the average height of the trees z_{tree} at the start of the measurements was 16.2 m and at the end of the measurement period 18.7 m. The under-growth was dense and consisted of grass with patches of stinging nettle (*Urtica dioica*) and cleavers (*Galium aparine*). The stinging nettle and cleavers reached a height of 1.5 m. Under the other tree species there was nearly no under-growth.

In 1995 and 1996 L_{AI} was measured using 5 leaf litter fall trays of 1 m^2 each. The Vegetation Area Index (VAI) measurements made with the LAI-2000 were converted into L_{AI} using Eq. 3.1. Based on the L_{AI} measurements made during the leafless period L_{AI} for the poplar trees was estimated as 0.72 m^2 m^{-2}. Comparing the resulting values with L_{AI} values from the litter trays yielded a correction factor of 1.91, which is comparable to the value of Chason et al. (1991). This calibration factor was used to correct the LAI-2000 measurements for the other years. The thus derived L_{AI} compares well with other studies, e.g. Breuer et al. (2003).

In 1997 the LAI-2000 sensor was also used to measure L_{AI} of the understory.

In Fig. 3.13 the projected one-sided L_{AI} of the poplar trees and of the undergrowth is depicted.

Most roots at the Fledite site were found in the upper 0.6 m of soil. Deeper down to a depth of 1.8 m, the roots followed the major cracks along the soil aggregates.

The soil profile consists of a 2 to 3 m layer of clay overlying sand. Fig. 3.14 shows a photograph of the soil profile.

Figure 3.14: *The soil profile at the Fleditebos site showing 3 distinctive layers. On top of the deepest layer sea shells are present. The large cracks that occurred after the land was reclaimed from the sea, can clearly been seen at the left side of the pit. The length of the tape in the photograph is 1.7 m.*

Table 3.8: *Volume fractions of sand X_q, clay X_c and organic material X_o and the densities ρ at the Fleditebos site.*

Depth (m)	X_q (m^3m^{-3})	X_c (m^3m^{-3})	X_o (m^3m^{-3})	ρ_{sample} (kg m^{-3})
0.07-0.34	0.35	0.09	0.06	880
0.36-0.70	0.28	0.16	0.02	980
0.90-1.10	0.20	0.11	0.05	1100

The volume fractions of sand X_q, clay X_c and organic material X_o as well as the soil density ρ for different depths are presented in Table 3.8. For convenience the weight fractions in kg kg^{-1} of sand, silt and clay are provided in Appendix B. These weight fraction show the large faction of soil particles < 16 μm in the lower layer, i.e. 60.8% of total dry matter. Table 3.9 shows the hydraulic characteristics of the soil at different depths.

It should be noted that the soil properties as presented in Table 3.9 for the Fledite-

Table 3.9: *The soil hydraulic parameters obtained by fitting $\psi(\theta)$ and $k(\psi)$ to respectively Eqs. 2.7 and 2.9 at the Fleditebos site. The last column shows the hydraulic conductivity k_s as determined separately for a saturated sample. The depth is given below the top of the mineral layer.*

Depth	θ_r	θ_s	α	n	m	l	k_s	
								sat. sample
(m)	(-)	(-)	(cm^{-1})	(-)	(-)	(-)	(cm d^{-1})	(cm d^{-1})
0.03-0.11	0.01	0.64	0.2641	1.156	0.135	-3.832	117.632	>1000
0.36-0.44	0.01	0.50	0.1045	1.104	0.094	-0.906	174.964	>1000
0.62-0.70	0.01	0.58	0.0961	1.075	0.070	-6.653	38.647	>1000
0.70-0.78	0.01	0.64	0.0507	1.026	0.025	-3.310	259.085	>1000

bos site are only valid for the hexagonal pedons and do not include the influences of permanent cracks. For these cracks the concepts for the flow of soil water in the unsaturated zone as discussed in Chapter 2 do not apply. They have to be adjusted for example as described by Van Dam (2000), who used field measurements of crack volume and crack depth to describe the swelling and shrinking of a clay soil. However, as these heavy clay soils at the Fledite site are non-swelling, the cracks are permanent and they function as artificial drains, due to which the saturated hydraulic conductivity k_s of these soil layers can be as high as 10 m d^{-1}. Groen (1997) even estimated the saturated permeability for similar soils at 300 to 500 m d^{-1}. He obtained satisfactory results for the outflow of pesticides of such heavy clay soils with permanent cracks. To obtain these results he simulated the permanent cracks as imaginary drains just above the soil layer were the cracks start.

The groundwater table in winter was approximately at 1.2 m below the surface and during summer at 2 m. The area was drained by plastic tube drainage with a spacing of 48 m. These drains discharged in two ditches running from south to north. The distance between the two ditches was 500 m. Fig. 3.15 shows a transect of the soil surface perpendicular to the direction of the two ditches. Also depicted in the same figure are the groundwater levels z_g in spring and at the end of the summer. The two ditches can clearly be seen by the drop in surface elevation. Even in the relatively wet period in March the angle of the slope of the groundwater table towards the ditches is very small. The relatively flat groundwater table is most likely caused by the existence of the large cracks in the lower parts of the soil.

In the northern part the ditches with a length of 1200 m ended in a channel. The water level in the channel was kept at 5.2 m below NAP. From visual observations it was concluded that the draining function of the tubes was almost zero. However, the draining was taken over by the permanent cracks in the clay. These cracks stayed

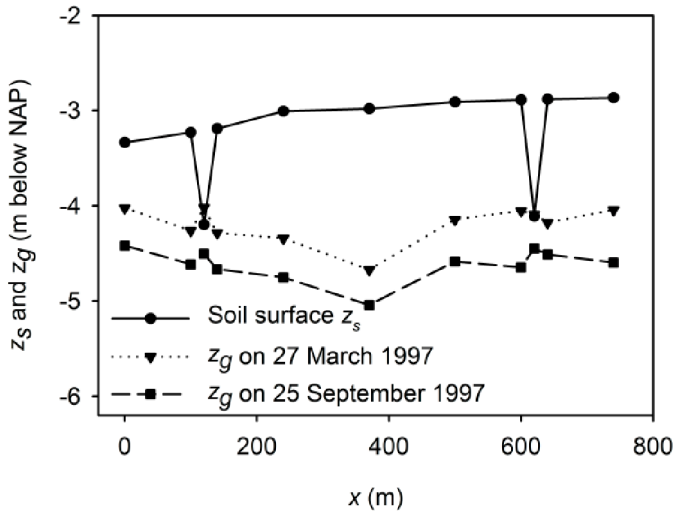

Figure 3.15: *Cross section of the soil surface z_s (solid line) at the locations of the groundwater observing tubes at the poplar forest of the Fleditebos site. Also depicted are the groundwater levels z_g in spring and at the end of summer.*

after the reclamation of the land and were at some places as wide as 10 cm.

Although the groundwater levels during the observing period were relatively high, in winter and summer a significant drop at the centre of the plot between the two ditches occurred. This drop shows the low hydraulic conductivity of these clay soils. Therefore it is questionable if during dry periods the roots will be able to extract water from the deeper layers at a sufficiently high rate to maintain an evaporation rate close to potential.

Figure 3.16: *View of the undergrowth below the birch and pine trees near the scaffolding tower at the mixed forest of the Kampina site. Low resolution picture taken with one of the first digital camera's.*

3.6 Kampina

The Kampina site (51°34′01″N – 5°17′27″E) was located near the town of Boxtel.

The stand is a mixed forest, both in species and tree age. Because of this mix the forest has a layered structure, as can be seen in Fig. 3.16. The forest to the west side is mainly beech (*Fagus sylvatica*) and oak (*Querqus robur*) with nearly no undergrowth. Most of these trees were planted between 1890 and 1900. The canopy cover of this part of the forest is mainly high (> 80%). To the east side the forest is more open and the trees are mainly pine (*Pinus sylvestris*) with some birch (*Betula pendula* and *Betula pubescens*) and an undergrowth of purple moor grass (*Molinia Carulea*) and wavy hair grass (*Deschampsia flexuosa*). The pine trees were partly planted around 1930 and partly natural regrowth. In between these two more or less distinct forest patches there is a strongly mixed forest with an undergrowth of purple moor grass and seedlings from the trees. The distribution of the main tree species in the area (500 m radius) around the tower was 33% pine, 29% beech, 27% oak, 10% birch. Fig. 3.17 shows the main land use in the surroundings of the flux tower. A more detailed description of the vegetation at Kampina may be found in Jonkheer

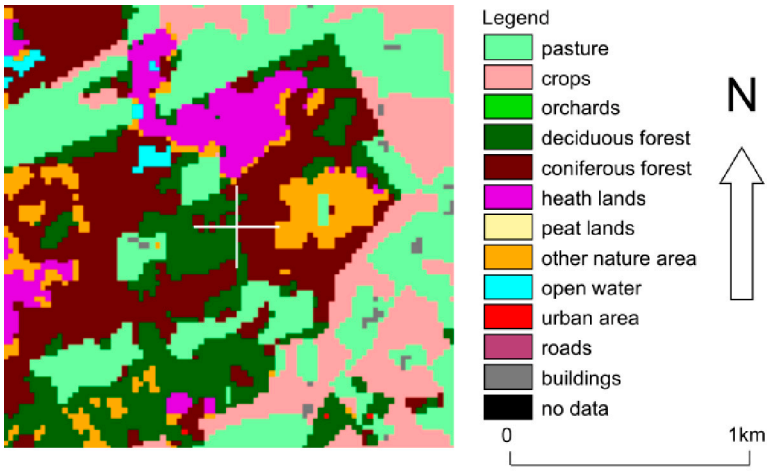

Figure 3.17: *Different types of land use in an area of 2 x 2 km surrounding the Kampina site as classified in the land use database LGN.*

(1989).

Table 3.10 summarizes the different parameters characterizing the vegetation of the Kampina site.

Because of the mixture of coniferous evergreen and broad-leaf deciduous trees at the Kampina site it was not possible to calibrate the average L_{AI} estimates of the LAI-2000 sensor. Hence for this site the minimum L_{AI} values reflect the average of the L_{AI} of all trees, i.e. deciduous and evergreen, as well as the needle area of the conifers. In Fig. 3.18 the projected one-sided L_{AI} of the trees and the grass undergrowth is depicted.

The majority of the roots were found in the first 0.5 m. Maximum rooting depth was 1.2 m.

The soil is sandy. The volume fractions of sand X_q, clay X_c and organic material X_o as well as the soil density ρ for different depths are tabulated in Table 3.11. Table 3.12 shows the hydraulic characteristics of the soil at different depths.

In winter the groundwater table was at approximately 0.5 m depth, in summer at 1.8 m depth. With a maximum rooting depth of 1.2 m it is expected that during our measuring period the trees had access to the groundwater reservoir all the time. The main management objective of the area was to restore the wetland vegetation. Therefore most of the ditches in the area surrounding the site were dammed in 1997, with the purpose to keep the groundwater table as high as possible. This high groundwater table sometimes caused parts of the area to be flooded in winter, however during the measuring period of this study it occurred in 1998 only for a

Table 3.10: *Vegetation characteristics near the tower at the Kampina site. All values are average values for the stand. The standard deviation if available is also provided. The tree heights z_{tree} are given at the start as well as at the end of the observation period. All other characteristics have been averaged over this observation period.*

Site	Kampina	Stand. dev.
Tree species	Mixed deciduous coniferous	
Undergrowth	Purple moor grass	
Planting year	1890,1930	
Observation period	1996-1998	
Tree density, N_{tree}	310 tree ha^{-1}	
Tree height, z_{tree}	16.6-17.0 m	$\pm$ 4.1 m
D_{BH}	0.26 m	$\pm$0.12 m
Crown radius	3.56 m	
Projected crown area	40 m^{2}tree^{-1}	$\pm$28 m^{2}tree^{-1}
Crown base	7.1 m	$\pm$3.8 m
L_{AI}tree, max.	3.8 m^{2}m^{-2}	0.09 m^{2}m^{-2}
L_{AI}under, max.	1.3 m^{2}m^{-2}	
Canopy cover fraction, c_{veg}, maximum	0.95	
Canopy cover fraction, c_{veg}, minimum	0.45	
Rooting depth, 90%/max.	0.4 m	
Rooting depth, z_{root}, maximum	1.2 m	

Table 3.11: *Volume fractions of sand X_q, clay X_c and organic material X_o and the densities ρ at the Kampina site.*

Depth (m)	X$_q$ (m^{3}m^{-3})	X$_c$ (m^{3}m^{-3})	X$_o$ (m^{3}m^{-3})	ρ_{sample} (kg m^{-3})
0-0.20	0.52	0.01	0.05	1320
0.20-0.50	0.53	0.01	0.01	1450

few days. These measures were mainly aimed to improve the hydrological conditions of the neighbouring fens, but are not necessarily beneficial to the trees in the area. Especially if the high groundwater table is maintained over a long period damage to the tree roots is likely to occur

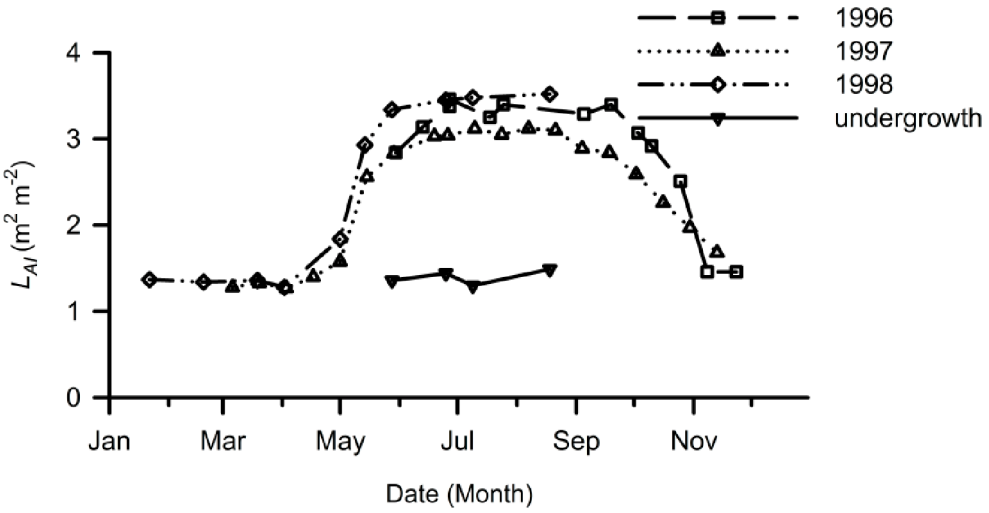

Figure 3.18: *Leaf Area Index (L_{AI}) of the trees and undergrowth at the mixed forest stand of the Kampina site for different years.*

Table 3.12: *The soil hydraulic parameters obtained by fitting $\psi(\theta)$ and $k(\psi)$ to respectively Eqs. 2.7 and 2.9 at the Kampina site. The last column shows the hydraulic conductivity k_s as determined separately for a saturated sample. The depth is given below the top of the mineral layer.*

Depth	θ_r	θ_s	α	n	m	l	k_s	
								sat. sample
(m)	(-)	(-)	(cm^{-1})	(-)	(-)	(-)	(cm d^{-1})	(cm d^{-1})
0.03-0.11	0.01	0.46	0.0195	1.657	0.397	2.0	38.372	30.2
0.30-0.38	0.01	0.45	0.0242	1.347	0.258	2.0	68.470	75.0
0.50-0.58	0.01	0.34	0.0109	2.891	0.654	1.0	37.646	217.0

3.7 Loobos

The Loobos site is located near Kootwijk (52°10′04″N – 5°44′38″E) The main tree species is Scots pine (*Pinus sylvestris*). The forest extends in all directions for more than 1.5 km. Around 1909 the trees were planted on sand dunes, being widely spaced with some open spots.

In a radius of 500 m around the flux tower almost 90% of the area is covered with Scots pine, 3% of the area is open and mostly covered with heather and grass, Fig. 3.19. Other tree species in the forest stand are Corsican or black pine, birch, Douglas fir and oak. The average tree height at the start of the measurements was

Figure 3.19: *Scots pine with an undergrowth of grass at the Loobos site.*

15.1 m. The undergrowth of the forest is a closed cover of mainly grass (*Deschampsia flexuosa*). Fig. 3.20 shows the main land use in the surroundings of the flux tower.

Table 3.7 summarizes the different parameters characterizing the vegetation of the Loobos site.

For the pine trees at the Loobos site destructive measurements were used to establish relations between sapwood area, branches and needle area. These relations were used to calculate L_{AI}. L_{AI} thus obtained was used to check the LAI-2000 measurements. Surprisingly enough the differences between both L_{AI} estimates were relatively small: an overestimation of 22% by the LAI-2000. This overestimation is in contrast with most other studies (e.g. Stenberg et al., 1994). Stenberg et al. (1994) measured L_{AI} of Scots pine using a LAI-2000 sensor, which was on average 43% too low. The overestimation found in the present study is probably because of the large amount of woody area of the tree stems and larger branches. At the Loobos site the tree density was about 1/3 of that at the sites investigated by Stenberg et al. (1994). Also at the Loobos site the average height of the lowest living branch was only at 9.5

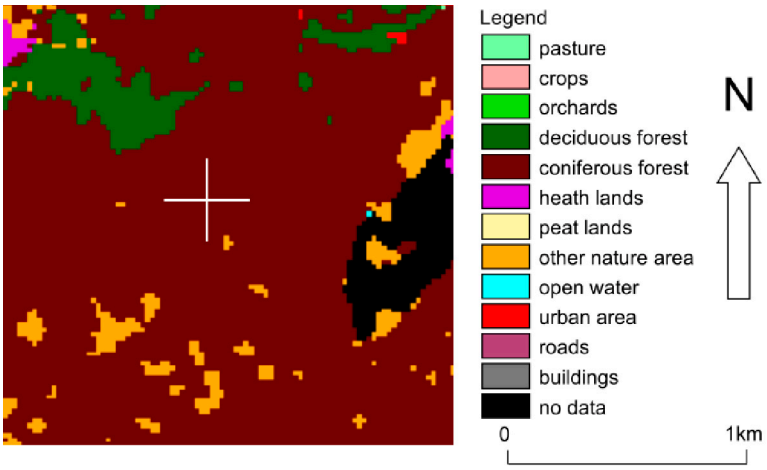

Figure 3.20: *Different types of land use in an area of 2 x 2 km surrounding the Loobos site as classified in the land use database LGN.*

Table 3.13: *Vegetation characteristics near the tower at the Loobos site. All values are average values for the stand with the standard deviation between brackets. The tree heights z_{tree} are given at the start as well as at the end of the observation period. All other characteristics have been averaged over this observation period.*

Site	Loobos	Stand. dev.
Tree species	Scots pine	
Undergrowth	Grass	
Planting year	1904	
Observation period	1995-2010	
Tree density, N_{tree}	403 tree ha^{-1}	
Tree height, z_{tree}	15.3-15.7 m	$\pm$ 2.0 m
D_{BH}	0.25 m	$\pm$ 0.05 m
Crown radius	2.45 m	
Projected crown area	21 m^2 $tree^{-1}$	$\pm$ 10 m^2 $tree^{-1}$
Crown base, z_{can}	9.5 m	$\pm$ 1.6 m
L_{AI} tree, maximum	1.9 m^2 m^{-2}	$\pm$ 0.01 m^2 m^{-2}
L_{AI} under, maximum	1.5 m^2 m^{-2}	$\pm$ 0.08 m^2 m^{-2}
Canopy cover fraction, c_{veg}, maximum	0.7	
Canopy cover fraction, c_{veg}, minimum	0.55	
Growth rate	2.49 $m^3 ha^{-1} yr^{-1}$	
Rooting depth, z_{root}, 90% of all roots	0.25	
Rooting depth, z_{root}, maximum	>2.5 m	

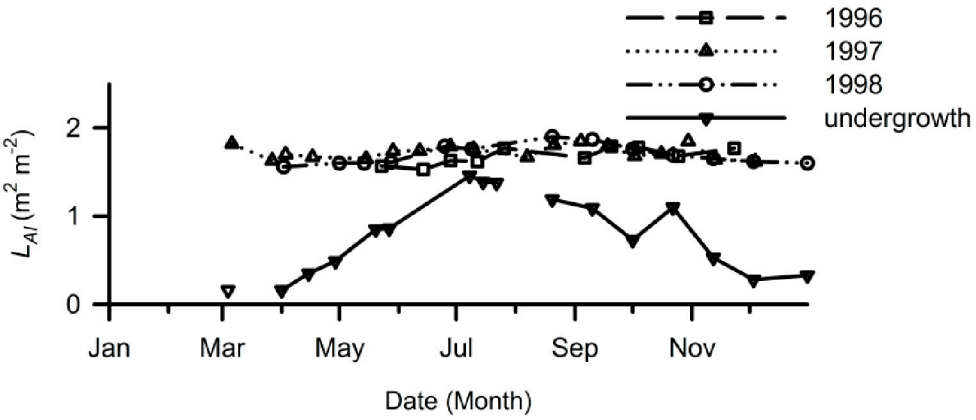

Figure 3.21: *Leaf Area Index (L_{AI}) (m^2 m^{-2}) of the pine trees and the undergrowth at the Loobos site for the different years.*

m.

Based on an analysis of 36 pictures taken vertically upward from below the canopy, 28% of the canopy cover as seen by the LAI-sensor consisted of twigs and branches. As for this study the temporal differences were more important than the absolute values of L_{AI}, and because of the large standard deviation of the sapwood derived L_{AI} ($\pm$ 0.89 m^2 m^{-2}), L_{AI} estimates of the Licor were not adjusted for the pine stand.

In 1998 the LAI-2000 sensor was also used to measure L_{AI} of the undergrowth. For the measurements of L_{AI} of the undergrowth dead biomass was excluded as much as possible. In Fig. 3.21 the projected one-sided L_{AI} of the different sites is depicted.

Most roots are found in the first 0.25 m. Although not encountered in the soil pits of this study, the trees are known to have a tap root reaching depths of more than 2.5 m (Personal communication Forestry Service).

On top of the sandy soil is an approximately 11 cm thick litter layer. Fig. 3.22 depicts a photograph of the soil profile at the Loobos site.

The volume fractions of sand X_q, clay X_c and organic material X_o as well as the soil density ρ for different depths are tabulated in Table 3.14. For convenience also the weight fractions of sand, silt and clay are presented in Appendix B. Table 3.15 shows the hydraulic characteristics of the soil at different depths.

Because of the local topography caused by the sand dunes the distance to the groundwater table depends on the location. At the base of the tower the groundwater table dropped in some years to depths of more than 6.5 m below the surface. In an adjacent valley the groundwater level varied between 2.0 and 4.0 m below the soil

Figure 3.22: *The soil profile at the Loobos site showing the thin organic layer on top of the mineral layer with its sparse root density.*

Table 3.14: *Volume fractions of sand X_q, clay X_c and organic material X_o and the densities ρ at the Loobos site.*

Depth (m)	X_q (m^3 m^{-3})	X_c (m^3 m^{-3})	X_o (m^3 m^{-3})	ρ_{sample} (kg m^{-3})
0-0.20	0.53	0.01	0.02	1560
0.40-0.60	0.60	0.01	0.00	1630

surface during the observing period. The differences in groundwater table depths at these two locations mainly reflect the topography. In figure 3.23 an example is given of the variation in topography in the neighbourhood of the measurement tower for a transect from north to south and from west to east. The surface of the dune shown at the west to east transect is one of the more pronounced dunes in the area. In

Table 3.15: *The soil hydraulic parameters obtained by fitting $\psi(\theta)$ and $k(\psi)$ to respectively Eqs. 2.7 and 2.9 at the Loobos site. The last column shows the hydraulic conductivity k_s as determined separately for a saturated sample. The depth is given below the top of the mineral layer.*

Depth	θ_r	θ_s	α	n	m	l	k_s	
								Sat. sample
(m)	(-)	(-)	(cm^{-1})	(-)	(-)	(-)	(cm d^{-1})	(cm d^{-1})
0.10-0.18	0.01	0.44	0.0239	3.429	0.708	0.5	19.717	268.0
0.50-0.58	0.01	0.38	0.0198	5.410	0.815	-0.9	9.334	178.0

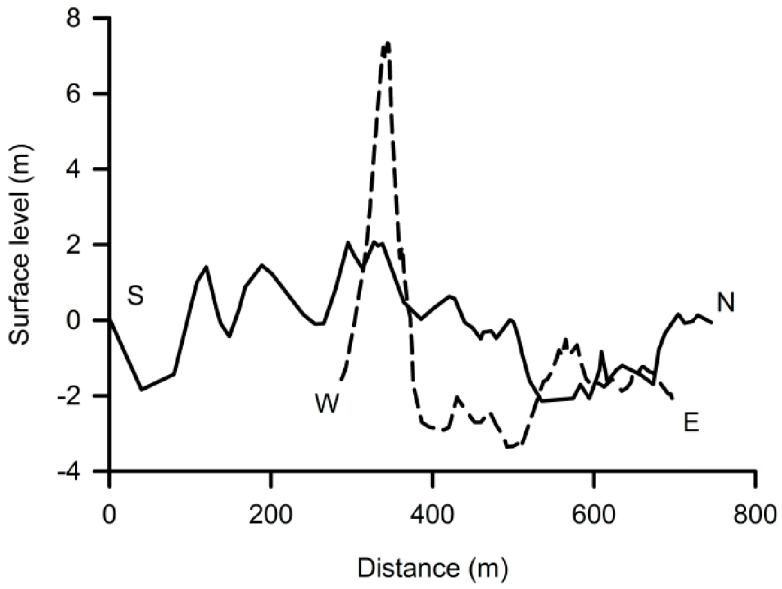

Figure 3.23: *Topography near the measurement tower at the Loobos site.*

general however, the topography is more like the north-south transect (see also Fig. 3.19).

Because of the topography, the hydraulic characteristics of the sandy soil and the relatively deep groundwater reservoir it is likely that in some years this water reservoir is inaccessible for the roots of the pine trees.

Table 3.16: *Total L_{AI} (m^2 m^{-2}), i.e. trees plus undergrowth, and the water holding capacity W (mm) for stressed conditions for the different sites. W is calculated for the soil profile extending to the depth where 90% of the roots are present, $z_{root}^{90\%}$ and for the total root zone, i.e. the soil profile extending to the maximum rooting depth, $z_{root}^{\max}$.*

	Banken-bos Larch	Edese-bos Oak	Fledite-bos Poplar	Kampina Mixed	Loobos Scots pine
Total L_{AI} (m^2 m^{-2})	2.3	5.3	6.1	5.0	3.3
W (mm) for $z_{root}^{90\%}$	81.6	73.4	88.8	107.4	7.9
W (mm) for $z_{root}^{\max}$	125.8	117.1	192.1	209.2	20.8

3.8 General differences between the sites

The two forest stands with the most pronounced differences in their site characteristics are the Loobos site with the stand of pine trees on sand and the Fleditebos site with the poplar trees on clay. The differences in soil type together with the low groundwater table at Loobos and the relatively high groundwater table at Fleditebos also create large difference in hydrological conditions between these two sites.

The differences in maximum total L_{AI} between the sites is mainly based both on the differences between broad-leaved and needle-leaved tree species (see Table 3.16) and the timing of the peaks in L_{AI} of the undergrowth and the trees (see e.g. Fig. 3.13). Both at the Fleditebos site as well as at the Loobos site L_{AI} of the undergrowth reached almost the same maximum L_{AI} (m^2 m^{-2}) as the trees at the specific sites. The largest variation in total L_{AI} was found for the poplar stand at the Fleditebos site, while the larch stand at the Bankenbos site showed the least amount of variation in L_{AI}.

Comparison of the groundwater table depths with the rooting depths at the different sites (see Fig. 3.24), shows that deep groundwater tables coincide with deep rooting depths and vice versa. This behaviour is in accordance with the findings by van den Burg (1996), who found that rooting depth for forests in the Netherlands correlated mainly to ploughing depth or the depth of the groundwater table.

If the water holding capacity W at the start of a drought is defined as the difference in soil water content at a pressure head $h = -10^{2.1}$ Pa (i.e. pF 2.1) and $h = -10^{4.2}$ Pa (i.e. pF 4.2), Table 3.16 shows that, except for the Loobos site, the amount of soil water easily extractable for evaporation is on average 87.8 mm. If it is assumed that there is no additional soil water available by lateral or vertical transport, the maximum amount of soil water available for evaporation is greatest at the mixed forest stand of the Kampina site. Even with the deepest roots of all

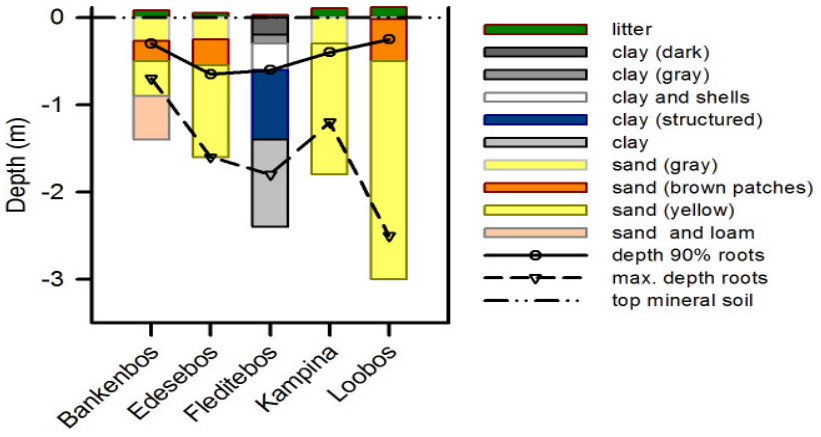

Figure 3.24: *Schematic representation of the soil profile at the different sites. Also shown are the maximum rooting depth and the depth where above 90% of the roots is found. The maximum depth of the roots at the Loobos site is estimated (pers. comm Forestry Service). The thickness of the litter layer is an average and varies throughout the year.*

sites, the maximum amount of available soil water at the pine stand of the Loobos site is very low, i.e. 20.8 mm. This low amount of available soil water implies that in principle the vegetation at the Loobos site is most prone to water stress, especially if the roots are not close to the groundwater table depth.

Chapter 4

Hydro-meteorological measurements at the sites

4.1 Measurement campaigns

The measurements used for this study have been collected during 2 campaigns.

- The campaign for the Edesebos site has been held in 1988 until 1990. To measure λE by means of the Bowen ratio, i.e. $\beta = H/\lambda E$, a Temperature Interchange System has been used. This Bowen ratio system has been running during the summer half year (May to October) only. Precipitation P has been measured continuously during the two years of the campaign.

- The campaign for the Bankenbos, Fleditebos, Kampina and Loobos sites lasted from the end of 1994 to 1998. All measurements were continued throughout the year. At these sites the eddy-correlation technique has been used to measure H, λE and τ. The Loobos site was the only site being continued after 1998.

At all sites most of the measurements were automatized. At the start all instruments were new and the factory calibrations were used. The tipping bucket raingauges were calibrated in the lab prior to installation in the field. Maintenance took place on a weekly basis and occasionally every two weeks. The Krypton hygrometers used for the eddy correlation system were factory calibrated regularly, i.e. every one to two years. For the long term Loobos site, the instruments were calibrated following the guidelines of the manufacturers. Kabat et al. (1997) compared at the same site H being measured with the Bowen ratio Temperature Interchange System with the measurements by the eddy correlation system. Good agreement between the two fluxes was obtained. Table 4.1 summarizes the heights at which the different variables were measured.

Table 4.1: *Heights (m) at which the different variables were measured. Heights are given in meters with the base of the tower as the reference level. Measuring instruments which were added in July 1996 are denoted by *).*

Variable	Edese bos 1988	Edese bos 1989	Loo-bos *) added in July 1996	Fledite bos	Fledite bos after 1997	Ban ken bos	Kampi na
	(m)	(m)	(m)	(m)	(m)	(m)	(m)
H, λE, u_*, u, T_{son}			25.99	23.17	25.44	27.80	29.60
β, u, T_a, $\varkappa$	18.25	18.70					
β, u, T_a, $\varkappa$	20.60	20.70					
β, u, T_a, $\varkappa$	22.95	22.70					
u			24.41	21.70	23.97	26.29	28.25
$\varkappa_r$, T_a	2.30	2.30	23.52	20.76	23.03	25.41	27.40
u, $\varkappa_r$, T_a			8.4*				
u, $\varkappa_r$, T_a							
u, $\varkappa_r$, T_a			5.0*				
u, $\varkappa_r$, T_a			2.5*				
u_{dir}	23.30	23.30	23.97	21.22	23.49	25.93	27.91
P (tower)	18.00	18.00	23.77	21.03	23.30	25.68	27.63
P (open field)	0.6	0.6	0.4	0.4	0.4	0.4	0.4
$R_s^{down/up}$, $R_l^{down/up}$	19.60	19.60	21.89	19.10	21.37	23.79	25.57
R_{net}	19.50	19.50					
p	2.00	2.00					
G	-0.05	-0.001	-0.05	-0.05	-0.05	-0.04	-0.05
G		-0.025					
T_{soil}	-0.025	-0.012					
θ, T_{soil}			-0.03	-0.03	-0.03	-0.03	-0.03
θ, T_{soil}			-0.10	-0.10	-0.10	-0.05	-0.10
θ, T_{soil}			-0.25	-0.20	-0.20	-0.12	-0.30
θ, T_{soil}			-0.75	-0.45	-0.45	-0.32	-0.60
θ, T_{soil}			-2.00	-1.00	-1.00	-0.57	-1.10
θ	-0.05	-0.05					
θ	-0.08	-0.08					
θ	-0.15	-0.15					
θ	-0.50	-0.50					
h		-0.40					
h		-0.60					
θ, h	-0.10	-0.10					
θ, h	-0.30	-0.30					
θ, h	-0.80	-0.80					
θ, h	-1.20	-1.20					
θ, h	-1.60	-1.60					

Table 4.2: *The variables being measured by the various instruments with their estimated field accuracy at the Edesebos site. Instruments only used in 1988 are denoted by* [1]*). Instruments installed in 1989 are denoted by* [2]*).*

Variable	Instrument	Manufacturer	Type	Field accuracy
T_d, T_w	Psychrometer	In Situ Instruments		0.02 K
R_s^{down}	Solarimeter	Kipp	CM5	1%
R_{net}	Net radiometer	Solar radiation Instruments	SRI4	5%
p	Pressure transducer	Aanderaa Instruments	2810	
T_a		Rotronic	YA-100	0.1 K
$\varkappa_r$		Rotronic	YA-100	5%
u	Cup anemometer	In Situ Instruments		0.5 m s^{-1}
u_{dir}	Wind vane	Aanderaa Instruments	2750	3^0
P	Pluviograph	Van Doorne		5%
	Tipping Bucket	Ogawa Seiki[2]	PR200	0.2 mm tip^{-1}
T_f	Pressure transducer	Validyne[1]	DP15	5%
		Trans Instruments[2]	BHL 4879-50-07MO	
S_f	Pressure transducer	Validyne[1]	DP15	5%
	Tipping bucket	Lambrecht[2]	LY100	0.001 mm tip^{-1}
G	Flux plate	BWD Precision Intruments		10%
T_{soil}	Platinum resistance		Pt100	0.1 K
h	Pressure transducer with ceramic cups	TFDL, MicroSwitch (Honeywell)	141PC	5%
θ	Capacity sensor	TFDL		5%

4.2 Edesebos site

Table 4.2 gives an overview of the variables measured, the instruments used and of the estimated field accuracy. The field accuracy incorporates the uncertainty after factory or laboratory calibration, as well as the uncertainty because of the placement of the sensor in the field and the operational practice being employed.

Figure 4.1: *The picture at the left shows the ladder mounted on top of the scaffolding tower and 3 of the 4 trolleys with dry and wet bulb temperature sensors. The cup anemometers are at a fixed height. The picture on the right shows a cup anemometer and the inlet for the aspirated temperature sensors.*

At the Edesebos site instead of an eddy correlation system, a Bowen ratio system has been exploited, using the Thermometer Interchange System (TIS) as was developed by "In Situ Instruments", Sweden. Here, two sets of air temperature differences and dry and wet bulb temperature differences were measured using four aspirated psychrometers. The temperature sensors were placed on trolleys fixed to a ladder on top of the scaffolding tower (see Fig. 4.1).

To eliminate instrument errors the trolleys and thus the sensors for each set were interchanged every 5 minutes. In addition the absolute temperatures were measured. H and λE were derived by combining Eq. (2.23) and Eq. (2.24) with the assumption $K_E \approx K_H$.

At the top of the scaffolding tower the standard meteorological measurements of u, u_{dir}, $\varkappa_r$ and T_a were made. Here, also R_{net} and R_s^{down} were measured at booms 2 m high and extending 2 m outside the tower, directing to the South. At 2 m above the ground level p was measured. G was measured using 2 heat flux plates and a soil temperature sensor. In 1988 the flux plates were installed at a depth of 5 cm with the temperature sensor being installed at 2.5 cm. In 1989 one flux plate has been covered with a thin layer of soil and the other was installed at 2.5 cm depth with the temperature sensor being installed at 1.2 cm depth. To estimate the change in energy storage in the forest T_a and $\varkappa_r$ were measured at 2.3 m height.

To measure P a tipping bucket raingauge (Ogawa Seiki, PR200, with a nominal resolution of 0.2 mm tip^{-1}) was installed at the top of the tower and a siphoning gauge (van Doorne) in the eastern corner of a nearby pasture. The rim of this gauge

was at 0.6 m height above the surface. The gauge has been set at this height because it was felt that otherwise the fence and the young trees at the other side of the fence would influence the catch of the gauge. In 1989 a collecting gauge was added to the tower and another was set next to the gauge in the open field. These gauges had the same funnel area (400 cm^2) as the others and were also set at the same height. The throughfall was collected in a reservoir using three gutters with a total length of 30 m and a width of 10 cm. Every 20 minutes the water level in the reservoir was measured by means of a pressure transducer (Validyne, DP15 in 1988 and Trans Instruments, BHL 4879-50-07MO in 1989). Total stem flow of 6 trees was measured automatically. In 1988 the stem flow was collected in a barrel where the water level was measured by means of a pressure transducer. In 1989 the barrel was replaced by a tipping bucket rain gauge (Lambrecht, LY100, with a resolution of 93 cm^3 tip^{-1}).

At the site soil water content θ and pressure head h were measured in 2 profiles 0.8 m apart, at 1 m and 2 m distance from the nearest tree. h was measured continuously using ceramic cups and pressure transducers. θ was measured twice a week with capacitive sensors (Hilhorst, 1984). The depth of the groundwater table z_g was measured every week in a well 30 m deep.

4.3 Bankenbos, Fleditebos, Kampina and Loobos sites

4.3.1 Measurement set-up

For the sites Bankenbos, Fleditebos, Kampina and Loobos a measurement system has been designed that was able to run as stand alone for at least a week. The system was powered by a solar panel and a wind generator. To reduce power consumption some sacrifices had to be made to the system set-up, which will be discussed below. In 1996 an infra-red gas analyser to measure H_2O and CO_2 fluxes was added to the measuring set-up of the Loobos site, causing the power consumption to increase considerably. To overcome this problem additional solar panels as well as a gasoline generator backup system were installed. This generator started automatically when the voltage of the batteries dropped below a certain threshold value. The generator was placed about 50 m NE (prevailing wind direction is SW) of the measuring tower. To prevent interference with the measurements, a tube has been connected to the exhaust with its opening at 12 m height above the generator. In the summer the generator was usually not needed. In the winter during prolonged overcast skies the generator may run up till 16 hours a week. Later the generator was replaced by a direct methanol fuel cell run on methanol.

To measure the contribution to total λE and H by the undergrowth, a second flux and automatic weather station was installed for limited periods below the canopy. In March 1997 this additional station was first installed at the Fleditebos site. After a couple of months the below canopy station was moved in June to the Loobos site. Here this below canopy station remained until November 1997.

In Table 4.3 the instruments used at the Bankenbos, Fleditebos, Kampina and the Loobos sites are given as well as the accuracy of each variable measured. In this Table the effects of site specific circumstances on the accuracy have not been taken into account.

4.3.2 Sensible and latent heat flux densities

To obtain the sensible heat flux density H and latent heat flux density λE the eddy-correlation technique has been applied. The eddy-correlation system used at the Bankenbos, Fleditebos, Kampina and Loobos sites, has originally been developed in collaboration with Copenhagen University and Wageningen Agricultural University (Moncrieff et al., 1997). The data processing software has been developed in mutual collaboration with the University of Edinburgh. The system is based on a 3D-ultrasonic anemometer in combination with a fast response device to measure $\varkappa_{abs}$ or $\varkappa$, being either a Krypton hygrometer or an infra-red gas analyser (see Fig. 4.2).

Because of drift, primarily originating from the scaling of the windows, the accuracy of the Krypton hygrometer to measure $\varkappa_{abs}$ as a absolute value is not high. However, the response time of the instrument is short and differences in $\varkappa_{abs}$ over a short time interval (e.g. 30 minutes) are measured accurately. To derive λE the measured differences are needed only. The humidity signals were passed to the analogue input ports of the sonic and from there recorded by a PC.

The PC calculated the 30 minute covariances and averages, which were stored after each 30 minutes. To calculate the 30 minute averages a running mean has been applied with a time constant of 200 seconds. For short periods at all sites "raw" high frequency data were stored. Since the time the infra-red gas analyser was installed at the Loobos site, "raw" high frequency data were continuously stored at this site. To derive final results the following corrections were used: rotation corrections following McMillen (1988), frequency response corrections based on Leuning and Moncrieff (1990) and on Moore (1986), density fluctuation corrections as described first by Webb et al. (1980) and cross wind contamination and humidity corrections for H as given by Schotanus et al. (1983). The density corrections are minimal for the closed path gas analysis system, but are needed for the Krypton hygrometer. For this device also a correction as suggested by Tanner et al. (1993) was made for the

Table 4.3: *The variables being measured by the various instruments with the accuracy provided by the manufacturer and their estimated field accuracy at the sites Bankenbos, Fleditebos, Kampina and Loobos. For R_l the offset because of window heating introduces an additional source of uncertainty.*

Variable	Instrument	Manufacturer	Type	Factory accuracy	Field accuracy
u, v, w	Sonic anemometer	Gill	Solent 1012R2	1.5%	0.02 m s^{-1}
T_v	Sonic anemometer	Gill	Solent 1012R2	0.5%	0.5%
$\varkappa_{abs}$	Fast response hygrometer	Campbell	Krypton KH2O	8%	10%
$\varkappa$	Infra-red gas analyser	LI-COR	LI-COR 6262	1%	5%
R_s^{down}, R_s^{up}	Pyranometer	Kipp	CM21	1%	1%
R_l^{down}, R_l^{up}	Pyrgeometer	Kipp	CG1	10%	10%
T of R_l-sensors	Platinum resistance	Kipp	PT100	0.1 C	0.2 C
T_a	Platinum resistance	Vaisala	HMP35A	0.1 C	0.1 C
$\varkappa_r$	Solid state	Vaisala	HMP35A	2% $\varkappa_r$	3.5% $\varkappa_r$
u	Cup anemometer	Vector	A101ML	1%	0.5 m s^{-1}
u_{dir}	Wind vane	Vector	W200P	2	3
P	Tipping bucket 0.2 mm resolution	Environmental Measurements	ARG100	0.5% at 10 mm h^{-1}	5%
T_f	Tipping bucket 0.07 mm resolution	SC-DLO	-	1.0% at 10 mm h^{-1}	5%
G (1x)	Flux disk	TPD-TNO	WS31	5%	10%
G (3x)	Flux ring	Hukseflux	SH1	5%	30%

absorption of light by oxygen in the detected wavelength. A full description of the data processing has been given in Appendix C. For a description of the system in combination with an infra-red gas analyser, as was applied since July 1996 at the Loobos site, one is referred to Moncrieff et al. (1997), Aubinet et al. (2000) and Gash and Dolman (2003).

Figure 4.2: *The left picture shows the top of the scaffolding tower, with the eddy-correlation system at the top of the extendible mast, rain gauge, temperature/humidity sensor, cup anemometer and wind direction sensor on top of the scaffolding tower and the radiation sensors extending 3 m horizontally out of the tower. The right picture shows the 3D-sonic anemometer and the krypton hygrometer of the eddy-correlation system.*

The limited storage capacity of the palmtop PC's applied did not allow for storage of the high frequency raw data. Thus the covariances and averages were calculated on-line and stored. However, due to the limited speed of the processor of the palmtop PC used not all covariances could be stored. Dyer et al. (1982) pointed out that the error in the fluxes of the scalars T and $\varkappa$ is only 3% per degree of tilt, whereas for momentum fluxes it is 14% per degree of tilt. With this error in mind it was decided to store all the covariances needed to rotate the momentum flux and leave out some of the covariances needed for the rotation of the scalar fluxes. For short periods during which all raw data were stored, the effects of not applying all rotation corrections has been quantified by comparing the fluxes based on the limited number of rotation corrections with those based on the full rotation corrections, as will be discussed in Section 5.2.1.

4.3.3 Measuring transpiration by sap flow

At the Loobos site sap flow has been measured using the Tissue Heat Balance-system of Čermák (Ecological Measuring Systems, model P4.1, Brno, Czech Republic). This system calculates the sapflow from temperature changes of the phloem, the amount

of energy needed for heating and the specific heat of water; the system needs no calibration (Swanson, 1994). In 1996 the system was applied at 3 trees while in 1997 and 1998 6 trees were used. Each tree was continuously measured at two sides. Scaling up to stand level was done on the basis of the relation between sapwood area and D_{BH}, determined by coring 59 trees, and the distribution of D_{BH} for the stand.

4.3.4 Radiation

The radiation sensors were mounted on horizontal booms extending 3 m outside of the scaffolding tower. The booms were directed to the South. To measure R_{net} the four components of the radiation balance were measured separately: $R_s^{down}$and R_s^{up} were measured with two pyranometers, $R_l^{down}$and R_l^{up} were measured by pyrgeometers, with the sensor for R_l^{down} being ventilated. Although the temperature dependence of the sensor is improved by the ventilation, the effect of heating of the window by the sun is still estimated as 25 W m^{-2} at 1000 W m^{-2} solar radiation. As mentioned in Table 4.3, the offset caused by this window heating should be added to the uncertainty of the measurements.

At the Fleditebos and Loobos sites for a short period a net radiometer has been placed below the canopy. To check the accuracy of this net radiometer it was for 3 weeks mounted on top of the scaffolding tower to compare with the radiation balance as measured with the separate long- and short-wave radiation sensors above the forest. To check for differences in sensitivity of the two sides of the instrument the net radiometer was turned 180^0 during this period. The comparison with the separate radiation sensors showed that the net radiometer deviated only by 3% from the 4 component net radiometer. Also the net radiometer had the same sensitivity at both sides.

4.3.5 Soil heat flux density

The soil heat flux density G was measured with 4 heat flux sensors installed below the litter layer at a depth of 3 cm in the mineral soil at each side of the soil temperature profile sensors with a distance of approximately 50 cm. Two types of sensors were used: the traditional one in the form of a plate and another one in the shape of a ring. van Loon et al. (1998) showed that the ring type flux sensors were not capable of measuring G accurately. To estimate G the measurements of the heat flux plates were used. The measurements of the flux rings were used only for estimating the effects of spatial variability.

Figure 4.3: *The champagne glass shaped tipping bucket raingauge as has been used at all sites, except Edesebos site, on top of the tower and in the open field.*

4.3.6 Meteorological background variables: u, u_{dir}, $\varkappa_r$ and T_a

At the top of the scaffolding towers standard meteorological measurements of u, u_{dir}, $\varkappa_r$ and T_a were made. At the Fleditebos site and at the Loobos site $\varkappa_r$ and T_a were also measured during a short period in 1997. At the Loobos site, since July 1996 $\varkappa_r$, T_a and u sensors were mounted on the scaffolding tower at 3 levels below the tree crown. The $\varkappa_r$ used are based on a capacity principle. This is one of the main reasons why the readings of this sensor slowly drop in time. As in the Netherlands for a large part of the year $\varkappa_r$ reaches saturation in the early morning, this phenomenon was used to linearly correct the readings of the $\varkappa_r$ sensor over the year in between calibrations.

4.3.7 Precipitation, throughfall and stemflow

Precipitation P was measured using tipping bucket rain gauges with a resolution of approximately 0.2 mm per tip.

At each site a rain gauge was located on top of the scaffolding tower. To minimize the error due to wind turbulence another raingauge was installed in an open space nearby. This gauge had the rim at 40 cm above the soil surface and was logged in event mode. Measuring P is not as evident as often is assumed, which is not only caused

by instrumental problems, but also by the sometimes very large differences observed in space and time. Most point precipitation data show an underestimation of the catch, mainly because of changes in the pressure fields around the rain gauge. The magnitude of this underestimation depends on the exposure of the rain gauge, u and the intensity of P. The biggest errors have been observed for high u in combination with low intensities of P and at high intensities of P because of the structure of tipping bucket rain gauges. This latter error was minimized by applying a static and dynamic calibration for each individual rain gauge. The first error was reduced as much as possible by the shape of the selected rain gauge which reduces the obstruction of the wind field by the champagne glass body look like of the gauge (see Fig. 4.3). Under the assumption of minor spatial differences at low rain intensities ($P < 0.5$ mm h^{-1}) and of minimal wind effects at the gauge in the open field, data of this gauge were used for the low intensities. For higher intensities of P spatial differences are more likely to occur. To prevent a decoupling of the measurements of T_f and P, for $P \geq 0.5$ mm h^{-1}, the data measured at the top of the scaffolding tower were used. Data differing more than 5% between the two gauges were flagged and excluded of the parameter estimation.

Throughfall rate T_f was measured by means of 36 manual gauges as well as one tipping bucket rain gauge at the end of an approximately 10 meter long gutter of 10 cm width (see Fig. 4.4).

Each week the average of the manual gauges was used to calibrate the readings of the tipping bucket for that week. Differences between the weekly throughfall of trough and manual gauges were generally less than 10%, only for rare conditions of snow larger differences were found. The manual gauges were set up at 4 m distance of each other in a fixed grid of 400 m^2. The diameter of the gauges was 9.72 cm with the rim being at about 10 cm above the surface. Vegetation around the gauges was kept short. The gauges were read either once a week or once every fortnight.

Figure 4.5 shows the frequency distribution of T_f as a fraction of P at the Loobos site for 2 showers with a different intensity.

To check if the set up of 36 gauges placed in a fixed grid was adequate to obtain a representative average of T_f, the data sets with different intensities of P for a number of weeks were tested. A chi-square test showed that at all sites only for amounts of $T_f < 0.4$ mm week^{-1}, there was reason to reject the hypothesis that the data were adequately described by a normal distribution. For these low throughfall amounts the canopy does not become completely saturated and hence the spatial variability pattern of throughfall is primarily determined by the degree of canopy opening (Loustau et al., 1992).

For the study of the processes of interception storage and evaporation only data with $P > 0.4$ mm week^{-1} have been used. To estimate the uncertainty in the

Figure 4.4: *The 10 m long and 10 cm wide throughfall gutter at the Loobos site, with at the end (just behind the left tree) the tipping bucket gauge.*

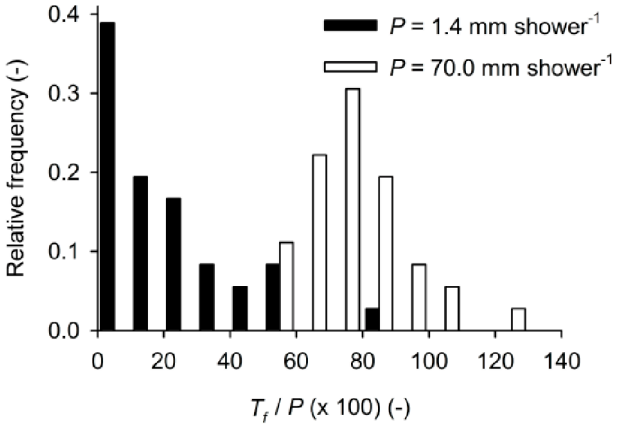

Figure 4.5: *Relative frequency of the throughfall rate T_f measured by the throughfall buckets at the Loobos site as a fraction of the precipitation rate P for two showers with a total precipitation amount of 1.4 mm respectively 70.0 mm.*

throughfall data the relative error was calculated by reducing the number of gauges to 30 and comparing their mean with the mean of all 36 gauges. The obtained relative

error was ± 2%, corresponding well with the findings of Helvey and Patric (1965). To achieve a 5% standard error of estimate in T_f for hardwoods in the eastern US, 24 and 46 gauges were needed for throughfall rates below 0.5 mm in the non-foliated and foliated period respectively and 6 to 18 gauges for higher throughfall rates. The fact that more gauges are needed during the foliated period is in line with the findings of Lloyd and Marques (1988). In order to obtain a 5% error in the mean throughfall rate 20 roving gauges were needed in a tropical rain forest with high rainfall rates and a large amount of foliage.

The resolution of the tipping bucket gauge is approximately 0.07 mm per tip depending on the exact length of the gutter. For this tipping bucket as well as the tipping bucket at the top of the tower the tips were accumulated and logged at 5 minute intervals.

Before the tipping bucket gauges were installed in the field, they were calibrated and the resolution was adjusted depending on the collecting surface of the gutter. The throughfall gauges were cleaned every week and the other gauges every two weeks.

As the undergrowth was dense at one site (Fleditebos), additional throughfall rate measurements were done here. Five gutters with a length of 2 m and a width of 10 cm were installed at soil surface level. Care was taken not to disturb the vegetation around the gutters. At 4 gutters the throughfall was collected using barrels, while at the outlet of the remaining gutter a tipping bucket was placed. This tipping bucket had the same specifications as the tipping buckets used on the tower and in the open field.

Stemflow was collected in barrels using spiral tubes fixed at breast height to 6 trees. The amount of water collected in the barrels was measured on a weekly basis.

4.3.8 Soil temperature and soil water

To obtain the temporal pattern of soil temperature T_{soil} and soil water content θ continuous measurements at 30 minute intervals were made. At the Bankenbos, Fleditebos, Kampina and Loobos sites T_{soil}, electrical conductivity k_e (Ω m^{-1}) and the dielectric permittivity ϵ (J V^2 m^{-1}) were measured at 5 different depths in 2 profiles 1.5 to 2.0 m apart. For this Frequency Domain sensors (FD) were used. These sensors measure ϵ at the 20 MHz frequency range. Every 30 minutes a measurement was made at all 10 sensors and stored on a palmtop PC. All θ profiles were placed in such a way that one profile was close (± 0.5 m) to the stem of a tree and the other profile further away from the tree (± 2.5 m). To obtain an accurate estimation of θ, calibration curves were made using undisturbed volumetric soil samples with a diameter of 20 cm and a height of 20 cm taken at the installation depths of the FD

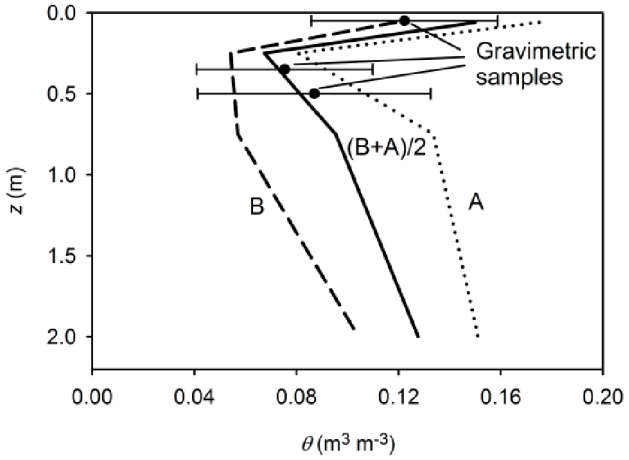

Figure 4.6: *Volumetric soil water content θ at the Loobos site on 1 April 1997, as measured by the 5 permanent FD sensors of each of the soil profiles A and B and as measured by taking gravimetric samples. The horizontal bars depict the standard deviation in θ of the gravimetric samples.*

sensors. To obtain an impression of the spatial variability of θ, we measured at a few occasions θ at 3 to 5 depths.

In 2005 at the Loobos site the soil water and soil temperature sensors were replaced by a new different system consisting of Campbell Scientific sensors (type CS615). The sensors, with pens of 30 cm length were placed horizontally at 5 cm depth in the litter layer and at depths of 0.03 m, 0.20 m, 0.50 m and at 1.00 m respectively in the mineral soil. The measurement interval was set at 1 hour.

To capture the *spatial variability* of the soil water content special measuring campaigns were held at each site. At the Loobos site 10 random spots with 3 points along a line of 10 m were sampled within 200 m of the tower. At each spot θ was measured using a TDR (Time Domain Reflectory) and volumetric soil samples were collected to determine θ. At the sites Kampina and Fleditebos $\pm$ 20 points were sampled along a transect of 250 m. At these sites θ was measured by a FD probe instead of a TDR. Fig. 4.6 depicts the variation in θ at the Loobos site. Especially at a larger depth, the measurements of θ made by the 2 profiles fall well within the range as measured by the gravimetric method. Similar results were obtained for the other sites.

Table 4.4: *Groundwater level monitoring wells at the Bankenbos, Fleditebos, Kampina and Loobos sites, with their total length, reference level and elevation of the soil surface.* [1] *) Reference is the base of the tower i.e. ± 22 m NAP.*

Location	Well number		Filter depth (m)	Reference level (m-NAP)	Soil surface (m-NAP)
Bankenbos	1	Tower	2.97	9.988	9.911
	2		2.80	9.415	9.323
Fleditebos	1		2.45	-3.242	-3.336
	2		2.45	-2.961	-3.230
	3	Ditch	1.75	-3.554	-4.199
	4		2.00	-2.976	-3.190
	5		2.45	-2.838	-3.008
	6	Tower	2.40	-2.540	-2.982
	7		2.00	-2.698	-2.911
	8		2.00	-2.530	-2.887
	9	Ditch	1.86	-3.444	-4.110
	10		1.99	-2.756	-2.882
	11		2.00	-2.683	-2.866
	12		2.45	-2.465	-2.840
	13		2.45	-2.767	-3.207
Kampina	1	Tower	2.50	1.128	0.597
	2	Ditch	2.00	0.963	-0.219
Loobos	1	Tower	6.50	+0.167[1]	-0.009[1]
	2		4.80	-2.463[1]	-2.674[1]

4.3.9 Groundwater level depth

At all locations 2 or more groundwater level observing tubes have been installed. The tubes had a diameter of 3.6 cm and a filter length of 50 cm. Every fortnight all tubes were monitored by hand. Additionally at every site one tube had a data logger with a pressure transducer installed. Depending on the range of the depth of the groundwater table z_g the resolution of the system was better than 0.8 cm (range of 2 m) or 0.04 cm (range of 1 m). At the Fleditebos and the Loobos site the measurement interval was 16 minutes. At the Bankenbos site the interval was 32 minutes. At these sites the raw A/D converter output was logged and in the office transferred to water level depths using a calibration curve. At the Kampina site the resolution of the system was 0.6 cm (range 1.50 m). Here, a measurement interval of 30 minutes was used.

4.3.10 Discharge

At two locations measurements of the discharge Q of the ditches draining the site were made with sharp crested weirs. At the Kampina site a triangular weir was used with an angle of 90°. And at the Fleditebos site two trapezium shaped weirs were used. Automatic water level recorders were used with a 20 cm diameter float in a stilling well. The accuracy of the recorder was 1 mm. Every minute a measurement was made and every 10 minutes the actual, average, minimum and maximum values were recorded. The discharge rate Q (m^3s^{-1}) was derived from the surface water levels z_{sw} (m) using the relationship:

$$Q = C_{1,2} z_{sw}^{a} \tag{4.1}$$

were $C_{1,2}$ and a (-) are calibration constants. The weirs were calibrated in the laboratory. For the V-notch $C_1 = 1.365$ $m^{-0.5}s^{-1}$ and a = 2.5. For the trapezium weir $C_2 = 1.860$ $m^{0.5}s^{-1}$ and a = 1.5 was found.

4.4 Main uncertainties in the hydro-meteorological measurements

The net radiometer used at the Edesebos site and later under the canopy at the Fleditebos and Loobos sites deviated only by 3% from the four component net radiometer. The net radiometer had the same sensitivity at both sides.

The mean and the standard deviation of the throughfall rate T_f based on the 36 manual gauges represents the true T_f well. The uncertainty in the mean of T_f is approximately ± 2%. Only for amounts of $T_f < 0.4$ mm $week^{-1}$ the uncertainty is higher.

The two soil profiles at each site are a good representation of the range in θ values that may be encountered in the footprint of the towers.

The groundwater level at the poplar stand of the Fleditebos site showed a concave profile even in the wet part of the year. This profile is an indication of the high transmissivity of the soil being caused by the permanent cracks.

Chapter 5

Quality control of the flux measurements

5.1 Introduction

The quality of the data is among others determined by the quality of the sensor. In the Tables 4.2 and 4.3 an overview has been given of the accuracy of the sensors used. Besides the instrument accuracy other factors such as electronic problems, frost or dew may influence the quality of the data.

After storing all data in a database a quality check was performed. The quality control consisted of a number of steps were each step could result in a different flag. Three major type of checks were distinguished.

- First the data were checked for acceptable ranges, for example upper and lower limits on the recorded mean and standard deviation and the maximum time step difference.
- Secondly the data were compared with data of different sensors at the site measuring the same quantity, for example on the maximum difference between the rain gauge installed on the tower and installed in the nearby open field.
- Thirdly the data were checked on consistency of physical relations, for example by comparing the ratio of R_s^{up}/R_s^{down} with known albedo α_s values.

These flags were used to distinguish between time slots with missing data, data accepted as good data and data of questionable quality. The accepted data were then used to derive relations between different variables.

In Chapter 6 a complete description will be given of the method used to derive an estimated value for a missing data. First the gaps in the data series of the prognostic variables were replaced. To ensure consistency in the time series a visual inspection was done. The data marked as questionable were compared with the newly derived data, checked for consistency in the time series and the quality check flags were checked. The original measurement was accepted if it complied to three conditions.

- Firstly, the measured data did not cause any inconsistency in the time series.

- Secondly, the data did not differ much, i.e. more than twice the standard deviation, from the derived data.
- Thirdly, the reason(s) the flag(s) were set (for this the comments in the field log book are consulted) could be considered as a warning instead of an error.

If the data did not comply to these conditions, the measurement was qualified as unreliable and the data were rejected.

Besides these kind of data problems which may be considered as causing erroneous data, also the representativeness of the measurements plays a role in the quality of the data. Especially the representativeness of the flux measurements is of major concern. The representativeness of the measurements may be influenced by the placement of the sensor. An impression of what is actually measured by the flux system is obtained from a footprint analysis. In the next section the fetch conditions and the roughness parameters that govern the location and the area of the footprint will be discussed.

For the fluxes that have been derived from turbulent components there are a number of factors that may influence the uncertainty in the data. A concern specifically for this study is the effect of not rotating all fluxes on data quality. The magnitude of this effect will be demonstrated by comparing fully rotated fluxes with partly rotated fluxes for short periods.

To provide an overall assessment of the quality of the flux data from the eddy-correlation system, firstly an indication of the quality of the system set-up was obtained and secondly the quality of the data was evaluated using as main criterion the degree of closure of the energy balance. To check the quality of the system set-up the measured (co-)spectra were compared with the theoretical functions. As an indication of the representativeness closure of the energy balance was used. This closure of the energy balance was also used for the assessment of the quality of the measurements of the different components of the energy balance.

5.2 Roughness parameters and fetch conditions

To estimate the displacement height and the roughness length the logarithmic wind profile relation has been used. The displacement height d (m) was derived from the measurement of the friction velocity u_* (m s^{-1}) and the average wind speed $\overline{u}$ (m s^{-1}) at two different levels:

$$\overline{u}(z_2) - \overline{u}(z_1) = \frac{u_*}{\kappa}\left[\ln\frac{z_2 - d}{z_1 - d} - \psi_M(\zeta_2) + \psi_M(\zeta_1)\right] \tag{5.1}$$

where κ is the Von Karman constant (-), $\zeta = \frac{z-d}{L}$ the stability parameter adjusted for the displacement height and ψ_M the integrated form of the stability function ϕ_M.

For unstable conditions we applied the form as given by Paulson (1970); for the stable case the form as given by Van Ulden and Holtslag (1985) (see Eq. 2.30) has been used.

To minimize the effects of stability only data under near neutral conditions i.e. $-0.01 < \zeta < 0.01$ were considered. For the wind profile data of the sonic anemometer and of the cup anemometer have been used. The scalar wind speed $\overline{u}$ as measured by the cup anemometer was transformed to the total wind speed in the direction of the average wind using the relationship as presented by Bosveld (1997):

$$\overline{u} = \overline{u_{cup}} \frac{1 - 0.5\frac{\sigma_v^2}{\overline{u_{cup}}^2} - \frac{\sigma_u^2}{\overline{u_{cup}}^2}}{1 - \frac{\sigma_u^2}{\overline{u_{cup}}^2}} \tag{5.2}$$

where $\overline{u_{cup}}$ denotes the scalar wind speed as measured by a cup anemometer (m s^{-1}), $\overline{u}$ the wind speed in the direction of the average wind (m s^{-1}), σ_u and σ_v the standard deviation (m s^{-1}) of the wind speed components u and v in the horizontal plane. It was assumed that the horizontal wind variances measured at the level of the sonic anemometer were similar to those at the level of the wind cup anemometer. No clear dependency of the displacement height on wind speed was found and only a weak correlation with wind direction. Differences between years were insignificant and could not be related to an increasing tree height for the period of observation (max. 4 years). For the calculation of the roughness length z_{0M} (m) the median value of the displacement height d (m) was used (see Table 5.1) with Eq. 5.1 extended to the surface at $z = 0$:

$$\overline{u}(z) = \frac{u_*}{\kappa}\left[\ln\frac{z_{ref} - d}{z_{0M}} - \psi_M(\zeta)\right] \tag{5.3}$$

where z_{ref} (m) is the reference height.

No significant correlation of z_{0M} with $\overline{u}$ was found at any of the locations. However, clear differences were found for periods with and without leaves (see Table 5.1). Also at nearly all sites a dependency on wind direction u_{dir} was found. Fig. 5.1 shows an example of the z_{0M} dependency on u_{dir} at the Loobos site. The increase in z_{0M} with u_{dir} from South to West corresponds to a slight decrease found in d.

In Table 5.1 the results are summarized. The standard error in the estimation of d varies from 0.7 m for the more heterogeneous Kampina site to 0.2 m for the homogeneous poplar stand of the Fleditebos site. For z_{0M} the standard error varies between 0.05 m in summer to 0.02 m in winter for the deciduous sites. At the pine stand of the Loobos site the error was $\pm$ 0.02 m.

Differences in the roughness parameters may influence the size and the location of the source area of the flux as detected by the sensor. The location of the sources of λE and H as measured by the sensors also depends on u_{dir} and atmospheric

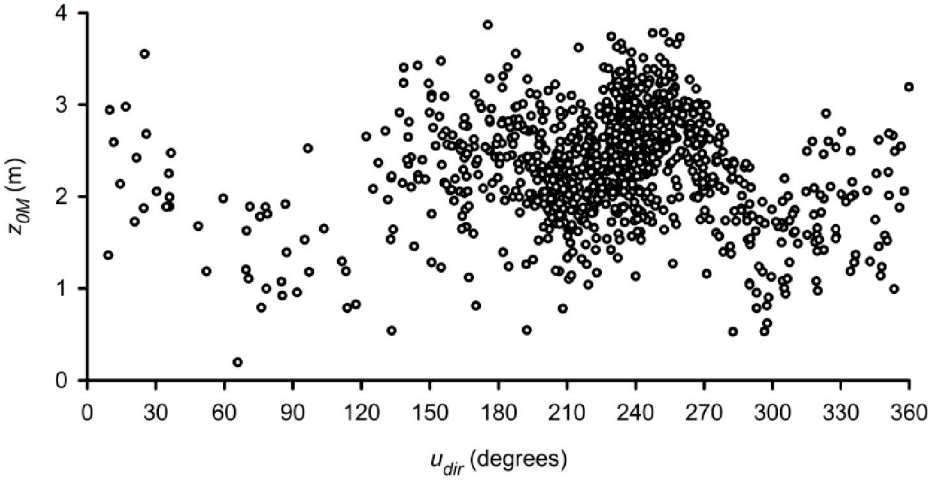

Figure 5.1: *The roughness length z_{0M} at different wind directions u_{dir} for the Loobos site in 1998.*

stability. To obtain an impression of the representativeness of the flux measurements at each site, use has been made of a model which describes the flux source areas in relation to the measuring set-up and the atmospheric stability. The model used is the one proposed by Schuepp et al. (1990) including the adjustments by Lloyd (1995) to incorporate the model response to stability effects. The relative contribution to the vertical flux at height z is given by:

$$\frac{1}{F_0}\frac{dF}{dx} = \frac{-2x_{F\,\max}}{x^2}\phi_M \exp\left(\frac{-2x_{F\,\max}}{x}\phi_M\right) \tag{5.4}$$

where F denotes the flux density (W m^{-2}), F_0 a unit area flux density (W m^{-2}), x the distance upwind of the sensor (m), $x_{F\,\max}$ the distance upwind of the sensor where the flux source is maximal (m). The latter is calculated as:

$$x_{F\,\max} \approx \frac{1.7 z_{ref}^{1.03}\left[\ln\left(\frac{z_{ref}-d}{z_{0M}}\right) - \psi(\zeta)\right]}{(1-\zeta)^{0.5}} \tag{5.5}$$

Table 5.1 shows for each site the distance at which the maximum source takes place as well as the distance where 90% of the flux contribution is accounted for. These distances are a rough estimation that apply for unstable conditions, i.e. for $L = -100$ m.

In Fig. 3.4, 3.8, 3.12, 3.17 and 3.20 the land use at each site has been depicted for a square of 2 x 2 km surrounding the tower. When interpreting the footprint area of

the fluxes, it should be kept in mind that the main wind direction in the Netherlands is SW. The land use depicted in the figures mentioned show that the maximum flux contribution at all sites is generated by the main vegetation type near the tower. It also shows that, except for the Fleditebos and the Loobos site, at the other sites the flux measured is partly composed of fluxes originating from other vegetation types than the main vegetation type near the tower.

At the Bankenbos site wind coming from the east will generate fluxes at the tower with the peat area as an important source of the fluxes. For wind directions between SW and SE larch will be the main contributor to the fluxes. For the other wind directions the fluxes from the larch will be mixed with fluxes from other tree species.

At the Edesebos site the area with oak trees is surrounded by coniferous forest, with the shortest distance at 200 m. Although the fluxes were measured relatively close to the canopy, it may be expected that part of the fluxes originates from the coniferous forest instead of from the oak trees.

At the Fleditebos site the fetch conditions are relatively good in all directions.

The site at Kampina was selected as a mixed site. Besides fluxes originating from the forest there are also fluxes originating from grassland and heather (with a high percentage grass), especially with wind directions from N to NE.

At the Loobos site the pine trees extend over a large area with some smaller areas covered with grass and occasionally with heather.

5.2.1 Non-rotated fluxes

Because of the priority given to year-round data collection and the fact that all sites were at remote locations without access to main power supply, it was at the start of the measurements not possible to store all raw data being collected in the early years. Hence not all corrections usually applied could be made. Therefore, it was decided to leave out the correction for the third rotation.

To estimate the size of the error caused by partly rotating λE and H, the raw data collected over short periods were processed both with all rotation corrections and the limited rotation correction, as done for the long term measurements. In Table 5.2.1 the regression results of the sites Loobos, Fleditebos and Bankenbos are shown.

No significant correlation was detected between rotated and non-rotated λE and H and u_{dir}. The influence of the omission of the rotations on λE is negligible. The differences found for H and the momentum flux, τ were accepted as a minor trade off with respect to the continuity of the data series. The third rotation correction to compensate for the twisting of the streamlines as suggested by Kaimal and Finnigan (1994) is disputable. Finnigan (2002) mentioned that later research showed that this

Table 5.1: *The height of trees z_{tree}, the height of the tower z_{ref}, the roughness length z_{0M}, the displacement height d and the distance where the maximum flux source x_{Fmax} is located as well as the distance for 90% of the total flux $x_{F90\%}$ for unstable conditions (L = -100 m).* [1]*) Estimated from the 1989 ratio z_{0M} and d to tree height.*

Site	Year		z_{tree} (m)	z_{ref} (m)	d (m)	z_{0M} (m)	$\frac{d}{z_{tree}}$ (-)	$\frac{z_{0M}}{z_{tree}}$ (-)	$x_{F\,\max}$ (m)	$x_{F90\%}$ (m)
Banken-	1995	s	21.4	27.80	17.8	1.95	0.78	0.091	67	914
bos		w				1.65		0.077	76	1015
	1996	s	22.3	27.80	17.8	2.15	0.76	0.096	62	854
		w				1.75		0.078	73	980
	1997	s	23.4	27.80	17.8	2.05	0.70	0.088	65	883
		w				1.65		0.071	76	1016
Edesebos	1988	s[1]	17.1	21.28	13.7	1.08	0.80	0.063	66	928
	1989	s	17.4	21.70	14.0	1.10	0.80	0.063	67	940
Fleditebos	1995	s	16.5	23.17	11.0	2.00	0.67	0.121	60	805
		w				1.40		0.085	75	980
	1996	s	17.2	23.17	11.0	2.20	0.64	0.128	57	757
		w				1.60		0.093	70	916
	1997	s	18.0	25.44	11.0	2.50	0.56	0.139	62	799
		w				1.60		0.089	82	1030
	1998	w	18.5	25.44	11.0	1.70	0.60	0.092	79	999
Kampina	1996	s	19.0	29.60	14.0	2.15	0.73	0.113	83	1028
		w				2.15		0.113	83	1028
	1997	s	20.0	29.60	14.0	2.25	0.70	0.113	80	1001
		w				2.15		0.108	83	1028
	1998	s	21.0	29.60	14.0	2.05	0.67	0.098	85	1055
		w				2.05		0.107	80	1001
Loobos	1995		15.3	25.99	9.9	2.19	0.65	0.139	72	906
	1996		15.3	25.99	9.9	1.60	0.65	0.105	86	1065
	1997		15.3	25.99	9.9	2.05	0.65	0.134	75	940
	1998		15.3	25.99	9.9	2.13	0.65	0.139	73	921

last rotation correction was best left out. Omitting the third rotation will reduce the differences between the two approaches even further.

5.3 Power (co-)spectra of turbulent components

To check the quality of the system set up and thus the quality of the flux measurements spectra and co-spectra of the turbulent components were compared with the theoretical spectral density functions. The spectra and co-spectra were calculated

Table 5.2: *Regression results of non-rotated versus rotated fluxes, where a is the slope, x_0 the intercept and R^2 the mean square error.*

Site	λE			H			u_*		
	a (-)	x_0 (W m^{-2})	R^2 (-)	a (-)	x_0 (W m^{-2})	R^2 (-)	a (-)	x_0 (m s^{-1})	R^2 (-)
Loobos	1.02	0.7	0.98	0.96	-3.4	0.98	1.05	0.01	0.99
Fleditebos	1.00	-0.3	0.99	0.94	-3.4	0.99	1.07	0.00	0.99
Bankenbos	0.98	2.1	0.97	0.97	-1.6	0.99	1.05	0.02	1.00

for approximately 10 day periods except for the Kampina location where because of logistics problems a shorter period was used. A Hamming window was used to filter the data in the low and high frequency range (Kaimal and Finnigan, 1994). For the calculations of the spectra two subroutines as described by Press et al. (1989) were slightly adjusted. To smooth the curves the spectra were binned using a logarithmic interval for the normalized frequency to ensure equidistant bins for the logarithmic plot. The power spectra compare well with the model spectra (Eq. C.27-C.39). Although there is some deviation from the model power spectrum of $\varkappa$ this deviation is not found in the co-spectra (see Fig. 5.2). The co-spectra of all 4 locations are similar in shape and have their peaks at $n \approx 0.1$. Their peaks seem to be more pronounced than the model co-spectra, which was derived over flat terrain. The co-spectra correspond well with the findings of Anderson and Pyatt (1986). Based on this spectral analysis the fluxes were considered to be of good quality.

5.4 Energy balance closure

Closure of the energy balance is a test of the quality of the data. As a measure of closure the ratio between the turbulent and the non-turbulent fluxes is used i.e.

$$\frac{(\lambda E + H)}{(R_{net} - G_0 + F_{lat} - J - \mu F_A)} \tag{5.6}$$

Here it is assumed that the lateral fluxes are small and hence their contribution to the total energy balance is negligible.

Photosynthetic energy may be calculated by:

$$\mu F_A = -\mu \overline{w' \rho_c'} \tag{5.7}$$

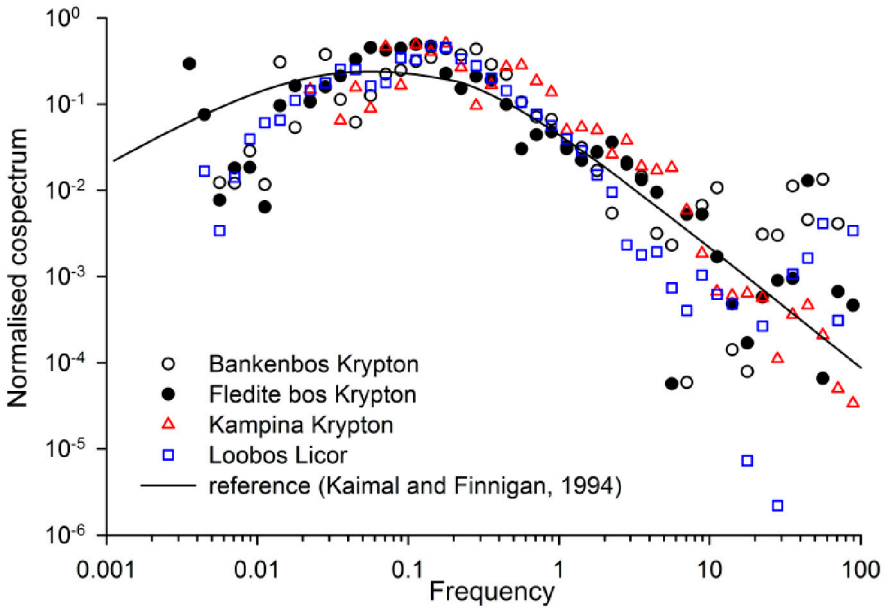

Figure 5.2: *Measured (symbols) and modelled (solid line) normalised co-spectra of vertical wind speed and specific humidity* $\overline{w'\varkappa'}$ *as a function of frequency i.e.* $n = fz \ / \ \overline{u}$ *under unstable conditions. The modelled co-spectra line is based on Kaimal and Finnigan (1994).*

where $\overline{w'\rho_c'}$ is the flux density of CO_2 from eddy-correlation measurements including the storage flux (μmol m^{-2} s^{-1}) and μ is the specific energy for conversion of energy by photosynthesis (J mol^{-1}). For a typical maximum daytime flux of 20 μmol CO_2 m^{-2} s^{-1} the energy consumed for photosynthesis is 10 W m^{-2}. As these values have not been measured at all sites and the contribution is relatively small as compared to the radiation flux, this component has been neglected for the calculation of the energy balance closure.

For short time steps (less than a day) the effect of energy storage should be taken into account. Storage of energy may take place in the vegetation and air space below the flux sensors of radiation, H and λE and in the soil above the sensors of G. This storage term is particularly important during periods of rapid change, i.e. for conditions such as occur during sunrise and sunset.

5.4.1 Heat storage in soil and litter layer

To determine the soil heat flux at the surface G_0 the heat storage above the heat flux plates has to be added to the measurements of the plates:

$$G_0 = G_z + \int_{t_2}^{t_1} \int_{z}^{0} C_{soil}(z) T(z,t) \mathrm{d}z \mathrm{d}t \tag{5.8}$$

where C_{soil} is the volumetric heat capacity of the soil (J m^3 K^{-1}), z is the depth at which the heat flux plate is installed. C_{soil} is composed of the weighted volumetric heat capacities of the different soil components (De Vries, 1963):

$$C_{soil} = \rho_{soil} c_{soil} = X_a \rho_a \mathrm{c}_p + X_o \rho_o \mathrm{c}_o + X_q \rho_q \mathrm{c}_q + X_c \rho_c \mathrm{c}_c + X_w \rho_w \mathrm{c}_w \tag{5.9}$$

where the subscript o stands for organic matter, q for quartz, c for clay minerals and w for water, X is the volume fraction (m^3 m^{-3}), ρ the density (kg m^{-3}) and c the specific heat (J kg^{-1} K^{-1}). The densities (kg m^{-3}) are respectively: $\rho_a = 1.2$, $\rho_o = 1300$, $\rho_q = 2660$, $\rho_c = 2650$ and $\rho_w = 1000$ and the specific heat (J kg^{-1} K^{-1}) $\mathrm{c}_p = 1010$, $\mathrm{c}_o = 1920$, $\mathrm{c}_q = 800$, $\mathrm{c}_c = 900$ and $\mathrm{c}_w = 4180$. x_w may be replaced by the measured soil moisture volume fraction θ, that of air by $\theta_s - \theta$.

It has been assumed that the T_s at the top of the litter layer was well represented by T_a below the canopy. T of the sensors above and below the soil heat flux plate were used to derive the temperature at the top of the mineral layer and at the depth of the plate by (Van Wijk and Vries, 1963):

$$T(z,T) = \overline{T} + A_T(z) \sin \left[\omega t - z \left(\frac{D_T{}'}{\omega} \right)^{-1/2} \right] \tag{5.10}$$

where A_T (K) is the amplitude of the soil temperature at depth z, ω the diurnal angular frequency ($\pi/12$ rad h^{-1}) and $D_T{}'$ (m^2 s^{-1}) is the apparent thermal diffusivity. For the mineral layer, assuming the physical properties being constant within a layer, $D_T{}'$ of the soil has been derived from:

$$A_T(z_2) = A_T(z_1) \exp \left[-(z_1 - z_2) \left(\frac{2 D_T{}'}{\omega} \right)^{-1/2} \right] \tag{5.11}$$

For the litter layer D_T for organic matter as given by Van Wijk and Vries (1963) has been used, i.e. $0.15 \cdot 10^{-6}$ m^2 s^{-1}. Here the assumptions were made that θ of the litter layer was close to that of the top mineral layer, and that T of the litter layer and of the soil layer above the highest soil temperature sensor was well represented by the temperature of that sensor. The temperatures thus derived were used to calculate the heat storage above the plate by means of Eq. 5.8 and 5.9.

5.4.2 Heat storage in the biomass

The heat storage in the biomass, J_{veg} W m^{-2} can be divided in a rapidly changing heat storage in the leaves and branches and a more slowly storage in the stems:

$$J_{veg} = J_{leaf+branch} + J_{stem} + J_{undergrowth} \tag{5.12}$$

As the biomass of the undergrowth is small as compared to that of the trees, the change in heat storage of the undergrowth is neglected. The method applied to derive the change in heat storage in branches and leaves and in the stem of the trees is described in Appendix D. In this Appendix also the values of the parameters for the different tree species at the sites are provided.

5.4.3 Results energy balance closure

Laubach et al. (1994) and many others reported gaps in energy balance closure varying between 11 and 30% for 1 hour averages of day time values for a spruce forest in Germany. Uncertainties in the half hour values are partly due to the changes in heat storage in the soil, air and canopy space below the reference level. To limit these uncertainties, the daily totals of H and λE are plotted against R_{net} in Fig. 5.3.

Deviations from the 1 : 1 line may be caused by the error introduced by omitting the rotation of the scalar fluxes. Also the heterogeneity of the site (see e.g. Fig. 3.17) in combination with the relatively small footprint of the radiation sensors as compared to the footprint of the eddy correlation system may cause deviations from the 1 : 1 line.

If the regression lines were forced through the origin all slopes were above 0.94, indicating a closure of the energy balance better than 6%. The Kampina site was the exception. For this site the slope was more than one. Indicating that H and λE were using 14% more energy than was supplied by R_{net}. If the Kampina data set was split up in summer and winter, the slope of the regression line (with a free offset), became 1.0 for the summer period and 0.85 for the winter. For both these data sets there was a positive offset of $\pm$ 20 W m^{-2}.

Using half hour data and calculating the different components of the energy balance as discussed previously gave similar results, however with a larger range of the data. As an example the energy balance of the Fledite site for the year 1997 is shown in Fig. 5.4).

Moncrieff et al. (1996) discussed the possible errors associated with flux measurements, distinguishing between random and systematic errors. Assuming a random error of 20% per half hour value for a data set of in total 44 days, may give an overall random error for the data set in the order of 13%. In general, independent random

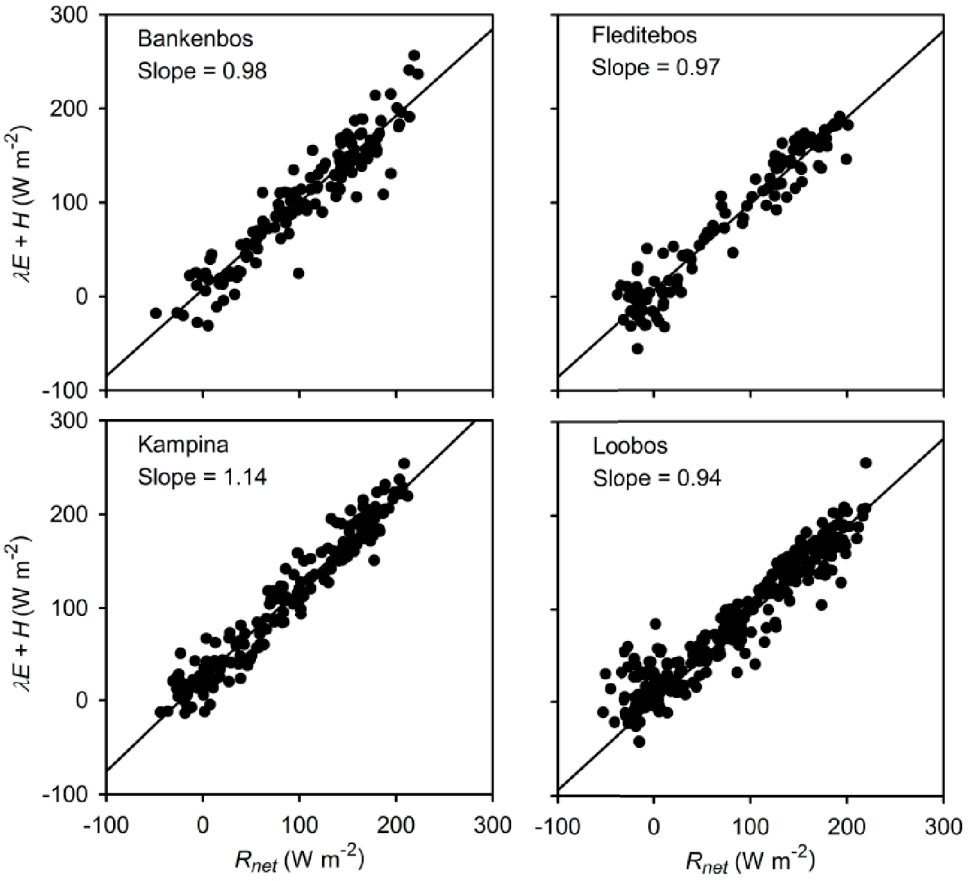

Figure 5.3: *Energy balance closure depicted as the ratio of daily averages of net radiation R_{net} and daily averages of the sum of sensible H and latent heat flux λE for dry days: for the Bankenbos, Fleditebos and Loobos sites data of 1995 were used, for the Kampina site data of 1996.*

errors decrease with the length of the data set by $1/\sqrt{N}$, where N represents the number of data. This decrease however, does not hold for systematic errors.

At the Loobos site an underestimation of λE was observed when comparing λE measured using a closed path system with an open path Krypton hygrometer. The difference between the two instruments was also evident when looking at the power spectra, which show a significant lack of flux, especially at high frequencies. This lack of flux became more pronounced during wet conditions. A possible reason could

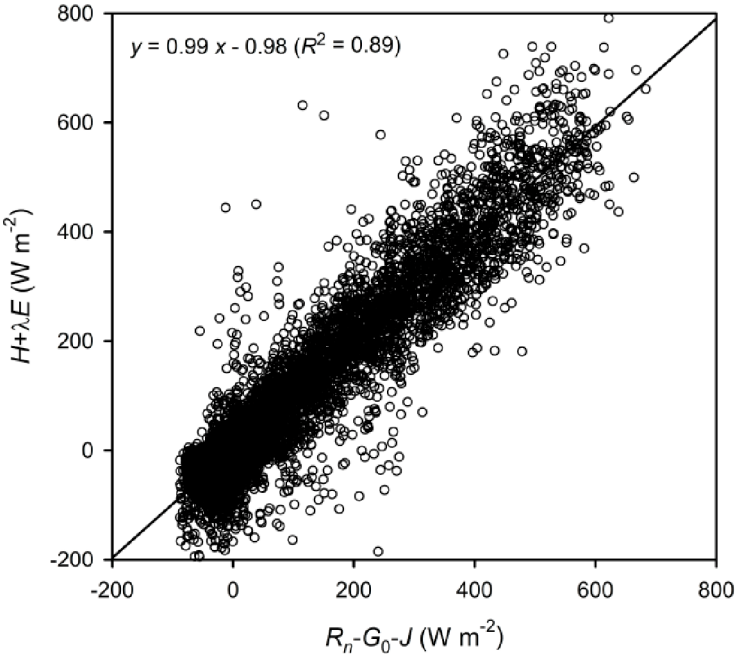

Figure 5.4: *Energy balance at the Fleditebos site 1997 using half hour averages of the sum of net radiation R_{net}, soil heat flux at the surface G_0 and the energy storage J in the vegetation and air layer between surface and reference level compared to the sum of sensible H and latent heat flux λE for dry periods.*

be damping of the high frequency water vapour fluctuations due to adsorption and desorption on the walls of the inlet tube. Goulden et al. (1996) reported, for a closed path system with an infra-red gas analyser, an underestimation for λE of 20%, for which they also reported a long term precision of $\pm 5\%$. Ibrom et al. (2007) showed that under moist condition the damping in the tube of the water vapour fluctuations increases. Hence, λE was corrected based on comparison with the measurements of the Krypton hygrometer for those periods during which $\varkappa$ was measured only by the closed path system.

The relatively good closure of the energy balance based on daily values, as well as the good resemblance of the measured and modelled co-spectra of $\overline{w'\varkappa'}$ gave confidence to the quality of λE. If closure of the energy balance is used as an estimate of the accuracy of the measurement, λE derived in this study using an eddy-correlation system is in summer better than 5% and in winter better than 15%. The error in λE when using a Bowen ratio system has been estimated for the Edesebos site following

Fuchs and Tanner (1970). If the error in the R_{net} is estimated at 5% and in G_0 as 25%, the average error in λE for day time values on a clear day in summer becomes 10%. For a dry day in spring with low humidity differences this error may increase up to 20%.

5.5 Data quality under wet conditions

For a similar sonic as is used in the present study, Gash et al. (1999) and Van der Tol et al. (2003) demonstrated that tests on the form of the power spectra of the different wind components and on the slope of the σw versus u_* gave no reason to doubt the functioning of the sonic during rain. This was confirmed by the data of our study. In addition the co-spectra of $w'T'$ were compared for dry and wet conditions as measured at the pine stand of the Loobos site. Fig. 5.5 shows that for the most common slightly stable atmospheric conditions found in these regions during showers a reasonably good agreement with the reference spectra as given by Kaimal and Finnigan (1994) is obtained. The closed path IRGA that has been employed at the Loobos site in 1996 continues to measure during rainy conditions. However due to smearing of water vapour on the inner walls of the inlet tube, λE will in general be underestimated. Here these data will only be used for comparison purposes and not to determine actual λE.

Due to these problems with the closed path IRGA, these data can not be used to check the closure of the energy balance. Also for the open path IRGA the check on the energy balance closure under wet conditions is limited. The reason is that during showers the Krypton hygrometer was always shut down automatically in order to prevent damage to the instrument. Therefore, there are only some λE data available during light showers and at the start of showers. To investigate the level of closure of the energy balance for these data, the different components of the energy balance of 1996 for the poplar stand at the Fleditebos site were plotted in Fig. 5.6. Although the scatter is relatively large ($R^2 = 0.47$), the absolute differences are in the same order of magnitude as under dry conditions. The energy balance closure expressed as $(\lambda E + H)/(R_{net} - G_0 - J)$ is for wet conditions 81%, for dry conditions 86%. For dry conditions, closure of the energy balance varied for the Fleditebos site between 0.86 and 0.99 for the different years. These findings support earlier findings by Gash et al. (1999) and demonstrate the small effect of rain on the performance of the sonic anemometer.

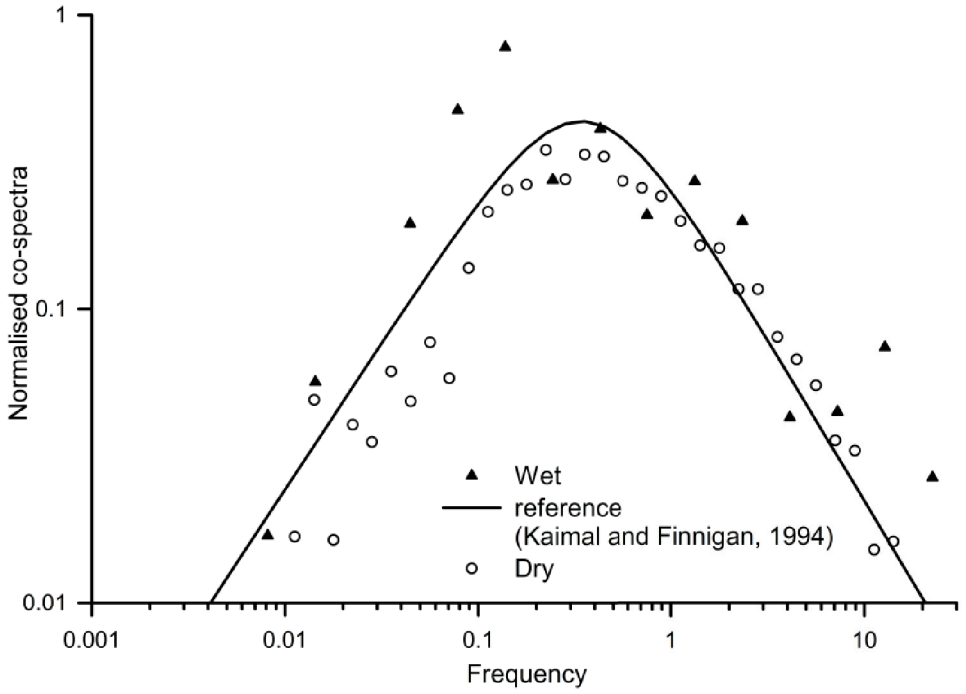

Figure 5.5: *Normalised co-spectra of $w'T'$ as a function of frequency $n = fz \,/\, \overline{u}$ for wet ($P > 0.2$ mm 30 min^{-1}) stable conditions during two showers and for dry stable conditions in the same period measured at the pine forest of the Loobos site.*

5.6 Conclusions

Analysis of the fetch conditions (see Table 5.1) shows that for the major wind direction at all sites the origin of the maximum flux is well within the footprint area of the towers. The Loobos site and the Fleditebos site may be considered most homogeneous for all wind directions.

From the comparison with the full rotation corrections it followed, that the influence of the omission of the rotations on λE is negligible, i.e. well below 5%.

The relatively good closure of the energy balance based on daily values (see Fig. 5.3), as well as the good resemblance of the measured and modelled co-spectra of $\overline{w'\varkappa'}$ (see Fig. 5.2) give confidence to the quality of λE. The fact that the closure of the energy balance for 30 minute data is less good, i.e. $> 80\%$, indicates that a large part of the uncertainty is in the estimates of the heat storage in both the soil and biomass.

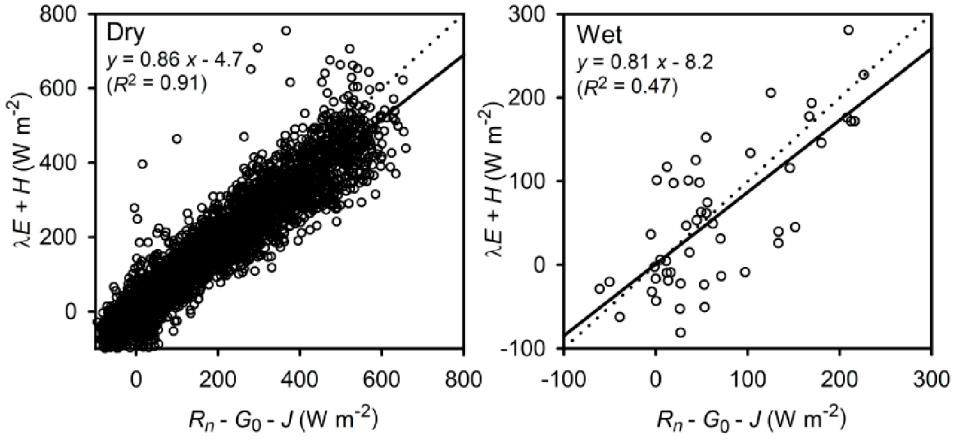

Figure 5.6: *The sum of turbulent fluxes $\lambda E + H$ plotted against the net radiation minus the storage fluxes in the soil, vegetation and air below the measurement level $R_{net} - G_0 - J$. For dry (left panel) and wet (right panel) conditions in 1996 at the poplar stand of the Fleditebos site.*

If closure of the energy balance is used as an estimate of the uncertainty of the measurement, λE derived in this study using an eddy-correlation system is in summer time better than 5% and in winter time better than 15% for the Bankenbos, Fleditebos and Loobos sites. For the Kampina site the percentage of energy balance closure in summer time is less good, i.e. the uncertainty is better than 15%.

The uncertainty in λE when using a Bowen ratio system is estimated for day time values on a clear day in summer as 10%, and for a dry day in spring with low humidity differences as 20%.

The analysis of the behaviour of the measured wind components with the sonic anemometer showed the small effect of rain on the performance of this sensor. Also the limited number of available data from the open path Krypton hygrometer at the Fleditebos site under wet conditions, showed a reasonably good closure of the energy balance i.e. better than 80% (see Fig. 5.6), as well as a reasonably good agreement with the modelled spectra (see Fig. 5.5).

These findings demonstrate the good performance of the sonic anemometer and thus the relatively good estimates of H under wet conditions. The associated uncertainty in λE based on the percentage of energy balance closure is better than 20%.

Chapter 6

Gap filling to generate continuous data sets

6.1 Introduction

Most models are highly sensitive to initial values of state variables, hence gaps in the forcing data sets are influencing the behaviour of the models. Therefore uninterrupted data series of the driving variables of the model are required.

Measurements over short time steps (e.g. 30 minutes) of environmental variables are inclined to have gaps, resulting from e.g. power failure, instrument breakdown and rejection of data by means of quality checks. The treatment of gaps depends among others on the length of the gap. For instance hourly data in one diurnal cycle, or daily data in a seasonal cycle may be missing. Because of e.g. differences in autocorrelation or significance of storage terms, both sorts of gaps should be treated differently.

A distinction should also be made between first order variables (e.g. $\overline{u}$) and second order variables (e.g. λE). Filling gaps in series of second order variables using first order variables (e.g. λE from R_{net}, T and $\varkappa$) is always possible.

Retrieving first order data from second order data is however generally not needed. For example, it is not useful to retrieve $\overline{u}$ from H as measured with a 3D sonic anemometer. Then it is more appropriate to use $\overline{u}$ as measured by the 3D sonic and to transfer those to the sensor with the missing data of $\overline{u}$. Also in practice, if there is a gap in first order data series, second order data will frequently be missing for that period.

Hence, before a long term model can be run these gaps in the data series need to be treated. Long term data series are also needed to study for example the variability between sites and between years. In these cases uninterrupted data series of the variables driving the process as well as the variables resulting from the process, such as λE, are essential. For these studies daily averages or totals are generally sufficient. *The main objective of gap filling is to derive high quality synthetic data being consistent with the measured data.* As has been discussed in Chapter 5, prior to filling data gaps, a data quality check has to be executed.

6.1.1 Overview of methods to fill gaps in time series

Moffat *et al.* (2007) provided an overview of methods available to fill gaps in data series of net carbon fluxes. Most of these methods can also be applied for fluxes of H or λE. These methods can be grouped as follows: (non)-linear interpolation (Xia et al., 1999), look-up tables (Falge et al., 2001), a method based on the mean diurnal variations of previous periods (Falge et al., 2001), (semi-)empirical models (e.g. Green, 1979; Desai et al., 2005) and (multiple) (non)-linear regression (Aubinet et al., 2000).

Interpolation may be preferred in between time steps or between data from different sites, applying either linear or non-linear interpolation techniques. As most relations in nature are complex, (non)-linear interpolation is reliable only when filling very short gaps (e.g. a 30-minute time step) and only then if other data series without gaps of more or less physically related variables show the same trend (e.g. T and R_s).

Look-up tables have the desired variable binned based on meteorological conditions. Falge et al. (2001) used PPFD (Photosynthetic Photon Flux Density) and vapour pressure deficit as the driving meteorological variables for λE and H. To represent different seasonal conditions the tables were split up in 6 or 4 parts. The advantage of lookup tables as compared to semi-empirical methods such as non-linear regression is that look-up tables are discrete and do not depend on a fixed continuous response function.

The *Mean Diurnal Variation* (MDV) method replaces missing data using the mean for that time slot based on measurements of previous as well as of subsequent days. This method is based on the assumption that the average of the previous and subsequent periods is representative for the period with the missing data. For (half-)hourly data, Falge et al. (2001) recommended averaging windows of either 7 or 14 days. Larger averaging intervals are generally not recommended as they will for each time slot introduce more deviations from the mean. The strong point of MDV is that no data are needed of other variables, which is particularly useful for remote locations when no data are available at all. At the same time it is also a weak point of this method, because there is no response to different conditions that may influence the variable to be filled (Falge et al., 2001).

(Semi-)empirical models are used to fill gaps in data series of fluxes e.g. the relation between T_{soil} and R_s and the night time CO_2 flux (e.g. Lloyd and Taylor, 1994). The disadvantage is however, that these models are based on either pre-defined physical or physiological relations, not necessarily representative for the period with missing data. For example, the assumption of energy balance closure, although the-

oretically correct, will not be easy to apply to a specific site under all conditions. A site may be influenced by either advection or by the problem that G_0 or J has not been accurately measured. Hence, fluxes derived from a model using the assumption of energy balance closure will then show an offset as compared to the fluxes measured.

(Multiple) (non)-linear regression during gap filling ensures conservation of the response to meteorological drivers. A non-linear regressor is capable of reproducing the highly non-linear relations that are common in nature. A distinct advantage of the use of regression techniques as compared to semi-empirical models is that in principal it is not necessary to make any prior assumptions about a physical relation between variables.

To derive artificial data use will be made of a non-linear regressor. Therefore a distinction will be made between first order data of an automatic weather station and second order data from a flux station. There is generally not just one cause for missing data. The availability of variables to be used to fill the gap may be different. Typical cases of missing data will be analysed and it will be demonstrated how different data being measured (at the same site and nearby sites) can be used to replace the missing data.

One of the risks in gap filling is that the periods with missing data are related to unusual conditions. For example if an open path sensor has been used to measure $\varkappa$ it is likely that gaps in the data series correspond to periods with showers. To establish a relationship between λE and meteorological data, using the periods with "good" data may bias the results to conditions during dry periods. How such a bias may affect the results will also be investigated.

6.2 Quality check and data gap filling procedure

Before starting the gap filling procedure a data quality check was executed. The three phases of the checks on the Automatic Weather Station data and the two phases of the flux data checks have already been described in more detail in Chapter 4. All data records that are flagged are considered as missing data. For training of the regressor only the remaining data will be used.

After the three phases of the data quality check, first the missing data of the meteorological and other prognostic data are replaced. Secondly, the missing data of λE are replaced. The data quality and data filling procedures are schematically presented in Fig. 6.1.

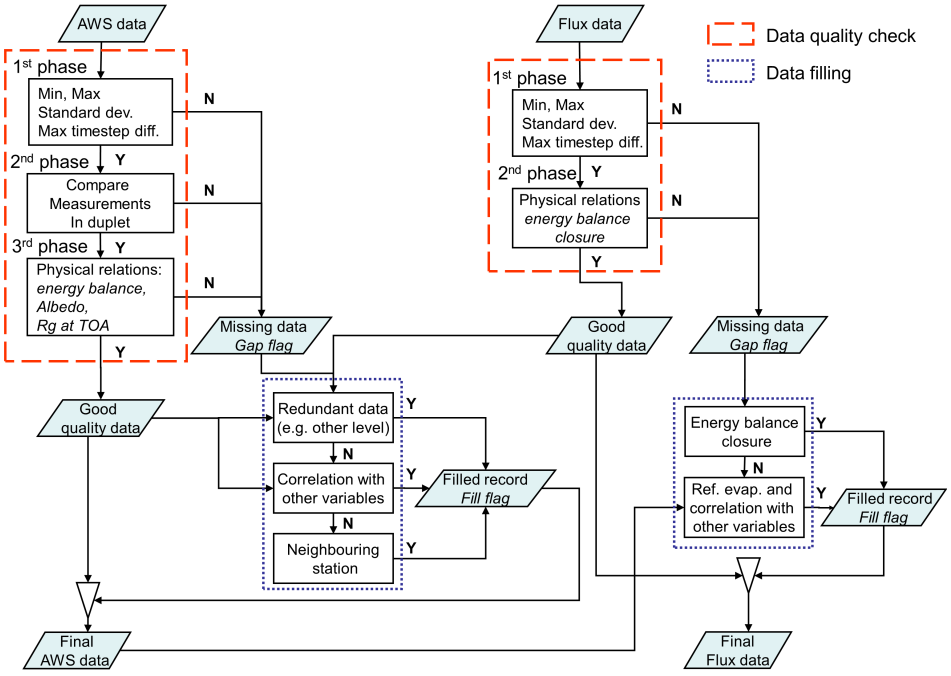

Figure 6.1: *Schematic representation of the data quality checking and gap-filling procedure for the Automatic Weather Station (AWS) data and the flux data.*

6.2.1 Automatic Weather Station data

For weather station data such as T_a, $\varkappa_r$, u, R_{net}, R_s and P there are a number of techniques for gap filling available which are based on comparing data at a specific site with those measured at neighbouring sites. Xia et al. (1999) tested 6 different methods to estimate missing values in forest climatology data for Bavaria, Germany. They found that a method based on multiple regression analysis (using the 5 nearest weather stations) gave the best estimations. The most accurately estimated variables were maximum and mean temperature, and water vapour pressure, followed by minimum temperature. The poorest results were obtained for wind speed and precipitation. The biggest problem arose when the station was located in an extended forested area and the neighbouring stations were located in an area with different land cover, such as grassland. They found that if the forest influence was not taken into account the errors increased significantly, especially for wind speed and precipitation.

Site information can be used that is implicitly available in other variables measured at the site with the data gap. This will partially overcome the problem of the differences between the sites. For example if wind speed data are missing at site A,

but radiation data are available, a non-linear regressor can be trained using not only the wind speed data at site A and site B, but also the radiation data at site A.

Based on these findings the following 3 possible options were used to derive a first estimate. The first option is to use "redundancy" available if other sensors are measuring the same variable, e.g. at other heights. The second option is to use other variables measured at the same site that are strongly correlated, e.g. T_a and $\varkappa_r$ or R_s and t (or R_s^{atm}). The third option is to use the same variable but measured at one or more neighbouring sites.

6.2.2 Flux data λE

For most variables measured by an automatic weather station simple physical relations with other variables exist. For λE, these relations are more complex and uncertain. In most cases λE can be simulated with any land surface scheme using the driving variables as input. However, the use of any particular land surface scheme will inherently reflect the concepts it is based on, and therefore strongly affect the outcome, e.g. the PILPS results of Qu et al. (1996). Continuous records of λE data are in general only of interest for longer time steps. Thus highly accurate gap filling of flux data at a short time step is often not needed. Therefore as the driving variables are the base to replace the second order data, the first emphasis of gap filling is on the driving variables.

Because for the analysis of the water balance terms λE at a daily or longer time step are of interest, gap filling of λE will be performed on daily data. This approach has the advantage of reducing the random uncertainty in the data. It also removes most of the uncertainties associated with the different storage terms such as present in the soil, the biomass and in the air volume below the reference level. Huntingford and Cox (1997) and Musters (1998) already demonstrated that to replace the Jarvis-Stewart functions controlling the stomatal or canopy conductance of the Penman-Monteith equation, non-linear regressors such as neural networks can be used with good results. Here this property is used to remove most of the seasonal fluctuation in the data by subtracting a calculated reference evaporation before starting the gap filling. Thereafter the neural network is used to explain the residue.

Because of the sparse distribution of flux stations, filling of missing flux data using neighbouring stations is not practical. To derive a first estimate of λE there are two options. The first option is to obtain λE as the residue of the energy balance. For this option the other energy balance terms H and R_{net} should be available. The second option is to use the reference λE, e.g. based on the Penman-Monteith equation (see Eq.2.35) with a fixed r_s.

6.2.3 Gap filling procedure

After establishing the first estimates, a non-linear regressor will be used to explain the differences between the measured data and these first estimates.

To select the input variables needed to drive the regressor, ideally a Principal Component Analysis will be performed, in particular if dependencies between variables are to be expected. If dependencies are found indeed, the variables will be combined to one new variable to be used as input for the regressor. This procedure will limit the number of degrees of freedom for the regressor. For linear dependencies there are currently a number of tools available, but to the author's knowledge, there are no reliable tools for non-linear dependencies. Because it is expected that most variables used in this study possess non-linear dependencies "expert judgement" will be used. To assure a good estimate and to avoid extrapolation, care will be taken to cover the variable space as well as possible. Variables in the regression that only cover a limited range will be excluded. To increase the coverage of the variable space (e.g. Haan, 1977) and if necessary variables will be combined, e.g. by the use of physical models.

Subsequently, to derive synthetical data for the missing records in the data sets the non-linear regressor will be used.

All the synthetical data will be added to the database with a flag marking the method used to derive the data. Before these data are to be accepted, they are compared with the original data flagged by the quality check. If the difference is small and removal of the quality flag can be justified (e.g. by checking the notes in the log book of the field station), the quality flag is removed and the original data are accepted as "reliable". For the opposite case, the synthetical data will be accepted and the quality flag is replaced by a flag marking the method used to derive the data.

6.3 Artificial Neural Network as non-linear regressor

Mathematically, the incorporation of known physical relations such as the conservation equations of mass and energy will remove much of the expected behaviour of the target variable. To predict the anomalies a regressor can then be used. Hence, instead of feeding the measurements directly to the regressor, the residuals of the measurements and the output of the simulated physical relations will be used. In a similar way differences between a variable measured with 2 different instruments at the same or at 2 different sites may be used as the target for the regressor. To simulate undefined non-linear relations that are common in nature, a non-linear regressor is the best choice, as it has the greatest flexibility. Therefore, to estimate the

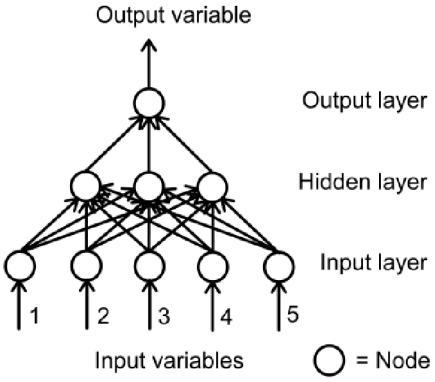

Figure 6.2: *Example of a neural network configuration with 5 input variables, a hidden layer with 3 nodes and 1 output variable.*

missing data an algebraic neural network will be used that is capable of reproducing highly non-linear relationships (Moors and Dolman, 2001; Gardner and Dorling, 1998; Huntingford and Cox, 1997). A typical neural network consists of a number of input nodes, a number of nodes in a hidden layer and one output node. In Fig. 6.2 an example is shown of a neural network configuration.

For this study the neural network of Saxén and Saxén (1995) has been used. In order to obtain the same weight for all input variables at the start of the training session, all input variables, denoted by x will be scaled to values between –1 and +1:

$$x' = \frac{x - \overline{x}}{\max(x) - \min(x)} \tag{6.1}$$

The output and input nodes will be activated by a linear function. To capture the non-linear behaviour of natural systems, a sigmoid activation function will be used for the nodes of the hidden layer, i.e.

$$y = -1 + \frac{2}{1 - e^{-x'}} \tag{6.2}$$

For the training of the network the Levenberg-Marquardt algorithm has been used (Press et al., 1989). This algorithm minimizes the sum of squares of the residuals by modifying the network weights. The search direction is an interpolation between the directions given by Gauss-Newton and the steepest descent methods (Saxén and Saxén, 1995). The behaviour of the network configuration is evaluated using the Root Mean Square Error (RMSE):

$$\mathrm{RMSE} = \sqrt{\frac{\sum (y - \widehat{y})^2}{n}} \tag{6.3}$$

To determine if a configuration is over-dimensioned a test data set has been used. An increase in the number of nodes will in general result in a decrease of the RMSE of the training data set. However, if at the same time the RMSE of the test set increases, this increase is an indication of over-dimensionalising of the network and this specific configuration will not be used.

6.4 Results

6.4.1 Automatic weather station data

Generally speaking there is not just one cause for gaps in the data series. The data available to fill the gap also vary. In Table 6.1 an overview is presented of the most common combinations and optimum network configurations used within this study. Table 6.1 is not meant to compare different network configurations, but it represents optimum configurations for parts of the data sets.

As mentioned earlier, this configuration depends on the availability of reliable data of the input variables for that part of the data set.

One of the most important variables missing in Table 6.1 is the precipitation. The calibration of a neural network to simulate the difference in precipitation between two sites yielded good results. The RMSE of the test set however had such a large value, that there was no benefit in using a neural network as compared to the use of a simple regression equation. The same conclusion applies to the simulation of the difference in precipitation between the rain gauge in the open field and the gauge mounted on the top of the scaffolding tower.

As an example of how the optimum network configurations are derived downward radiation flux density R_l^{down} has been used. Modelling R_l^{down} is not trivial especially under cloudy conditions. There exist however a number of models for clear sky conditions that yield acceptable results (e.g. Brutsaert, 1982). For cloudy skies however the results become less satisfactory.

In general physical relations to model R_l^{down} are based on T_a and $\varkappa$ as driving variables. R_s^{down} and H are other variables commonly not used for modelling of R_l^{down}. However, a strong physical relation can be very useful to fill missing R_l^{down} data. R_s^{down} is related with R_l^{down} through the radiation balance, and H through T_s. Table 6.2 shows a number of such relations for R_l^{down}. It also shows how the optimum network configurations were derived from a number of possible configurations.

To prevent the neural network from solving the well known temperature dependency of R_l^{down}, the desired output R_l^{down} has been replaced by the differences: $\sigma T^4 - R_l^{down}$. The data set was selected such that alternatively 48 consecutive records

Table 6.1: *Different neural network configurations as being used for the gap filling of the automatic weather station variables. For each diagnostic variable the neural net input and output signals, the number of nodes of the hidden layer, the flag identifying the method used to derive the data, the RMSE of the training set and the mean of the output variable is given. The variables used are u wind speed, u_* friction velocity, u_{dir} wind direction, $\varkappa$ specific humidity, H sensible heat flux density, E evaporation rate, ζ $(=\frac{z-d}{L})$ stability parameter, R_s^{atm} solar radiation at the top of the atmosphere, c_c cloud cover and R_l^{down} (mV) refers to the incoming long wave radiation in millivolts, t time of day. The subscripts refer to: the instruments kry: krypton hygrometer and son: sonic anemometer, the locations lev2: level 2, soil, etc., the subscript res stands for the residue of the variable.*

Variable	Output signal	Input signals	Nodes	Flag	RMSE	$\overline{y}$
u	$u - u_{son}$	u_{son}, u_*, ζ	2	NN1	0.141	2.48
(m s^{-1})	$u - u_{loc}$	$u_{loc}, u_{dir}, T, R_s^{down}$	2	NN2	0.566	
	$u - u_{lev1}$	$u_{lev1}, u_{lev2}, u_{loc}, R_s^{down}$	3	NN4	0.446	
	$u - u_{loc}$	$u_{loc}, R_s^{down}, x_{lev1}, x_{lev2}$	3	NN5	0.559	
T	$T - T_{son}$	$T_{son}, u_{son}, u_*, \zeta$	3	NN1	1.024	15.97
(^{o}C)	$T - T_{son}$	$T_{son}, T_{soil}, u_{son}, \zeta, t$	3	NN2	0.847	
	$T - T_{son}$	u_{son}, u_*, ζ, t	3	NN3	0.982	
	$T - T_{son}$	$T_{son}, T_{soil}, u_{son}, u_*, \zeta, H, t$	5	NN4	0.677	
	$T - T_{loc}$	T_{loc}, t	0	NN5	0.772	
x	$x - x_{kry}$	$x_{kry}, T, u, H, u_*, \zeta, t$	3	NN1	0.452	9.47
(g kg^{-1})	$x - x_{lev2}$	x_{lev2}, T, u, R_s, t	3	NN2	0.352	
	$x - x_{lev2}$	$x_{lev2}, T, u, H, u_*, \zeta, t$	5	NN3	0.393	
	$x - x_{loc}$	$x_{loc}, T, u, u_{dir}, t$	2	NN4	0.579	
R_s^{down}	$R_s^{down} - R_s^{atm}$	$R_s^{atm}, T, x, H, E_{res.}, u, u_*, \zeta, t$	6	NN1	27.05	263.2
(W m^{-2})	$R_s^{down} - R_{loc}^{down}$	$R_{s,loc}^{down}, T, R_s^{atm}, x, u, R_l^{down}(mV)$	4	NN2	41.27	
R_l^{down}	$R_l^{down} - \sigma T^4$	$T, R_s^{down}, \varkappa_r, u, t, R_s^{atm}, \sigma T^4, c_c$	4	NN1	20.18	312.8
(W m^{-2})	$R_l^{down} - \sigma T^4$	$T, R_s^{down}, \varkappa_r, H, \zeta, \sigma T^4, c_c$	3	NN2	19.31	

with measured reliable data were selected for the calibration data set followed by 48 records for the validation data set.

For the calibration data set ($N = 1486$) the average of the measured R_l^{down} was 312.81 W m^{-2}. The validation data set consisted of 1536 records with the average measured $R_l^{down} = 317.58$ W m^{-2}. As was to be expected the network set-up with the largest number of degrees of freedom (i.e. number of input nodes plus hidden nodes) showed the best calibration results.

The best validation results were obtained using R_s^{down}, $\varkappa_r$, H, u_*, ζ, R_s^{atm}, σT^4 and c_c as input variables and 5 hidden nodes, i.e. the simulated $R_l^{down} = 314.20$ W m^{-2}. Leaving out ζ, u_*, σT^4 or R_s^{atm} as input variables did not yield a significant

decrease in the results. Leaving out R_s^{down} had the biggest impact, followed by H. A network configuration with R_s^{down}, H and 2 or 3 other input variables provided nearly always reasonable results. It should be noted that cloud cover indirectly uses R_s^{down} as it was calculated as the ratio R_s^{down}/R_s^{atm}. If no turbulent data from the flux station were available the input variables providing the best results were R_s^{down}, T, $\varkappa_r$, u, R_s^{atm}, σT^4 and c_c. Of these variables R_s^{down} and $\varkappa_r$ explained most of the variance. Use of only artificially obtained data, such as time and R_s^{atm} was not adequate to explain any variation whatsoever. However, to improve the results R_s^{atm} could be used in combination with other variables.

Table 6.2: *Simulation of $\sigma T^4 - R_l^{down}$ by different neural network configurations. Also shown are the number of hidden nodes, the RMSE and the ranking of the results of the calibration (cal) and the validation (val) data set.*

Input signals	Nodes	RMSE cal.	RMSE val.	Order cal.	Order val.
$R_s^{down}, \varkappa_r, H, \zeta, \sigma T^4$	3	23.00	24.48	27	29
$R_s^{down}, \varkappa_r, H, \zeta, \sigma T^4, c_c$	3	18.60	20.30	9	7
$R_s^{down}, \varkappa_r, H, \zeta, \sigma T^4, c_c$	4	18.64	20.50	10	9
$R_s^{down}, \varkappa_r, H, \zeta, \sigma T^4, c_c$	2	20.14	21.05	16	11
$R_s^{down}, \varkappa_r, H, \zeta, R_s^{atm}, \sigma T^4, c_c$	3	19.15	21.67	12	17
$R_s^{down}, \varkappa_r, H, u_*, \zeta, R_s^{atm}, \sigma T^4, c_c$	4	16.84	20.40	4	8
$R_s^{down}, \varkappa_r, H, u_*, \zeta, R_s^{atm}, \sigma T^4, c_c$	5	16.52	19.49	2	1
$R_s^{down}, \varkappa_r, H, u_*, \zeta, R_s^{atm}, \sigma T^4, c_c$	7	16.83	19.49	3	1
$R_s^{down}, T, \varkappa_r, H, \zeta, \sigma T^4, c_c$	3	19.31	21.08	13	12
$R_s, T, \varkappa_r, H, \zeta, \sigma T^4, c_c$	4	17.96	21.35	7	16
$R_s, T, \varkappa_r, H, \lambda_E E_{res}, u_*, \zeta, R_s^{down}, \sigma T^4, c_c$	7	16.08	19.99	1	6
$R_s, T, H, \sigma T^4, c_c$	3	21.41	22.97	24	22
t, R_s^{atm}	3	31.94	32.00	45	45
t, R_s^{atm}	8	30.70	31.42	41	40
t, R_s^{atm}	4	31.40	31.71	43	43
$R_s^{down}, T, \varkappa_r, u, R_s^{atm}, \sigma T^4, c_c$	4	20.18	22.17	18	20
$T, \varkappa_r, u, R_s^{atm}, \sigma T^4, c_c$	4	24.64	25.94	32	34
R_s^{atm}	4	31.56	31.86	44	44
c_c	4	25.65	26.20	35	35
c_c	2	25.78	26.20	36	35
c_c	1	25.93	26.24	37	36
$t, T, \varkappa_r, u, R_s^{atm}, \sigma T^4$	4	24.19	25.49	31	31
$T, \varkappa_r, u, R_s^{atm}, \sigma T^4$	4	24.64	25.88	33	33

continued on next page

continued from previous page

Input signals	Nodes	RMSE cal.	RMSE val.	Order cal.	Order val.
$t, H, u_*, \zeta, R_s^{atm}$	4	30.30	30.53	40	39
H, u_*, ζ, R_s^{atm}	4	27.58	29.12	39	38
H, u_*, ζ, R_s^{atm}	3	25.08	26.86	34	37
H, u_*, ζ, R_s^{atm}	2	31.13	31.65	42	42
$T, \varkappa_r, c_c$	2	23.68	24.37	29	27
$T, \varkappa_r, c_c$	6	21.45	24.95	25	30
$T, \varkappa_r, c_c$	3	23.60	24.41	28	28
$T, \varkappa_r, u$	2	26.13	25.87	38	32
$\varkappa_r, u, c_c$	2	23.71	24.21	30	26
$\varkappa_r, H, u, c_c$	2	21.83	21.27	26	15
$\varkappa_r, H, u, c_c$	3	21.06	21.73	23	19
$R_s^{down}, \varkappa_r, u, H, u_*, \zeta, R_s^{atm}, \sigma T^4, c_c$	4	17.32	19.50	5	3
$R_s^{down}, \varkappa_r, H, u_*, \zeta, \sigma T^4, c_c$	4	17.71	19.84	6	5
$R_s^{down}, \varkappa_r, H, u_*, \sigma T^4, c_c$	4	18.30	19.74	8	4
$R_s^{down}, T, \varkappa_r, H, c_c$	4	18.90	20.60	11	10
$R_s^{down}, T, \varkappa_r, H, c_c$	3	20.48	21.18	20	14
$R_s^{down}, T, \varkappa_r, u_*, c_c$	4	20.16	23.77	17	25
$R_s^{down}, T, \varkappa_r, \zeta, c_c$	4	19.74	23.32	15	24
$\varkappa_r, H, \zeta, \sigma T^4, c_c$	3	20.57	22.27	21	21
$\varkappa_r, H, \zeta, \sigma T^4, c_c$	4	19.52	23.02	14	23
$\varkappa_r, H, u_*, \sigma T^4, c_c$	3	20.81	21.71	22	18
$R_s^{down}, \varkappa_r, H, \sigma T^4, c_c$	3	20.47	21.12	19	13

6.4.2 Gap filling λE

To derive the optimal neural network configuration for the differences of λE, i.e. $\lambda E - \widehat{\lambda E}$, a number of neural network configurations has been tested using L_{AI}, R_s^{down}, R_l^{down}, $\varkappa_r$, $\varkappa$, T_a, u, θ, D_θ.

Measuring λE during wet conditions is extremely difficult. Open path sensors tend to produce spiky results or are shut down. Because of smearing of water vapour in the tubes under such conditions, closed path sensors often underestimate λE. If under these conditions data are excluded from the training data set of the regressor there is a risk of results becoming biased towards dry conditions. For example in the Netherlands wet periods in summer are often associated with mainly westerly winds, while prolonged dry periods are associated with easterly winds. Also during wet conditions, λE is more controlled by the efficiency of the aerodynamic transport of water vapour. This control is in contrast to dry conditions when λE is largely

regulated by the land surface. To overcome these problems inherently associated with the measurement of λE during wet conditions, and following Gash et al. (1999), λE has been calculated as the residual of the energy balance. Hence, a neural network was separately trained on relatively dry conditions NN_{dry} ($P \leq 0.5$ mm d^{-1}) respectively wet conditions NN_{wet}($P > 0.5$ mm d^{-1}).

For *dry* days the flux differences were calculated using the measured λE with $\widehat{\lambda E}$ calculated using the "Penman-Monteith equation"with a fixed surface resistance $r_s = 100$ s m^{-1} and also applying the Makkink equation (Makkink, 1959). The latter equation is applied in the Netherlands to calculate the reference evaporation and provides a simple estimate of the maximum λE based only on R_s^{down} and T:

$$\lambda E_{ref} = 0.65 \frac{\Delta_\varkappa}{\Delta_\varkappa + \gamma} R_s^{down} \tag{6.4}$$

For *wet* days the differences were calculated using λE being derived as the residual of the energy balance and $\widehat{\lambda E}$ based on the Penman-Monteith equation using a fixed surface resistance set to $r_s = 0$ s m^{-1}. Also the interception loss calculated as the difference between P and T_f was tested as an extra input variable for the neural network.

For the pine forest at the Loobos site, λE was most sensitive to $\varkappa_r$ and T_a. For the years studied, this site did not show a significant influence of θ on λE as simulated by the neural network. Although the pine forest at this site is located on a sandy soil with a relatively deep groundwater table, the corresponding deep rooting system made the trees less sensitive to the soil water deficit θ_D.

This insensitive behaviour towards θ is in contrast to that of the poplar forest at the Fleditebos site, which is located on a fine textured clayish soil with a shallow groundwater table. λE of this forest showed to be sensitive to θ during two years with a relatively dry soil and low groundwater table and no sensitivity during the relatively wet year. Including θ as an input variable for the neural network improved the simulation results of λE at this site.

Fig. 6.3 shows the 1996 measured evaporation rate and the evaporation rate simulated using a neural network trained on the data of the years 1995, 1997 and 1998 for the poplar stand at the Fleditebos site.

Setting $r_s = 0$ s m^{-1} overestimated λE. It thus increased the scatter in the differences to be explained by the neural network and did not improve the results. Using θ during dry periods improved the results, also for the relatively wet year. Including the interception did not improve the results.

Using a different regressor for wet and dry conditions, provided a "best estimate" for E in 1996 of 632 mm yr^{-1} (see Table 6.3).

This "best estimate" for E corresponds well with E derived as the residual of the water balance, i.e. 653 mm yr^{-1}. The use of only dry periods to train the neural

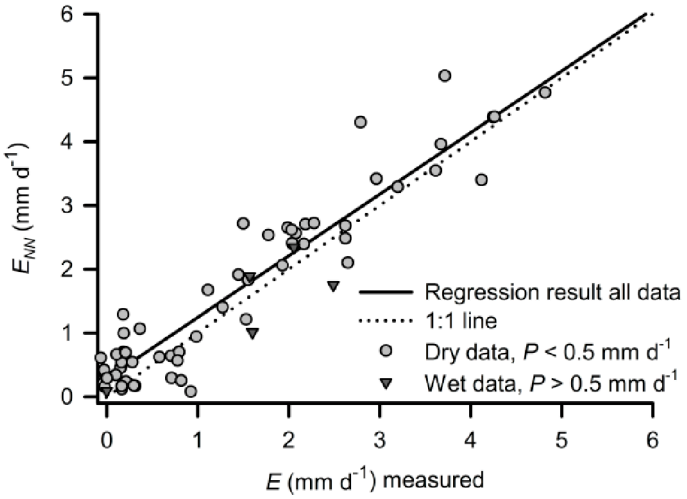

Figure 6.3: *Daily sums of measured evaporation E and simulated evaporation E_{NN} for the poplar forest at the Fleditebos site in 1996. The simulation results are the combined results of a neural network trained separately for dry and for wet periods in the years 1995, 1997 and 1998. The regression results are: $E_{NN} = 0.28 + 0.97E$ ($R^2 = 0.88$).*

Table 6.3: *Total evaporation E at the Loobos site with missing data filled using different filling techniques. "Best estimate" (NN), i.e. a combination of measured data and data of NN_{dry} and NN_{wet}, NN trained for dry periods only (NN_{dry}), NN trained for wet periods only (NN_{wet}), E derived as the residue of the water balance (Water balance), precipitation (P), change in soil moisture storage (ΔS), all in mm yr^{-1}.*

Year	E				P	ΔS
	NN	NN_{dry}	NN_{wet}	Water balance		
1996	632	546	708	653	699	46

network clearly underestimated E, while the neural network trained only for wet periods overestimated $\dot{E}$.

In Table 6.4 the results of different filling techniques are compared. The estimates of the diurnal variation, look-up tables and the non-linear regression have been taken from Falge et al. (2001). The following remarks on these 3 methods can be made.

- The most important drivers for the look-up tables and the non-linear regression methods were R_{net} and $\varkappa_D$, taking into account the negative H and hence the additional energy available during wet conditions;

- Total E resulting from the look-up tables and the non-linear regression were

Table 6.4: *Total evaporation E at the Loobos site with missing data filled using different filling techniques. Neural Network (NN), NN trained for dry periods only (NN_{dry}), diurnal variation (Diur. var.), look-up table (Look-up), non-linear regression (regr.), precipitation (P), throughfall (T_f), interception (E_i), all in mm yr^{-1}. Also shown are the number of missing days and the number of days with $P > 0.5$ mm d^{-1}.*

Year	E					P	T_f	E_i	Number of days	
	NN	NN_{dry}	Diur. var.	Look-up	Regr.				Missing	Rain
1997	605	433	444	333	333	787	546	241	49	75
1998	703	399	392	362	362	1266	898	368	125	87
1999	691	574	618	607	607	861	541	320	156	83

identical;

- Diurnal variation technique provided the highest estimates of E of these three methods;
- Magnitude of the differences between the methods varied from year to year.

The NN_{dry} compared relatively well with the 3 methods mentioned before. NN in Table 6.4 yielded the highest estimates. This difference is mainly because a better measure for λE during wet periods was used to train the regressor of NN.

The fact that the other methods underestimated E is evident when comparing with the amount of E_i. Especially in 1998, which was a relatively wet year, this is clear. The part of the total E left for transpiration was negative for the look-up tables and the non-linear regression methods. From Table 6.4 it is also clear that the results of the filling procedure did not only depend on the number of missing data, but also on the specific period for which the data were missing. For example, the results of all methods were much better comparable to each other in 1999 than in 1997. This difference may be caused by:

- Combination of a large number of days missing in the spring of 1999;
- High E-values for the days with measurements;
- Relatively high R_{net} (50% higher than in 1997 and 1998) in the spring of 1999 resulting in a relatively high E due to the strong dependency on radiation.

The average uncertainty due to the gap filling in the daily E for all years and different sites using the neural network technique described here was 0.39 mm d^{-1} (σ = 0.05 mm d^{-1}). However as stated before, the uncertainty involved in the

Table 6.5: *Percentage of missing data of the Automatic Weather Station (AWS) and of missing data of the eddy correlation system (sensible heat flux H) with the uncertainty due to the gap filling in the total latent heat flux, $\Delta_{\lambda E}$.*

			Bankenbos %	Fleditebos %	Kampina %	Loobos %
1995	Missing data	AWS	16	0	-	4
		H	28	15	-	20
	Uncertainty	$\Delta_{\lambda E}$	6	4	-	6
1996	Missing data	AWS	22	3	8	0
		H	21	10	7	21
	Uncertainty	$\Delta_{\lambda E}$	7	3	2	7
1997	Missing data	AWS	2^{*}	16	0	0
		H	28^{*}	39	3	8
	Uncertainty	$\Delta_{\lambda E}$	7^{*}	10	1	2
1998	Missing data	AWS	-	0^{+}	$0^{\#}$	14
		H	-	8^{+}	$21^{\#}$	31
	Uncertainty	$\Delta_{\lambda E}$	-	2^{+}	$5^{\#}$	7

*) Measurements ended on DOY 265 1997 (for the whole year: missing data AWS 29%, H 48%, $\Delta_{\lambda E}$ 13%)
$^{+}$) Measurements ended on DOY 117 1998 (for the whole year: missing data AWS 68%, H 70%, $\Delta_{\lambda E}$ 19%)
$^{\#}$) Measurements ended on DOY 231 1998 (for the whole year: missing data AWS 37%, H 50%, $\Delta_{\lambda E}$ 11%)

simulated data depends on several aspects and thus varies from period to period and from site to site.

In Table 6.5 total uncertainty $\Delta_{\lambda E}$ for each site per year is given. To estimate the uncertainty for each site one year was selected and artificial gaps with different lengths were created. $\Delta_{\lambda E}$ is based on the estimated bias and the length of the data gaps in the flux data. The total uncertainty that can be attributed to the gap filling is well below 10% for all sites and all years. If more than 50% of the data are missing, $\Delta_{\lambda E}$ may become 20%, i.e. see remark $^{\#}$) in Table 6.5.

6.4.3 Effect of the number of missing records on uncertainty

The influence of the number of missing data on the uncertainty of the simulated data was studied by creating artificial gaps in a data set of incoming long-wave radiation R_l^{down}. The network configuration being used is depicted in Fig. 6.4.

The activation function for these nodes was Eq. 6.2. All data have been taken from the Loobos site. Training data were mainly selected from periods before and

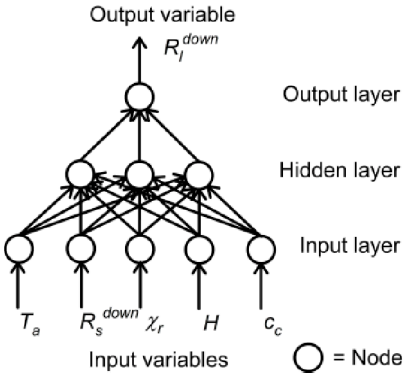

Figure 6.4: *Neural network configuration used for the simulation of the downward long wave radiation* R_l^{down}.

after the gap periods. The data set covered the period between 1 February and 24 June. The data records were selected in such a way that the period with missing data (gap) was followed by a period with good quality data. An exception was the data set with the longest data gap. For this data set the data gap was located either in the winter period with the calibration period (training) in the summer or vice versa. Fig. 6.5 shows the RMSE of the calibration and of the validation runs as a function of the number of missing data. Total number of records being used is 3025 and the average value of R_l^{down} for all data used is 307.0 W m^{-2}. For all runs the same total number of records (i.e. calibration plus validation data) has been used. The use of the same total number of records implies that, the more data were missing, the less data were available for training. This difference in available training data explains why the RMSE of the calibration sets was slightly decreasing with the number of missing data increasing. For about 40% of the missing data the RMSE of the calibration and validation set are comparable. At higher percentages the RMSE of the validation set increases slowly, above 90% rapidly.

6.5 Discussion

Because of the discrete character of the precipitation data, the use of neighbouring stations is often the only method to fill missing precipitation data. The results improved with decreasing distance between the stations and with increasing time step, i.e. daily or longer time steps. For our study the use of two completely independent rain gauges assured almost 100% data coverage.

The comparison between different methods to fill gaps in data sets (see Table 6.4), demonstrated that satisfying results were obtained using a neural network as

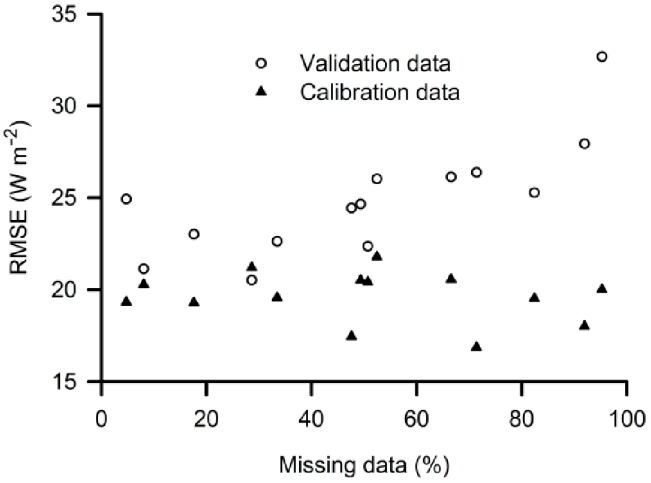

Figure 6.5: *The RMSE of the calibration data set respectively of the validation (missing) data for the incoming long wave radiation R_l^{down} at the Loobos site using data sets with increasing length of the period with missing data.*

non-linear regressor. These results are in line with findings of Moffat et al. (2007). Although their study was focused on net carbon fluxes, the differences between the gap filling techniques are applicable to all eddy-correlation data.

Selection of reliable data may create a data set biased towards specific conditions. Comparing E after gap filling with $E_i = P - T_f$, demonstrated unrealistic results if gap filling is exclusively based on dry conditions (see Table 6.4). The latter implies that the values of E as presented by Falge et al. (2001) are most likely underestimates of the true E-value. Our results show that at least for the Loobos site the underestimation is mainly attributed by the exclusion of wet periods. To a lesser extend it may also be caused by the gap filling technique used, i.e. either Look-up table or Regression.

The main advantage of the use of a neural network is that there is no need to find a consensus model to generate the flux data: consensus on the input data and the transfer function is sufficient.

Most studies comparing gap filling techniques assume the same set of data being available, which implies an automatic weather station data set. However, having in addition the sonic anemometer measurements available and hence the friction velocity and sensible heat flux data will also be available. As shown in our study, using this information will greatly improve the performance of the gap filling technique. Incorporating these other measurements in a standard protocol is complicated, because as shown in Table 6.1 a large number of different neural network configurations

is possible. The best configuration will depend on the site characteristics as well as the data available.

Filling data sets of which the number of missing data are less than the number of data available for training of the regressor, gave an uncertainty to the simulated data being comparable to the calibration data set. For these cases the uncertainty depended primarily on the capability of the regressor to simulate the physical dependencies and it was independent of the size of the data gap. If the number of missing data became more than the number of training data the uncertainty in the estimates increased as well. The magnitude of the uncertainty depends strongly on the size of the data gap (see Fig. 6.5).

The uncertainty due to the use of simulated data to fill the missing records is for E in normal years well below 10% (see Table 6.5). Large parts of this uncertainty can be attributed to the measurement uncertainties (see Chapter 5) rather than the gap filling uncertainties.

6.6 Conclusions

The application of neural networks contributes to highly consistent data series. The algorithm used is only valid for the conditions it is trained for. Hence it gives no guarantee for the ultimate quality of the results. This dependency on the training conditions was especially clear in the comparison of the filling methods being used for the estimation of E.

Not taking into account the weak points of the measuring technique used and the differences in conditions during wet and dry periods leads to a serious underestimation of E (up to 50% of total E).

The best validation results simulating E were obtained using a neural network configuration with R_s^{down}, $\varkappa_r$, H, u_*, ζ, R_s^{atm}, σT^4 and c_c as input variables and 5 hidden nodes. A network configuration with R_s^{down}, H and 2 or 3 other input variables provided nearly always reasonable results.

The magnitude of the uncertainty depends strongly on the size of the data gap. The uncertainty in E because of gap filling is in an average year well below 10%.

Chapter 7

Dry canopy evaporation

7.1 Introduction

Under dry conditions the evaporation from a forest consists of two parts: transpiration by the vegetation and evaporation from the bare soil underneath the vegetation. Of these two evaporation processes, transpiration is for forested surfaces the main contributor. Under conditions with a relatively moist soil, water loss is largely controlled by the physical boundary layer resistance r_a. The magnitude of r_a depends on the roughness characteristics of the canopy and the wind speed. Under conditions when the soil is drying out, the major control of water loss becomes physiological, often represented by a single surface or canopy resistance r_s. (e.g. Monteith and Unsworth, 1990).

Forests, however, are complex eco-systems, usually with great variability in space, both horizontally as well as vertically. The most extreme compositions are: on one side a forest with a single tree species and no or nearly no understorey (e.g. beech forest in the mid latitudes), and on the other side a forest with such a diversity in tree species and a lush understorey that there is no free air space left (e.g. tropical rain forest). In the northern mid latitudes where the Netherlands is located, there is almost no natural forest and most forest stands are basically planted single tree species. In these forests the undergrowth composition is influenced by the available radiation which depends on shading by the trees, available nutrients which depends on soil type, litter quality and atmospheric deposition, and hydrological regime. The fact that the undergrowth is seen as a competitor of trees, e.g. bracken (*Pteridium aquilinum*) in the UK (Roberts et al., 1980), dwarf bamboo (*Sasa kurilensis*) in Japan (Ishii et al., 2008), rhododendron (*Rhododendron ponticum*) in Belgium (Nadezhdina et al., 2004) and wild berry (*Prunus serotina*) in the Netherlands (Koop et al., 2000), illustrates the potential impact of the undergrowth on the water balance of a forest.

To overcome periods of droughts it is necessary for forests, i.e. a combination of trees and undergrowth, to reduce the evaporation rate to preserve water. To achieve this reduction in water loss, some tree species drop their leafs, e.g. *poplar* trees, while others close their stomata, e.g. *pine* trees.

It is expected that climate change will come among others with prolonged dry periods without rain (Christensen et al., 2007). For areas like the lower parts of the Netherlands, the connection between the root zone and the groundwater level often determines the composition and hence the quality of the natural vegetation cover. Prolonged disconnection from the groundwater may thus have serious consequences for such eco-systems. In this chapter special attention will be given to the derivation of parametrizations for water stress of forests in The Netherlands.

Transpiration loss of water is not only regulated by the availability of water at the root-soil interface, but also by other bio-physical processes causing stomatal closure.

Cochard et al. (2002) have shown that trees are able to "sense" a coming drought, while the trees are still being supplied with water at rates adequate to meet maximum transpiration requirements. Here we postulate that this process is related to the drying of the top soil layer where most roots are present combined with extractable water being available at deeper layers. It has been shown that vegetation, and especially trees are able to extract water from deeper layers enabling them to survive periods of drought (e.g. Rambal, 1984; Talsma and Gardner, 1986). The "sensing" of drought is most likely a combination of different drivers affecting the leaf water potential, as a dry top soil layer is mostly coinciding with relatively high radiation load R_s^{down}, high air temperature T_a and a large vapour pressure deficit e_D. The exact functioning is however still unclear (e.g. Woodruff et al., 2007) and may or may not be caused by feedback mechanisms using enzymes such as ABA (e.g. Franks, 2004; Franks et al., 2007).

The flow of soil water to the roots is much better understood (e.g. Feddes and Raats, 2004). The rate of water uptake depends on rooting density, soil hydraulic conductivity, and the pressure difference in the soil and at the soil-root interface. Non-uniformity of root water uptake from different soil depths as caused by differences in root densities and water availability, greatly complicates the understanding of the feedbacks of water stress on canopy resistance. In general the feedback of soil water on canopy conductance is simulated using a single function based on a single soil water parameter, such as used in Eq. 2.51. However, this soil water parameter is not necessarily a good representation of the complex relationship between stomatal closure and available soil water. To improve on this relationship, we will test a model for the stomatal closure that is able to represent the feedbacks by two distinct soil water sources, i.e. the water content of the top soil and of the soil layer at the depth of the deepest roots.

The flow of water from the soil, through the plant into the atmosphere is determined by a series of resistances: flow of soil water from a point in the soil towards the interface with the roots, - i.e. through the epidermis of the roots, - from the roots to the leaves and finally through the stomata into the stomatal cavities. Under

conditions of limited water availability, the main contributor to soil water stress is the resistance of the transport of water from the soil to the roots. The magnitude of this resistance depends on the root distribution and the hydraulic characteristics of the soil. Root distribution is variable in space and time and depends among others on plant species, bulk density of the soil and on the water and nutrient availability. Hence, a comprehensive study of effects of soil water stress on stomatal closure would consist of a dynamic root growth model as well as a dynamic unsaturated zone flow model. However, for field studies and for land surface schemes for regional models such an approach is hardly achievable. Hence a simplified approach is proposed.

The *first objective* of Chapter 7 is to derive parameter sets for a number of different forest types in the relatively small area of the Netherlands as well as to investigate if these sets add any additional information that may be used to describe regional heterogeneity in the transpiration rates of forest. Special attention will be paid to conditions of possible water stress and the effect of the groundwater reservoir.

The *second objective* of this Chapter is to analyse the separate contributions of the trees and the undergrowth to the total water loss of the forest sites studied.

Data from 5 sites in the Netherlands will be used. For a detailed description of the characteristics of the sites the reader is referred to Chapter 3. For a description of the continuous measurement system used, see Chapter 4. In the present chapter only some additional information on the undergrowth at the *poplar* forest of the Fleditebos site and at the *pine* forest of the Loobos site will be given. At these 2 sites additional eddy correlation measurements were taken below the tree canopy. The measurements of sapflow at the *pine* stand will be used as an independent check of the performance of the dual source model.

7.2 Leaf area development of undergrowth at Fleditebos and Loobos site

To enable the study of the undergrowth as a separate evaporation source a second flux station has been employed below the canopy at the two sites with a significant undergrowth. At the Fleditebos site the herbal undergrowth is covered by an almost closed canopy cover of *poplar* trees i.e. $c_{veg} = 0.8$ in summer time and covered by bare trees in winter time i.e. $c_{veg} = 0.2$. At the Loobos site the grass undergrowth is covered by a relatively open canopy of *pine* trees i.e. $0.55 < c_{veg} < 0.7$.

7.2.1 L_{AI} of the herbal undergrowth of the *poplar* forest

At the *poplar* site the herbal undergrowth started as early as February, with a maximum growth rate in April, leading to a L_{AI} close to 4 m^2 m^{-2}. In the second half of May L_{AI} started to decline although the height still increased to reach its maximum of 1.2 m to 1.3 m in July and August. Towards the end of September the height of the undergrowth decreased to 0.4 m and L_{AI} became $\leq$ 1.0 m^2 m^{-2}. In October some regrowth occurred, i.e. average height 0.15 m and L_{AI} 1.5 m^2 m^{-2}, which lasted until the end of November.

7.2.2 L_{AI} of the grass undergrowth of the *pine* forest

At the *pine* site the grass undergrowth showed a similar seasonal pattern as the herbal undergrowth of the *poplar* forest. However, the maximum L_{AI}, i.e. 1.5 m^2 m^{-2} of the living grass biomass was reached somewhat later at the end of June and started to decline at the end of July. Regrowth in October was observed with L_{AI} reaching 1.0 m^2 m^{-2}. It should be noted that in more recent years there was an increase in other species of the undergrowth. A survey done in 2009 showed next to the grass fractional cover of 46% also a fractional cover of 5% by *Vaccinium Myrtillus* and 5% by young *pine* trees. Total L_{AI} of the undergrowth i.e. also including mosses varied in 2009 between 1.1 and 2.3 for winter and summer respectively.

7.3 Root water uptake

7.3.1 Root water uptake parametrization

The parametrization of the root water uptake can be separated into two coupled processes:

1. Effects of water stress on the closure of the stomata,

2. Location of the root water uptake.

The first process determines the total amount of water that will evaporate and is influenced by stress on the stomata as caused by water shortage. The second process determines how root water uptake of this total amount of water is distributed over the different soil layers. It is assumed that allocation of root water uptake is based on minimizing the consumption of energy i.e. most of the water will be taken up in soil layers having the lowest soil water pressure and the highest root density (see Fig. 2.2).

For most forests root distribution can be split into two parts: the upper part with a high root density and the lower part with a low root density often existing of tap roots only.

To model the effect of water stress on stomatal closure we take the differences between shallow and deeper soil layers into account. This distinction in soil depth leads to a function for the soil water induced stress being composed of a fast and a slow reacting component. The fast reacting component reflects mainly the vegetation characteristics towards water stress and depends on the soil water content of the upper soil layer. The slow reacting component takes into account the slow depletion of the available water storage as well as the possible additional water available by capillary rise from the groundwater reservoir. The latter is mainly determined by changes in hydraulic conductivity. In the case of a tree canopy with undergrowth, the upper soil layer will include both: roots of trees and undergrowth, while the deeper layer may consist of tree roots only. For time steps less than a day, it is assumed that the upper and the lower soil layer act as two independent parallel sources of soil water.

Taking into account the distinction between the upper and lower soil layer, the soil water stress function becomes (see also Fig. 7.1):

$$f(\theta) = f(\psi(z_1))f(\psi(z_2)) \tag{7.1}$$

The function $f(\psi(z_1))$ represents primarily the direct and indirect feedback mechanisms of the vegetation to limited water availability in the upper soil layer z_1.

The function $f(\psi(z_2))$ represents available soil water under relatively dry conditions, reflecting the soil water conditions of a relatively thick layer at the bottom of the root zone z_2. The thickness of the layer allows to take potential vertical root growth under drying conditions into account.

As the exact functioning of stomatal closure is still unclear and complex feedback mechanisms may exist for the stress functions, the following empirical approach will be used for the feedbacks by the soil water stress in the top layer. Here we assume for $f(\psi(z_1))$ an exponential function similar to Eq. 2.51.

To simulate the influence of added soil water available to the vegetation by for example capillary of a groundwater reservoir, 2 options will be tested for $f(\psi(z_2))$:

The *first* option $f(\psi(z_2))_A$ is based on the assumption that at the deeper soil layers the availability of water is mainly driven by the hydraulic characteristics of the soil. It is assumed that soil layers z_1 and z_2 function as two parallel sources of soil water. Based on Sinclair (2005) and Sinclair et al. (2005) we derived a simplified equation for g_s:

$$\frac{g_s}{g_{s,\max}} = 1 - \frac{\psi(z_2)}{\psi_c} \tag{7.2}$$

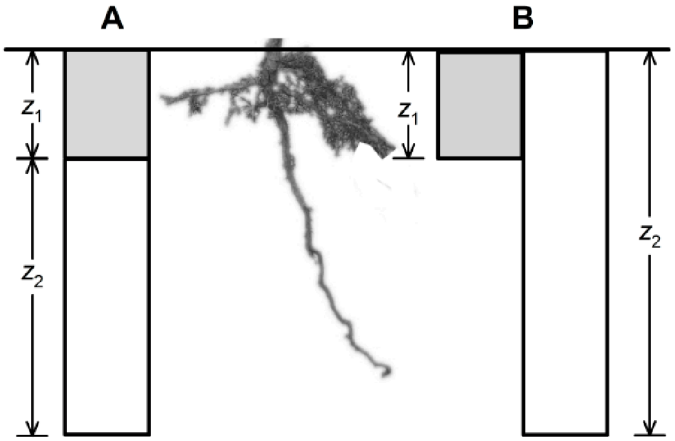

Figure 7.1: *The soil water stress model $f(\theta) = f(\psi(z_1))f(\psi(z_2))$, with $f(\psi(z_1))$ representing the soil water feedbacks of the upper soil layer where 80 - 90% of the roots are found. The left hand side of the figure shows model option A for $f(\psi(z_2))_A$ representing the feedback of the deepest roots. The right hand side shows model option B for $f(\psi(z_2))_B$ representing the soil water feedback of the total root zone.*

where $\psi(z_2)$ is the soil water pressure at depth z_2 and ψ_c represents the water pressure of the canopy. Sinclair (2005) showed that changes in the hydrostatic pressure of the leaves has no significant impact on the relative transpiration rate. Hence ψ_c is assumed to be constant at -1.5 MPa. The resulting curve is independent of the soil type.

The *second* option $f(\psi(z_2))_B$ is based on the assumption that roots have access to all soil water, i.e. from the surface down to the depth of the deepest roots.

Because in the Netherlands really dry conditions are at the moment relatively scarce, there is a lack of field measurements during prolonged dry periods. To overcome the limited number of data available representing the feedbacks under dry conditions, for the second option $f(\psi(z_2))_B$, a parametrization based on measurements under more extreme conditions is used. Here an empirical function based on data of 5 different forests in France, i.e. *oak*, *beech*, *fir*, *spruce* and *pine* will be used (Granier et al., 2000):

$$f(\theta_D) = \frac{\mathrm{p}_1 + \mathrm{p}_2(1-\theta_D) - \left[\{\mathrm{p}_1 + \mathrm{p}_2(1-\theta_D)\}^2 - 2.8\mathrm{p}_1\mathrm{p}_2(1-\theta_D)\right]^{1/2}}{1.4} \tag{7.3}$$

where $\mathrm{p}_1 = 1.154$ and $\mathrm{p}_2 = 3.0195$. The soil water deficit θ_D will be based on available soil water in the entire root zone.

Both options do not require site specific parameters. To derive site specific parameters sets only the parameters for $f(\psi(z_1))$ have to be optimized.

The soil water pressure ψ is defined as (see also Eq. 2.8):

$$\psi = -\frac{\rho_w g}{\alpha}\left[\left(\frac{1}{S}\right)^{1/m} - 1\right]^{1/n} \tag{7.4}$$

where S denotes the relative soil water saturation (see Eq. 2.50).

To convert measured θ into ψ, parametrizations will be used either determined by analysing soil samples in the laboratory or taken from standard soil databases (e.g. Wösten et al., 1999).

7.4 Methods used to derive surface conductance

The response of the transpiration rate to changes in environmental conditions will be analysed based on two separate assumptions:

- The forest is a unique eco-system that behaves as one "big leaf";

- The undergrowth is an important part of the forest eco-system and needs its own parametrization.

To model the effects of water stress both assumptions need a parametrization depending on the water uptake by roots. The parametrization to simulate water stress as has been described in Chapter 2 is adequate if the objective is to derive a unique set of parameter values for a specific site, i.e. a unique combination of vegetation and soil.

If the objective however, is to derive parameter sets allowing to change vegetation cover at sites, disentangling of the vegetation and soil characteristics is required. This latter objective will not be completely achievable. Not only the vegetation species, but also soil characteristics, such as dry bulk density and nutrient availability have major impacts on the rooting system. Also over longer periods, vegetation itself is one of the drivers in the soil formation processes.

With these shortcomings in mind, an attempt will be made to have a first order separation of the controls on water flow affecting stomatal closure by soil characteristics and vegetation. This separation is especially aimed at vegetation types with deep rooting systems, tapping from water sources such as the unsaturated zone just above a groundwater aquifer, which may be considered being independent of the present daily weather.

7.4.1 "Big leaf" approach

The "big leaf" stomatal conductance g_s has been derived from flux measurements taken above the canopy and by inverting the Penman-Monteith equation (Eq. 2.35):

$$g_s = \frac{1}{r_s} = \frac{\gamma \lambda E}{r_a \Delta_e A + \rho c_p e_D - r_a \left(\Delta_e + \gamma\right) \lambda E} \tag{7.5}$$

The available energy A is derived as the sum of measured H and λE.

7.4.2 Dual source model for two vegetation layers

The separate responses of trees and undergrowth have been analysed based on eddy-correlation measurements taken above as well as below the tree canopy at the *poplar* forest of the Fledite site and the *pine* forest at the Loobos site. The contribution of the two vegetation layers has been simulated using the sparse canopy model of Shuttleworth and Wallace (1985) and Dolman (1993), as has been described in Section 2.5.5.

7.4.3 Radiative transfer scheme for sparse canopies

In many studies the upper layer vegetation is assumed to be a continuous horizontal layer. For sparse forest, with $c_{veg} < 1$ as often found in managed forests at mid latitudes, this assumption is not necessarily a good one. A number of processes such as soil respiration, undergrowth transpiration and photosynthesis need a proper estimation of the amount of energy available below the tree canopy. Begue et al. (1996) showed that not taking inhomogeneity of discontinuous vegetation into account may result in an overestimation of PAR (Photosynthetic Active Radiation) interception by a factor of 1.5.

Continuous measurement of radiation under a canopy is rather complicated. To at least partly overcome this problem, use has been made of a two layer radiative transfer scheme (Hanan, 2001). This scheme also provides the opportunity to study the sensitivity of total transpiration in relation to the structure of the tree canopy: it makes use of both a macro structure and a micro structure sub-model. The macro structure sub-model describes the geometric distribution of the tree structure. The micro structure sub-model describes the fate of radiation in the tree crown as well as in the lower layer vegetation.

The tree canopy is modelled as a discontinuous canopy. The individual tree crowns have a cylindrical form. The gap probability is estimated using the fractional projected canopy cover. The macro structure model also provides the path length needed to calculate the radiation attenuation in the vegetation by the micro structure

model. A negative binomial distribution is used to estimate interception and scattering of radiation by leaves and branches. Leaves and branches each have their own surface and spectral properties. In the lower vegetation layer differences in spectral properties are used to distinguish between green and senescent leaves.

7.4.4 Stomatal conductance parameter optimization

The parameter values (i.e. constants) of the conductance functions (Section 2.5.3) are obtained by optimizing against the measured surface conductance g_s and by minimizing the sum of squares of model predictions and measurements using a Marquardt-Levenberg algorithm (SigmaPlot v10, Systat Software, Inc). All stomatal conduction functions were optimized simultaneously, resulting in curves maximizing the conductance for the different drivers.

7.5 Stomatal conductance using the "big leaf" approach

To analyse the differences in the behaviour of the stomatal conductance g_s between sites and years, the parameters for the Jarvis-Stewart model were optimized for each site and each year (Table 7.5). For this analysis the soil water content deficit θ_D was derived from θ measured in the root zone. The root zone is here defined as the soil layer where 80 to 90% of the roots are present (See Fig. 3.24). To reduce the effect of soil structural differences, θ_D has been normalized using the expression:

$$\theta_D = \frac{1}{\sum_{i=1}^{n} \Delta z_i} \sum_{i=1}^{n} \left(\frac{\theta_{\max} - \theta}{\theta_{\max} - \theta_{\min}} \Delta z \right)_i \tag{7.6}$$

where the difference between $\theta_{\max}$ and $\theta_{\min}$ determines the maximum amount of soil water being available for root water uptake during periods of drought. Often $\theta_{\max}$ and $\theta_{\min}$ are based on limits for ψ such as Field Capacity ψ_{FC} and Wilting Point ψ_{WP}. For agricultural crops the expressions $\psi_{FC} = -10^{2.0}$ Pa and $\psi_{WP} = -10^{4.2}$ Pa are usually taken. For $|\psi| > |\psi_{WP}|$ the vegetation will die. The exact value of ψ_{FC} may vary depending among others on the groundwater level. The crop type determines at what soil water pressure water ψ stress starts about to occur, e.g. for grass $\psi = -10^{2.7}$ Pa and for grains $\psi = -10^{3.0}$ Pa.

For forest these values differ, not only because of physiological differences between trees and crops, but also because of the extensive rooting system of trees. This rooting system compensates for differences in ψ both in the horizontal as well as in the vertical direction. To calculate θ_D for forest, Granier et al. (2007) used $\psi_{FC} = -10^{1.5}$ Pa and $\psi_{WP} = -10^{3.3}$ Pa.

The table in Appendix E gives an overview of θ at these different ψ by using the retention curves found at the sites. Fig. 7.2 shows for the 5 sites the amount of available θ between different ψ at depths close to the surface and at depths at, or close to the maximum rooting depth. The value $\psi = -10^{1.5}$ Pa coincides with the maximum change in slope of θ, from which point onwards an increase in water stress is to be expected.

However, comparing the values of θ at $\psi = -10^{1.5}$ Pa with the measured θ-values throughout the year shows that these values are extremely high and do rarely occur. In order to obtain a value better representing the amount of soil water available during a dry period under field conditions, $\theta_{\max}$ was determined based on two assumptions. Firstly: $\theta_{\max}$ was based on the lowest values for θ measured during the months with negligible evaporation, i.e. from November until April. Secondly: these data were only used when the soil was allowed to drain for at least 10 days with $P < 10.0$ mm 10d^{-1} and $P < 2.0$ mm d^{-1}.

These assumptions showed to be similar to the assumption of a fixed h over the different soil layers, i.e. for the sites with sandy soils $\psi = -10^{1.8}$ Pa, and for the Fleditebos site with its clay soil $\psi = -10^{2.1}$ Pa. Only the soil at 1.0 m depth under the *oak* forest at the Edesebos showed a sharp decline in θ at a much lower ψ, i.e. $\psi = -10^{0.4}$ Pa. This decline could imply that at this site the *oak*s may experience a stress signal from the roots at this depth at a much earlier stage than from the roots at other depths. Summarizing and following Granier et al. (2000) $\theta_{\min}$ was at all sites defined at $\psi = -10^{3.3}$ Pa.

To prevent evaporation of intercepted water contaminating the optimization of g_s dry records were used only. "Dry" was defined here as records being preceded by a period of at least 48 h without rain. To reduce the number of data with limited accuracy, the following additional data selection criteria were used: $H > 25$ W m^{-2}, $\lambda E > 25$ W m^{-2}, $T_a > 0$ ^{0}C, $\varkappa_r < 98\%$.

For the poplar forest at the Fleditebos site, the L_{AI} of trees and undergrowth reached their maximum in different months (see Fig. 3.13). These differences in timing of L_{AI} were used to separate the data set of the Fleditebos site in a period in which the undergrowth was dominant and a period in which the trees were considered dominant. Table 7.2 shows the optimized parameter sets for those two periods based on the "Big leaf" approach. The most distinct differences were found in the much higher $g_{s,max}$ and optimum temperature for the trees. If compared to the parameter set for all years of the poplar forest of Table 7.5, it shows the significant impact of the undergrowth on the magnitude of the overall parameters for this site.

The optimization results in Table 7.5 are presented for each year for the periods when the trees and/or undergrowth are most active, i.e. the period from June until the end of September. In Table 7.3 the maximum g_s is presented based on total L_{AI},

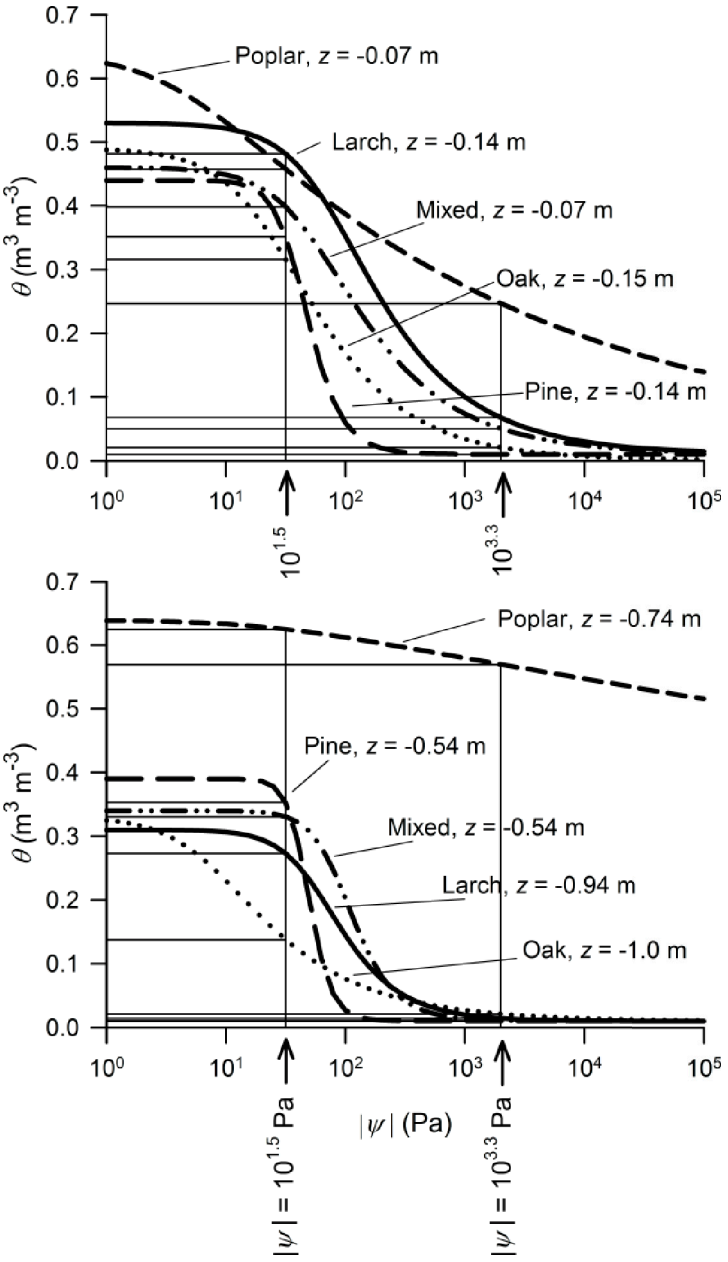

Figure 7.2: *The soil water content θ (m^3 m^{-3}) as a function of soil water pressure ψ (Pa). The top panel depicts the soil properties just below the soil surface (0.07 - 0.15 m), the lower panel depicts the properties of the deepest soil layer (0.54 - 1.0 m) measured. The amount of available soil water θ between $\psi = -10^{1.5}$ Pa and $\psi = -10^{3.3}$ Pa is illustrated by the horizontal lines (See also Appendix E).*

Table 7.1: *Optimized maximum surface conductance $g_{s,max}$ and stomatal conductance functions for each year and each site for the periods that trees and/or undergrowth were active, i.e. end of June until end of September. Also shown are the results of a specific site for all years. The constants a_R, a_T, c_eD, a_eD, c_{θ_D} and a_{θ_D} refer to the equations of Section 2.5.3. As a measure of fit, R^2 and the Standard Error of Estimate (SEE) are given. In 2001 at the Loobos site no soil water measurements were available because of lightning damage.*

Site	Year	$g_{s,max}$	a_R	a_T	c_{e_D}	a_{e_D}	c_{θ_D}	a_{θ_D}	R^2	SEE
Tree species		mm s^{-1}	W m^{-2}	^{0}C	hPa	hPa^{-1}	m^3 m^{-3}	-	-	mm s^{-1}
Bankenbos	1995	7.3	295.3	21.3	0.703	0.076	0.01	1.70	0.56	0.7
Larch	1996	8.1	78.5	17.3	0.323	0.096	0.85	0.27	0.51	0.9
	1997	7.2	374.0	20.7	0.460	0.072	0.01	0.10	0.59	0.7
	All	**7.3**	**233.7**	**19.4**	**0.164**	**0.075**	**0.58**	**0.35**	**0.50**	**0.8**
Edesebos	1988	7.5	280.0	16.3	0.233	0.070	0.49	1.68	0.66	0.7
Oak	1989	8.1	309.7	24.1	1.068	0.090	0.45	3.14	0.62	0.7
	All	**7.7**	**290.3**	**18.9**	**0.578**	**0.079**	**0.40**	**2.27**	**0.67**	**0.7**
Fleditebos	1995	8.0	251.1	19.0	0.182	0.076	0.20	0.39	0.52	1.1
Poplar	1996	8.8	165.5	14.9	0.001	0.093	0.57	0.01	0.47	1.3
	1997	7.8	57.7	14.7	0.069	0.063	0.57	1.04	0.58	1.2
	All	**8.3**	**146.6**	**16.8**	**0.034**	**0.082**	**0.30**	**0.22**	**0.48**	**1.2**
Kampina	1996	6.2	151.7	14.2	0.001	0.086	0.49	1.68	0.49	0.9
Mixed	1997	8.8	443.7	16.1	0.136	0.093	0.49	1.68	0.60	1.0
Forest	1998	6.5	0.1	11.5	0.001	0.060	0.49	1.68	0.56	1.2
	All	**7.7**	**216.8**	**16.0**	**0.045**	**0.100**	**0.49**	**1.68**	**0.49**	**1.1**
Loobos	1995	6.6	192.8	14.7	0.001	0.052	0.35	0.64	0.65	0.7
Pine	1996	11.9	166.1	15.6	0.397	0.127	0.12	0.45	0.61	1.1
	1997	10.0	438.4	16.1	0.293	0.076	0.15	0.26	0.62	0.9
	1998	10.5	479.0	19.8	0.439	0.075	0.16	0.25	0.63	0.8
	1999	10.3	323.0	16.2	0.644	0.086	0.27	0.54	0.69	0.9
	2000	11.1	363.3	17.5	0.763	0.100	0.49	1.68	0.65	1.2
	2001	12.9	321.4	24.6	0.107	0.115	-	-	0.60	1.0
	2002	8.0	126.6	20.1	0.102	0.070	0.01	0.04	0.50	1.0
	2003	9.4	385.8	16.8	0.248	0.088	0.43	0.66	0.50	0.9
	2004	14.2	548.5	19.5	0.101	0.102	0.49	1.68	0.80	0.9
	2005	9.1	217.4	19.0	0.222	0.079	0.60	0.08	0.62	0.9
	2006	10.4	465.3	22.1	0.794	0.078	0.55	0.01	0.74	0.7
	2007	10.2	144.2	17.6	0.231	0.085	0.48	1.00	0.74	1.2
	2008	12.4	511.1	15.3	1.153	0.090	0.56	0.01	0.80	0.7
	2009	14.1	309.6	23.7	0.655	0.114	0.52	1.00	0.73	1.0
	All	**9.9**	**289.3**	**17.8**	**0.390**	**0.090**	**0.38**	**0.44**	**0.62**	**1.0**

Table 7.2: *Optimized maximum surface conductance $g_{s,max}$ and stomatal conductance functions for the periods that the poplar trees or the undergrowth were dominantly active at the Fleditebos site. The constants a_R, a_T, c_eD, a_eD, c_{θ_D} and a_{θ_D} refer to the equations of Section 2.5.3. As a measure of fit, R^2 and the Standard Error of Estimate (SEE) are given.*

Vegetation	$g_{s,max}$ mm s^{-1}	a_R W m^{-2}	a_T ^{0}C	c_{e_D} hPa	a_{e_D} hPa^{-1}	c_{θ_D} m^3 m^{-3}	a_{θ_D} -	R^2 -	SEE mm s^{-1}
Tree	16.5	208.4	12.2	0.322	0.082	0.38	1.46	0.66	1.0
Undergrowth	7.4	174.2	6.2	0.205	0.145	0.49	1.68	0.09	1.6

Table 7.3: *The maximum surface conductance $g_{s,max}$ and actual conductance g_s for each site, with all reduction functions set to 1 and using the maximum total L_{AI}, i.e. combined L_{AI} of trees and undergrowth, of the site.*

Site	Tree species	$g_{s,max}$ mm s^{-1}	$L_{AI,max}$ m^2 m^{-2}	actual g_s mm s^{-1}
Bankenbos	*Larch*	7.3	1.8	13.1
Edesebos	*Oak*	7.7	4.9	37.7
Fleditebos	*Poplar*	8.3	6.3	52.3
Kampina	*Mixed forest*	7.7	5.0	38.5
Loobos	*Pine*	9.9	3.3	32.7

i.e. including L_{AI} of the undergrowth. The highest g_s during the year is found at the forest with the highest total L_{AI}, i.e. at the *poplar* forest of the Fledite site g_s = 52.3 mm s^{-1}. The *oak* forest of the Edesebos and the *mixed* forest of Kampina have almost identical $g_{s,max}$ and L_{AI} resulting in similar g_s, i.e. g_s = 37.7 mm s^{-1} and g_s = 38.5 mm s^{-1} for the *oak* and *mixed* forest respectively. Although at the *pine* forest of the Loobos site the L_{AI} is relatively low, this is compensated by the highest $g_{s,max}$ resulting in an almost identical g_s = 32.7 mm s^{-1} as the *oak* and the *mixed* forest. The *larch* forest at the Bankenbos site with almost no undergrowth has the lowest $g_{s,max}$ and L_{AI}, resulting in the lowest g_s = 13.1 mm s^{-1} of all 5 sites.

Fig. 7.3 shows the behaviour of the stress functions for the different sites, based on the parameter sets of all years of investigation as listed in Table 7.5.

As a reaction to the radiation load the *poplar* forest shows an almost on-off behaviour of the stomatal opening. The *pine* forest and to a lesser extend the *oak* forest demonstrate a much greater dependency on radiation.

The *larch* and *oak* forests show the highest optimal air temperature T_a, differing 3.4 °C with the lowest optimal T_a of the *mixed* forest. With the daytime T_a during the growing season being well above 10 °C, T_a will mainly have a negative feedback

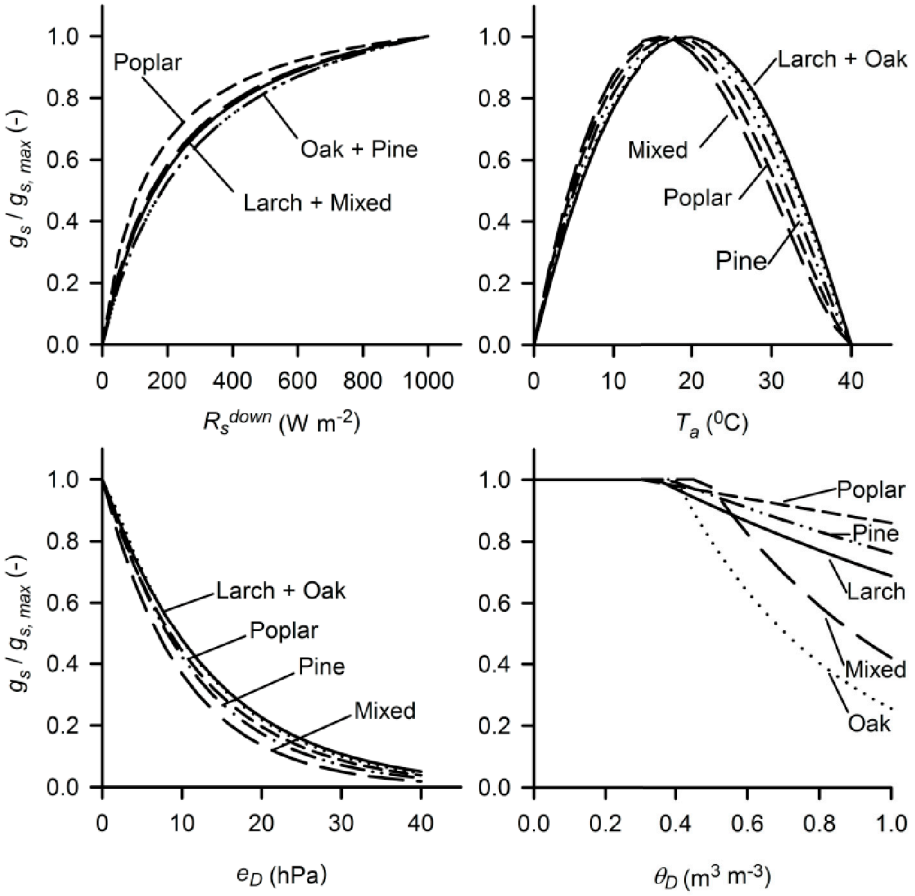

Figure 7.3: *The fractional surface conductance $g_s/g_{s,max}$ as a function of radiation R_s^{down}, air temperature T, vapour pressure deficit e_D and soil water deficit θ_D for all sites optimised for all years as listed in Table 7.5.*

on g_s. The strength of this feedback at the higher T_a range increases from *larch*, *oak*, *pine*, *poplar* to *mixed* forest.

As vapour pressure deficit e_D is strongly related to T_a, the same order in the decrease in strength in the negative feedback signal of increasing e_D to g_s is observed for the different forest types. The *mixed* forest and the *pine* forest are especially for $e_D < 15$ hPa most sensitive to an increase in e_D. The least sensitive to an increase e_D are the *oak* and *larch* forests.

For the *pine* forest g_s is influenced over the whole range by θ_D. The other forests start to be influenced at $\theta_D \gtrsim 0.3$ (m^3 m^{-3}). The *oak* and *mixed* forest follow the

Table 7.4: *t-test values, testing the Null hypothesis that the independent variable does not contribute to predicting the surface conductance g_s for each site.*

Site	Tree species	$g_{s,max}$	a_R	a_T	c_{e_D}	a_{e_D}	c_{θ_D}	a_{θ_D}
Bankenbos	*Larch*	0.86	8.89	28.30	0.01	21.03	9.41	5.03
Edesebos	*Oak*	0.86	12.22	24.09	0.04	19.27	22.22	6.77
Fleditebos	*Poplar*	0.00	8.90	28.74	0.00	20.05	1.99	3.09
Kampina	*Mixed forest*	0.74	7.91	30.92	0.00	25.31	0.00	0.00
Loobos	*Pine*	0.00	14.04	44.59	0.00	34.02	1.10	9.44

relationship $g_s/g_{s,max} = f(\theta_D)$, which has also been found by different authors at other sites (e.g. Fig. 5 of Granier et al. (2000). The fact that at the *poplar*, *pine* and *larch* forests g_s does not drop to low values at high θ_D may have 2 reasons. The first reason being the data set not covering the whole parameter space, i.e. not including dry periods. The second reason could be the fact that the used θ_D was based on the soil layer where 80-90% of the roots were present. Soil layers deeper down could also have functioned as a source of soil water regulating g_s.

7.5.1 Effect of parameter reduction on uncertainty

Reducing the number of parameters in a model will generally make the model more robust. To analyse the variance explained in g_s by each individual parameter of Eq. 2.46 a t-test was used. We tested the Null hypothesis that the coefficient of the independent variable is zero, i.e. the independent variable does not contribute to predicting the dependent variable g_s.

The low t-values for $g_{s,max}$ and c_{e_D} indicate that these variables did not contribute much in explaining the variance of g_s (see Table 7.4). Therefore, replacing both of these parameters by fixed values will most likely not reduce the explained variance significantly. In addition at the *mixed* forest of the Kampina site θ did not explain any of the variance in g_s. And at the *poplar* and the *pine* forest the parameter c_{θ_D} did not contribute much to explain the variance of g_s.

To check how important the different functions are to simulate g_s, each function, one by one was set to 1. The complete data series of each site was used (see Table 7.5). The resulting R^2 shows that except for the *oak* forest, $f(e_D)$ contributed most to explain the variance of g_s. Not including $f(T_a)$ to simulate g_s even increased R^2. This increase in explained variance is mainly because of the relatively high values for g_s at T_a below the optimum temperature a_T. Adding the lower temperature limit T_l as an independent variable improved R^2 for 2 sites. However, the resulting value for T_l became unrealistically low, i.e. > -200 °C for the *poplar* forest of the Fleditebos site. Such values for T_l imply that in the data sets studied, there is no evidence for

Table 7.5: *The correlation coefficient R^2 of the surface conductance g_s for each site. R^2 is listed using the relationships for all dependent variables and R^2 is listed excluding each relationship one by one by setting $f(x) = 1$. Also listed is R^2 using all relationships but adding the minimum temperature T_l as an independent variable.*

Site	Tree species	All	$f(R_S^{down}) = 1$	$\mathbf{f}(T_a) = 1$	$f(e_D) = 1$	$f(\theta_D) = 1$	T_l
Bankenbos	*Larch*	0.50	0.41	**0.59**	0.26	0.48	-
Edesebos	*Oak*	0.67	0.27	**0.69**	0.56	0.60	0.57
Fleditebos	*Poplar*	0.48	0.42	**0.52**	0.36	0.47	0.51
Kampina	*Mixed forest*	0.48	0.43	**0.53**	0.26	0.48	-
Loobos	*Pine*	0.62	0.47	**0.64**	0.44	0.60	0.63

a decrease of g_s with lower T_a.

Comparison of the variance explained by the different variables showed that for all sites the temperature dependency did not improve the results significantly. For the *larch* forest at the Bankenbos site when removing the temperature dependency, R^2 of the optimization results improved by approximately 15%. Removal of the soil water stress function reduced the variance explained by approximately 4%. For the *pine* site, Loobos, there was no major change in the results by removing either the temperature or the soil water function for 1996. For 1997 R^2 improved to 0.66 and for 2003 R^2 improved to 0.54 after setting g_s as $f(T_a) = 1$.

7.5.2 Stress from different soil water sources in the unsaturated zone

In Section 7.5 $f(\theta_D)$ was analysed based on θ_D of the soil profile with $> 90\%$ of the roots present (see Fig. 3.24 3.24). The fact that at most sites and years under dry conditions there was nearly no decrease in g_s, may have been caused by water being available at deeper soil layers. At other sites, for example the *larch* forest of the Bankenbos site, the limited parameter space could well be the reason for the limited range of the θ_D stress function, i.e. the length of the data set is limited and θ_D ranges from 0 to 0.7.

For the *pine* forest at the Loobos site and depending on which soil layer has been used to determine θ_D (Fig. 7.4), the parameter space is well covered with θ_D ranging from 0 to 0.8 or 1.0 $m^3\ m^{-3}$.

Comparing θ_D of the different depths and layers as depicted in Fig. 7.4 shows the strong dampening influence of θ measured at the deeper layers, i.e. at 2.00 m depth. Choosing a deeper soil layer to model water stress also implies that the stress is expected to develop later in time. The peak after DOY 30 is caused by a short period with temperatures well below zero and has not been taken into account.

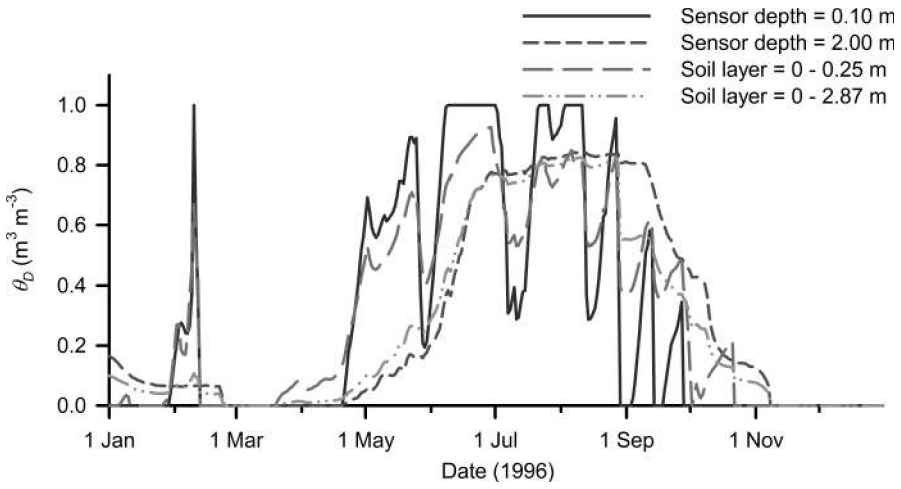

Figure 7.4: *Soil water deficit θ_D measured at specific depths of 0.10 m and 2.0 m for the pine trees at the Loobos site. Also shown are θ_D for the top soil layer 0 - 0.25 m of the soil and θ_D for the entire soil profile 0 - 2.87 m, i.e. down to the maximum rooting depth. Data are for the year 1996.*

To analyse for the Loobos site with its deep sinker roots of the *pine* trees if other soil layers play an important role, the data set of 1996 has been optimized using θ_D based on different soil layers. All stress functions except the θ_D stress functions were fixed. To put more emphasis on the relatively dry conditions, only data between mid June and end of September were used.

Taking different soil layers in account to determine θ_D, while keeping the other g_s dependencies fixed, did not change R^2 much (Fig. 7.5A). Only for θ_D based on θ measured at 0.75 m and 2.00 m, R^2 reduced from 0.66 down to 0.59 and 0.60 respectively (Fig. 7.5B). The difference in the function for θ_D at 0.03 m and at 0.10 m depth with the same $R^2 = 0.66$, reflects the fact that the layer at 0.03 m depth does not release soil water as fast as the soil layers deeper down.

For the *pine* forest of the Loobos site all relationships $g_s/g_{s,max}$ as a function of θ_D as shown in Fig. 7.5 demonstrate that for the relatively dry year of 1996, the vegetation is not severally stressed. For θ_D measured in 1996 (see Fig. 7.4), $g_s/g_{s,max}$ is always larger than 0.4, which is the limit at which severe stress starts to occur. For the deep layer this may be caused by the limited range of θ_D values, i.e. 0 - 0.52 available for the parameter optimization. It could however, also have been caused by these deep roots having access to the groundwater reservoir.

The frequency distribution of θ_D of the root zone of 0 - 0.25 m (using the same records as have been used for the analysis of g_s for the years 1995-2009) is depicted

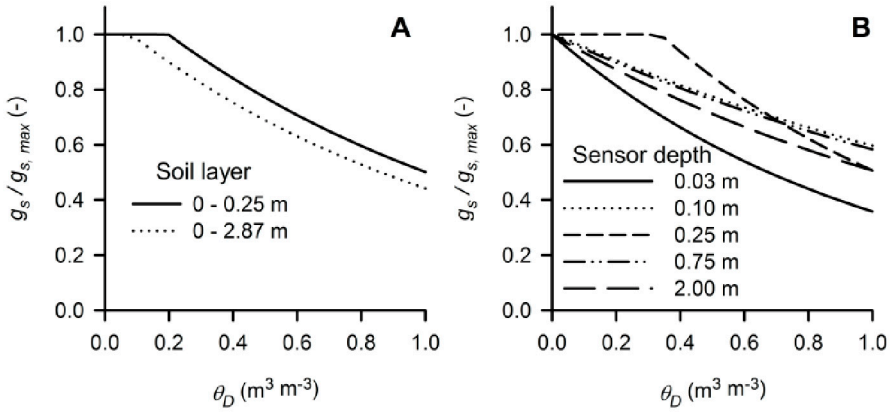

Figure 7.5: *The relative stomatal conductance $g_s/g_{s,max}$ of the pine forest at the Loobos site as a function of soil water deficit θ_D in different soil layers (left panel, **A**) and for soil water deficits at the different depths at which the sensors were installed (right panel, **B**).*

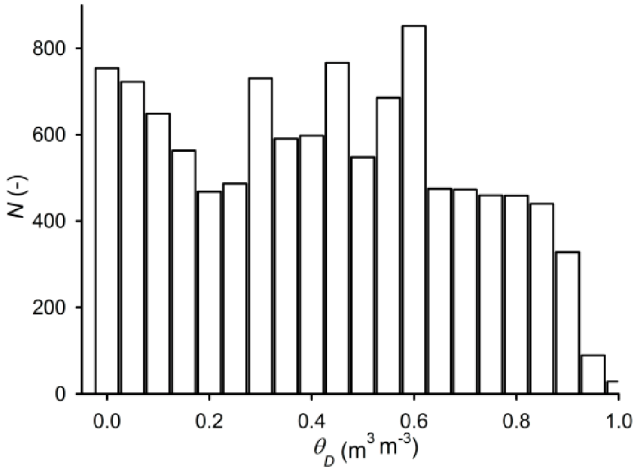

Figure 7.6: *The frequency N (-) distribution of the θ_D (-) for the top 0.25 m soil depth of the pine forest at the Loobos site. The data depicted have been selected using the same selection criteria as were used for the g_s optimization (see Section 7.5).*

in Fig. 7.6. This figure shows the large number of moist data points $\theta_D < 0.45$ as well as the relatively uniform distribution of dry data points at $\theta_D > 0.45$. This uniform distribution indicates that if θ_D of the root zone of 0 - 0.25 m drives the stomatal closure, it should be reflected in the data of g_s. However, the data of g_s do not demonstrate a strong decrease with an increasing θ_D (see Fig. 7.5), not even for

the relatively dry years 1995-1997. Hence, it strengthens the hypothesis that *pine* trees are able to access other, i.e. deeper water resources.

The *poplar* forest at the Fleditebos site demonstrated similar results for g_s based on θ_D of different soil layers. For this site a small improvement in R^2 was obtained using θ_D measured at 0.03 m and at 0.10 m, i.e. $R^2 = 0.50$ and $R^2 = 0.51$ instead of θ_D measured over the top soil layer of 0.60 m.

7.5.3 The effect of groundwater uptake by roots

One of the most important determinants of the maximum rooting depth in The Netherlands is the depth of the groundwater level z_g (van den Burg, 1996). For sites with a relatively high groundwater level droughts are a combination of low precipitation amounts and dropping groundwater levels. Hence drought is a combination of both a low soil water content in the top layer of the soil, where most roots of the trees and undergrowth are allocated and a low groundwater level that can no longer be reached by the tap or sinker roots of the trees.

In order to calculate soil water deficit θ_D of the top 0.50 m of the soil, a simple soil water balance study has been made. The water balance has been calibrated for periods when soil water content was measured. Under the assumption that roots may adjust to an average groundwater level, periods with lower levels were earmarked as periods in which tree roots were not able to tap into the groundwater reservoir. Drought affecting the whole eco-system was defined as at least 10 consecutive days of $\theta_D \geq 0.95$ with z_g being below average.

In Fig. 7.7 the 15 year average groundwater level z_g was computed for the *pine* stand of the Loobos site, i.e. 2.90 m below the soil surface. Fig. 7.7 shows periods of drought occurring not only in the years with the least amount of rain, but also in wet years, such as 1998. This behaviour reflects the slow reaction of the groundwater reservoir to surface fluxes as well as regional influences on the groundwater system.

In times of water shortages, it is to be expected that the surface conductance g_s decreases more rapidly at lower groundwater levels. To test this hypothesis, the data of 1995 - 2005 of the *pine* forest at the Loobos site have been split in two parts. In the first data set g_s was selected on the basis of $z_g < 2.3$ m below the soil surface. The second data set consisted only of records of g_s with $z_g > 3.3$ m below the soil surface. As can be seen in Fig. 7.8B there is no clear effect of z_g on g_s. Contrary to what had been expected, at $z_g > 3.3$ m below the soil surface more high values of g_s occur at high θ_D, than for the cases with $z_g < 2.3$ m below the soil surface. The outliers in Fig. 7.8B are mainly cases with exceptionally low $e_D < 2$ hPa during both winter and summer months.

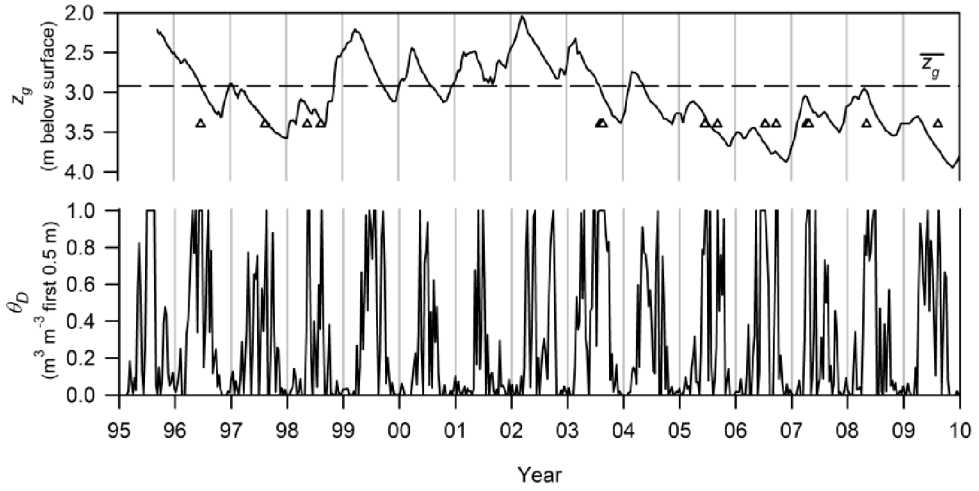

Figure 7.7: *The combination of a deep groundwater level z_g (top panel) and a high soil water deficit θ_D (bottom panel) is an indicator for periods of potential water stress, as shown by the triangles for the pine stand at the Loobos site. The dashed line at 2.9 m in the top figure shows the 15 year average $\overline{z_g}$.*

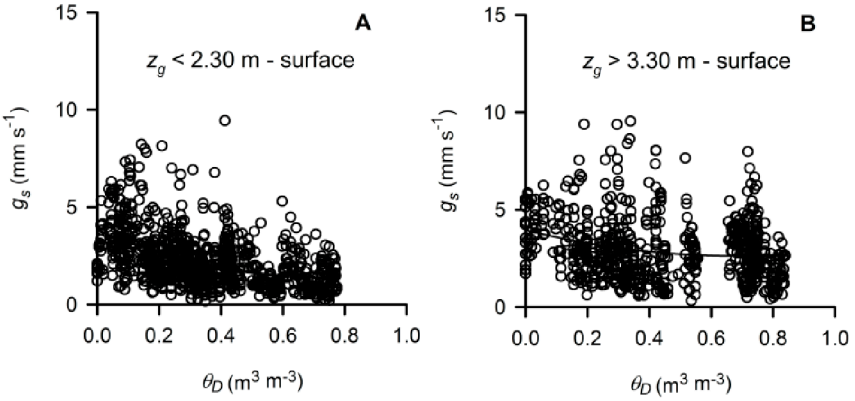

Figure 7.8: *Surface conductance g_s as related to soil water deficit θ_D for the pine forest at the Loobos site, 1995-2009. In the left panel, **A** only data records with the ground water level $z_g < 2.3$ m below the surface are shown. In the right panel, **B** only data records with $z_g > 3.3$ m below the surface have been selected. The solid lines depict the results of a second order regression.*

7.5.4 Modelling soil water feedbacks from deeper soil layers

At the *pine* forest of the Loobos site, both options to include possible feedbacks from the soil water deeper down in the soil $f(\psi(z_2))_A$ and $f(\psi(z_2))_B$, did not improve the

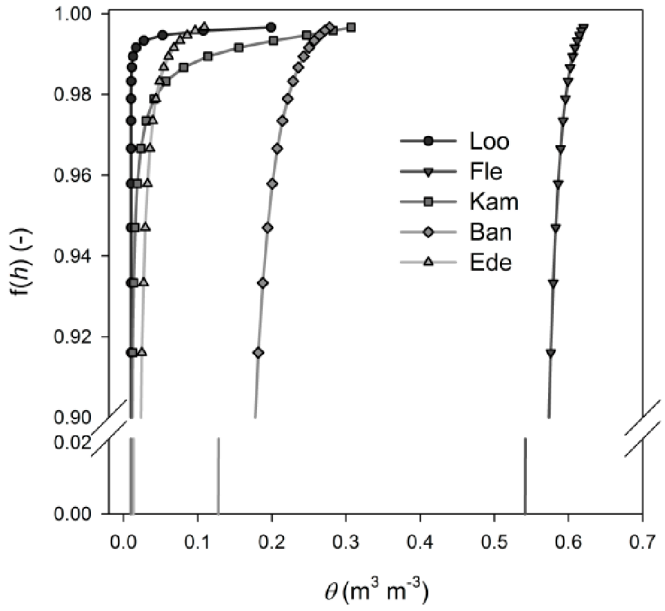

Figure 7.9: *The relative reduction of soil water stress in the deeper soil layers for all test sites based on option A for $f(\psi(z_2))_A$ (see Eq. 7.2) as a function of the volumetric soil water content θ.*

explained variance of the fit of g_s.

Fig. 7.9 depicts $f(\psi(z_2))_A$ as a function of soil water based on Eq. 7.2 for the different sites. This figure shows that sites with soils having a higher content of sand, demonstrate almost no reduction on $g_s/g_{s,\max}$ for a relatively large range of soil water content. Only at low water content $g_s/g_{s,\max}$ is reduced sharply. For the *pine* trees at the Loobos site because of changes in hydraulic conductivity the effect of water stress is almost non existent for most soil water conditions. Only at extreme dry conditions $f(\psi(z_2))_A$ acts almost as a on-off switch for the Loobos site. The clayey and loamy soils of respectively the Fledite and Bankenbos site, show a much more gradual decline of $f(\psi(z_2))_A$ with decreasing θ.

Fig. 7.10 shows for the results of the fitted $g_s/g_{s,\max}$ for the relatively dry year 1996 at the *pine* forest of the Loobos site using 2 different models:

- The classical model $\mathrm{f}(\theta)_{\mathrm{classic}}$ (see Eq. 2.51) using θ_D of the layer were 80-90% of the roots are found, i.e. the upper 0 - 25 cm of the soil, and
- The model using Eq. 7.1 based on option *B*, i.e. the combination of $\mathrm{f}(\theta(z_2))_B$ with $z_2 = 0$ - 2.87 m using Eq. 7.3 and $\mathrm{f}(\theta(z_1))$ with $z_1 = 0$ - 0.25 m using Eq.

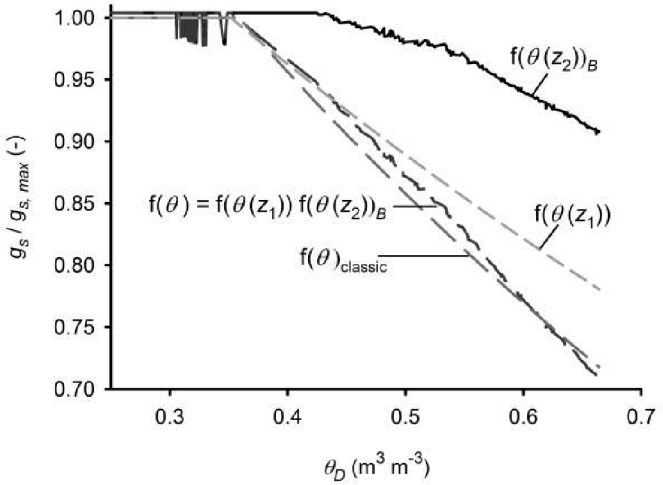

Figure 7.10: *The relative $g_s/g_{s,max}$ as a function of θ_D representing the upper 0 - 25 cm of the soil. Two models are depicted: the classical model f(θ)$_{classic}$ using θ_D of the soil layer where 80-90% of the roots are found, i.e. the upper 0 - 25 cm of the soil, and the model f(θ) = f($\theta(z_1)$) f($\theta(z_2)$)$_B$. The latter model also takes into account θ_D of the soil layer 0 - 2.87 m, i.e. until the maximum rooting depth. The fitted functions are based on the data of the year 1996 at the pine forest of the Loobos site.*

2.51.

The fitted functions are based on the data of 1996 measured at the *pine* forest at the Loobos site. The deviations from the spikes in the curve of f($\theta(z_2)$)$_B$ and the combined function f($\theta(z_1)$) f($\theta(z_2)$)$_B$ are caused by the differences in changes of θ in the soil layer 0 - 0.25 m and in the soil layer 0 - 2.87 m (see also Fig. 7.4). The soil water content of soil layer 0 - 0.25 m was used to calculate θ_D for the x-axis of Fig. 7.10. The graph shows the slow reaction of g_s to decreasing θ_D of the root zone and the relatively fast reaction to θ_D of the upper 0 - 25 cm of the soil. The graph also shows that the standard model f(θ) and the model using option B fit the 1996 data of the *pine* forest at the Loobos site equally well.

Fig. 7.11 shows how the fitted model B behaves under more extreme conditions of soil water stress in upper 25 cm of the soil $\theta_D(z_1)$ and in the total rootzone $\theta_D(z_2)$. The effects on g_s of the changes in $\theta_D(z_1)$ are largest for $\theta_D(z_2) < 0.6$. It should be noted that changes in $\theta_D(z_2)$ will include changes in $\theta_D(z_1)$, as demonstrated by the measured θ_D in Fig. 7.11. Therefore, especially the combination of low $\theta_D(z_1)$ and high $\theta_D(z_2)$ as depicted in Fig. 7.11 are unrealistic.

At the *poplar* forest of the Fleditebos site the use of $f(\psi(z_2))_A$ improved the

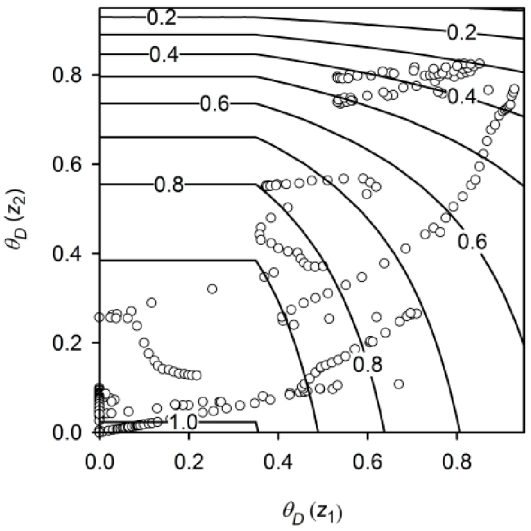

Figure 7.11: *The contour lines are the relative conductance $g_s/g_{s,max}$ as a function of $\theta_D(z_1)$ and $\theta_D(z_2)$ based on model option B. $\theta_D(z_1)$ represents the soil layer where 80-90% of the roots are found, i.e. the upper 0 - 25 cm of the soil. $\theta_D(z_2)$ represents the soil layer 0 - 2.86 m, i.e. from the surface to the deepest roots. The graph is based on the fitted data of the year 1996 at the pine forest of the Loobos site. The circles are the measured $\theta_D(z_1)$ and $\theta_D(z_2)$ in 1996.*

explained variance by 5% if compared to the standard model. Option $f(\psi(z_2))_B$ did not improve the explained variance.

7.5.5 Seasonality in surface conductance parameters

In most cases found in literature the parametrizations for the surface conductance g_s have been derived for the summer months. These relations are assumed to be valid also for the remainder of the year. In the period outside the summer months, the development of the leaf area has been used as the main driver representing growth and phenological changes over the year. Especially for evergreen vegetation evaporation outside the summer months can be substantial. This may also be the case for forest with an active undergrowth at the start and at the end of the growing season Therefore it is important to know if similar relationships for g_s as found in summer time also hold for the other months of the year.

Table 7.6 shows the parameter sets of the *pine* forest at the Loobos site being valid for each season. The dependency on air temperature T_a has not been taken into account as this dependency reduced the goodness of fit in all periods for this site.

Table 7.6: *Optimization results of surface conductance g_s for different seasons for all years measured at the pine forest of the Loobos site. Also shown are the results for all years (1995-2009) and all seasons both with and without temperature T dependency. As a measure of fit, R^2 and the Standard Error of Estimate (SEE) are given.*

Season	$g_{s,max}$ mm s^{-1}	a_R W m^{-2}	a_T ^{0}C	c_{e_D} hPa	a_{e_D} hPa^{-1}	c_{θ_D} m^3 m^{-3}	a_{θ_D} -	R^2 -	SEE mm s^{-1}
Winter	15.6	212.7	-	1.279	0.180	0.42	0.11	0.63	1.4
Spring	11.3	323.9	-	0.700	0.101	0.12	0.41	0.63	1.0
Summer	11.9	403.2	-	0.156	0.095	0.01	0.42	0.66	0.9
Autumn	11.4	155.2	-	0.217	0.119	0.01	0.85	0.22	1.4
All seasons f(T)	9.9	289.3	17.8	0.390	0.090	0.38	0.44	0.62	1.0
All seasons	12.0	280.4	-	0.097	0.099	0.38	0.49	0.64	1.0

In winter, soil water deficit θ_D plays no role and solar radiation R_S is the main driver. In spring the main drivers were e_D, and to a lesser extend θ_D. In summer e_D had the strongest reducing effect on g_s, while R_S plays almost no role. In autumn g_s is dominated by R_S and θ_D. The results for the winter period indicate that the vegetation is active. The measured CO_2 uptake during parts of the day in winter at this site indeed confirms that photosynthesis is taking place and hence the stomata are open to take up CO_2 and release water vapour during winter. Comparing the parameter values for the different seasons with those of all seasons, shows that the main differences were found for winter and autumn. Especially a_R is relatively low compared to the parameter values of all seasons. For both winter and autumn, the standard error is relatively high. For autumn also R^2 is low.

The higher value of $g_{s,\max}$ in winter may be caused by the fact that even with the selection criteria of a preceding dry period of at least 48 hours does not warrant the undergrowth or trees to be completely dry.

7.6 Separating evaporation of trees and undergrowth

To study the different stomatal response functions of the undergrowth and the tree canopy, the *dual source* model has been used as described by Eqs. 2.52 to 2.61. The available energy of the upper A_{Up} respectively lower layer A_{Low} is given by:

$$\begin{aligned} A_{Up} &= A_{Tot} - A_{Low} \\ A_{Tot} &= \lambda E_{Up} + H_{Up} \\ A_{Low} &= \lambda E_{Low} + H_{Low} \end{aligned} \tag{7.7}$$

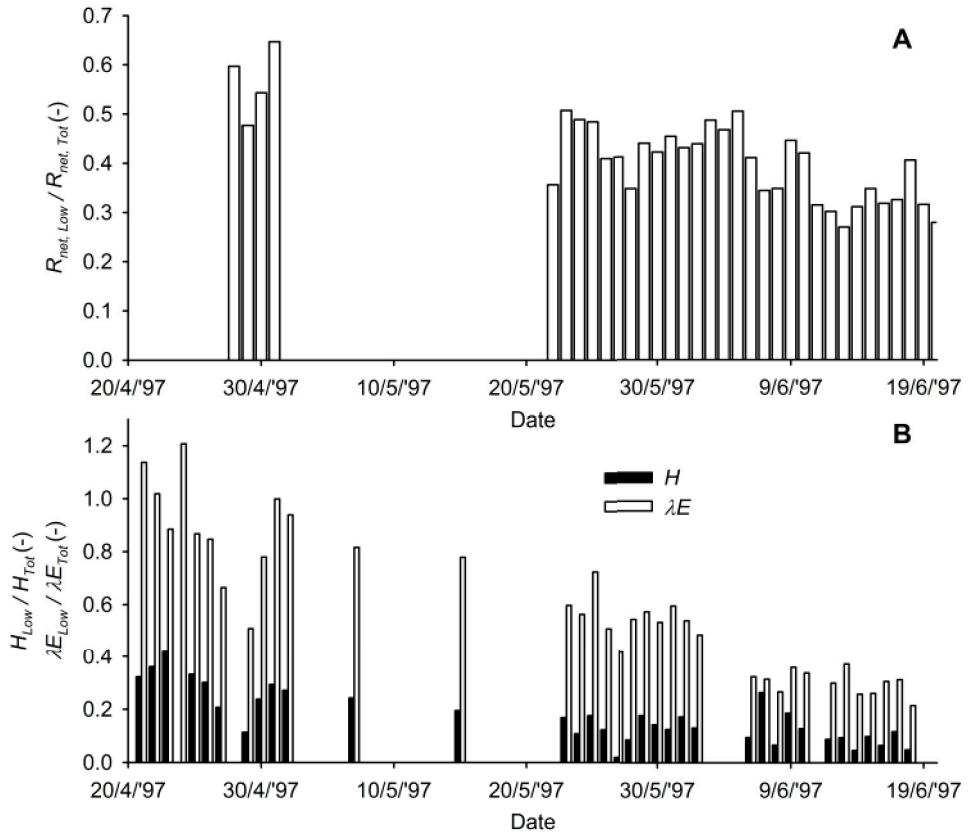

Figure 7.12: *Panel **A**: Net radiation R_{net}. Panel **B**: latent heat flux λE and sensible heat flux H measured below the canopy as a fraction of the total flux measured above the poplar trees in 1997 at the Fleditebos site.*

The latent heat flux of the tree canopy λE_{Up} is derived from λE_{Tot} i.e. the measured latent heat flux by the eddy-correlation system above the canopy, and λE_{Low}, i.e. measured by the eddy-correlation system below the canopy. Hence:

$$\lambda E_{Up} = \lambda E_{Tot} - \lambda E_{Low} \tag{7.8}$$

For the *pine* forest at the Loobos site and the *poplar* forest at the Fleditebos site the undergrowth is a well defined vegetation layer, being separate from the above tree canopy. To investigate if the undergrowth should be treated as a separate layer an additional flux station has been exploited in between the undergrowth and the tree canopy (See Section 4.3.1).

Fig. 7.12 shows the influence of emerging leaves of the *poplar* trees of the Fledite site from April to June. The appearance of the leaves also caused the Bowen ratio to change both above and below the canopy. In April almost all λE measured above the canopy originated from undergrowth and soil. In June λE originating from undergrowth and soil reduced to 0.25 to 0.30 of total λE.

The ratio of the daily average daytime (between 10h00 and 16h00) λE for dry conditions (defined as records preceded by at least 24 dry hours) at the *poplar* site for the undergrowth as a fraction of total λE changed from 1.0 in March down to 0.35 at the end of June. The latter coinciding with the start of the decline in L_{AI} of the undergrowth and reaching the maximum L_{AI} by the *poplar*s.

At the *pine* site the average undergrowth λE as a fraction of total λE during the months July and August amounted to 0.10. At the end of August this increased to 0.20 which was maintained in the month September and the first part of October, later decreasing to 0.15.

7.6.1 The eddy-decay coefficient for undergrowth

The transport of scalars and momentum in the dual source model is determined by the eddy-decay coefficient η (see Eq. 2.54).

At the *poplar* forest of the Fleditebos site no dependency on wind direction was found. Because of the large differences in plant height and leaf area of the undergrowth during the season, the surface roughness changed in time. Hence z_{0M} and u_*/u (for near neutral conditions) were made dependent on plant height.

The presence of dunes underneath the *pine* trees at the Loobos site influences the measurements below the canopy. To minimise disturbance of dunes on the turbulent measurements, data were used only with the wind coming from directions between 130 and 230 degrees N. For the *pine* forest the data of the undergrowth were according to the wind direction classified into 2 groups. A distinction has been made between the wind directions 120 to 240 and 270 to 355 degrees N for one group and the remainder of the wind directions for the second group. Table 7.7 shows the roughness characteristics for the two wind directions at the Loobos site.

Table 7.7 shows the roughness characteristics at the start and at the middle of the growing season.

Based on wind speed measurements above and below the canopy, for the *pine* site on average $\eta = 2.3$ and for the *poplar* site $\eta = 2.1$.

7.6.2 Radiative forcing

An important driver for the opening and closure of the stomata and therefore of the evaporation rate is the radiation load. For the lower layer direct measurements

Table 7.7: *Roughness characteristics d, z_{0M}, u_*/u (for near neutral conditions) and eddy-decay coefficient η for the undergrowth of the pine forest at the Loobos and the poplar forest at the Fleditebos sites.*

Site	Selection	d	z_{0M}	u_*/u	η
Loobos (*Pine*)	$120 < u_{dir} < 240$	0.0	0.4	0.22	2.3
	$270 < u_{dir} < 355$	0.0	1.4	0.40	
Fleditebos (*Poplar*)	Spring	0.1	0.35	0.18	2.1
	Summer	0.1	0.95	0.35	

of the incoming radiation are complicated because of the irregular structure of the tree canopy above in combination with the limited area that can be viewed by a radiation sensor. To overcome this problem, R_s^{down} for the lower vegetation layer was estimated using the radiative transfer scheme for sparse canopies as developed by Hanan (2001).

Fig. 7.13 shows for a clear day at the *pine* forest of the Loobos site the daily variation of the ratio between R_s^{down} for the lower vegetation layer and the total R_s^{down}. For a cloudy day with primarily diffuse radiation the ratio becomes as a straight line, similar to applying a Beer-Lambert type equation with a fixed extinction factor (e.g. Whitehead and Kelliher, 1991). The average extinction factor for the *pine* trees at the Loobos site is 0.53, which corresponds well with the average extinction factor of 0.52 for 7 coniferous stands as reported by Pierce and Running (1988).

For the *poplar* trees at the Fleditebos site a large change in the ratio between R_s^{down} for the lower vegetation layer and the total R_s^{down}, associated with the leaf development and senescence, was obtained. On top of this seasonal pattern, daily patterns similar to those of the *pine* forest were simulated.

7.7 Surface conductance using the dual source approach

The additional separate flux measurements taken below the tree canopy at the Fleditebos and Loobos site in combination with the *dual source* model, allowed to distinguish between the surface conductance g_s of the upper layer, i.e. the trees, and the undergrowth beneath the trees. In Table 7.8 the optimization results are shown of the stomatal conductance functions (see Section 2.5.3) for the separate vegetation layers.

As driving variables for g_s of the undergrowth, in Table 7.8 the separate measurements taken below the canopy of air temperature T_a and relative humidity $\varkappa_r$ and

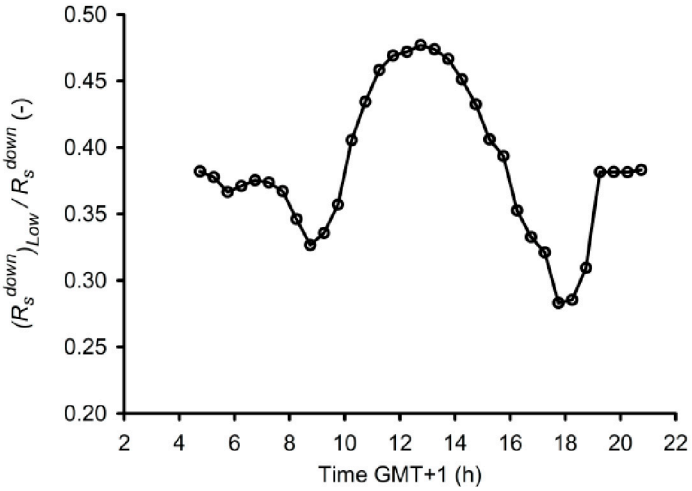

Figure 7.13: *The simulated diurnal variation of the incoming short wave radiation R_s^{down} above the lower vegetation layer as the ratio of that above the higher vegetation layer for a clear day at the pine forest of the Loobos site.*

Table 7.8: *Optimized maximum surface conductance $g_{s,max}$ and stomatal conductance functions for the trees and/or undergrowth at the Fleditebos and Loobos sites. Two flux stations were used simultaneously above and below the canopy. The constants a_R, a_T, c_eD, a_eD, c_{θ_D} and a_{θ_D} refer to the equations of Section 2.5.3. As a measure of fit, R^2 and the Standard Error of Estimate (SEE) are given.*

Site	Vegetation Layer	$g_{s,max}$ mm s^{-1}	a_R W m^{-2}	a_T ^{0}C	c_{e_D} hPa	a_{e_D} hPa^{-1}	c_{θ_D} m^3 m^{-3}	a_{θ_D} -	R^2 -	SEE mm s^{-1}
Fle-	Tree (*Poplar*)	7.2	0.1	22.0	0.001	0.055	0.38	1.47	0.10	2.7
dite-	Under	11.0	540.0	19.0	0.767	0.114	0.49	1.00	0.33	1.6
bos	Tree & under	5.5	51.0	22.0	0.001	0.065	0.49	1.68	0.22	1.1
Loo-	Tree (*Pine*)	12.9	254.8	19.7	1.756	0.055	0.54	1.00	0.46	1.9
bos	Under	5.9	376.4	12.1	0.001	0.047	0.01	1.10	0.38	0.7
	Tree & under	7.8	354.7	14.9	0.001	0.050	0.11	0.01	0.64	0.8

the modelled down-dwelling short-wave radiation R_s^{down} penetrating the canopy (see Section 7.6.2) were used. The thus obtained parameter values were almost identical to those when using the modelled driving variables for the lower layer, i.e. T_0 and e_{D0}.

The results for the *poplar* trees of the *dual source* approach are significantly different from the results obtained by the *big leaf* approach, marked as "Tree" in Table 7.2. The main reasons for the differences obtained by the two approaches are:

the different periods used, i.e. spring versus summer, possibly reflecting different phenological stages, and the contamination of the signal by the undergrowth that is still present in the data set used for Table 7.2. Based on the relatively small leaf area of the undergrowth, it was assumed for the *big leaf* approach, that during the summer months the tree evaporation was so dominant that the undergrowth evaporation could be neglected. Although the measurements show the relatively small contribution of the undergrowth to the total evaporation of the forest (see e.g. Fig. 7.12), the undergrowth signal is still strong enough to influence the optimization results of the *big leaf* model.

The undergrowth parameter set of the *poplar* forest also differs from that of Table 7.2. Especially a_R and a_T differ significantly. These differences may be caused by the relatively low temperatures and radiation for the data set used for Table 7.2.

The combined trees and undergrowth parameter set of the *pine* forest at the Loobos site compares relatively well with the parameter set for 1997 in Table 7.5. To a lesser extent these parameter sets of the combined vegetation layers also compare well for the *poplar* forest at the Fleditebos site.

Except for the combined trees and undergrowth of the Loobos site optimization, the fitting results were less good, i.e. R^2 between 0.1 and 0.46, than when using longer datasets, i.e. R^2 between 0.58 and 0.62 (see Table 7.5). This lesser fit implies that there is a larger uncertainty associated with the results of the *dual source* model if compared with the *big leaf* model. Partly this lesser fit is caused by the limited length of the datasets available at both sites: after mid of April to the end of June at the Fleditebos site and end of June to end of October at the Loobos site.

At the Fleditebos site, the data used reflect the first two months of the growing season of the *poplar* trees. During this period L_{AI} changes rapidly and as a result also total g_s. Fig. 7.14 shows that g_s of the *poplar* undergrowth starts to decrease faster than the trees with high T_a, e_D and low R_s^{down}. Although the range of θ is limited and therefore care should be taken when using the data, the results suggest that the trees will reduce g_s earlier than the undergrowth of the *poplar* forest.

At the *pine* forest of the Loobos site the differences between the trees and the undergrowth is much less pronounced than for the *poplar* forest. The trees and the undergrowth react almost identically to changes in e_D and R_s^{down} (see Fig. 7.15). Even more pronounced than the undergrowth of the *poplar* forest, the undergrowth of the *pine* forest reaches its optimum g_s at lower T_a than the trees. Also identical to the *poplar* forest the *pine* trees experienced more water stress than the undergrowth. In this data set of the Loobos site no water stress was detected at all for the undergrowth.

Fig. 7.16 shows the total maximum g_s for the different vegetation layers at both sites. The timing of the undergrowth contribution to total g_s differs between the sites. Where the undergrowth of the *poplar* forest at the Fleditebos site mainly influences

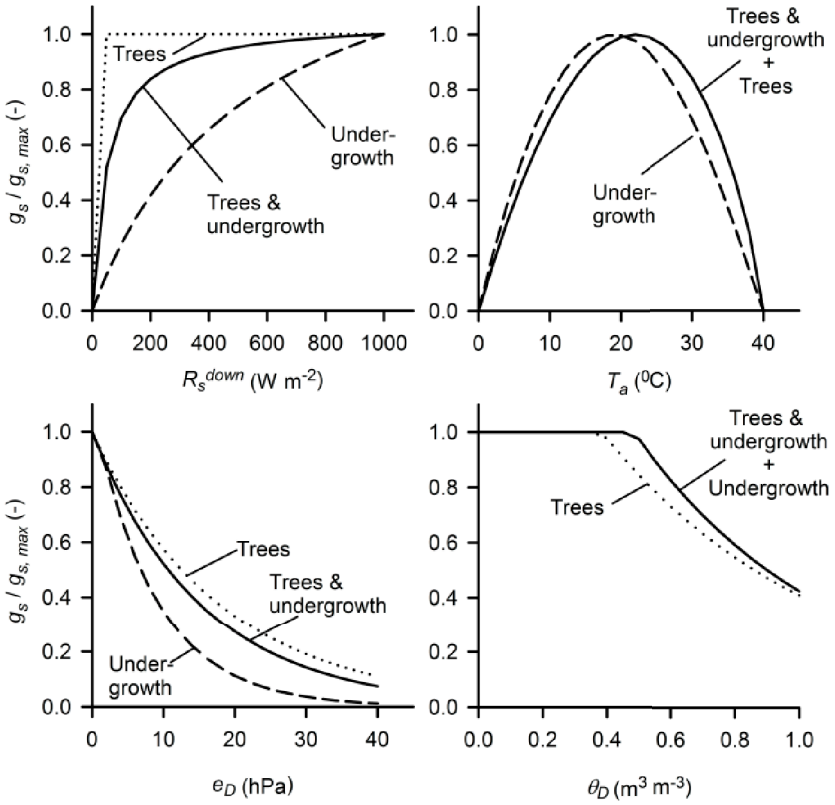

Figure 7.14: *The fractional surface conductances $g_s/g_{s,max}$ as a function of radiation R_s^{down}, air temperature T_a, vapour pressure deficit e_D and soil water deficit θ_D for the tree layer, the undergrowth layer and for the total vegetation at the poplar forest of the Fleditebos site in 1997.*

the total g_s during the first 3 months of the growing season, the undergrowth of the *pine* forest at the Loobos site especially influences total g_s during the summer months.

7.7.1 Evaluation of the *dual source* model

To validate the model performance the results were compared with the sapflow measurements of the *pine* stand at the Loobos site for the years 1997 and 1998. Because the sapflow data are lagging behind in time as compared to the actual evaporation rate, daily sums were used for the evaluation. Table 7.9 shows the evaluation results using the dual source model in combination with the calibrated parameters for the

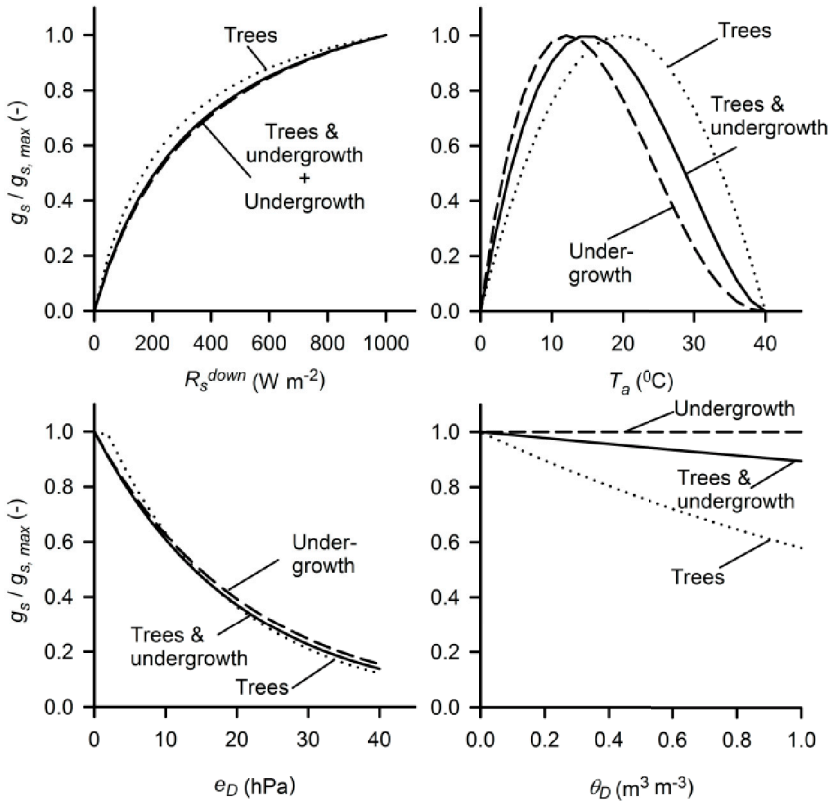

Figure 7.15: *The fractional surface conductances $g_s/g_{s,max}$ as a function of radiation R_s^{down}, air temperature T_a, vapour pressure deficit e_D and soil water deficit θ_D for the tree layer, the undergrowth layer and for the total vegetation at the pine forest of the Loobos site in 1997.*

pine forest at the Loobos site been taken from Table 7.8. For both years the sapflow derived evaporation rate of the *pine* trees E^{Sap} compares equally well with the modelled evaporation rate for the upper vegetation layer E_{Up} using the dual source model. These data include dry as well as wet data.

In addition the modelled total evaporation rate E_{Tot} is compared to the measured evaporation rate using an eddy-correlation system above the canopy E^{EC}. As may be expected the period 170 < DOY< 300 in 1997 for which the model was calibrated gives the best fit. The same period in 1998 also gives a reasonable fit. Both full years 1997 and 1998 show an overestimation of 25 to 30% of E_{Tot} as compared to E^{EC}. In this comparison only days with $E_I < 0.1$ mm d^{-1} were used.

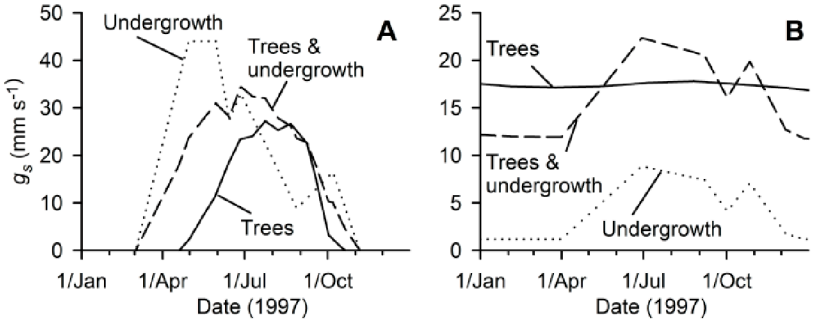

Figure 7.16: *The total maximum surface conductance g_s, i.e. correcting $g_{s,max}$ for L_{AI} with all reduction functions set to 1, for the trees, the undergrowth and the combination of trees and undergrowth. The results are based on the period of 20 April to 17 June 1997 at the poplar forest of the Fleditebos site (panel* **A***), and the period 20 June to 1 November 1997 at the pine forest of the Loobos site (panel* **B***).*

Table 7.9: *Evaluation of the dual source model evaporation results for the pine forest at the Loobos site for the years 1997 and 1998. The tree evaporation E_{Up} is validated using sapflow measurements E^{Sap} and total evaporation E_{Tot} using eddy-correlation measurements taken above the canopy E^{EC}. For E_{Tot} the total year as well as the period for which the calibration was done are provided. In both cases only days with modelled interception evaporation $<$ 0.1 mm d^{-1} were used. As a measure of fit R^2 and p are given. *) This dataset is used to calibrate the model.*

Year	Evaluation dataset	Period	Regression results	R^2	p
1997	Sapflow	$120 < \text{DOY} < 252$	$E^{Sap} = -0.13 + 1.03E_{Up}$	0.75	<0.0001
	Eddy corr.*	$170 < \text{DOY} < 300$	$E^{EC} = -0.07 + 0.95E_{Tot}$	0.86	<0.0001
	Eddy corr.	$1 < \text{DOY} < 365$	$E^{EC} = 0.31 + 0.69E_{Tot}$	0.79	<0.0001
1998	Sapflow	$140 < \text{DOY} < 228$	$E^{Sap} = 0.28 + 0.96E_{Up}$	0.73	<0.0001
	Eddy corr.	$170 < \text{DOY} < 300$	$E^{EC} = 0.63 + 0.84E_{Tot}$	0.79	<0.0001
	Eddy corr.	$1 < \text{DOY} < 365$	$E^{EC} = 0.40 + 0.76E_{Tot}$	0.76	<0.0001

The satisfactory modelling results in comparison to the sapflow data together with the overestimation of E^{EC} suggests that the model overestimates the evaporation rate of the undergrowth. During the months May to September the ratio of E_{Low} to E_{Up} ranges on average between 15 to 22% (see Fig. 7.17 B). This ratio increases

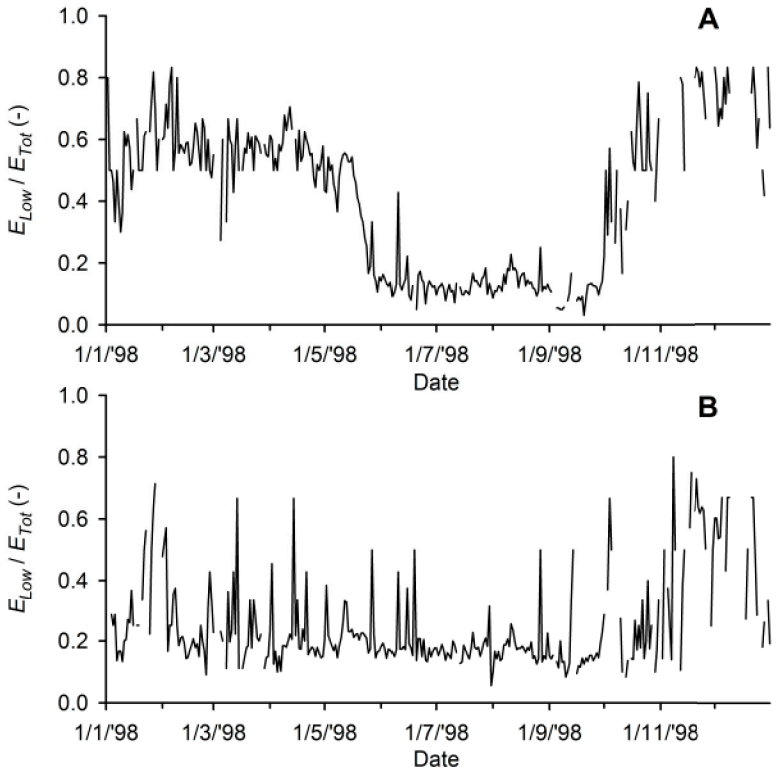

Figure 7.17: *The ratio of the simulated daily evaporation rate of the undergrowth E_{Low} to the total evaporation rate E_{Tot} for the poplar forest at the Fleditebos side (**A**) and the pine forest at the Loobos site (**B**) in 1998. These data represent the dry evaporation rate, i.e. transpiration, and do not include evaporation of intercepted rain.*

during the other months of the year to between 20 and 35%. The high contribution of the undergrowth E_{Tot} during the months October to March, suggests that the overestimation for the total year is mainly because of the overestimation during these months by the simulated E_{Low}. At the *poplar* forest of the Fleditebos site the relative contribution of the undergrowth compares well with the ratio based on the measurements of 1997 (see Fig. 7.12 B).

7.8 General discussion

Soil water stress is an important, but a difficult to parametrize aspect regulating stomatal opening and closure. Especially in mid latitude regions with relatively high

groundwater tables and rain showers well distributed in time these conditions may be hard to detect. Still, with the expected increase of relatively dry periods in these regions, knowledge of the effect of water stress on evaporation rate is important.

Main drivers of surface conductance g_s at the different forest stands

Poplar forest is most sensitive to radiation and least sensitive to soil water. *Oak* forest is least sensitive to radiation and most sensitive to soil water. *Mixed* forest is most sensitive to vapour pressure deficit and has the lowest optimum air temperature of all 5 forest stands. Soil water does not seem to have a great effect on the surface conductance of the poplar pine and larch forest. Granier et al. (2000) showed that for forest the critical value for soil water deficit θ_D equals 0.6. Above this value the transpiration rate reduces rapidly. The most important unknown in the amount of available water is the rooting depth that determines the total available soil water.

Soil water availability determined by rooting depth

In most models water stress is parametrized as a mean value over the depth where 80 - 90% of the roots are present. For agricultural crops that are harvested every year the rooting depth is well known, however for perennial grasslands and trees with permanent rooting systems the root distribution is less uniform (see e.g. Canadell et al., 1996) and the rooting depth may vary between years. Root growth and mortality will depend among others on available soil water. For coniferous trees in the Netherlands Olsthoorn (1998) found a critical soil water pressure of $\psi = -10^{2.1}$ Pa above which primary roots started to die. This growth and mortality of roots implies that in a relatively dry year the depth to which the roots are active, is not a fixed depth, but is the result of a complex process of growth and decline depending among others on soil water availability. This change in depth of active roots, is however not reflected in the soil water deficit θ_D stress functions for the sites of this study. Optimizing g_s for different soil depths showed for the sites with relatively deep roots, i.e. Loobos and Edesebos, the best fit was obtained, by using soil water of the root zone where most roots are found, and not necessarily by using θ of the total root zone.

Redistribution of groundwater to the upper soil layers by hydraulic lift is a possible explanation although not observed in our soil water measurements. However, the latter could have been caused by the relatively low detection rate of the sensors used.

Rooting depth of trees

Canadell et al. (1996) reported average maximum rooting depths of 2.6 $\pm$ 0.2 m for temperate grassland, 3.9 $\pm$0.4 m for temperate coniferous forest and 2.9 $\pm$ 0.2 m for temperate deciduous forest. Maximum and minimum values for these biomes differ by at least a couple of meters. Coniferous forests were among the eco-systems with the deepest root profiles. For the temperate coniferous forest of

their study the percentage of roots observed at 20 cm varied between approximately 25% and 80%. In a review of rooting patterns of forest trees in the Netherlands, van den Burg (1996) reported that besides ploughing depth, only the groundwater table depth explained a part of the variance in the rooting depth for fir, *poplar* and *oak* trees. The stand average maximum rooting depth reported by van den Burg (1996) were for *larch* 1.00 m, *poplar* 1.62 m, *oak* 1.4 m (for the tree species found at the Edesebos site, *Querqus rubra* the depth was 0.95 m) and for Scots *pine* 4.25 m. These values are somewhat low when compared with the study of Canadell et al. (1996), but correspond well with the data of our study. These rather shallow root systems may be caused by the relatively shallow groundwater table in the Netherlands in comparison to other countries. The relatively large rooting depths for Scots *pine* were attributed to the existence of a tap root in soil types such as are found at the Loobos site, i.e. an inland dune system with poor sandy soils. Taking into account the capillary rise of water in the combination with the existence of tap roots means that these eco-systems are often well in reach of groundwater resources. At the same time the average groundwater table depth will limit the maximum rooting depth, but as long as the groundwater table does not fall below levels that can be compensated by capillary rise, these trees will not experience serious stress because of water shortage. These conditions seem to have prevented severe water stress during the period the 5 sites were studied. The importance of the groundwater reservoir has also been demonstrated by among others Nadezhdina et al. (2007) and Vincke and Thiry (2008). The latter reported for Scots *pine* with a maximum groundwater table at 180-200 cm below soil surface, a contribution of 61% of the groundwater reservoir during the growing season, with a maximum of 98.5% during the drought period in June.

Rooting depth of undergrowth

The maximum rooting depths as reported by Canadell et al. (1996) suggest that the undergrowth of forest has rooting depths similar to those of trees. Neither in the *pine* forest, nor in the *poplar* forest, which had the most prominent undergrowth, such deep roots for the undergrowth were observed. Also at both sites the undergrowth partly died in the middle of the growing season and demonstrated a regrowth at the start of autumn. For the *poplar* forest dying and regrowth will also be caused by the competition for light. At the site with *pine* trees with only a minimal variability in the tree leaf area over the year, water shortage is more likely to cause the dieback of the undergrowth in the middle of the growing season. Bakker et al. (2006) observed the highest rooting densities for maritime *pine* in the first 20 cm of the soil profile. This was also true for the undergrowth species at their sites, except for Molinia that had a significant amount of roots at 40 cm depth. These findings are in line with the observations at the *pine* site Loobos. At this site 90% of the roots were found in the

top 30 cm of the soil, with most roots found in the lower part of the litter layer and the first 20 cm of the mineral soil (see Fig. 3.24). Still little is known about what environmental factors govern the variation in root growth and how this may effect the functioning of plants (Brunner and Godbold, 2007), making it difficult to include dynamic roots in land surface models.

It is possible to use total available soil water as an optimization parameter, which implies that an optimal combination is sought for the root distribution and the soil hydraulic characteristics. The thus derived parameter set will however only be applicable for the site under study and will be difficult to apply to other sites. Even for the site studied such a technique does not guarantee a root distribution that resembles reality, see e.g. van Wijk and Bouten (2001).

Modelling root water stress under extreme conditions

Under extreme conditions the water uptake by deep roots is of paramount importance. It was shown that under moderate conditions the use of the soil water content of the total rooting depth gives less optimal results, if compared to the soil water content of the top soil layer. To accommodate the fact that for extremely dry conditions also the water content at the deeper soil layers should be taken into account as is done in the proposed model (see Fig. 7.1). Although the proposed model compared well to the data measured for this study (see Fig. 7.10), severe drought conditions were not observed and an additional test under more extreme conditions is recommended. The proposed model for the simulation of the feedbacks of water stress on the stomatal conductance g_s works well in combination with a model that distributes the root water uptake over the different soil layers based on the optimality-approach (see e.g. Schymanski et al., 2008). This approach assumes that plants have evolved mechanisms that minimise costs related to the maintenance of root system while meeting their demand for water.

Contribution of undergrowth to total evaporation rate

The undergrowth at the two sites with additional measurements showed a clear decrease in evaporation in the summer. This decrease relative to that of the trees could be caused by the low sensitivity to radiation, low optimum temperature and low sensitivity to soil water deficit θ_D of the undergrowth at the pine and poplar site. In addition at the poplar site also the high sensitivity of the undergrowth to vapour pressure deficit e_D plays an important role.

These findings are in contrast to the findings by Körner (1985), who marked *pine* trees as sensitive to high e_D values, and grass species as much less sensitive. The average transpiration rate of the grass undergrowth was 30% of that of the *pine* trees under non water-limiting conditions. During a drought period the transpiration rate of the undergrowth became twice that of the *pine* trees. Similar high evaporation

ratios between trees and undergrowth were reported by Roberts et al. (1980) and Black et al. (1980). Other researchers such as Lindroth (1984) and Kelliher et al. (1986) reported much lower ratios, which are more in line with our results for the undergrowth of the poplar forest at the Fleditebos site and of the pine forest at the Loobos site.

The effect of trees shadowing the undergrowth depends on the canopy cover and the inclination of the sun. Running the radiative transfer model with a tree crown diameter of 4.0 m for different tree densities showed that although the canopy cover reached its maximum value at 300 trees ha^{-1}, the fraction of short wave radiation reaching the undergrowth already reached its minimum at 210 trees ha^{-1} at low solar elevation angles (winter) and at 390 tree ha^{-1} at higher solar elevation (summer). In winter time this fraction is especially high at the beginning and the end of the day, while in summer the maximum values are reached at mid day.

Modelling undergrowth and tree evaporation

The dual source model allowed to simulate the tree and undergrowth contribution to the total evaporation rate separately. The relatively high modelled contribution by the undergrowth at the Loobos site in autumn and winter, i.e. 20 to 40% of total evaporation E_{Tot}, is in contrast to the observed values in October 1997 which were approximately 15%. This overestimation could mainly be attributed to the high simulated undergrowth evaporation.

Although the location of the lower eddy correlation system was selected carefully and as much as possible in the footprint of the higher eddy correlation system, differences may be expected due to the much smaller (factor of 100) footprint of the lower system as compared to the system above the canopy. Wilson et al. (2001) estimated that due to high frequency loss of flux, the flux of the undergrowth may be low by 5-10%. The main cause of uncertainty in the sapflow evaporation data is in the up-scaling to stand level evaporation. The up-scaling is based on the relationship between sapflow, sap wood, trunk diameter and tree density of the stand. At the Loobos site the tree density is variable and changes slightly within the footprint area of eddy correlation set-up on top of the tower. This variability has been taken into account as added uncertainty in the sapflow evaporation data and amounted to 14% of the total stand level sapflow evaporation. The uncertainty in the evaporation rate measured by the eddy correlation equipment was estimated to be between 5 - 15% (see Chapter 5). Taking these uncertainties into account the modelled evaporation of the trees compared well with the sapflow derived evaporation of the pine trees at the Loobos site.

The findings of our study are in line with the undergrowth strategy towards limited water resources as reported by Baldocchi and Xu (2007). At the Loobos and Fleditebos site undergrowth avoids summer drought and is active only during spring

and autumn, when soil water is ample and for the poplar site the tree leaf area is limited.

7.9 Conclusions

The main driver for surface conductance g_s at all sites was vapour pressure deficit e_D. Although a parabolic response function was used for the temperature relationship of g_s, this relationship was not well established at the lower air temperature T_a range. At lower temperatures i.e. below a_T there was no clear reduction of g_s found for these sites at a mid latitude location. This behaviour may be caused by the fact that at lower T_a at these sites the dew on the undergrowth never completely disappeared.

This unclear relationship of g_s at lower T_a and the strong correlation between T_a and e_D for higher T_a makes the temperature relationship of g_s redundant.

Hence, in view of the limited variation between the sites, the parameter values for g_s as $f(T_a)$ may be set to a fixed value. Based on the improved R^2 for almost all years at the different sites after setting $f(T_a) = 1$, it is recommended to use $f(T_a) = 1$ for all forests sites in the Netherlands.

The low sensitivity of the forests to θ_D shows that these forests are not very sensitive to the range of changes in soil water experienced during this study. Whether these forests are sensitive to more severe droughts cannot be concluded from the present data sets. The proposed soil water stress model including a separate soil water feedback from deep soil layers, worked well for the conditions of this study, but needs to be tested for more extreme dry conditions.

The important contribution of the undergrowth to total evaporation rate E_{Tot} has been demonstrated for 2 forest sites in The Netherlands, i.e. the *pine* forest with its undergrowth mainly consisting of grass at the Loobos site and the *poplar* forest with its undergrowth mixture of grass, nettle and cleavers at the Fleditebos site.

The results of the tree evaporation applying the dual source model compared well (see Table 7.9) with the sapflow measurements at the Loobos site. The overestimation of the simulated undergrowth evaporation E_{Low} was most likely because of the limited data set being used for the derivation of the parameter set of Table 7.8. Such datasets are still limited. More extensive datasets will help to decrease the uncertainty in the modelled undergrowth evaporation rate. The considerable contributions of the undergrowth at the *pine* and the *poplar* forest during a large part of the year showed the importance of this component of the total forest water use.

Considering λE of the trees and the undergrowth separately will enable an improved understanding of the functioning of the forest ecosystem. It will also improve

our interpretation of changing conditions affecting trees and undergrowth differently and to determine the combined effect such a change may have on E_{Tot} of the forest. To support such a set-up, the rather limited number of plant functional types (*pft*s) as are being used at the moment to describe forests need to be replaced by *pft*s describing tree species in combination with undergrowth species. These *pft*s should not only allow to take L_{AI} of the undergrowth into account, but also the different phenological phases of the trees and of the undergrowth. The latter will help to improve the simulation of the seasonal differences in the behaviour of g_s, which will provide better estimates of E_{Tot} also outside the growing season.

Chapter 8

Wet canopy evaporation

8.1 Introduction

In the previous Chapter the evaporation rate of a forest under dry conditions was discussed. In contrast to shorter and aerodynamically smoother vegetations, the evaporation rate of forests under wet conditions may be considerable. Under some conditions this may even be as high as 50% of the gross precipitation (e.g. Dolman, 1988).

However, at present there is still no consensus on the best way to model and measure the interception loss and more specifically the canopy storage C (e.g. Aston, 1979; Leyton et al., 1967; Klaassen et al., 1998; Bouten et al., 1991) as well as the evaporation rate of the intercepted water E_i (e.g. Rutter et al., 1975; Gash, 1979; Teklehaimanot et al., 1991; Hormann et al., 1996; Gash et al., 1999; Lankreijer et al., 1999; Crockford and Richardson, 2000; Bosveld and Bouten, 2003; Van der Tol et al., 2003).

The causes for this lack of understanding will be outlined below and the remainder of this chapter will attempt to improve our understanding of how to best estimate canopy storage and interception evaporation. The main questions to be addressed in this Chapter are:

- What is the magnitude of the evaporation rate E_i and the interception water storage capacity C under wet conditions?
- Do E_i and C change for different meteorological conditions?
- Are E_i and C different for different tree characteristics?

In this Chapter the differences in E_i and in C for the forest sites described in Chapter 3 will be analysed, and an attempt will be made to derive improved parametrizations for these sites. The basis for these parametrizations is both the water balance of the vegetation cover (e.g. Rutter et al., 1971) and the energy balance (e.g. Gash et al., 1995). These approaches will be applied to demonstrate the variability and

magnitude of E_i and C at short time steps and to improve the present conceptual ideas on E_i. These new concepts will be applied to derive parametrizations for the sites studied. The main aim of the thesis is to develop a water balance model that is applicable not only for the present well equipped research sites, but also for less well monitored forested sites. Therefore the aim is to derive general physically-based relationships. The applicability of these relations will be demonstrated for the oak forest at the Edesebos site.

8.2 Precipitation characteristics, number of showers per day

Most of the analysis of interception parameters is based on the characteristics of single shower events. However, as the definition of a shower event, particularly its beginning and ending is arbitrary, *often daily data are being used, based on the assumption of one single shower per day.* To check the validity of this assumption characteristics of daily rainfall data were compared with those of showers, defined as continuous rainfall with intermittent dry periods of less than 30 minutes.

Applying this definition, Fig. 8.1 left panel shows that in only 50% of the cases a single shower per day occurs. It also shows that in relatively dry years such as 1996 ($P = 688$ mm) this assumption appears more robust than in relatively wet years such as 1998 ($P = 1270$ mm).

The right panel of Fig. 8.1 shows the frequency distribution of the length of the dry periods in between the showers. In wet years there are more short dry periods than in dry years. Dry periods longer than 5 days (not shown in Fig. 8.1) occur more than 3 times as often in the dry year 1996 as in a wet year 1998.

It is generally assumed that a wet canopy needs 10 hours or more to dry up. For the Loobos site more than 60% of the showers start within 5 hours of the previous one. These numbers may change if an arbitrary start and end of the day, for example mid night or 8 o'clock GMT is used, which will not only change the number of showers, but will also create events that start with a wet canopy. For the relatively wet year 1998 this start has the highest impact and using daily data the number of showers is decreased by 50%.

There is also a shift in the shower distribution: the number of showers between 0.2 and 3 mm are halved, while the frequency of showers greater than 5 mm is almost doubled. The impact of these differences on the parameter estimation will be discussed in Chapter 8.6.

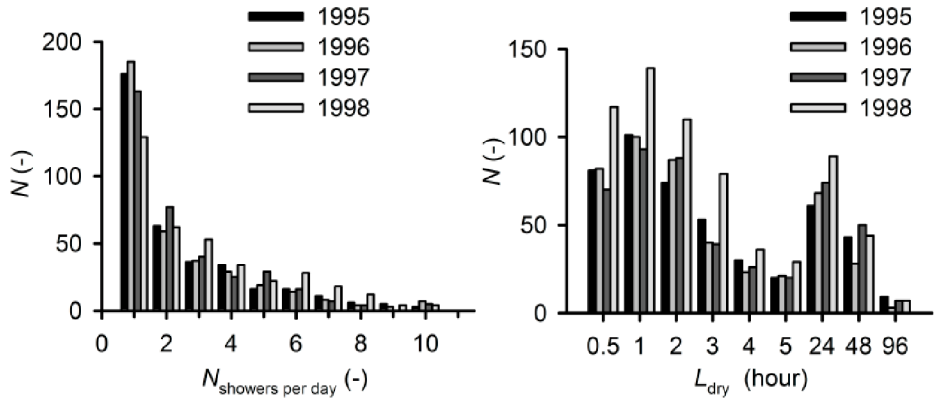

Figure 8.1: *The frequency distribution of the number of showers occurring at one day $N_{showers\ per\ day}$ (left panel) and the time between showers L_{dry} (right panel) measured at the Loobos site in the years 1995 -1998. A shower is defined as one rainfall event with intermittent dry periods of less than 30 minutes. Remark: in the right panel the ticks are at irregular intervals.*

8.3 Evaporation rate of intercepted rain

As suggested earlier, next to the amount of energy available, the rate of evaporation of water from a wet surface E_i is primarily determined by the aerodynamic resistance r_a. The magnitude of r_a is related to the roughness lengths z_0 of the underlying surface for vapour, heat and momentum transport (see Eqs. 2.41 and 2.43). In this Section firstly the behaviour of z_{0H} and z_{0M} under dry and wet conditions will be studied and secondly E_i.

8.3.1 Aerodynamic resistance

At all sites the general trend observed in z_{0H} showed an increase at the start of a shower, a decrease during the showers and an increase again just after the shower ceased. the aerodynamic resistance z_{0M} showed an increase during the shower. Using Eq. 2.67 the behaviour of z_{0H} and z_{0M} is shown in Fig 8.2 as kB^{-1} for dry and wet, i.e. $P \geq 0.4$ mm 30 min^{-1} conditions. Here the assumption is made of equal displacement heights d for momentum and heat.

To reduce possible differences between the radiative T_s and aerodynamic T_s, data were selected for $u_* > 0.2$ m s^{-1}.

Fig. 8.2 shows for pine forest with its relatively open canopy under unstable conditions that z_{0H} and z_{0M} do not differ much, i.e. kB^{-1} is close to zero. If the stability corrections are applied, the horizontal part of the graph lowers on average

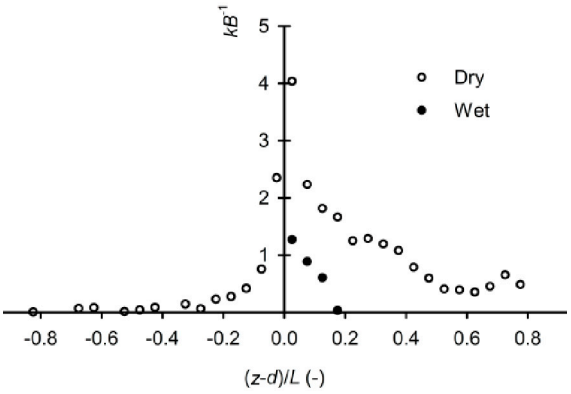

Figure 8.2: *Averaged values of kB^{-1} (not including the stability terms) as a function of equidistant bins of the stability $(z-d)$ / L for the pine stand at the Loobos site in 1997 for both dry and wet conditions.*

with 0.34, resulting in a slightly negative kB^{-1}.

For *dry stable* conditions kB^{-1} decreases with increasing stability classes showing the dependency on u_*. Often this relationship is reported as a function of the root or a power close to 0.5 of u_* or the Reynolds number Re (e.g. Garratt and Hicks, 1973; Mölder and Kellner, 2002) in combination with vegetation characteristics such as the leaf width and L_{AI} (e.g. Brutsaert, 1982; McNaughton and Van den Hurk, 1995).

For *dry unstable* conditions the relation with the friction velocity and kB^{-1} can be modelled as a weak function of the Reynolds number. For the pine site this relationship would result in $kB^{-1} = 0.003Re^{0.54} - 1.55$ ($R^2 = 0.25$), where $Re = u_* z_{0M}/\nu$ with ν ($\mathrm{m^2 s^{-1}}$) being the kinematic viscosity. This equation resembles similar equations as being derived for other vegetated surfaces (e.g. Mölder and Lindroth, 2001). In view of the very weak dependency on u_* however, a constant value for kB^{-1} seems to be more appropriate. The value found for dry unstable conditions at noon for the month July $kB^{-1} = -0.43$ corresponds well with the value of -0.5 reported by Mölder and Lindroth, 1999) for a mixed pine spruce forest with a L_{AI} varying between 4 and 6 $\mathrm{m^2\ m^{-2}}$. Similar findings were obtained by Hall (2002) for coppiced poplar and by Bosveld (1999) kB^{-1} for a Douglas fir plantation with a L_{AI} of 8-11 $\mathrm{m^2\ m^{-2}}$. These authors explain the negative value by the near zero bluff body contribution of the very thin needles causing a high eddy diffusivity for heat within the roughness sub-layer and in the canopy.

For *wet* conditions the atmospheric stability is mainly *stable*. For these conditions the average kB^{-1} is distinctly lower as compared with stable dry conditions, but on

Table 8.1: *Average values for kB^{-1} for the years 1996 and 1997 for four sites. At the Bankenbos, Fleditebos and Kampina sites the data used encompass the three summer and winter months of each year. Dry conditions were defined as periods preceded by 12 hours without rain, wet as periods with $P \geq 0.4$ mm (30 min)$^{-1}$. σ denotes the standard deviation.*

Site		kB^{-1} (-)						u_* (m s^{-1})		
		Unstable		Stable				Unstable	Stable	
		Dry	σ	Dry	σ	Wet	σ	Dry	Dry	Wet
Bankenbos	s	0.39	0.98	2.47	2.58	1.56	2.24	0.72	0.41	0.58
(Larch)	w	2.07	1.79	6.04	3.88	1.46	2.38	0.73	0.50	0.82
Fleditebos	s	0.23	1.44	4.09	3.14	3.26	2.64	0.60	0.40	0.53
(Poplar)	w	3.09	2.62	8.70	4.84	5.28	3.96	0.64	0.49	0.66
Kampina	s	-0.39	0.68	4.79	4.09	4.43	4.31	0.62	0.44	0.56
(Mixed)	w	0.60	1.40	8.15	4.57	6.22	4.36	0.66	0.47	0.60
Loobos	All	-0.14	1.26	3.25	3.40	1.53	2.53	0.59	0.44	0.67
(Pine)										

average higher if compared with unstable dry conditions. Similar trends were found at all four sites (see Table 8.1).

The averages of Table 8.1 were calculated taking for unstable conditions $(z - d)/L < -0.01$ and for stable conditions $(z - d)/L > 0.01$. The relatively large standard deviation is mainly caused by values close to neutral. Overall the results show a tendency for low kB^{-1} values during the foliated summer months and high values during the non-foliated winter months. Comparison between sites shows high values of kB^{-1} corresponding with sites having a high L_{AI} for both dry and wet stable conditions. For unstable conditions however such a trend is not clear. The relatively small value for the mixed site during unstable conditions may be caused by the presence of pine trees. The reason why this value does not hold under stable conditions is not clear.

Differences in *tree characteristics* and u_* may influence the magnitude of kB^{-1}.

For *wet* conditions the sites can be split in two groups: needle leaf trees with a low value of $kB^{-1} \approx 1.5$ and broad leaf trees with a high value of $kB^{-1} \approx 3.2 - 6.2$. In contrast to dry conditions, the presence of needles at the larch site for wet conditions seems to have little effect. For wet conditions no relationship between kB^{-1} and u_*, L_{AI} and leaf length scale L_c (m) could be derived.

For *dry unstable* conditions using average values of u_*, L_{AI} (and W_{AI} for the non–foliated season) and taking a typical value for $L_c = 0.01$ m, the following relationship

($R^2 = 0.88$) could be established:

$$kB^{-1} = -1.32 + \frac{36.2}{L_{AI}}\sqrt{L_c u_*} \tag{8.1}$$

This relationship resembles the theoretical relation for a relatively open canopy as given by McNaughton and Van den Hurk (1995) reasonably well. However the uncertainty of this relation is large, for example omitting the data of the winter period at the deciduous sites reduces the slope as well as the explained variance by 50%. Also differences between years can be considerable.

In conclusion: our results show that kB^{-1} changes with stability classes. In general kB^{-1} is lower for wet conditions than for dry stable conditions. This behaviour seems to be caused mainly by changes in z_{0H} during showers. Under wet conditions, only for rare occasions with relatively high atmospheric stability kB^{-1} approaches 0, while under these conditions r_a is well defined by z_{0M}. Applying a fixed value $kB^{-1} = 1.5$ instead of $kB^{-1} = 2.0$ for the pine site changes an underestimation of 32% to just 8% in the calculated E as compared to the measured E. For this site with $kB^{-1} = 0.0$ i.e. $z_{0M} = z_{0H}$, an average overestimation in E of 30% has been found.

8.3.2 Evaporation rate of wet vegetation

Measurements of *precipitation* P, *throughfall* T_f and *stemflow* S_f and Eq. 2.66, i.e. the Gash-model, can be used to derive E. The amount of water intercepted by the vegetation and subsequently evaporated E_i is:

$$E_i = P - T_f - S_f \tag{8.2}$$

Plotting the derived interception losses E_i against P for events large enough to saturate the canopy gives the ratio $\overline{E}/\overline{P}$ (Gash, 1979; Loustau et al., 1992). Table 8.3.2 shows the sensitivity of this method for the integrating time step being applied, i.e. $\overline{E}$ decreases by a factor of 2 if the duration of showers is used instead of hourly data. This sensitivity is primarily caused by the rainfall distribution as shown in Fig. 8.1.

Another method to derive λE is based on *micro-meteorological techniques*. However, particularly during and after showers, λE appears to be underestimated by the direct measurements using a closed path gas analyser. For the open path, however, showers tend to cause many spikes in the measurements, resulting in data gaps. Calculating λE as a residual of the energy balance is a good alternative under such conditions. In Fig. 8.3a E measured above the canopy using the infra-red gas analyser is plotted against E derived as the residual from the energy balance. During and

Table 8.2: *The ratio $\overline{E}/\overline{P}$ and the average evaporation rate $\overline{E}$ for the period 1995 to 1998 at the pine forest of the Loobos site. With an average precipitation rate P of 1.54 mm h^{-1} (with a minimum of 1.31 and a maximum of 1.63 mm h^{-1}) for $P > 0.4$ mm h^{-1}. For the hourly data the canopy was assumed being saturated for $P > 0.4$ mm h^{-1}. Showers were defined as a rainfall event preceded by a dry period of more than 10 hours.*

	Hourly		Daily		Shower	
	Mean	R^2	Mean	R^2	Mean	R^2
$\overline{E}/\overline{P}$ (-)	0.19	0.30	0.13	0.41	0.10	0.25
$\overline{E}$ (mm h^{-1})	0.29		0.20		0.15	

just after rainfall for the Loobos site sensible heat flux H above the canopy is often negative with values ranging between -25 to -100 W m^{-2} (see Fig. 8.3b). This behaviour is caused by $T_s < T_a$ above and below the canopy (± 0.5 ^{0}C). During daytime and under wet conditions H below the canopy is small but positive (± 10 W m^{-2}). This situation, together with the negative H above the canopy causes the canopy to act as a well-ventilated wet bulb and enhances the energy available for evaporation of the overlying canopy layer. The average contribution of the undergrowth at the pine forest for hours with $P > 0.4$ mm h^{-1} is 11% of the total evaporation and 14% at the poplar forest for the months April and June.

Total duration of evaporation of intercepted water: From the sapflow measurements it is clear that at least for the shower analysed in Fig. 8.3 there is no transpiration taking place. For smaller showers during daytime also an abrupt although delayed decrease in transpiration is observed. The lag in time of the transpiration as measured by the sapflow compared to that measured by micro-meteorological techniques is in general due to changes in the amount of water stored in the sapwood of the tree (e.g. Swanson, 1994).

Kume et al. (2006) argued that the time needed to restore the sapflow to its normal level may be considered as the time needed to dry the canopy. Using this assumption shows that after a continuous shower started at 20h00 the day before at the pine site, between 10 to 13 hours are needed before the sapflow is returned to its normal level (see Fig. 8.4). Using the sapflow signal to indicate the moment when the canopy is dry, and using the end of throughfall as the time the canopy is saturated and drainage has stopped, makes it possible to estimate C and $\overline{E}$ during this period. The thus derived C is 1.65 mm and $\overline{E}$ for this period is 0.19 mm h^{-1}. The latter is approximately twice as high as $\overline{E}$ during the hours with rain (0.11 mm h^{-1} for $P > 0.4$ mm h^{-1}).

A third alternative to estimate E of intercepted precipitation is the use of the *Penman-Monteith equation* (see Eq. 2.35) with $r_s = 0$. The results of this approach

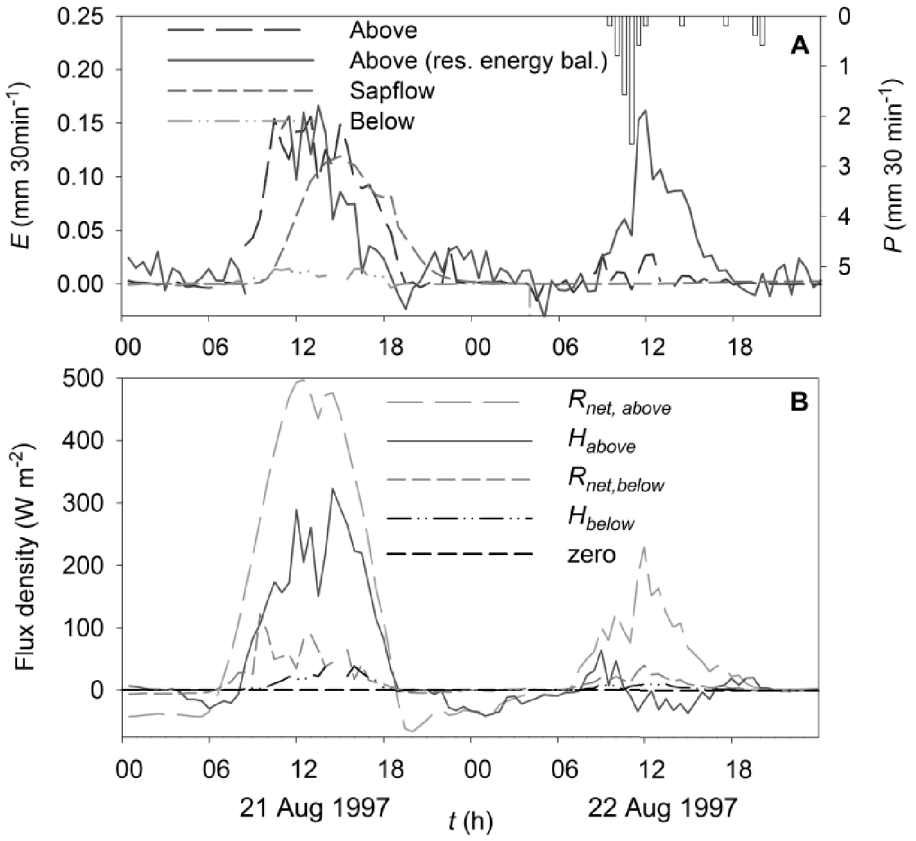

Figure 8.3: *Panel* ***A*** *shows the evaporation rates E at the Loobos site for 21 and 22 August 1997: measured above the canopy using a Licor 6262 gas-analyser, as derived from the energy balance, from sapflow measurements and measured below the canopy. The vertical bar graph represents the precipitation rate P. Panel* ***B*** *shows net radiation* R_{net} *and sensible heat H flux densities both above and below the canopy.*

are sensitive to the correct parametrization of r_a, which depends on z_{0M} and z_{0H}. For vegetation often the ratio between these roughness lengths is taken as $kB^{-1} = \ln(z_{0M}/z_{0H}) \approx 2.0$ (Brutsaert, 1982). Fig 8.5 shows for the pine site the variation of E under wet conditions, applying flux measurements and solving the energy balance. Also depicted are E using Penman-Monteith with $kB^{-1} = 2.0$ depicted as r_{aH} and $kB^{-1} = 0.0$ depicted as r_{aM}. Fig. 8.5 shows that in the first two years at this site the use of a value $kB^{-1} = 2.0$ provides estimates of E best resembling the measurements, however especially in the last year $z_{0M} = z_{0H}$ gives best results. In conclusion: using

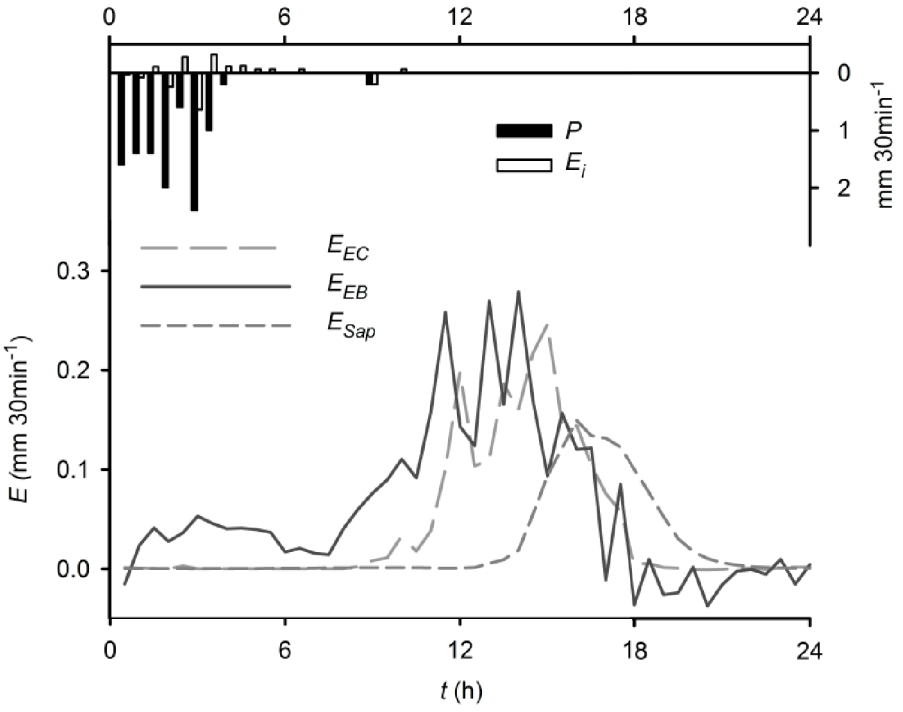

Figure 8.4: *Gross precipitation P, interception rate E_i $(= P - T_f - S_f)$, evaporation rates as derived directly from the eddy-correlation system E_{EC}, as the residue of the energy balance E_{EB} and transpiration from the sapflow measurements E_{Sap} at the pine forest of the Loobos site on 2 September 1997.*

a value for kB^{-1} based on measurements at a specific site gives a good estimation of E as compared to E derived by flux measurements, i.e. differences are less than 10% if a site and year specific average is used.

For the sparse canopy model the Penman-Monteith derived E is considered to be per unit canopy cover and should thus be multiplied by the cover fraction c_{veg} to derive E per unit ground area (Gash et al., 1995). The measured monthly average E for the 11 years of the pine site compared best with the canopy cover corrected $c_{veg}E_{PM,r_{aH}}$ using r_{aH} (see Table 8.3.2).

At the mixed forest site with its almost closed canopy in summer and open canopy in winter similar results were obtained (see Fig. 8.6). During the summer months it is evident that the use of z_{0M} gives an overestimation. E using z_{0H}, based on the kB^{-1} values of Table 8.1, and corrected for the canopy cover, resembles the best measured E.

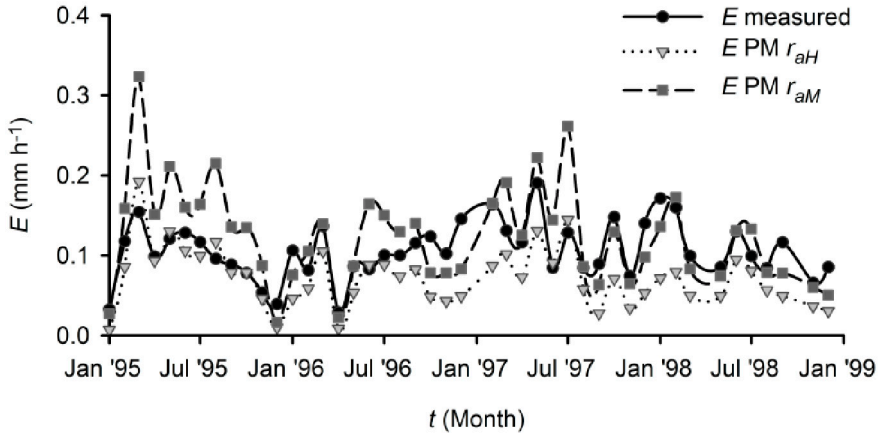

Figure 8.5: *Monthly averages of the evaporation rate under wet conditions ($P \geq 0.4$ mm h^{-1}) at the pine forest. The measured evaporation rate E is based on both flux measurements and solving the energy balance. Also depicted are the Penman-Monteith evaporation using $kB^{-1} = 0.0$ (E PM r_{aM}) and $kB^{-1} = 2.0$ (E PM r_{aH}).*

Table 8.3: *The slope a of the regression line ($E_{meas} = x_0 + aE_{PM}$) using roughness length of momentum $E_{PM,r_{aM}}$ and the roughness length of heat $E_{PM,r_{aH}}$. Also shown are the regression results for the canopy cover corrected E, i.e. $c_{veg}E_{PM,r_{aM}}$ and $c_{veg}E_{PM,r_{aH}}$. Where $x_0 = 0.05$ mm h^{-1} and c_{veg} is the fractional canopy cover. ($R^2 = 0.53$ for r_{aM} and $R^2 = 0.55$ for r_{aH}).*

	$E_{PM,r_{aM}}$	$E_{PM,r_{aH}}$	$c_{veg}E_{PM,r_{aM}}$	$c_{veg}E_{PM,r_{aH}}$
a	0.44	0.60	0.63	0.86

$\overline{E}$ based on the ratio of $\overline{E}/\overline{P}$ derived by regression analysis are relatively high (0.15 - 0.29 mm h^{-1}), if compared to E during showers ($P \geq 0.4$ mm h^{-1}) derived from the measured H and if compared to E calculated based on the Penman-Monteith formulation. However, these high rates correspond reasonably well with $\overline{E}$ just after a shower (see Fig. 8.4). The difference between the two rates may well be caused by the fact that E based on throughfall totals per hour, day or shower include E taking place after the throughfall has ceased. When using hourly data of E derived from flux measurements for wet conditions (i.e. $P \geq 0.4$ mm h^{-1}) these relatively high values of E after the rainfall has ceased are not included.

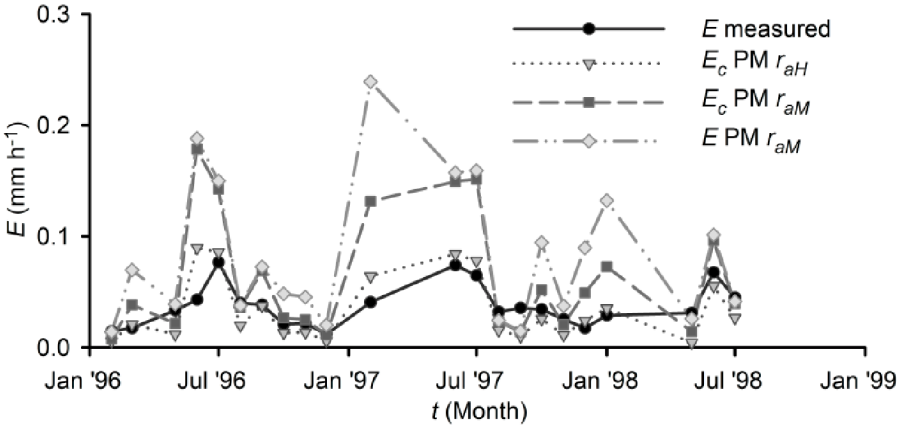

Figure 8.6: *Monthly averages of the evaporation rate E under wet conditions ($P \geq 0.4$ mm h^{-1}) for the mixed forest at the Kampina site. The Penman-Monteith evaporation rate is given per unit canopy cover using the surface roughness length for heat E_c PM r_{aH}, as well as using the surface roughness length for momentum per unit canopy cover E_c PM r_{aM} and per unit ground area E PM r_{aM}.*

Table 8.4: *The water storage capacity C (mm) calculated for different periods and different forest sites using daily totals and applying the analysis as outlined by Leyton et al. (1967).*

Period	Larch Bankenbos		Oak Edesebos		Poplar Fleditebos		Mixed Kampina		Pine Loobos
	Foli-ated	Bare	Foli-ated	Bare	Foli-ated	Bare	Foli-ated	Partly fol.	Foliated
1988	-	-	0.7	0.2	-	-	-	-	-
1989	-	-	0.5	0.2	-	-	-	-	-
1995	0.4	0.3	-	-	0.6	0.2	-	-	0.5
1996	0.5	0.3	-	-	0.5	0.2	0.7	0.3	0.6
1997	0.4	-	-	-	0.5	0.3	0.8	0.4	0.5
1998	-	-	-	-	-	-	0.8	-	0.5

8.4 Storage of intercepted precipitation

The capacity of a vegetation layer to store water i.e. C, plays a major role in most models simulating interception losses.

Leyton's analysis: The method commonly used to derive this storage capacity is based on the work of Leyton et al. (1967). The results for the 5 sites using their method are presented in Table 8.4.

Dependency of C on tree characteristics For these 5 sites an exponential model

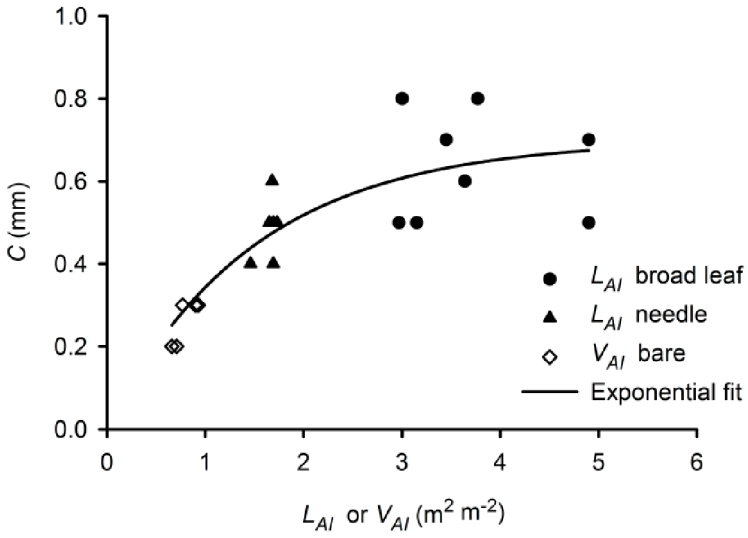

Figure 8.7: *The water storage capacity C as derived by Leyton's analysis using daily data as a function of the Vegetation Area Index V_{AI}. During the foliated period instead of V_{AI} L_{AI} has been used.*

describes best the $C(V_{AI})$ relationship (see Fig. 8.7):

$$C(V_{AI}) = 0.7(1 - \exp^{-0.67\ V_{AI}}) \qquad R^2 = 0.75 \tag{8.3}$$

For values of $L_{AI} > 3$ the increase in C with increasing leaf area becomes less. This exponential rise of C to a maximum is partly due to the fact that for $L_{AI} > 3$ the canopy cover of most forests in The Netherlands is almost 100%. These results also show the amount of variation associated with these numbers. Hence care should be taken when applying these results to different sites. Besides the leaf area, other characteristics of the tree such as the angle of leaves and branches and the distribution of the leaves also play a role in the relationship between C and L_{AI} (see e.g. Appendix F). For example adding the leaf angle or the gap fraction will increase the variance explained by approximately 10% ($R^2 = 0.87$).

The above mentioned strong link between L_{AI} and canopy cover can be well explained in analogy with radiative transfer models for canopies. To simulate the extinction of radiation by a canopy often a Beer-Lambert type equation is used :

$$x = x_0(1 - \exp^{-\vartheta L_{AI}}) \tag{8.4}$$

where ϑ denotes the extinction factor. This relationship is among others used by the LAI-2000 sensor (LiCor) to estimate the gap fraction. For mid latitude forests

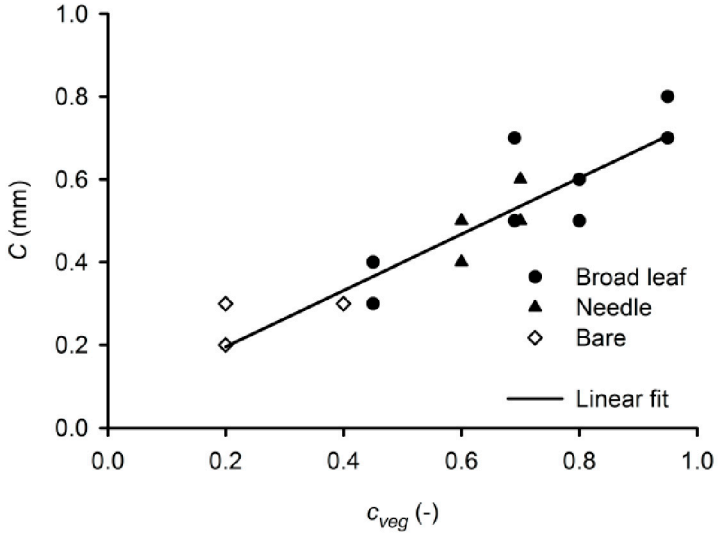

Figure 8.8: *The water storage capacity C as a function of the fractional vegetation cover c_{veg}. Broad leaf: oak, poplar and mixed forest (leaf bearing period). Needle: pine and larch (leaf bearing period). Bare: poplar, oak, larch (non-foliated period).*

ϑ usually ranges between 0.6 and 0.8. The gap fraction obtained by the LAI-2000 sensor gives a rough estimate of the fractional canopy cover c_{veg}. With maximum c_{veg} set equal to 1 and combining Eqs. 8.3 and 8.4 shows that C depends linearly on c_{veg}, with $C_{\max} = 0.7$ mm. This is confirmed by our data. Fig. 8.8 shows the almost linear relation ($R^2 = 0.86$) found for the forests studied

$$C = 0.06 + 0.68\ c_{veg} \tag{8.5}$$

where c_{veg} is obtained by analysing digital photographs of the canopy cover using image processing software.

It is evident that this linear relationship only holds for forest with relatively low L_{AI} and low c_{veg}. Completely closed canopies often associated with high L_{AI} will most likely produce higher C than the maximum found for these mid latitude forests. However, the scatter in the data of van Dijk and Bruijnzeel (2001a) on C for forests with high L_{AI} is such that it is impossible to obtain a unique relation between tree characteristics and C. It should be kept in mind that part of the scatter in these studies is due to the use of different methods to derive C. Hence when estimating interception losses with non site specific estimates of C the large variation in C may lead to erroneous results, especially for forests with $L_{AI} > 3$ m^{2}m^{-2}.

Inverse model: As an alternative to the method of Leyton, C was also derived

Table 8.5: *Water storage capacity C on an areal basis (mm), average measured evaporation $\overline{E}$ (mm h^{-1}) and average precipitation rate $\overline{P}$ (mm h^{-1}) for the three winter and the three summer months.*

Period		Larch Bankenbos			Poplar Fleditebos			Mixed Kampina			Pine Loobos		
		C	$\overline{E}$	$\overline{P}$	C	$\overline{E}$	$\overline{P}$	C	$\overline{E}$	$\overline{P}$	C	$\overline{E}$	$\overline{P}$
1995	w		0.10	1.01	-	0.10	1.26	-	-	-	-	0.13	1.21
	s	1.58	0.14	1.49	0.94	0.14	1.70	-	-	-	1.25	0.11	1.81
1996	w	0.60	0.08	0.60	1.43	0.10	1.28	0.65	0.06	0.73	0.92	0.09	1.22
	s	2.16	0.12	1.95	0.90	0.13	1.45	1.52	0.11	1.63	1.88	0.11	1.87
1997	w	0.98	0.14	1.20	1.12	0.09	1.12	1.48	0.07	0.88	1.07	0.16	1.20
	s	1.18	0.16	1.32	0.88	0.13	1.32	1.03	0.12	1.19	1.48	0.12	1.85
1998	w	-	-	-	1.16	0.12	1.36	1.83	0.04	1.04	1.88	0.13	1.53
	s	-	-	-	-	-	-	1.26	0.12	1.31	-	0.11	1.85

using the sparse canopy Gash model (see Eq. 2.68). To ensure saturated conditions only daily data with $P > 1.5$ mm d^{-1} have been used. Average precipitation $\overline{P}$ and evaporation $\overline{E}$ rates were calculated for those hours when $P > 0.4$ mm h^{-1} per period of three months, i.e. summer: July-September and winter: January-March (see Table 8.5). E was derived as the residual of the energy balance.

For all sites the highest $\overline{P}$ has been found in the summer months. To a lesser extend this also holds true for $\overline{E}$. At the pine site the differences in $\overline{E}$ between years is relatively small, the continuous presence of the needles seems to keep $\overline{E}$ at the same level. The trends in C are however less clear. The two sites with needle leaf trees show a high C-value in summer, while for the poplar site and the mixed site the highest values are found in winter time. In general the thus derived C is 2 to 4 times as high as has been found using the Leyton analysis (Table 8.4); for the non-foliated period the difference is even larger.

In Fig 8.9 the storage capacity on a canopy cover basis C_c for the pine site is depicted as averages per three month period. Based on the measurements of P on top of the scaffolding tower a threshold of $P > 1.5$ mm h^{-1} gave the best simulated E_i for this 11 year period resulting in an average C of 1.67 mm ($\sigma = 1.23$ mm) and an underestimation of measured E_i of 0.5% with a total RMSE = 0.54 mm and RMSE = 0.84 mm for saturated conditions only.

Fig 8.9 shows a slow increase in C_c until the end of 2001, after that a slow decrease. Although there is no significant correlation with $\overline{P}$ or $\overline{E}$, the increasing trend corresponds to a slightly increasing trend in both $\overline{E}$ and somewhat stronger in $\overline{P}$. This increasing trend in $\overline{E}$ and $\overline{P}$ is opposite to the trend observed in V_{AI}, which shows a small but continuous decrease after 1996.

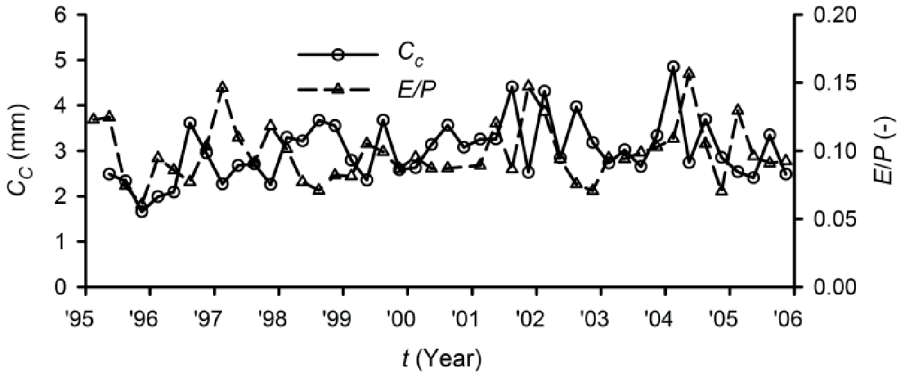

Figure 8.9: *The average water storage capacity per season on canopy cover basis, i.e. C_c, and the ratio of average measured evaporation rate and precipitation, i.e. $\overline{E}/\overline{P}$ for the pine site calculated applying the Gash-model (Eqs. 2.65 and 2.66).*

Dependency of C on meteorological variables

To further investigate if there is any dependency between the amount of water on the leaves and parameters such as u and P, two approaches have been used.

For the first approach showers were selected for which the canopy was not saturated i.e. total $P \leq 1.5$ mm, E was almost negligible i.e. total $E < 0.1$ mm. For these showers $(P - T_f - S_f)$ should equal the amount of water on the leaves C.

These values of C were checked for correlation with wind speed u, standard deviation of the wind speed σ_u, precipitation P, net radiation R_{net}, evaporation E and vapour pressure deficit e_D. To minimize the effect of different L_{AI} the data set was split up in summer and winter months. For both data sets there was no correlation found with any of these parameters, with the exception of P giving the highest positive correlation ($R^2 = 0.20$ in winter and $R^2 = 0.47$ in summer).

As a second approach daily values of C derived by the Gash-model (Eq. 2.68) have been used. As a consequence of the model concept used, showers less than the saturation threshold contain no information on C. On a yearly basis, for showers saturating the canopy, the strongest correlation of C found was with E and P ($R^2 = 0.3-0.4$ depending on the year). There exists, however, neither significant correlation with the daily averages nor with the averages being based on wet hours only of available energy A, sensible heat H, air temperature T_a, vapour pressure deficit e_D, wind speed u and friction velocity u_*.

Selecting data on the basis of the size of rainfall events, showed that the correlation between C and E becomes stronger for bigger showers especially during the summer months (see Table 8.4). During the winter half year a negative correlation between C

Table 8.6: *Dependency of the storage capacity C on E, H, A, T_a, D_e, u and u_* expressed as R^2 (significant at the 95 percent confidence level). The data set is split by different intensities of P and seasons.*

	$P > 1.5$ mm d^{-1}	$1.5 < P < 1.7$ mm d^{-1}		$2.0 < P < 4.0$ mm d^{-1}		$P > 4.0$ mm d^{-1}	
	All year	Summer	Winter	Summer	Winter	Summer	Winter
E	0.4	<0.1	<0.1	0.23	0.3	0.39	<0.1
H	<0.1	<0.1	<0.1	<0.1	<0.1	<0.1	<0.1
A	<0.1	<0.1	<0.1	<0.1	0.3	<0.1	<0.1
T_a	<0.1	<0.1	<0.1	<0.1	<0.1	<0.1	<0.1
e_D	<0.1	<0.1	<0.1	<0.1	0.3	<0.1	<0.1
u	<0.1	<0.1	0.29	<0.1	<0.1	<0.1	<0.1
u_*	<0.1	<0.1	0.37	<0.1	0.15	0.21	<0.1

and u ($R^2 = 0.29$) and u_* ($R^2 = 0.37$) was found. For larger showers this correlation weakened ($R^2 = 0.15$; significant at the 95% confidence level, but not at the 99% confidence level) and changed to a positive slope. For $P > 4.0$ mm d^{-1} there existed no correlation with any of the parameters tested in winter time, while in summer time the strongest positive correlation was observed with E ($R^2 = 0.39$) and to a lesser extend with u_* ($R^2 = 0.21$).

8.5 Verification of interception parametrization

8.5.1 Application of the interception parametrization to the Edesebos site

To test the applicability to other sites of the above parametrizations for E and C, the sparse Gash model i.e. Eq. 2.66 using daily P as input is applied to an independent site.

As verification data the measurements of the oak forest at the Edesebos site are used. This site is the same site as has been used by Lankreijer et al. (1993) and is based on the work of Hendriks et al. (1990). The small differences in their results and the present study are among others caused by the fact that, contrary to the present study, in these other studies only part of the data set have been used.

It was assumed that besides information on z_{tree}, c_{veg} and the almost always present automatic weather station variables no other information was available. As for the year 1990 only precipitation data were available, the ratio $\overline{E}/\overline{P}$ had to be based on the data of 1989. For all model runs d and z_{0M} were calculated based on relations with tree height, z_{tree} as found by Dolman (1986) for an oak forest in a

different part of the Netherlands. In Table 8.7 the interception losses for the oak forest at the Edesebos site are shown.

For the verification of E two options have been compared:

- Run 2 and 4 with $\overline{E}$ based on $kB^{-1} = 0$ corrected for the fractional canopy cover following Gash et al. (1995), and
- Run 1 and 3 with $\overline{E}$ using $kB^{-1} = 3$ for the foliated months and $kB^{-1} = 5$ for the non-foliated months based on the values for stable wet conditions of the poplar site (see Table 8.1).

For the verification of C two options have been compared:

- Run 1 and 2 with C based on C derived by the method of Leyton (see Fig. 8.8), and
- Run 3 and 4 with C obtained by inverting the Gash-model for the poplar site (see Table 8.5).

The parameters used and the results of the model runs are summarized in Table 8.7.

For this data set measured $\overline{E}$ is best simulated using the values of kB^{-1} as measured at the poplar site (run1 and run 3). If it is assumed that $\overline{E}$ with a $kB^{-1} = 0$ is on a canopy cover basis, $\overline{E}$ of run 2 and 4 is also close to the measured rates. Consequently the differences in $\overline{E}$ between run 1 and 2 and run 3 and 4 are minor.

The main differences in $\overline{E}$ are caused by the different values of C. C based on the values derived solving the Gash model for the poplar site (run 3 and 4) approach the site specific values based on the use of Leyton's analysis for the foliated months. For the partly foliated months the storage capacity is much higher. As to be expected the values of C based on the relation of Fig. 8.8 (run 1 and 2) resemble much better the site specific C using Leyton's analysis, especially for 1989.

The overall effect on the interception loss differs between periods and years. Run 1 and 2 give the best results for the foliated months of 1988 and 1990 and for the partly foliated months of 1989. For this data set the use of $kB^{-1} = 0$ and assuming all available energy is used by the evaporation of the wet canopy provides similar good results as the use of kB^{-1} values of the poplar site. The value of C based on the data of the poplar site (run 3 and 4) is clearly too high for the foliated period of 1988, although it is only 0.1 mm higher than the value derived by Leyton's analysis, $C = 0.7$ mm. For the partly foliated periods of 1988 and 1990 the results compare fairly well with the measurements.

Table 8.7: *Interception parameters and total measured and modelled interception loss for the oak forest at the Edesebos site. "Fol." stands for foliated period (July, August and September), Part fol. represents the partly foliated period at the beginning and end of the growing season (May, June and October). The symbol Δ indicates the differences between modelled and measured interception loss as percentage of the measured value.*

	Quantities	1988		1989		1990	
		Fol.	Part fol.	Fol.	Part fol.	Fol.	Part fol.
	d (m)	$0.75z_{tree}$					
	z_{0M} (m)	$0.1z_{tree}$					
	c (-)	0.69	0.4	0.69	0.4	0.69	0.4
	$\overline{P}$ (mm h^{-1})	1.90	1.87	2.33	1.73	2.33	1.73
Meas.	$\overline{E}$ (mm h^{-1})	0.11	0.09	0.10	0.17	-	-
	C (mm)	0.7	0.2	0.5	0.2	-	0.2
	E_i (mm)	41.6	26.1	27.2	18.6	4.0	16.3
Run 1	kB^{-1} (-)	3.0	5.0	3.0	5.0	3.0	5.0
	$\overline{E}$ (mm h^{-1})	0.10	0.08	0.07	0.09	0.07	0.09
	C (mm)	0.53	0.20	0.53	0.20	0.53	0.20
	E_i (mm)	41.0	16.3	20.9	18.1	6.1	10.8
	Δ (%)	-1	-37	-23	-2	+53	-34
Run 2	kB^{-1} (-)	0	0	0	0	0	0
	$\overline{E}$ (mm h^{-1})	0.21	0.24	0.13	0.25	0.13	0.25
	C (mm)	0.53	0.20	0.53	0.20	0.53	0.20
	E_i (mm)	47.1	17.4	22.0	17.8	6.4	11.0
	Δ (%)	+13	-33	-19	-5	+59	-33
Run 3	kB^{-1} (-)	3.0	5.0	3.0	5.0	3.0	5.0
	$\overline{E}$ (mm h^{-1})	0.10	0.08	0.07	0.09	0.07	0.09
	C (mm)	0.80	1.15	0.80	1.15	0.80	1.15
	E_I (mm)	59.0	26.0	27.2	29.3	8.6	17.4
	Δ (%)	+42	-0	+0	+57	+114	+7
Run 4	kB^{-1} (-)	0	0	0	0	0	0
	$\overline{E}$ (mm h^{-1})	0.21	0.24	0.13	0.25	0.13	0.25
	S (mm)	0.80	1.15	0.80	1.15	0.80	1.15
	E_I (mm)	64.6	27.0	28.3	29.2	8.7	17.6
	Δ (%)	+55	+3	+4	+57	+118	+8

8.5.2 Effect of temporal variation in $\overline{E}/\overline{P}$ and water storage C

To know the behaviour of the model during the non-foliated period and to minimise the differences caused by changes in $\overline{E}$ and $\overline{P}$, the model has also been run using the complete records of precipitation data and using monthly averages for $\overline{E}$ and $\overline{P}$. For

the months May until October these averages were based on calculations as described above for run1 and run2. For the winter months no data were available to calculate $\overline{E}$, however from Table 8.1 it was concluded that the ratio $\overline{E}/\overline{P}$ is fairly constant for these months at the mixed forest and poplar site. Thus for the winter months a fixed ratio $\overline{E}/\overline{P} = 0.08$ was used for the run using kB^{-1} of the poplar site and $\overline{E}/\overline{P} = 0.136$ for the run using $kB^{-1} = 0$. For the storage capacity the values based on the Leyton analysis for the site were used.

Fig. 8.10 shows the results if monthly values are used for $\overline{E}/\overline{P}$ and seasonal values for C. For all three years total P is 1392 mm, total measured E_i is 188.2 mm, simulated E_i using the kB^{-1} values of the poplar site (run 1) gives a small overestimation, 192.4 mm (+2%) and using $kB^{-1} = 0$ (run2) there is a slight underestimation 184.0 mm (-2%). The model efficiency F expressed as:

$$F = 1 - \frac{1}{N}\sqrt{\sum (x_{meas} - x_{sim})^2} \tag{8.6}$$

is 0.97 for both runs, indicating that the day to day estimates of the two runs are equally good. However, on average over longer periods run1 has a positive and run2 a negative bias. The model runs behave similarly during the foliated months and show an overestimation in 1988 and 1990 and an underestimation in 1989. During the non-foliated period run1 has a tendency to overestimation while run2 tends to an underestimation in all years. For 1989 the differences between the two model runs are non existent, except after the end of October when run2 underestimates the measured interception loss while run1 shows an almost equally sized overestimation. In 1990 both, run 1 and run2 perform badly for the months April until July. However, the underestimation by run1 for this period is compensated by the overestimation of the three months before.

The differences between the two runs are caused by the different values for the threshold required to saturate the canopy for the non-foliated period. The overestimation during the foliated period in 1988 is caused by the relatively high C. The latter in combination with the high $\overline{E}$ for run2 causes this run to even further overestimate E_i. During the foliated period of 1989 $\overline{E}$ for both runs is almost identical, combined with a lower value for C than was used for 1988 gives the good modelling results.

The differences between the runs change from year to year, indicating that fixed parameter values may decrease the model's daily performance considerably. These differences are not because of the use of monthly averages of $\overline{E}$ and $\overline{P}$, but mainly because of the higher measured value of C used for the foliated period of 1988. These higher C-values for the foliated period decrease the model performance by an extra 15% for both runs.

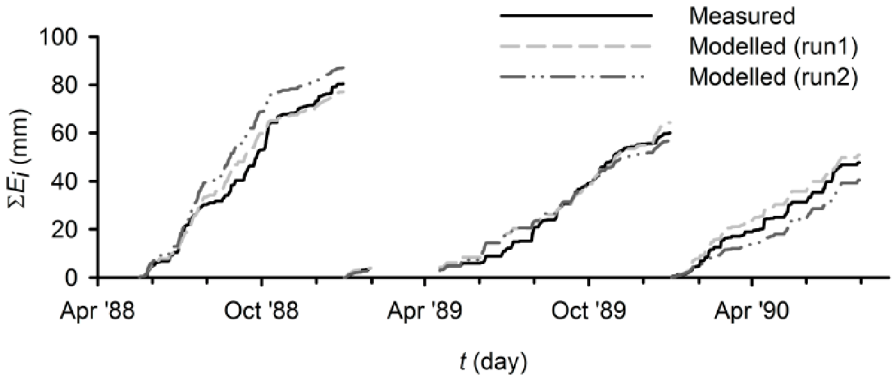

Figure 8.10: *Measured and modelled interception losses E_i for 3 years at the oak forest of the Edesebos site. Monthly values values have been used for $\overline{E}/\overline{P}$, seasonal values for C.*

8.6 Discussion

E, C and c_{veg} are the most sensitive parameters of interception models (e.g. Gash, 1979; Loustau et al., 1992). Valente et al. (1997) introduced the sparse canopy concept and showed that c_{veg} is the most sensitive parameter of the sparse Rutter and Gash model. In these concepts c_{veg} is assumed to linearly influence C and E.

8.6.1 Evaporation rate

Several authors mention that evaporation measurements under wet conditions using micro meteorological techniques such as the Bowen ratio and eddy-correlation methods can be used (Stewart, 1977; Gash et al., 1995; Grelle et al., 1997; Van der Tol et al., 2003), there are still unexplained differences between the results of these measurements and if compared with theoretical formulations such as the Penman-Monteith equation. A possible explanation could be differences in the diffusivities for heat and vapour during wet and dry conditions, caused by different location of the sources of heat and vapour (e.g. Mizutani and Ikeda, 1994; Lankreijer et al., 1999; Stewart, 1977; Van der Tol et al., 2003). Underestimation by the Penman-Monteith equation can be attributed to the advection of H (negative), increasing the total available energy (e.g. Stewart, 1977). Another but smaller contribution can come from a positive H originating from the understorey, as occasionally happens during showers at the pine forest of the Loobos site (see 8.3). An overestimation may be caused by the use of $z_{0H} = z_{0M}$ (Lankreijer et al., 1993).

As most experiments describe unstable dry conditions there is not much experimental evidence supporting or rejecting the hypothesis $z_{0H} = z_{0M}$. The present

study shows the logarithm of the ratio of the roughness length for heat and momentum expressed as kB^{-1} is not constant, differs between sites, seasons and changes between wet and dry conditions. For dry unstable conditions the values found are in the same range as found in other studies (see e.g. Bosveld, 1999; Mölder and Lindroth, 1999; Mölder and Lindroth, 2001). Although for wet conditions the scatter in the data is large the following observations could be made:

- For the two needle leaf forests the average value for kB^{-1} is approximately 1.5 for wet conditions,
- For the poplar and the mixed forest site, kB^{-1} varies between 3 and 4 during the foliated period and between 5 and 6 during the non-foliated period.

The relatively high values in winter time may be caused by the rigid structure of the twigs and branches acting as a bluff rough surface when there are no leaves present. In rare cases kB^{-1} may depend on the precipitation intensity, corresponding to events with relatively high atmospheric stability. During such events kB^{-1} approaches zero (see Fig. 8.2).

Using the Penman-Monteith equation and a fixed long term average (11 years of data) of $kB^{-1} = 1.0$ for the pine site, showed that the calculated wet evaporation rate only underestimated the measured evaporation rate by 4% of the observed values.

Gash et al. (1999) showed that similarly good results can be obtained by using a sparse canopy approach. To account for open spaces in a sparse canopy it is assumed that all available energy is used to evaporate the water layer on the canopy surface, i.e. there is no energy being used by the layer below the canopy. Although the resulting evaporation rate per unit ground area compares well with the measurements, redirecting R_{net} and G only to the canopy seems a case of compensating errors. Since measurements of R_{net} and G are based on unit ground area, there is no reason to assume that these will become zero under wet conditions for the lower layer. Moreover, although a limited amount of data is available, the eddy-correlation measurements below the canopy show that during rainfall E of the lower layer varies between 11 and 14% of total E for the pine and poplar site respectively. Indicating that indeed almost all evaporation is coming from the wet canopy layer. Thus the elegant and easy to apply assumption by Gash et al. (1995) and Valente et al. (1997), i.e. assigning all available energy to the canopy layer, does not seem valid, but provides reasonable results as long as c_{veg} compensates for the incorrect kB^{-1} value. Using a correct value for kB^{-1} is physically more appropriate, and provides the same results, i.e. a correct estimate of E on a unit ground area basis instead of a unit canopy area basis. Following Gash et al. (1995) and Valente et al. (1997), calculating the wet evaporation rate with $kB^{-1} = 0$, multiplying this by c_{veg} to obtain the wet evaporation rate per unit ground area shows that their sparse canopy concept works well

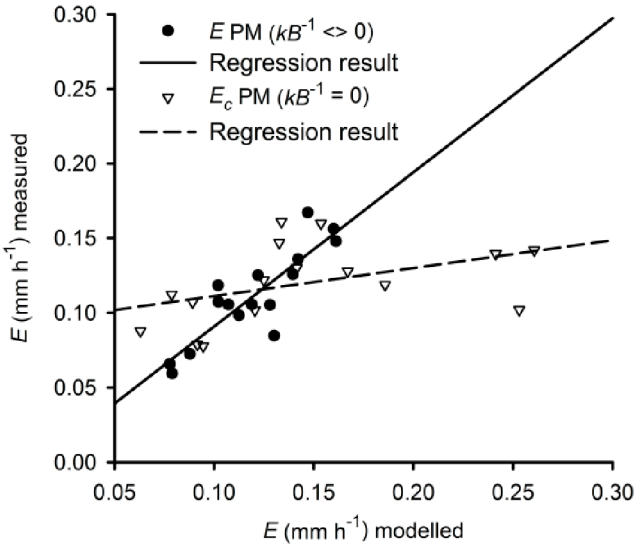

Figure 8.11: *The seasonally averaged measured wet evaporation rate E of 1996 and 1997 for the larch, pine, poplar and mixed site and the Penman-Monteith evaporation rate E PM using the site dependent kB^{-1} values and the fractional canopy cover corrected Penman-Monteith evaporation rate E_c PM using $kB^{-1} = 0$ for the spring and summer season averages. The solid line represents the regression line of the site dependent kB^{-1} values, the dashed line represents the regression line of the $kB^{-1} = 0$ values.*

for the relatively open larch, poplar and pine forest during the foliated season (see Fig. 8.11). The outliers in the figure are the data points of the mixed forest with its closed canopy, for which the sparse canopy concept does not seem to work and overestimates E per unit ground area by almost double. For the non-foliated period of the larch and the poplar site the sparse canopy concept underestimates E.

This study largely supports Gash's discussion (Gash et al., 1999), and at the same time explains why Lankreijer et al. (1993) obtained good results for the closed canopy site Ede. Good agreement can be obtained when these two approaches are combined. Site and tree specific kB^{-1} values in combination with C per unit canopy cover, improve the applicability of the interception models. The kB^{-1} values presented here, may well be used for similar forests under roughly the same conditions. More experimental data is needed to enable parametrization of the differences between sites, before the current results can be generally applied to different regions.

8.6.2 Storage capacity

The other important quantity that determines the magnitude of E_i for each shower is C. The size of C depends on the leave characteristics and the surface tension forces.

Grelle et al. (1997) show that by using a water balance and eddy-correlation measurements the resulting maximum C was 2 to 3 times as high in comparison to the values derived by applying the method of Leyton. These high values for C support the conclusion by Klaassen et al. (1998). They attributed the underestimation by Leyton's method to the neglect of drainage of a partly saturated canopy. However, in my opinion it is a combination of errors, where the selection of data points with a saturated canopy and negligible evaporation has the biggest impact. In case daily data are used, also the inclusion of data points with wet canopies at the start of the day have a strong impact. For example, using measured E to select data points with almost no evaporation and showers defined as continuous rainfall events ($P \geq 0.2$ mm 30 min^{-1}) preceded by at least 10 hours without rain, provided estimates of C between 0.9 and 2.1 mm for the pine site of our study. Of this 4 year data set only 10 data points remained after applying these selection criteria. This low number for a 4 year record in combination with the large scatter shows the sensitivity of the results to measurement errors. However, these values correspond well with the average value of C (see Table 8.5) derived using the Gash model for sparse canopies with measured E to estimate $\overline{E}$ under wet conditions. These values for C are also in the same range as the values presented by Lankreijer et al. (1999) applying the same method. The high degree of variation in C suggests, as remarked by among others Hormann et al. (1996), Calder et al. (1996), Lankreijer et al. (1999), Price and Carlyle-Moses (2003), Keim (2004) and Carlyle-Moses (2004), that a variable value for C may improve the modelling performance. However, no clear dependency on for example wind speed or rain intensity could be retrieved from the sites of this study (see Table 8.4).

More common approaches attribute differences in C to tree characteristics. The most widely used tree characteristic to explain differences in C is L_{AI}. An ideal situation would be to compare C at the same site for different L_{AI}. However, the changes in maximum or average L_{AI} between years are in general to small to establish any relation between L_{AI} and C. Also for deciduous forest changes in L_{AI} due to leaf fall are difficult to use as the branches of the trees play an important role by acting as preferential flow paths in the (partly) non-foliated period. Better relations are found when comparing results between sites with more pronounced differences in L_{AI}. For the present study, comparing C based on Leyton's analysis of all sites with L_{AI} does not support the often used assumption of a linear relation, but showed an exponential relation with L_{AI}, and an even better linear relation with c_{veg} (see Fig. 8.8).

Fleischbein et al. (2005) found a similar relation for their montane forest in Ecuador with the free throughfall fraction as the better predictor for differences in C. Considering the good relation with c_{veg}, an exponential relation with L_{AI} is to be expected, as it is known that c_{veg} and L_{AI} often have an exponential relation. It should be noted that this is not necessarily the case for sites with L_{AI} greater than 5 m^2m^{-2}. At L_{AI} values above 5 m^2m^{-2} the canopy cover will be closed in most forests and the linear relation between C and c_{veg} will no longer be valid. A possible better option to derive C from tree characteristics would be to have a linear relation with $c_{veg} < \approx 0.8$ and for (almost) closed canopies a relation with L_{AI}. This last part is not straightforward and the uncertainty for a specific site will be large due to the large scatter in the data. This becomes clear when combining our dataset to those from other studies such as provided by Turner and Lambert (1987) and Deguchi et al. (2006). The resulting data set shows a relationship (significance level $p > 0.05$) between C with L_{AI} and c_{veg}, but with a large scatter respectively $R^2 = 0.31$ ($C = 0.48 + 0.11L_{AI}$, $N = 53$) and $R^2 = 0.15$ ($C = 0.23 + 0.88c_{veg}$, $N = 66$). Thus C seems to vary between sites and this variation is globally not well described by tree characteristics such as L_{AI}, c_{veg} or basal area.

Dependency of C on parameters such as P and u are even less evident. Teklehaimanot and Jarvis (1991) found a good relation between N_{tree} and the throughfall fraction. However, their relation is questionable for low N_{tree}. Turner and Lambert (1987) compared 18 studies on Pinus radiata in different parts of the world and derived a similar relation between interception and N_{tree} expressed as basal area ($R^2 = 0.61$). Adding P to the relation improved the regression by almost 10% ($R^2 = 0.67$). That such general relations may have limited value for individual sites becomes clear when comparing individual data points: the site with the highest basal area (57 m^2ha^{-1}) has the lowest interception loss (10%) while the site with the lowest basal area (22.5 m^2ha^{-1}) has the second lowest interception loss (13%).

At the study sites for showers not saturating the canopy $P < 1.5$ mm, a positive correlation was found between C and the precipitation intensity for the summer months ($R^2 = 0.47$). This increasing C with increasing P is in contrast to the findings of Calder (1986), Calder et al. (1996) and Price and Carlyle-Moses (2003). who found a decreasing C with increasing drop size. However, the experiments by Calder were made with a rainfall simulator, where the lowest rainfall rate was almost as high as the highest rate observed in the eleven year period at the Loobos site, which makes it doubtful if these results can be compared. Also differences in tree characteristics may play a role in this relation (e.g. Pook et al., 1991).

The negative correlation of C and u_* for showers just saturating the canopy ($1.5 < P < 1.7$ mm) as observed at the sites during the winter half year can be attributed to the loss of water on the canopy due to movement of the leaves and

branches. This supports the findings of Hormann et al. (1996), however it seems that this effect is most of the time overshadowed by the positive correlation between E and u_*. This may be enhanced by the fact that in most cases the layer of water on the leaves concentrates in drops at the edges of the leaf (see e.g. Butler, 1985). This forming of drops will conserve energy by reducing the evaporative surface and will thus reduce E. Higher u will not only enhance the evaporation process, but will also shake the drops off the leaves, reducing C as observed by Hormann et al. (1996). Efforts have been made to model these drops or patches of wet leaf area and the exchange of energy between these surfaces (Shuttleworth, 1976, Butler, 1986, Bosveld and Bouten, 2003), however due to lacking information on the size of the wet patches these models are difficult to apply.

For the time being, the relation between C and c_{veg} found for the 5 sites supports the sparse canopy concept introduced by Gash et al. (1995) and Valente et al. (1997). This implies that the applied L_{AI} dependent storage capacity used in among others GCM's (General Circulation Models) can be improved if c_{veg} is taken into account. It also suggests that for the study sites, based on Leyton's analysis, for $c_{veg} < 0.9$ a fixed value of $C_c = 0.7$ can be used, including the non-foliated period for deciduous trees. Including sites from other studies (e.g. Marin et al., 2000; van Dijk and Bruijnzeel, 2001a; Price and Carlyle-Moses, 2003; Bryant et al., 2005; Loescher et al., 2005; Deguchi et al., 2006), this value will increase to $C_c = 0.9$. It should be taken into account that this increase is possibly due to the lack of data in non-foliated periods. The relatively large scatter when plotting C_c against L_{AI} in this and other studies shows that besides the leaf area other factors determine the size of C. For forest with $c_{veg} \approx 1$ it seems more appropriate to select values that resemble the site tree species best. In this respect, it is unfortunate that Breuer et al. (2003) lack information on c_{veg}, the only temperate forest ecosystems distinguished are deciduous and coniferous forests. No distinction is made between needle dropping species such as larch with its relatively low L_{AI} and species with a high L_{AI} such as Douglas fir. The latter causing relatively high mean values for coniferous forest $C = 1.8$ mm. Although this value corresponds with the average value found for the pine site Loobos $C = 1.65$ mm, it is doubtful if these two can be compared due to the different methods used. Using the average $C = 1.4$ mm for European deciduous forest as supplied by Breuer et al. (2003) overestimates E_i for the oak stand at the Edesebos with 80% and 44% for the summer months in 1988 and 1989 respectively. The overestimation reduces to 45% and 16% if we assume that the value for C corresponds to a closed canopy and is adjusted according to c_{veg} of the site. This decrease in E_i supports the suggestion that improvements can be made if besides tree species and total precipitation also c_{veg} is reported as well as precipitation intensity.

8.7 Conclusions

Attempts have been made to improve the estimates of wet evaporation E_i and canopy water storage C, two of the most important parameters to simulate interception loss.

Measurements show that, both the roughness length for heat z_{0H} and for momentum z_{0M} are subject to changes under wet conditions. Use of a value for $kB^{-1} = 1.0$ to express the ratio between the aerodynamic resistance for heat and momentum (see Eq. 2.67) seems more appropriate for the pine site of this study. The use of the value $kB^{-1} = 1.0$ changes a 30% underestimation of the calculated evaporation rate using Penman-Monteith with $kB^{-1} = 2.0$ and an 30% overestimation with $kB^{-1} = 0.0$ to an underestimation of 4%.

The magnitude of kB^{-1} differs per site, is in general higher for the winter period and is different for wet and dry periods. For the sites studied only for relatively rare occasions kB^{-1} approached zero under wet conditions. These events were associated with large storms. Based on the data available for this study as a rule of thumb $kB^{-1} = 1.0 - 1.5$ may be used for needle leaf forests and $kB^{-1} = 3.0 - 4.0$ in summer and $kB^{-1} = 5.0 - 6.0$ in winter for broad leaf deciduous forests (see Table 8.1).

Estimates of the evaporation rate E during wet conditions based on regression analysis using measured throughfall T_f, stemflow S_f and precipitation P are approximately twice as high as E derived from the energy balance closure during showers. Possible causes for this are the systematic underestimation of measured P, but also for hourly data not having taken into account the drip taking place after the end of the time step. For event based data the use of measured T_f implicitly includes the amount of water left on the leaves at the end of the shower and thus also the relatively high E taking place after the shower has ceased (see Fig. 8.4).

Although the use of daily data instead of an arbitrary definition of a shower reduces the total number of showers in a year by 50%, the consequences for the magnitude of the ratio $\overline{E}/\overline{P}$ are minimal.

The fact that events without E are very rare or non existent are the main cause for the often found low values of C when using techniques based on the method of Leyton et al. (1967). Using the sparse canopy model of Gash et al. (1995) and E derived from the energy balance closure to calculate C gives values 3 times as high as when using the method of Leyton. The largest differences occur especially during the winter months. The relatively good modelling results obtained with the Gash model using different parameter sets for the same location, exhibit the trade off between C and E. Thus, although in my opinion the lower values of E for wet conditions presented in this study are physically more consistent, it is even more important to assure that the parameters to be used to simulate interception losses are consistent

with one another and with the concept used.

For the sites and years of this study there is a clear relation between the fractional canopy cover c_{veg} and C. For sparse canopies, i.e. $c_{veg} \lesssim 0.9$, c_{veg} is a better proxy for C than Leaf Area Index L_{AI} (see Fig. 8.8 and 8.7). C seems not only to depend on vegetation characteristics such as L_{AI}, c_{veg} and the tree density N_{tree}, but also on the precipitation regime. This implies that parameters derived for a specific tree species at a specific site will only be applicable to other sites having the same climatic conditions. As a consequence parameter estimations based on tree species only (or more specifically land cover and L_{AI}) are not sufficient to provide accurate values for water balance studies if climatic differences between sites are not taken into account.

Fixed parameter values can decrease the model's daily performance considerably. For the Edesebos site this was mainly caused by differences in C.

Using site and tree specific kB^{-1} values in combination with C per unit canopy cover, will improve the general applicability of the interception models. The presented kB^{-1} and C values may well be used for similar forests under approximately the same conditions. More experimental data, however, will be needed to enable parametrization of the differences between sites, before the present results can be generally applied to regions with different climatic conditions.

Chapter 9

Epilogue

9.1 Main conclusions

An example of the possible value of improved knowledge on the water use of forests may be obtained from the spring drought in the Netherlands of 2011.

The Dutch National Weather Service (KNMI) reports the continuous sum of potential excess of precipitation, which is precipitation minus potential evaporation as based on Makkink (1959) corrected for land cover type. This potential excess precipitation is a good measure to compare between different years. It is, however, of limited use when evaluating the actual effect of the depletion of water resources.

For the dry spring over the period 1 April to 9 May 2011, KNMI reported for the forested area of the Veluwe a potential excess precipitation of -80 to -100 mm. However, the measurements at the pine stand of the Loobos site on the Veluwe showed over the same period an actual excess precipitation of -35 mm. An absolute difference of 45 to 65 mm is considerable and it makes the use of the potential excess precipitation in reporting drought situations questionable.

Reporting actual excess precipitation would provide a much better insight on the actual status of the water resources. Although the status of the water resources can be simulated by using numerical models (see e.g. Section 7.5.4) and/or estimated from remote sensing images, it is recommended to use for verification direct measurements (see Section 4.3.2). At present the measurements of actual evaporation are not incorporated in operational reports. The Loobos site is at present the only long-term continuously run forest station in the Netherlands and could be used for such purposes.

The results of the present doctoral thesis may contribute to improve operational water management issues related to forest hydrology as it discusses the water use of a number of different forest types in the Netherlands. The leading question was: "What is the difference in water use of different tree species in The Netherlands?". This question has been divided into three underlying research questions. In the following paragraphs the main findings will be briefly discussed.

"*What are the main processes controlling the magnitude of the different components of the water balance of forested areas in the Netherlands?*". The main components of the soil water balance over a certain period of time are precipitation, evaporation, soil water change and the resulting discharge. Evaporation is arguably its most important component as it controls land-atmosphere feedbacks through the land surface energy budget. The processes controlling the evaporation rate are different for both dry and wet conditions. During dry conditions the processes controlling the availability of soil water and the flow of this water to the leaf surface of trees and undergrowth are most important (see Chapter 7). During wet conditions the processes controlling the amount of water stored at the leaf surface and the vertical location of the vapour sources will determine the evaporation rate (see Chapter 8).

"*What are the controlling parameters of these processes and are they related to tree species?*". In comparison to other vegetated surfaces, forests have a relatively large surface roughness providing a low aerodynamic resistance r_a, which makes the magnitude of stomatal conductance g_s the determinant of the evaporation rate under dry conditions.

In Chapter 7 it has been shown that not only g_s of the trees, but also g_s of the undergrowth plays an important role in determining the evaporation rate under dry conditions. Fig. 7.3 and Table 7.5 show the resulting conductance functions and parameter values based on the equations of Section 2.5.3 for the 5 forest stands of this study. The low sensitivity to soil water deficit θ_D shows that the forest stands of this study are not very sensitive to the range of changes in soil water encountered during this study. The sensitivity of these forests to more severe droughts cannot be concluded from the present data sets. The relatively good performance for moderate soil water stress conditions by the model introduced to represent the feedback of θ_D on g_s under more extreme dry situations (see Fig. 7.10 and Fig. 7.11), shows the potential of such a parametrization taking into account drought conditions. Especially situations of extreme drought leading to cessation of root water uptake from the groundwater reservoir.

During and just after showers have ceased, the main parameters governing the quantity of water evaporated are those parameters that determine the water holding capacities of the vegetation as well as the rate of evaporation. In Chapter 8 attempts have been made to improve the estimates of interception evaporation E_i and canopy water storage C, being two of the most important parameters that simulate interception loss. It has been shown that it may take up to 13 hours before transpiration is returned to its normal level (see Fig. 8.4).

During such a drying period the rate of interception evaporation E_i is largely depending on the roughness length for heat z_{0H} as well as for momentum z_{0M}.

Measurements show that under wet conditions, both the roughness length for heat z_{0H} and for momentum z_{0M} are subject to changes. Applying site and tree specific values for the ratio of roughness length for heat z_{0H} and for momentum z_{0M} in combination with C per unit canopy cover, will improve the general applicability of the interception models. The in Chapter 8 presented ratio's of z_{0H} and z_{0M} (see Table 8.1) and C values (see Fig. 8.8 and 8.7) may well be used for similar forests under approximately the comparable conditions.

To enable parametrization of the differences between sites, more experimental data however will be needed before the present results can be generally applied to regions with different climatic conditions.

The relatively large contributions of the undergrowth at the *pine* and the *poplar* forest during large parts of the year showed the importance of this component of total forest water use (see e.g. Fig. 7.12).

"*Will this knowledge be of added value to predict effects of different tree species on the water balance?*". Parametrizations as are found in this study that allow to quantify the effect of most common forest types on the water balance in the Netherlands. These capabilities have among others being demonstrated by the modelled interception evaporation E_i for the Oak forest at the Edesebos site (see run1 in Fig. 8.10).

9.2 Deriving actual evaporation for forests in the Netherlands

At present hydrological practitioners mainly use numerical models based on the input of a reference evaporation rate. Direct measurements of forest evaporation by the eddy-correlation technique, such as has been used in the present study (see Chapter 4), are often not part of general hydrological practice. For a more complete overview of different methods to measure actual evaporation see e.g. Moors (2008). Each of these methods has their own advantages and disadvantages. Issues to be considered are the temporal and spatial scale of the measurements, operational requirements and the associated uncertainty.

For the eddy-correlation technique as has been employed for this study on forest evaporation, it was shown that the uncertainty during dry conditions in summer at almost all sites was less than 5% (see Chapter 5). In winter the uncertainty was less than 15%. During wet conditions the uncertainty has been estimated as being less than 20%. Often longer time steps than the typical 30 minutes measurement time step of micro-meteorological measurements are required.

In Chapter 6 it has been shown that because of filling missing data the added uncertainty is less than 10%. A large part of the measurement error will depend on the experience of the user, i.e. doubling this error. Malfunctioning of equipment may cause a considerable additional error i.e. 5 - 100% (Allen et al., 2011).

To improve the estimates of actual evaporation by numerical models, the findings of Chapter 7 and Chapter 8 for the parametrizations of dry and wet evaporation can be used. In addition: the undergrowth contribution to evaporation can be made explicit, enabling improved evaporation estimates in all seasons of the year.

Further improvements can be achieved by taking seasonal differences into account among others by introducing parametrizations reflecting the differences in phenological phases.

Also capabilities to include human influences, for example the effect of deliberate or unintentional application of nutrients on the controls of trees on their transpiration rate, will help to improve evaporation estimates of unmeasured forest stands.

In the long run climate change may not only affect the evaporation rate by changing the magnitude of the physical drivers such as radiation, temperature, wind and precipitation, but also through changes in physiological characteristics of forest plant communities (see e.g. Kruijt et al., 2008; Milly and Dunne, 2011).

To implement improvements a five step approach is suggested:

1. Direct measurement of the actual evaporation rate at strategic sites is recommended for process understanding and verification purposes. Especially the real time use for verification is recommended during extreme conditions, such as droughts (see also Section 9.1).

2. Continuous use of crop factors will only be sustainable if the effects of elevated CO_2 and nutrient application will be taken into account and if updated crop coefficients will become available.

3. Replacing the crop factors by effective surface resistances will allow for the use of land surface models that take into account forest properties, such as albedo and L_{AI}. Such properties are almost constant with respect to changes in soil water content, but are important for the spatial differences of the energy balance.

4. A promising way forward to overcome the presently missing impact of elevated CO_2 and nutrient availability on the physiological processes, is an improved coupling between biogeochemical and hydrological models. This coupling will also pave the way to incorporate issues such as tree phenology, which is the main process dictating changes in seasonal patterns.

5. Finally the use of an atmospheric meso-scale model coupled to the land surface model will not only enable weather services to provide a forecast of the actual evaporation. Even more importantly this coupling will also ensure a consistent feedback of the atmosphere on the vapour pressure deficit. The latter being especially important if land surface models based on the vapour pressure gradient such as the Penman-Monteith model are to be used.

To improve in steps 1 to 5 the spatial variability (e.g. vegetation characteristics measured by Lidars) and the initial state of the models (e.g. soil water, Dolman and de Jeu, 2010), the use of remote sensing could greatly contribute.

Step 4 will allow support for the introduction of improved local feedbacks in climate models, which may help to investigate critical transitions in our climate (see e.g. Rietkerk et al., 2011). This knowledge will also support respectively step 3 and step 5, that will contribute to the implementation of more spatial explicit surface properties our land surface schemes.

The forecasts of the water use of forests of step 5 may be further extrapolated by for example taking into account the statistical depletion rate e.g. the historical draw-down characteristics of the groundwater table.

The approaches suggested above are primarily aimed to support proper water management and are for a part in line with the recommendations by Droogers (2009). Some of these approaches can also contribute to improve evaporation estimates of the land surface schemes being used in meteorological forecasting and climate modelling. For these land surface schemes improvements can be achieved by better representing the spatial heterogeneity in land surface schemes (see Jacobs et al., 2008; Shuttleworth, 2007).

9.3 Research perspectives

The *first* research challenge is related to the increased risk of droughts. Managing the available fresh water resources during situations of water scarcity requires reliable measurements and forecasts of water use. At present not much is known regarding how the water use of different forest types will change under more severe prolonged dry periods. Especially in areas with historically relatively high groundwater levels such as in The Netherlands, no data are available on how the water use of forest will change during dry periods with falling groundwater tables.

The *second* research challenge is related to the still often ignored contribution of the undergrowth to the forest evaporation. Considering the evaporation rate of the trees and the undergrowth separately will enable an improved understanding

of the functioning of forest ecosystems. It will also improve our interpretation of the changing climatic and hydrological conditions affecting evaporation of trees and undergrowth differently.

To support such an approach, the rather limited number of plant functional types as are being used at the moment to describe forests, need to be replaced by plant functional types describing tree species in combination with undergrowth species. These plant functional types should not only allow to take leaf area index L_{AI} of the undergrowth into account, but also the different phenological phases of the trees and of the undergrowth. The latter will help to improve the simulation of the seasonal differences in the behaviour of the stomatal conductance g_s, which will provide better estimates of the total evaporation rate, i.e. also outside the growing season.

To enable research in these directions, additional data sets will be needed. These data sets should especially aim at representing the different phenological phases of the vegetation and should include:

- Evaporation data sets of undergrowth,
- Evaporation and soil water data sets for forests under water stress.

The release of water vapour and the intake of carbon dioxide by trees are both for an important part controlled by the opening and closing of the stomata. Because of this stomatal control, there is a strong link between the evaporation rate and the rate of the carbon dioxide uptake by forests. Therefore, most issues that are valid for the evaporation rate as mentioned above also hold for the photosynthesis rate.

It is still unclear what is driving inter annual variability in net ecosystem exchange of carbon. Extreme events such as droughts are clearly important, but the quantification of the impact is still a major challenge.

Measurements at the pine forest of the Loobos side showed that the undergrowth contribution to the total carbon uptake by photosynthesis was on average similar to the contribution of undergrowth to the evaporation rate. Thus the undergrowth also plays an important role in the total photosynthesis of a forest. In addition, the undergrowth has an effect on the respiration rate through the input of substrate and the influence on the soil water content of the top soil layer can have a significant effect on net carbon exchange of a forest. Research on the separate contribution to evaporation and photosynthesis of trees and undergrowth will improve our understanding of the net carbon exchange. Emphasis on drought situations will add to our knowledge on the effect of lowering groundwater tables on the net carbon sequestration by forests.

Appendix A

Stemflow

The amount of stemflow S_f is directly related to P. Table A.1 shows the regression results for the four experimental sites at which stemflow was measured. To investigate a possible relation between S_f and L_{AI} distinction has been made between summer and winter. In summer S_f decreased in the order: oak - poplar - pine - larch. In winter the order is: oak - poplar - larch - pine. At all sites investigated S_f is low, in most cases $S_f < 0.01P$. At the pine site there exists hardly any difference between summer and winter, because the differences in the Vegetation Area Index V_{AI} amounted only to 0.2 m^2 m^{-2}.

Only for oak and poplar trees the ratio of S_f/P as a function of V_{AI} is significantly different between the foliated and the non-foliated periods (see Fig. A.1). This relationship shows an increase in leaf area reducing the ratio of S_f/P. The increase of S_f with decreasing leaf area is a confirmation of the findings of Giacomin and Trucchi (1992). At their beech forest site in Italy S_f was found to be 12% higher in the lesser foliated period for precipitation events > 5 mm.

Tree characteristics that may explain the differences in S_f between tree species are differences in the angles of the branches, the capacity of the bark of the trees to absorb and retain water and the foliage. For the tree species of this study the branch angle increases in the order: poplar - oak - larch - pine. As a rule of thumb one may conclude that the smaller the branch angle the greater the stemflow. Additionally the capacity of the bark of the trees to absorb and retain water will influence the

Table A.1: *Stemflow parameters at four forest sites assuming a linear relationship with precipitation P: $S_f = x_0 + aP$ (mm) , where P (mm) is the precipitation based on weekly data.*

Location	Summer			Winter		
	x_0 (mm)	a	R^2	x_0 (mm)	a	R^2
Larch (Bankenbos)	-0.0012	0.0005	0.53	-0.0092	0.0035	0.88
Oak (Edesebos)	-0.0956	0.0148	0.63	-0.4412	0.0738	0.91
Poplar (Fleditebos)	-0.0557	0.0107	0.60	-0.0966	0.0341	0.88
Pine (Loobos)	-0.0039	0.0007	0.77	-0.0055	0.0013	0.75

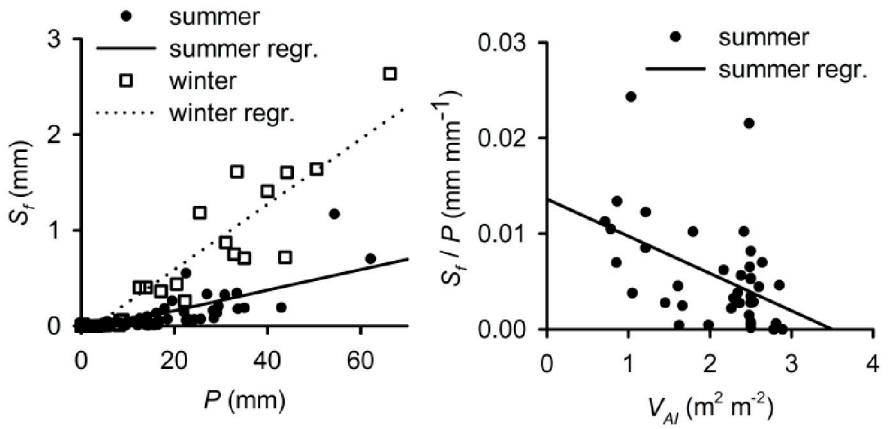

Figure A.1: *Left panel: The amount of stemflow S_f as a function of precipitation amount P on a weekly basis of the poplar trees at the Fleditebos site during foliated (summer) and non-foliated (winter) period. Right panel: For the same site S_f / P as a function of the Vegetation Area Index V_{AI} during the foliated period.*

amount of stemflow. The intercept of the regression line in the left graph of Fig. A.1 gives an indication of this capacity. At this poplar stand during the non-foliated period S_f only starts at $P > 3.5$ mm week^{-1}.

The right hand graph of Fig. A.1 shows the influence of the amount of foliage on the stemflow fraction S_f / P. Foliage influences S_f in two ways. It prevents rain from wetting branches and trunk and also the weight of the foliage may bend the branches downward, increasing the angle of the branches with the stem and thus reducing S_f. The influence of the foliage is evident as during the foliated period S_f starts at $P > 6.0$ mm week^{-1}.

In view of the low numbers found for S_f at the sites presented here, a detailed assessment of this quantity seems unnecessary as compared to the uncertainties of the other components of the water balance. Except in the winter periods S_f will not be taken into account for the oak and poplar sites, when $S_f > 0.01P$.

Appendix B

Weight fractions of the soil

The tables below show the weight fraction of the soil at the Bankenbos, Fleditebos, Kampina and the Loobos sites. The sand fraction is defined as the fraction of dry matter with particle size between 16 μm - 2000 μm, the silt fraction with particle size 2 μm - 16 μm and the clay fraction with particle size 0 μm - 2 μm.

Table B.1: *Weight fractions x of sand, silt and clay and the densities ρ at the Bankenbos site.*

Depth (m)	x_{sand} ($kg^3\ kg^{-3}$)	x_{silt} ($kg^3\ kg^{-3}$)	x_{clay} ($kg^3\ kg^{-3}$)	ρ_{sample} ($kg\ m^{-3}$)
0-0.30	0.41	0.01	0.05	1260
0.55-0.70	0.64	0.01	0.02	1650
0.60-0.90	0.65	0.02	0.01	1760

Table B.2: *Weight fractions x of sand, silt and clay and the densities ρ at the Fleditebos site.*

Depth (m)	x_{sand} ($kg^3\ kg^{-3}$)	x_{silt} ($kg^3\ kg^{-3}$)	x_{clay} ($kg^3\ kg^{-3}$)	ρ_{sample} ($kg\ m^{-3}$)
0.07-0.34	0.61	0.12	0.18	880
0.36-0.70	0.42	0.15	0.32	980
0.90-1.10	0.25	0.32	0.29	1100

Table B.3: *Weight fractions x of sand, silt and clay and the densities ρ at the Kampina site.*

Depth (m)	x_{sand} ($kg^3\ kg^{-3}$)	x_{silt} ($kg^3\ kg^{-3}$)	x_{clay} ($kg^3\ kg^{-3}$)	ρ_{sample} ($kg\ m^{-3}$)
0-0.20	0.52	0.01	0.05	1320
0.20-0.50	0.53	0.01	0.01	1450

Table B.4: *Weight fractions x of sand, silt and clay and the densities ρ at the Loobos site.*

Depth (m)	x_{sand} ($kg^3\ kg^{-3}$)	x_{silt} ($kg^3\ kg^{-3}$)	x_{clay} ($kg^3\ kg^{-3}$)	ρ_{sample} ($kg\ m^{-3}$)
0-0.20	0.96	0.01	0.02	1560
0.40-0.60	0.98	0.00	0.02	1630

Appendix C

Data processing for the eddy correlation technique

One of the main objectives of the experimental work of the forest hydrology project was to obtain long term (about three years) of continuous measurements. All sites were located in remote areas where no main power was available. This was solved by using batteries powered by solar and wind energy and by minimizing the power consumption. Due to this some concessions had to made to the quality of the flux data. Reduction of the power consumption was achieved among others by using palmtop PC's and not storing the raw data continuously, but instead storing the means, variances and covariances. However, the disadvantage of the use of these palmtops is, besides the limited data storage capacity, the processor speed. This lead to the second concession, namely not calculating the covariances of the wind speed components in x- and y-direction u and v with temperature T and scalar $\varkappa$ and the covariance of T and $\varkappa$. To check if the mentioned concessions caused unacceptable data quality loss, raw data were collected for short periods (maximum a couple of weeks at each site).

For a complete description of the eddy-correlation technique in combination with infra red gas analyser and the processing software for the raw data the reader is referred to Moncrieff et al. (1996) and Aubinet et al. (2000). Here the data processing is described as used for a 3D sonic and an open path hygrometer applying eddy correlation technique. This was the basis for the long term data collection of this study.

The equipment used for the measurement of the momentum, sensible and latent heat flux is a 3-D sonic anemometer (SOLENT 1012R2, Gill) and a Krypton hygrometer (KH_2O, Campbell). The three wind components are derived from the calibrated relation between the wind speed and the transit time for a sound pulse travelling over the known distance between one of the three transmitters to the corresponding receiver. The temperature fluctuations needed for the sensible heat flux density are derived from the known relation between the speed of sound in air c_s (m s^{-1}) and

the absolute air temperature T in K (Kaimal and Finnigan, 1994):

$$c_s^2 = \gamma \frac{R}{M_d} T(1 + 0.32\frac{e}{p}) \tag{C.1}$$

where M_d the molar mass of dry air (0.028965 kg mol^{-1}), R is the universal gas constant (8.314 J mol^{-1} K^{-1}), $\gamma_c = c_p/c_v$ is the ratio of specific heat, with c_p and c_v the specific heat (J kg^{-1} K^{-1}) of dry air at constant pressure and constant volume respectively ($\gamma_c R/M_d$ = 403 m^2 s^{-2} K^{-1}), e denotes the vapour pressure of water (hPa) and p the atmospheric pressure (hPa).

The sonic temperature is defined as $T_{son} = c_s^2/403$ and is close to the virtual temperature T_v (K):

$$T_v = T(1 + 0.38\frac{e}{p}) \tag{C.2}$$

The absolute humidity $\varkappa_{abs}$ measured by the Krypton hygrometer relates to the vapour pressure by:

$$\varkappa_{abs} = \frac{eM_w}{RT} \tag{C.3}$$

where M_w is the molar mass of water (0.0180153 kg mol^{-1}). In the case of high vapour pressure the difference between the sonic temperature and the virtual temperature becomes more pronounced, but are still small enough (±0.01 K) for most micrometeorological purposes (Kaimal and Kristensen, 1991). Corrections for the effect of humidity on the sensible heat flux are applied following Schotanus et al. (1983). The three wind speed components, the speed of sound (all in m s^{-1}) and the humidity concentration (in mV) are measured at 20.825 Hz. Each 30 minute interval the sound of speed is converted into sonic temperature using Eq. (C.1), where after the fluctuations of all quantities are calculated using a non-centralized running mean algorithm with a 200 s time constant. Means and variances are calculated and stored of u, v, w, T_{son} and $\varkappa$, as well as the covariances $\overline{u'w'}$, $\overline{u'v'}$, $\overline{v'w'}$, $\overline{w'T'_{son}}$ and $\overline{w'\varkappa'}$.

After collecting the data in the field the mean absolute humidity (kg m^{-3}) measured by the Krypton hygrometer is calculated using the calibration parameters supplied by the manufacturer. The same parameter of the humidity calibration span is used for the covariance of vertical wind speed and humidity. The wind speed and direction are calculated from the means of u and v. The wind direction is also corrected for the non alignment with the magnetic North.

C.1 Oxygen absorption

The Krypton H_2O hygrometer emits ultraviolet light between 123.58 and 116.47 nm. This implies that the sensor is besides to hydrogen also sensitive to ozone and

oxygen. Due to the high relative concentration of oxygen a correction is needed. Differences in the density of oxygen depend on temperature and air pressure. For the absolute humidity measured by the Krypton this correction is assumed constant in the calibration coefficients (i.e. constant temperature and pressure) and implicit in the calibrated offset supplied by the manufacturer. To incorporate a site dependent oxygen correction in the absolute humidity measurement by the Krypton hygrometer, the offset caused by the oxygen concentration during calibration should be subtracted. This gives the following equation

$$\overline{\varkappa_{abs}} = \frac{\ln V_0 - \ln \overline{V_q}}{x_p k_v} + \frac{k_{O_2}}{k_v}(\rho_{O_2 0} - \rho_{O_2}) \tag{C.4}$$

where V_0 is the calibration offset (V), V_q the measured voltage (V), x_p the path length (m), $k_{O_2}$and k_v are the absorption coefficients for oxygen and water vapour (0.0085 and 0.143 $\mathrm{m^3\ g^{-1}\ cm^{-1}}$ respectively), $\rho_{O_2 0}$ the oxygen density during calibration (kg $\mathrm{m^{-3}}$), ρ_o the density during the measurement (kg $\mathrm{m^{-3}}$). The oxygen density is given by

$$\rho_{O_2} = \frac{C_{O_2} M_{O_2} p}{RT} \tag{C.5}$$

where C_{O_2} is the relative concentration of oxygen (0.21), M_{O_2} is the molecular weight of oxygen (32 kg $\mathrm{mol^{-1}}$), p the air pressure (Pa), R the universal gas constant (8.314 J $\mathrm{mol^{-1}K^{-1}}$) and T the air temperature (K).

The covariance of the absolute humidity and the vertical wind speed is corrected for the oxygen sensitivity by

$$\overline{w'\varkappa'_{abs}} = \frac{-\overline{w'V_q'}}{x k_v \overline{V_q}} + \frac{C_{O_2} M_{O_2} p}{RT^2} \frac{k_{O_2}}{k_v} \overline{w'T'} \tag{C.6}$$

This correction is in the order of 10% of the sensible heat flux. For this study no correction is made for the ozone sensitivity.

C.2 Axis rotation

Although the sites are relatively flat and some effort was made to install the sonics in the mean wind direction perpendicular to the surface the data are processed using stream line coordinates.

To align the u-component to the mean horizontal wind speed and to align the mean wind vector parallel to the mean stream lines of the wind speed, a two axis coordinate rotation is applied to the means, variances and covariances of the wind

speed components following McMillen (1988) and Kaimal and Finnigan (1994). The horizontal wind vector is defined as

$$\overline{u_{hor}} = \sqrt{\overline{u}^2 + \overline{v}^2} \tag{C.7}$$

and the total wind vector

$$\overline{u_{tot}} = \sqrt{\overline{u}^2 + \overline{v}^2 + \overline{w}^2} \tag{C.8}$$

from this the angle between $\overline{u}$ and $\overline{u_{hor}}$ is

$$\alpha = \arccos\left(\frac{\overline{u}}{\overline{u_{hor}}}\right) \tag{C.9}$$

and the vertical tilt

$$\gamma = \arccos\left(\frac{\overline{u_{tot}}}{\overline{u_{hor}}}\right) \tag{C.10}$$

With these angles the first two rotations can be calculated. In effect the first rotation sets $\overline{v}$ to zero and the second rotation sets $\overline{w}$ to zero.

The covariances of the wind speed components and temperature and humidity (i.e. sensible and latent heat flux) were not rotated. Also the third rotation as proposed by Kaimal and Finnigan (1994), which forces the lateral momentum flux to zero was not performed. This rotation is necessary when the streamlines incline with respect to the local surface. For the present sites this was not considered to have a major influence on the results.

After the rotation corrections, a first estimate of the friction velocity u_* (m s^{-1}) is calculated as:

$$u_* = \sqrt{\overline{w'v'}^2 + \overline{w'u'}^2} \tag{C.11}$$

as well as the Monin-Obukhov stability length L (m):

$$L = -\frac{\overline{T_{son}}u_*^3}{\kappa g \overline{w'T'_{son}}} \tag{C.12}$$

After the frequency response corrections the friction velocity and the stability length are recalculated.

C.3 Frequency response corrections

Due to sensor response, sensor separation, path length averaging, and signal processing, a part of the transporting eddies may be influenced or not detected by the system. To correct for this the flux loss is calculated using transfer functions describing the spectral loss of the system and model (co-)spectra (Moore, 1986). To prevent

aliasing, the effective transfer functions are calculated for frequencies n not exceeding the Nyquist frequency (i.e. half of the sampling frequency n_s). The convolution integral of the model spectra and the effective transfer function is calculated over the frequency range 0.00001 Hz to the Nyquist frequency.

Detrending of the data was done using an auto regressive moving average filter with a time constant τ_d of 200 s. The response gain for this high pass filtering is:

$$T_d(n) = \frac{(2\pi n\tau_d)^2}{1 + (2\pi n\tau_d)^2 / \alpha_d} \tag{C.13}$$

were the time coefficient α_d is taken as one.

The co-spectral transfer function for the transformation of analogue to digital signals is given by:

$$T_a(n) = 1 + \left(\frac{n}{n_s - n}\right)^3 \tag{C.14}$$

where n_s is the sampling frequency.

The frequency response gains for the wind speed components, the sonic temperature (all from the Solent sonic anemometer) and for the humidity (from the Krypton hygrometer) are considered to be negligible.

The transfer functions for spatial averaging over a path with length x_p (x_p = 0.149 m for the sonic anemometer and $x_p \approx 0.0125$ m for the Krypton hygrometer) are for the humidity, the sonic temperature and the wind components u and v:

$$T_p(n) = \frac{1}{2\pi\frac{n}{u}x_p}\left[3 + \exp\left(-2\pi\frac{n}{u}x_p\right) - \frac{4\left(1 - \exp\left(-2\pi\frac{n}{u}x_p\right)\right)}{2\pi\frac{n}{u}x_p}\right] \tag{C.15}$$

and for the vertical wind component w:

$$T_p(n) = \frac{4}{2\pi\frac{n}{u}x_p}\left[1 + \frac{1}{2}\left\{\exp\left(-2\pi\frac{n}{u}x_p\right) - \frac{3\left(1 - \exp\left(-2\pi\frac{n}{u}x_p\right)\right)}{2\pi\frac{n}{u}x_p}\right\}\right] \tag{C.16}$$

The transfer function for sensor separation of the Krypton hygrometer and the sonic anemometer is given by:

$$T_s = \exp\left(-9.9\left[\frac{n}{u}s\right]^{1.5}\right) \tag{C.17}$$

were s (s = 0.2 m) is the distance between the two sensors.

The composite transfer functions for the equipment used for this study are calculated as:

$$T_{uu} = T_{pu}T_aT_d \quad \text{(C.18)}$$
$$T_{vv} = T_{pv}T_aT_d \quad \text{(C.19)}$$
$$T_{ww} = T_{pw}T_aT_d \quad \text{(C.20)}$$
$$T_{TT} = T_{pT}T_aT_d \quad \text{(C.21)}$$
$$T_{qq} = T_{pq}T_aT_d \quad \text{(C.22)}$$
$$T_{uw} = \sqrt{T_{uu}T_{ww}}T_aT_d \quad \text{(C.23)}$$
$$T_{vw} = \sqrt{T_{vv}T_{ww}}T_aT_d \quad \text{(C.24)}$$
$$T_{Tw} = \sqrt{T_{TT}T_{ww}}T_aT_d \quad \text{(C.25)}$$
$$T_{qw} = \sqrt{T_{qq}T_{ww}}T_aT_d \quad \text{(C.26)}$$

For the theoretical spectra and co-spectra the formulations of Kaimal et al. (1972) are used. In their formulations the spectra are functions of the normalized frequency $f = \frac{n(z-d)}{\overline{u}}$ and stability $\zeta = \frac{z-d}{L}$.

For stable conditions ($\zeta < 0$):

$$S_{uu} = \frac{1}{n}\frac{f}{0.2(0.838+1.172\zeta)+f^{5/3}3.124\left[0.2(0.838+1.172\zeta)\right]^{-2/3}} \quad \text{(C.27)}$$
$$S_{ww} = \frac{1}{n}\frac{f}{(0.838+1.172\zeta)+f^{5/3}3.124(0.838+1.172\zeta)^{-2/3}} \quad \text{(C.28)}$$
$$S_{TT} = \frac{1}{n}\frac{f}{\left[0.0961+0.644\zeta^{3/5}\right]+f^{5/3}3.124\left[0.0961+0.644\zeta^{3/5}\right]^{-2/3}} \quad \text{(C.29)}$$
$$S_{wT} = \frac{1}{n}\frac{f}{0.284\left[1.0+6.3\zeta^{3/4}\right]+f^{2.1}2.34\left\{0.284\left[1.0+6.3\zeta^{3/4}\right]\right\}^{-1.1}} \quad \text{(C.30)}$$
$$S_{uw} = \frac{1}{n}\frac{f}{0.124\left[1.0+7.9\zeta^{3/4}\right]+f^{2.1}2.34\left\{0.124\left[1.0+7.9\zeta^{3/4}\right]\right\}^{-1.1}} \quad \text{(C.31)}$$

For unstable conditions ($\zeta < 0$) the spectra are dependent of the boundary layer height. For the horizontal and vertical wind speed the formulations of Hojstrup (1981) are used. Here Moore (1986) is followed and the spectrum of temperature and the co-spectra of vertical wind speed with temperature and horizontal wind speed as

given by Kaimal et al. (1972) are also used for unstable conditions:

$$S_{uu} = \frac{1}{n}\left[\frac{210.0f}{(1.0+33.0f)^{5/3}} + \frac{f(-\zeta)^{2/3}}{(\frac{z}{z_i})^{5/3}+2.2\,(f)^{5/3}}\right] \left[\frac{1}{9.546+1.235(-\zeta)^{2/3}(\frac{z}{z_i})^{-2/3}}\right] \tag{C.32}$$

$$S_{ww} = \frac{1}{n}\left[\frac{16.0f(-\zeta)^{2/3}}{(1.0+17.0f)^{5/3}} + \frac{f}{1+5.3\,(f)^{5/3}}\right] \left[\frac{1}{0.7285+1.4115(-\zeta)^{2/3}}\right] \tag{C.33}$$

$$S_{TT} = \frac{1}{n}\left[\frac{14.94f}{(1.0+24.0f)^{5/3}}\right] \qquad f<0.15 \tag{C.34}$$

$$S_{TT} = \frac{1}{n}\left[\frac{6.827f}{(1.0+12.5f)^{5/3}}\right] \qquad f\geq 0.15 \tag{C.35}$$

$$S_{wT} = \frac{1}{n}\left[\frac{12.92f}{(1.0+26.7f)^{1.375}}\right] \qquad f<0.54 \tag{C.36}$$

$$S_{wT} = \frac{1}{n}\left[\frac{4.378f}{(1.0+3.8f)^{2.4}}\right] \qquad f\geq 0.54 \tag{C.37}$$

$$S_{uw} = \frac{1}{n}\left[\frac{20.78f}{(1.0+31.0f)^{1.575}}\right] \qquad f<0.25 \tag{C.38}$$

$$S_{uw} = \frac{1}{n}\left[\frac{12.66f}{(1.0+9.6f)^{2.4}}\right] \qquad f\geq 0.25 \tag{C.39}$$

where z_i (m) denotes the boundary layer height, which is not known most of the time and taken here as constant at 1000 m. Again according to Moore (1986) the same functions may be used for $S_{uu}=S_{vv}$, $S_{TT}=S_{qq}$, $S_{uw}=S_{vw}$ and $S_{wT}=S_{wq}$.

The flux loss correction factor $c_{F_{xy}}$ is then the ratio of the integrated theoretical (co-)spectral distribution functions $S_{xy}$to the convolution integral of the (co-)spectral transfer functions T_{xy} and S_{xy}

$$c_{F_{xy}} = \frac{\int_0^\infty S_{xy}\mathrm{d}n}{\int_0^\infty T_{xy}S_{xy}\mathrm{d}n} \tag{C.40}$$

With the now corrected variances and covariances the friction velocity and stability length are recalculated.

C.4 Sensible heat flux and air temperature

The sonic temperature is close to virtual temperature (Kaimal and Kristensen, 1991) and is transformed to mean air temperature by a simplified relation:

$$\overline{T} = \frac{\overline{T_{son}}}{1 + 0.51\frac{\overline{\varkappa_{abs}}}{\rho_a}} \approx \overline{T_{son}}\left(1 - 0.51\frac{\overline{\varkappa_{abs}}}{\rho_a}\right) \tag{C.41}$$

where $\overline{\varkappa_{abs}}$ (kg m^{-3}) denotes the absolute humidity and ρ_a (kg m^{-3}) the density of dry air at the sonic temperature. If available the humidity measured by the automatic weather station is used, if not the measurement of the eddy correlation system is used. Cross wind and humidity corrections are done on the covariance of the vertical wind speed and the temperature (Schotanus et al., 1983):

$$\overline{w'T'} = \left(\overline{w'T'_{son}} - \frac{0.51}{\rho_a}\overline{T_{son}}\,\overline{w'\varkappa'_{abs}} + 2\overline{u}\,\overline{T_{son}}\frac{\overline{u'w'}}{c_s^2}\right) \tag{C.42}$$

If the latent heat flux is not available, the humidity correction is derived form the latent heat flux calculated as the residue of the energy balance.

The sensible heat flux H (W m^{-2}) is:

$$H = c_p\rho_a\overline{w'T'} \tag{C.43}$$

where c_p is specific heat of moist air (J kg^{-1} K^{-1}) and ρ_a the density of dry air (kg m^{-3}).

It should be noted that, except for the short periods during which raw data were collected, due to the limited number of covariances stored in the field the sonic temperature variance was not corrected for cross wind contamination nor for humidity fluctuations.

C.5 Latent heat flux

To correct for the fact that the vertical wind speed is unequal to zero if a sensible heat flux exists, Webb et al. (1980) proposed a correction for all scalars where the density is measured instead of the mixing ratio, which is the case when using a Krypton H_2O hygrometer

$$\overline{w'\varkappa'_{abs}} = 1 + \frac{M_d}{M_w}\frac{\overline{\varkappa_{abs}}}{\rho_a}\left(\overline{w'\varkappa'_{abs}} + \frac{\overline{\varkappa_{abs}}}{\overline{T_{air}}}\overline{w'T'}\right) \tag{C.44}$$

The latent heat flux (W m^{-2}) is calculated as:

$$\lambda_E E = \overline{w'\varkappa'_{abs}}\lambda_E \tag{C.45}$$

where λ_E is the latent heat of water vapour (J kg^{-1}).

Appendix D

Storage of heat in biomass

The heat storage in the biomass, J_{veg} W m^{-2} can be divided in a rapidly changing heat storage in the leaves and branches and a more slowly storage in the stems:

$$J_{veg} = J_{leaf+branch} + J_{stem} + J_{undergrowth} \tag{D.1}$$

As the biomass of the undergrowth is small as compared to that of the trees, the change in heat storage of the undergrowth is neglected. The change in heat storage in branches and leaves is given by:

$$J_{leaf+branch} = \int_0^{z_{tree}} \rho_{leaf+branch} \mathrm{c}_{leaf+branch} \frac{\mathrm{d}T_{veg}}{\mathrm{d}t} \mathrm{dz} \tag{D.2}$$

where $\mathrm{c}_{leaf+branch} = 2647\ Jkg^{-1}K^{-1}$ based on c of dry wood corrected for the water content of the leaves and the branches.

For the estimation of the heat storage in the trunks, the method of Moore (1986) was followed, i.e. that the heat flux across the surface of a tree trunk with a diameter larger than 14 cm can be treated as an infinite slab. Ignoring the surface conductance the heat flux across a unit trunk surface at height z is given by:

$$F(z) = \sqrt{\rho_{stem} \mathrm{c}_{stem} k_T} A_T \cos\left(\omega t + \phi_T + \frac{\pi}{4}\right) \tag{D.3}$$

where k_T (W m^{-1} K^{-1}) is the thermal conductivity of the stems and ϕ_T is the phase angle of the diurnal cycle of T. As T_{veg} was not measured, is was assumed that it was equal to T_a. For those cases where no measurements of T_a under the canopy were available, the T_a measured above the canopy was used. Under the assumption that the variation of F with height is negligible the change of heat storage in the trunk has been calculated as:

$$J_{stem} = F\ T_{AI} \tag{D.4}$$

where T_{AI} (-) is the tree area index.

If no specific measurements were available, the mass of the tree stems has been calculated using the volumes and the specific mass of the stems. The mass of the branches and leaves was estimated as a fraction of the stem biomass. The specific

Table D.1: *Constants to calculate stem volume V_{stem} , density of fresh and dry wood, ρ_{stem} and biomass of branches and leaves as percentage of stem biomass, M_{stem} for different species.*

Species	constants of V_{stem}			ρ_{stem} (kg m^{-3})		% of M_{stem}	
	a_1	a_2	a_3	fresh	dry	branches	leaves
Scots pine	0.0724	1.933	0.859	700-850	510	11.4	4.3
Japanese larch	0.0546	1.909	0.979	850	590	10.7	2.5
Poplar	0.0463	1.789	1.106	880	450	8.6	1.8
Beech	0.0492	1.843	1.055	960	700	25.4	1.2
American oak	0.0578	1.845	1.008	900-1150	-	44.1	3.6
Inland oak	0.0519	1.861	1.039	1000	-	28.3	2.8
Birch	0.0674	1.712	1.060	-	-	11.0	3.7

heat of the stems was estimated as the weighted average of the specific heat of dry wood and water and adding a correction for heat of wetting hygroscopic material (Moore, 1986). The relation of Skaar (1972) $c_0 = 4.85T + 1113$ (J kg^{-1}K^{-1}) for the specific heat of cellulose was used for that of dry wood. The thermal conductivity k_T of the stems was calculated applying (Siau, 1971):

$$k_T = [\rho_{stem}(2.0 + 5.5\theta_{stem}) + 238] \cdot 10^{-4} \tag{D.5}$$

where θ_{stem} (m^3 m^{-3}) is the moisture content of the stem.

To estimate the stem volumes V_{stem} (m^3) the allometric functions of Dik (1990) and Dik (1996) were used:

$$V_{stem} = a_1 D_{BH}^{a_2} \, z_{tree}^{a_3} \tag{D.6}$$

where a_1, a_2 and a_3 are tree species specific constants, D_{BH} (cm) is the diameter at breast height, z_{tree} (m) the tree height. The values of a_1, a_2 and a_3 for the main tree species of this study are given in Table D.1.

The density of the stems is taken from Laming et al. (1978). Estimates of the percentage biomass of branches and leaves are from Cannell (1982).

For the pine trees at the Loobos site specific measurements were available and allometric relations for the dry weight of the biomass M_X (kg) were derived, using the same type of model as for V_{stem}:

$$M_X = a_1 D_{BH}^{a_2} \, z_{tree}^{a_3} \tag{D.7}$$

In Table D.2 the values of the constants to estimate the dry weight of the biomass are shown.

For beech the allometric relations found by Bartelink (1998) for the central part of the Netherlands have been used (see Table D.3).

Table D.2: *Parameters for the allometric relations between the dry biomass M_X (kg) of leaves, branches and stems for Scots pine.*

	a_1	a_2	a_3
Leaves	0.0178	3.889	–2.575
Branches	0.0269	4.439	-3.053
Stems	0.0322	1.726	1.099

Table D.3: *Parameters for the allometric relations between the dry biomass M_X (kg) of leaves, branches and stems for beech.*

	a_1	a_2	a_3
Leaves	0.0167	2.951	-1.101
Branches	0.0114	3.682	-1.031
Stem	0.0109	1.951	1.262

For American oak at the Edesebos site a specific estimation of the total biomass has been derived during an earlier study by Hendriks et al. (1990), and this estimate of the total biomass has also been used for this study. The volume of twigs and branches with a diameter less than 5 cm was estimated as 15% of the volume of the stem and branches greater than 5 cm. The wet biomass including small branches and twigs was estimated in 1988 as 19.7 kg m^{-2} and in 1989 as 20.9 kg m^{-2}.

Appendix E

Soil water availability

Table E.1: *Soil water content θ (m^3 m^{-3}) for different soil water pressures ψ (Pa) at different soil depths at the different forest sites. The negative depth at the Edesebos site indicates that the sample is taken in litter layer. *) At the Bankenbos site the second sample at $z = 0.94$ m has a high loam content.*

Site	Depth	θ (m^3 m^{-3})				
	(m)	$\lvert\psi\rvert = 10^{1.5}$	$= 10^{1.7}$	$= 10^{2.1}$	$= 10^{3.3}$	$= 10^{4.2}$
Bankenbos	0.14	0.48	0.44	0.32	0.07	0.02
Forest: larch	0.36	0.35	0.30	0.18	0.03	0.01
Soil: loamy	0.60	0.30	0.23	0.08	0.01	0.01
sand	0.94	0.27	0.23	0.12	0.01	0.01
	0.94*	0.29	0.28	0.25	0.17	0.13
Edesebos	-0.03	0.50	0.42	0.25	0.03	0.01
Forest: oak	0.15	0.32	0.25	0.14	0.02	0.01
Soil: loamy	0.37	0.20	0.12	0.03	0.00	0.00
sand	0.55	0.25	0.20	0.11	0.01	0.00
	1.00	0.14	0.11	0.07	0.02	0.01
Fleditebos	0.07	0.46	0.43	0.37	0.25	0.18
Forest: poplar	0.40	0.43	0.42	0.38	0.29	0.24
Soil: clay	0.66	0.52	0.51	0.48	0.39	0.34
	0.74	0.62	0.62	0.61	0.57	0.54
Kampina	0.07	0.40	0.35	0.24	0.05	0.02
Forest: mixed	0.34	0.39	0.37	0.19	0.12	0.07
Soil: sand	0.54	0.33	0.31	0.16	0.01	0.01
Loobos	0.14	0.35	0.21	0.04	0.01	0.01
Forest: pine	0.54	0.35	0.20	0.02	0.01	0.01
Soil: sand						

Appendix F

Small scale spatial variability in storage capacity of intercepted water

The year to year changes in L_{AI} and c_{veg} for a specific site are relatively small if compared to the variation in C. The use of the fixed throughfall buckets allows to compare for each individual bucket the throughfall fraction T_f/P for the same tree species with different V_{AI}. At such a small spatial scale P and other meteorological conditions can be assumed identical for each time step, differences in T_f/P between the buckets can be attributed directly to differences in C and V_{AI}. Fig. F.1 shows the relation between V_{AI} and T_f/P for each individual bucket at the pine forest of the Loobos site. The results are based on the sum of T_f measured the week preceding the date when the V_{AI} measurements were made. Weekly P varied from 1.8 to 57 mm in this period.

For all weeks in the period December 1996 to December 1997 the regression results

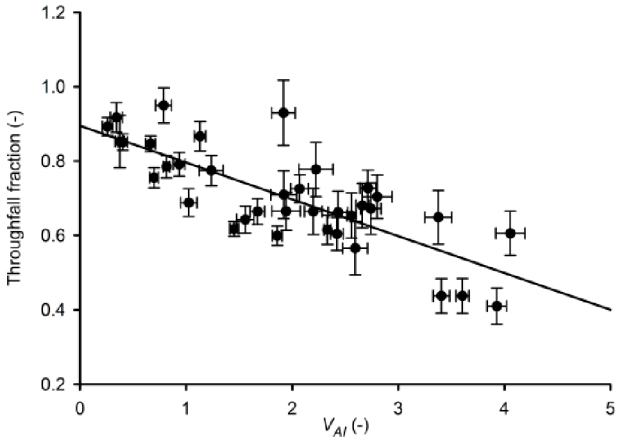

Figure F.1: *Weekly throughfall T_f measured at each bucket as a fraction of gross precipitation P on a weekly basis depicted as a function of the vegetation area index (V_{AI}). The data are averaged values (with standard errors) over 12 weeks in the period of December 1996 to December 1997 for the pine stand at Loobos.*

($R^2 = 0.61$) are:

$$\frac{T_f}{P} = 0.90 - 0.099\,V_{AI} \tag{F.1}$$

For this site with its relatively low L_{AI}, an almost similar relation can be obtained by using the gap fraction instead of V_{AI}. Plotting the interception loss E_i, i.e. P minus T_f, shows slightly more scatter ($R^2 = 0.46$):

$$E_i = 2.44 + 2.13\,V_{AI} \tag{F.2}$$

In all cases drip points show up as outliers. At these drip points sometimes the throughfall exceeded the gross precipitation amount resulting in a negative interception loss as is observed by many other studies (e.g. Lloyd and Marques, 1988). The slope of the regression line and the variance explained ($R^2 = 0.19$) reduces for high values of P e.g. for $P > 40$ mm:

$$\frac{T_f}{P} = 0.88 - 0.051\,V_{AI} \tag{F.3}$$

This change in the relationship may be explained as at high rainfall intensities the influence of the amount of water intercepted by the leaves and eventually evaporated will be relatively small. At the same time the amount of water falling freely to the soil surface and the water dripping from the leaves will be relatively large. These two effects combined reduce the differences in water retention between the covered and non-covered areas and at the same time increase the relative effects of drip points.

At the poplar forest of the Fleditebos site the canopy varies from an almost closed cover in summer to bare in winter. This change in leaf area gives a negative correlation in summer; similar to the pine forest, but for the winter period the correlation between T_f/P and V_{AI} is positive (see Fig. F.2).

This positive correlation during the non-foliated period of the trees is caused by the V_{AI} that is measured, representing the amount of branches above the bucket during this period. The bare branches do not block the throughfall as in the summer period, but enhance throughfall by functioning as drip points. These data of the poplar forest show that E_i in winter even for deciduous trees are an important component of the water balance (10 - 20% of P).

The change in the direction of slope over the year may be explained by the smaller branches and twigs acting as preferential flow paths towards drip points during the non-foliated period. However, the wide scatter ($R^2 = 0.09 - 0.16$) for the individual dates especially during the leaf bearing period seems to point to the conclusion that at least at this deciduous site there is no clear simple relation between the leaf area and C at this spatial and temporal scale. In contrast, at the pine forest of the Loobos site, changes in V_{AI} or c_{veg} have a linear effect on T_f/P and thus on C. This relationship

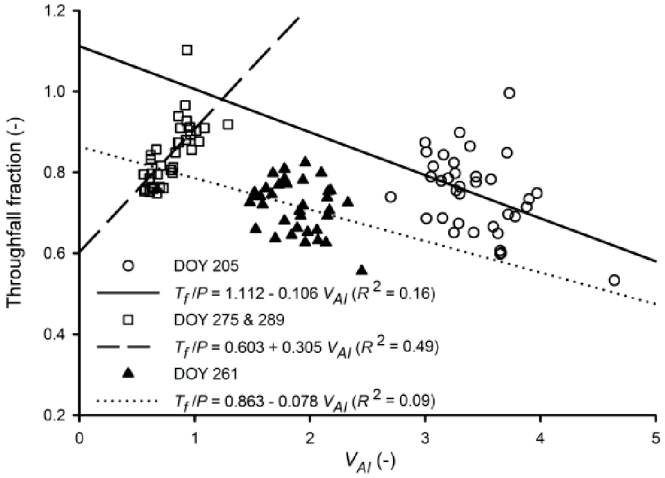

Figure F.2: *Weekly throughfall T_f measured at each bucket as a fraction of gross precipitation P on a weekly basis as a function of the vegetation area index V_{AI}. The data are averaged values for 3 periods of 1, 2 and 1 week in 1997 for the poplar forest at the Fleditebos site.*

makes it possible to extrapolate the results of the pine forest to different sites with approximately the same tree characteristics (tree height and crown diameter), but with different V_{AI} or c_{veg}.

Summary

Water use of forests in the Netherlands

Introduction

This thesis analyses the water use of five different forest types in the Netherlands. The main question leading to the present PhD thesis was: "What is the difference in water use between different tree species in the Netherlands?". This question was divided into the following three underlying research questions:

- "What are the main processes controlling the magnitude of the different components of the water balance of forested areas in the Netherlands?";
- "What are the controlling parameters of these processes and are they related to tree species?";
- "Will this knowledge be of added value to predict effects of different tree species on the water balance?".

Theory of forest evaporation

Evaporation is arguably the component of the water balance with the highest uncertainty. To improve on this uncertainty the main focus of this study is on the processes that govern the evaporation rate of forests. Two main conditions are distinguished: the evaporation from a wet canopy and the evaporation from a dry canopy. As the controls of the evaporation rate are different for these conditions, they are discussed in separate chapters: Chapter 7 "Dry canopy evaporation" and Chapter 8 "Wet canopy evaporation". The theory and equations governing the water and energy flow of a forested plot are introduced in Chapter 2 "Theory of forest evaporation". The theory and equations provide the basis for the parametrizations of a numerical model. In the subsequent Chapters, the concepts behind these equations

are evaluated to determine possible conceptual improvements to simulate the effects of land-use changes on the water balance.

Characteristics of the research sites

For this thesis an extensive amount of data has been collected at five different forest sites in the Netherlands, i.e. Bankenbos, Edesebos, Fleditebos, Kampina and Loobos (see Fig. 3.1). A detailed description including most of the parameters representing the characteristics of the vegetation and the soil at these sites is provided in Chapter 3. Table UK.1 provides an overview of the forest characteristics at the different sites.

The two forest stands with the most pronounced differences in their site characteristics are the Loobos site with a stand of *pine* trees on sand soil and the Fleditebos site with a stand of *poplar* trees on a clay soil. The differences in soil type together with the low groundwater table at Loobos and the relatively high groundwater table at Fleditebos also create large variety in hydrological conditions between these two sites.

The differences in maximum total L_{AI} between the sites is mainly based both on the differences between broad leaved and needle leaved tree species (see Table 3.16) and on the timing of the peaks in L_{AI} of the undergrowth and the trees (see e.g. Fig. 3.13). Both at the Fleditebos site as well as at the Loobos site the L_{AI} of the undergrowth reached almost the same maximum L_{AI} (m^2 m^{-2}) as the trees at the specific sites. The largest variation in total L_{AI} was found for the *poplar* stand at the Fleditebos site, while the *larch* stand at the Bankenbos site showed the least amount of variation in L_{AI}.

Comparison of the groundwater table depths with the rooting depths at the different sites (see Fig. 3.24), shows that deep groundwater tables coincide with deep rooting depths and vice versa.

If the water holding capacity W at the start of a drought is defined as the difference in soil water content at a pressure $\psi = -10^{2.1}$ Pa (i.e. pF 2.1) and $\psi = -10^{4.2}$ Pa (i.e. pF 4.2), Table 3.16 shows that, except for the Loobos site, the amount of soil water easily extractable for evaporation is 87.8 mm on average. If it is assumed that there is no additional soil water available by lateral or vertical transport, the maximum amount of soil water available for evaporation is greatest at the *mixed forest* stand of the Kampina site. Even with the deepest roots of all sites, the maximum amount of available soil water at the *pine* stand of the Loobos site is very low, i.e. 20.8 mm. This low amount of available soil water implies that in principle the vegetation at the Loobos site is most prone to water stress, especially if the roots are not close to the groundwater table.

Table UK.1: *Vegetation characteristics near the observation towers at the sites. All values are average values for the stand. If available, the standard deviation is given between brackets. The tree heights z_{tree} are given at the start as well as at the end of the observation period. All other characteristics have been averaged over this observation period.*

	Banken-bos	Edesebos	Fledite-bos	Kampina	Loobos
Tree species	Larch	Oak	Poplar	Mixed deciduous and coniferous	Scots pine
Undergrowth	Purple moor grass	Bare soil and some regrowth of oak	Stinging nettle, cleavers and grass	Purple moor grass	Grass
Planting date		1944	1985	1890,1930	1904
Observation period	1995-1997	1988-1989	1995-1998	1996-1998	1995-1998
Tree density (tree ha^{-1})	300	600	440	310	403
Tree height (m)	22.0-23.4 (1.5)	17.1-17.4 (n.a.)	16.2-18.7 (0.5)	16.6-17.0 (4.1)	15.3-15.7 (2.0)
DBH (m)	0.29 (0.04)	n.a.	0.24 (0.02)	0.26 (0.12)	0.25 (0.05)
Projected crown area (m^2 $tree^{-1}$)	35 (11)	n.a.	20 (4)	40 (28)	21 (10)
Crown base (m)	14.7 (1.5)	n.a.	8.7 (0.8)	7.1 (3.8)	9.5 (1.6)
L_{AI} tree (-) max.	1.8	4.9	3.7	3.8	1.9
Canopy cover fraction (-) max./min.	0.6/0.4	0.69/0.2	0.8/0.2	0.95/0.45	0.7/0.55
L_{AI} under (-) max.	-	-	4	1.3	1.5

Hydro-meteorological measurements at the sites

All sites, except for the *oak* stand at Edesebos had the same general set-up with some minor differences depending on the specific site. This set-up is discussed in Chapter 4 and consisted of a scaffolding tower with an extendable mast mounted at the top. On top of this mast a 3D sonic anemometer and a Krypton hygrometer were mounted. These were used to derive the latent and sensible heat fluxes using eddy correlation techniques. To measure the carbon flux, at the *pine* stand the inlet of an infra-red gas-analyser was added next to the hygrometer in 1996. In 2000 this closed

path system and hygrometer were replaced by an open path sensor measuring water vapour and carbon dioxide. An automatic weather station measuring wind speed, wind direction, temperature, humidity, incoming and outgoing long and short wave radiation was set up on the scaffolding tower. Here, also a tipping bucket rain gauge was mounted. In addition there was a tipping bucket installed in an open space nearby. Under the canopy the throughfall was measured using 36 manual gauges as well as a tipping bucket rain gauge at the end of an approximately 10 meter long trough. Stemflow was measured from 6 trees on a weekly basis. The soil heat flux was measured using 4 flux plates in combination with 2 temperature/soil moisture profiles. All data were stored at 30 minute intervals, except for the tipping bucket rain gauges for which a 5 minute interval was used.

At the Edesebos site in the *oak* stand a Bowen ratio system was used instead of an eddy correlation system. The Bowen ratio was measured using the Thermometer Interchange System. Most of the other measurements were set-up similar to those at the other sites.

In 1997 two special campaigns for a duration of several months were held. During these campaigns additional measurements were made below the canopy of the *poplar* stand and of the *pine* stand. For this an eddy-correlation system was set-up similarly to the one used above the canopy and in combination with measurements of air temperature, humidity and net radiation.

The data used for this thesis concern the years 1988, 1989 for the *oak* stand at the Edesebos site and the years 1995, 1996, 1997 and 1998 for the other sites. The longest time series used are the data from 1995 to 2009 of the *pine* stand at the Loobos site.

Quality control of the flux measurements

As the fetch conditions of the site determine the location and the magnitude of the contribution of the sources upwind of the flux sensor an estimation is made of the length of the fetch. The length of the fetch together with the quality assessment of the measurements are discussed in Chapter 5.

After storing all data in a database a quality check was performed (see Fig. 6.1). Flags were used to distinguish between time slots with missing data, data accepted as good data and data of questionable quality. The accepted data were then used to derive relations between different variables. Based on these relationships synthetic data were produced.

The data marked as questionable were compared with the synthetic data, checked for consistency in the time series and their quality check flags were checked. The original measurement was accepted if it complied to three conditions:

- Firstly, the measured data did not cause any inconsistency in the time series.

- Secondly, the synthetic and measured data did not differ much.
- Thirdly, the reason(s) the flag(s) were set could be considered as a warning instead of an error.

If the data did not comply to these conditions, the measurement was qualified as unreliable and the data were rejected.

Analysis of the fetch conditions (see Table 5.1) shows that for the major wind direction at all sites the origin of the maximum flux is well within the footprint area of the towers. The Loobos site and the Fleditebos site may be considered most homogeneous for all wind directions.

From the comparison with the full rotation corrections it followed, that the influence of the omission of the rotations on λE is negligible, i.e. well below 5%.

The relatively good closure of the energy balance based on daily values (see Fig. 5.3), as well as the good resemblance of the measured and modelled co-spectra of $\overline{w'\varkappa'}$ (see Fig. 5.2) give confidence to the quality of λE. The fact that the closure of the energy balance for 30 minute data is less good, i.e. $> 80\%$, indicates that a large part of the uncertainty is in the estimates of the heat storage in both the soil and biomass.

If closure of the energy balance is used as an estimate of the uncertainty of the measurement, λE derived in this study using an eddy-correlation system is in summer time better than 5% and in winter time better than 15% for the Bankenbos, Fleditebos and Loobos sites. For the Kampina site the percentage of energy balance closure in summer time is less good, i.e. the uncertainty is better than 15%.

The uncertainty in λE when using a Bowen ratio system is estimated for day time values on a clear day in summer as 10%, and for a dry day in spring with low humidity differences as 20%.

The analysis of the behaviour of the measured wind components with the sonic anemometer showed the little effect of rain on the performance of this sensor. Also the limited number of available data from the open path Krypton hygrometer at the Fleditebos site under wet conditions, showed a reasonably good closure of the energy balance i.e. better than 80% (see Fig. 5.6), as well as a reasonably good agreement with the modelled spectra (see Fig. 5.5).

These findings demonstrate the good performance of the sonic anemometer and hence the relatively good estimates of H under wet conditions. The associated uncertainty in λE based on the percentage of energy balance closure is better than 20%.

Gap filling to generate continuous datasets

Long term measurements rarely produce continuous records. Gaps in the data series may be caused by instrumental failure such as power breaks or because data are deemed to be of insufficient quality. However, continuous data sets are of paramount importance in modelling studies and interpreting measurements of different sites. Sometimes the data gaps in this study were biased towards certain meteorological conditions. For example a number of sensors tended to work less well under wet conditions. In the Netherlands wet conditions are in winter and summer often associated with specific wind directions. If this bias was not taken into account and relations derived for dry periods were used to replace missing data in wet periods, serious biases could be obtained.

To provide an unbiased method for filling data gaps, the capabilities of a neural network were explored in Chapter 6. Results showed that for data, such as temperature or specific humidity, gap filling could be much improved by including nodes representing the seasonal and diurnal cycle or by including measurements of the same variable measured by a different instrument at the same or at an other site. A distinct advantage of a neural network in gap filling is that it is not necessary to make assumptions about a physical relation between variables. For short time steps as used for this study, care should be exercised when only variables of different sites are used to feed the network. Because a neural network makes no assumptions about the physical relations between the variables the results are as good (or bad) as the data used to train the network.

Dry canopy evaporation

Chapter 7 describes the variation in parameter values determining the transpiration rate for five typical forests in the Netherlands and the contribution of the understorey for two of these forest stands. The main objective is to improve our understanding of the processes determining the transpiration rate of forest, with special attention to the differences between stands with different tree species and the contribution of the understorey. In view of the expected increasing frequency of periods of prolonged droughts, special attention is paid to the root water uptake and the parametrization of water stress. For the two sites with more abundant undergrowth an attempt is made to separate the evaporation rate of the understorey and the trees. To explain the variation in evaporation between years and between sites the Jarvis-Stewart parametrization using a sparse canopy single and dual source model is optimized for different periods.

The main driver for surface conductance g_s at all sites was vapour pressure deficit e_D. Although a parabolic response function was used for the temperature relationship of g_s, this relationship was not well established at the lower air temperature T_a range.

At lower temperatures i.e. below the optimum air temperature there was no clear reduction of g_s found for these sites at a mid latitude location. This behaviour may be caused by the fact that at lower T_a at these sites the dew on the undergrowth never completely disappeared.

This unclear relationship of g_s at lower T_a and the strong correlation between T_a and e_D for higher T_a makes the temperature relationship of g_s redundant.

Hence, in view of the limited variation between the sites, the parameter values for g_s as $f(T_a)$ may be set to a fixed value. Based on the improved R^2 for almost all years at the different sites after setting $f(T_a) = 1$, it is recommended to use $f(T_a) = 1$ for all forests sites in the Netherlands.

The low sensitivity of the forests to θ_D shows that these forests are not very sensitive to the range of changes in soil water experienced during this study. Whether these forests are sensitive to more severe droughts cannot be concluded from the present data sets. The proposed soil water stress model including a separate soil water feedback from deep soil layers, worked well for the conditions of this study, but needs to be tested for more extreme dry conditions.

The important contribution of the undergrowth to total evaporation rate E_{Tot} has been demonstrated for 2 forest sites in The Netherlands, i.e. the *pine* forest with its undergrowth mainly consisting of grass at the Loobos site and the *poplar* forest with its undergrowth mixture of grass, nettle and cleavers at the Fleditebos site (see Fig. 7.12). The contribution of undergrowth evaporation to total evaporation varied at the *poplar* forest of the Fleditebos site between 0.25 and 1.0, and at the *pine* forest of the Loobos site between 0.10 and 0.20.

The results of the tree evaporation when applying the dual source model compared well (see Table 7.9) with the sapflow measurements at the Loobos site. The overestimation of the simulated undergrowth evaporation E_{Low} was most likely because of the limited data set being used for the derivation of the parameter set of Table 7.8. Such datasets are still limited. More extensive datasets will help to decrease the uncertainty in the modelled undergrowth evaporation rate.

Wet canopy evaporation

Chapter 8 discusses the main parameters determining the amount of precipitation stored on the vegetation and subsequently evaporated. Attempts have been made to improve the estimates of wet evaporation E_i and canopy water storage C, two of the most important parameters to simulate interception loss.

Measurements show that both the roughness length for heat z_{0H} and for momentum z_{0M} are subject to changes under wet conditions. Use of a value for $kB^{-1} = 1.0$ to express the ratio between the aerodynamic resistance for heat and momentum (see Eq. 2.67) seems more appropriate for the *pine* forest of this study. The magnitude

of kB^{-1} differs per site, is generally higher for the winter period, and is different for wet and dry periods. Only for relatively rare occasions kB^{-1} approached zero under wet conditions. These events were associated with large storms. Based on the data available for this study as a rule of thumb $kB^{-1} = 1.0 - 1.5$ may be used for needle leaf forests and $kB^{-1} = 3.0 - 4.0$ in summer and $kB^{-1} = 5.0 - 6.0$ in winter for broad leaf deciduous forests (see Table 8.1).

Estimates of the evaporation rate E during wet conditions based on regression analysis using measured throughfall T_f, stemflow S_f and precipitation P are approximately twice as high as E derived from the energy balance closure during showers. Possible causes for these differences are the systematic underestimation of measured P, but also the hourly data not taking into account the drip that occurs after the end of the time step. For event based data the use of measured T_f implicitly includes the amount of water left on the leaves at the end of the shower and thus also the relatively high E after the shower has ceased (see Fig. 8.4).

The fact that events without E are very rare or non-existent is the main cause for the often low values of C found when using techniques based on the method of Leyton et al. (1967). Using the sparse canopy model of Gash et al. (1995) and E derived from the energy balance closure to calculate C gives values 3 times higher as compared to using the method of Leyton. The largest differences occur especially during the winter months. The relatively good modelling results obtained with the Gash model using different parameter sets for the same location, exhibit the trade-off between C and E.

Fixed parameter values can decrease the model's daily performance considerably. For the Edesebos site this was mainly caused by differences in C.

Using site and tree specific kB^{-1} values in combination with C per unit canopy cover, will improve the general applicability of the interception models. The presented kB^{-1} and C values may well be used for similar forests under approximately the same conditions. More experimental data however will be needed to enable parametrization of the differences between sites, before the present results can be generally applied to regions with different climatic conditions.

Epilogue

To improve estimates of the actual evaporation of forests a five step approach is suggested in Chapter 9. An important part of this approach is the implementation of direct measurement of the actual evaporation rate at strategic sites for process understanding and verification purposes. Especially the real time use for verification is recommended during extreme conditions, such as droughts.

For future research related to the water use of forests there are two main challenges. The *first* is related to the increased risk of droughts and the effect of lowering

groundwater tables on the physiology and water use of forests. The *second* research challenge is related to the still often ignored contribution of the undergrowth to the forest evaporation. To enable research in these directions, additional data sets will be needed. These data sets should especially aim at representing the different phenological phases of the vegetation and should include:

- Evaporation data sets of undergrowth,
- Evaporation and soil water data sets for forests under water stress.

Because of the strong link between transpiration and photosynthesis, the above mentioned challenges are also important for the research on the carbon exchange of forests.

Samenvatting

Watergebruik van bossen in Nederland

Inleiding

In dit proefschrift wordt het watergebruik van vijf verschillende bosopstanden in Nederland geanalyseerd. De hoofdvraag en aanleiding voor het schrijven van dit proefschrift was: "Wat is het verschil in watergebruik van verschillende boomsoorten in Nederland?". Deze vraag is onderverdeeld in de drie onderliggende onderzoeksvragen:

- "Wat zijn de belangrijkste processen die de grootte van de verschillende waterbalanscomponenten van beboste gebieden in Nederland bepalen?";
- "Welke parameters controleren deze processen en zijn deze gerelateerd aan de boomsoorten?";
- "Is deze kennis van toegevoegde waarde voor het voorspellen van de effecten van verschillende boomsoorten op de water balans?".

De theorie van de verdamping van bossen

Verdamping wordt vaak gezien als de component van de waterbalans met de hoogste onzekerheid. Om deze onzekerheid te verminderen ligt de nadruk van deze studie op de processen die bepalend zijn voor de verdampingssneheid van bossen. Er kunnen twee belangrijke condities onderscheiden worden: de verdamping die plaatsvindt bij een natte kruin en de verdamping die plaatsvindt bij een droge kruin.

Aangezien de variabelen die de hoeveelheid verdamping bepalen verschillend zijn voor de beide condities, worden ze in verschillende hoofdstukken besproken: Hoofdstuk 7 "Droge kruin verdamping" en Hoofdstuk 8 "Natte kruin verdamping". De

theorie en vergelijkingen die de water en energie stromen van een bosopstand bepalen worden in Hoofdstuk 2 “De theorie van bosverdamping” besproken. Deze theorie en vergelijkingen zijn tevens de basis voor de parameterisatie van een numeriek model. Om te bepalen of er verbeteringen mogelijk zijn voor het simuleren van de effecten van landgebruiksveranderingen op de waterbalans, worden in de volgende hoofdstukken de concepten achter deze vergelijkingen geëvalueerd.

Kenmerken van de onderzoekslocaties

Voor dit proefschrift is een grote hoeveelheid data verzameld op vijf verschillende boslocaties in Nederland: Bankenbos, Edesebos, Fleditebos, Kampina en Loobos (zie Fig. 3.1). Een gedetailleerde beschrijving, inclusief de meeste parameters die de vegetatie - en bodemkarakateristieken van de sites beschrijven, wordt gegeven in Hoofdstuk 3. Tabel NL.1 geeft een overzicht van de kenmerken van het bos op de verschillende sites.

De twee bosopstanden met de meest uitgesproken verschillen in hun locatiekenmerken zijn de Loobos locatie met een opstand van dennebomen op een zandgrond en de Fleditebos locatie met een opstand van populieren op een kleibodem. De verschillen in bodemtype samen met de lage grondwaterstand van het Loobos en de relatieve hoge grondwaterstand van het Fleditebos creëeren tevens grote verschillen in de hydrologische condities tussen de twee locaties.

De verschillen in maximale totale L_{AI} tussen de locaties zijn hoofdzakelijk gebaseerd op zowel de verschillen tussen loof- en naaldboomsoorten (zie Tabel 3.16) als op de tijdstippen dat de L_{AI} van de ondergroei en de bomen maximaal is (zie bijvoorbeeld Fig. 3.13). Zowel op de Fleditebos locatie als op Loobos locatie bereikt de L_{AI} van de ondergroei bijna de zelfde maximum L_{AI} (m^2 m^{-2}) als de bomen op de betreffende locaties. De populierenopstand van de Fleditebos locatie heeft de grootste variatie in de totale L_{AI}, terwijl de lariksopstand van de Bankenboslocatie de minste variatie in L_{AI} heeft.

Vergelijking van de grondwaterstanden met de worteldiepten op de verschillende locaties (zie Fig. 3.24), laat zien dat de diepste grondwaterstanden samenvallen met de grootste worteldiepten en vice versa.

Indien het vochthoudendvermogen W aan het begin van een droge periode wordt gedefinieerd als het verschil in bodemvocht bij een druk $\psi = -10^{2.1}$ Pa (= pF 2.1) en $\psi = -10^{4.2}$ Pa (= pF 4.2), dan laat Tabel 3.16 zien, dat behalve voor de Loobos locatie, de hoeveelheid bodemvocht beschikbaar voor verdamping gemiddeld 87.8 mm is. Indien wordt aangenomen dat er geen additioneel water via lateraal of vertikaal transport aanwezig is, dan is de hoeveelheid beschikbaar vocht voor verdamping het grootst voor de gemengde bosopstand van de Kampina site. Zelfs met de grootste bewortelingsdiepte van alle locaties, is de hoeveelheid beschikbaar bodemvocht van

Table NL.1: *De vegetatiekenmerken in de nabije omgeving van de meettorens op de verschillende locaties. Alle waarden zijn gemiddelde waarden voor de opstand. De standaarddeviatie wordt, indien beschikbaar, tussen haakjes weergegeven. De boomhoogte z_{tree} wordt zowel voor het begin als voor het einde van de meetperiode gegeven. Alle andere kenmerken zijn gemiddeld over de meetperiode.*

	Banken-bos	Edesebos	Flediteb-os	Kampina	Loobos
Boom soorten	Lariks	Eik	Populier	Gemengd loof- en naaldhout	Grove den
Ondergroei	Pijpe-strootje	Kale grond en enige hergroei van eik	Brand-netels, kleefkruid en gras	Pijpe-strootje	Bochtige smele
Plant datum		1944	1985	1890,1930	1904
Observatie periode	1995-1997	1988-1989	1995-1998	1996-1998	1995-1998
Boom dichtheid (boom ha^{-1})	300	600	440	310	403
Boom hoogte (m)	22.0-23.4 (1.5)	17.1-17.4 (n.a.)	16.2-18.7 (0.5)	16.6-17.0 (4.1)	15.3-15.7 (2.0)
DBH (m)	0.29 (0.04)	n.a.	0.24 (0.02)	0.26 (0.12)	0.25 (0.05)
Geprojecteerd kruin opp. (m^2 $boom^{-1}$)	35 (11)	n.a.	20 (4)	40 (28)	21 (10)
Basis van de kruin (m)	14.7 (1.5)	n.a.	8.7 (0.8)	7.1 (3.8)	9.5 (1.6)
L_{AI} boom (-) max.	1.8	4.9	3.7	3.8	1.9
Kruin fractie (-) max./min.	0.6/0.4	0.69/0.2	0.8/0.2	0.95/0.45	0.7/0.55
L_{AI} onder (-) max.	-	-	4	1.3	1.5

de dennenopstand op de Looboslocatie erg klein, 20.8 mm.

Deze kleine hoeveelheid beschikbaar bodemvocht impliceert dat de vegetatie op de Loobos locatie in principe het meest gevoelig is voor watertekorten, speciaal wanneer de wortels niet dicht in de buurt zijn van het grondwater.

Hydro-meteorologische metingen op de locaties

Alle gebruikte meetlocaties, op de eikenopstand van de Edesebos locatie na, hadden dezelfde meetopstelling met slechts enkele kleine verschillen afhankelijk van de

specifieke locatie. Deze opstelling is besproken in Hoofdstuk 4 en bestaat uit een steigertoren met een uitschuifbare mast, gemonteerd bovenop de toren. Bovenaan deze uitschuifbare mast zijn een 3D sonische anemometer en een Krypton hygrometer geplaatst. Deze instrumenten werden gebruikt om, met gebruik van de eddy-correlatietechniek, de latente en voelbare warmtestroom te bepalen. Om de koolstofdioxide uitwisseling van de dennenopstand te meten is in 1996 de inlaat voor een instrument dat op basis van infrarood de waterdamp- en kooldioxideconcentratie meet naast de hygrometer geplaatst. In 2000 zijn dit gesloten pad systeem en de hygrometer vervangen door een open pad systeem. Aan de bovenkant van de steigertoren was een automatisch weerstation geplaatst dat de windsnelheid, windrichting, temperatuur, luchtvochtigheid, inkomende en uitgaande lange en korte golfstraling meet. Hier was ook een "tipping bucket" regenmeter geplaatst. Daarnaast was er een zelfde type regenmeter op een dichtbij zijnde open plek geïnstalleerd. Onder de boomkruin is de doorval gemeten met behulp van 36 handregenmeters en ook automatisch, met een "tipping bucket" regenmeter die geplaatst was aan het eind van een ongeveer 10 meter lange goot. De stamafvoer van 6 bomen is gemeten op een wekelijkse basis. De bodemwarmtestroom is gemeten met gebruik van 4 bodemwarmtestroomplaten in combinatie met 2 temperatuur- en bodemvochtprofielen. Alle gegevens zijn opgeslagen met een interval van 30 minuten, behalve die van de "tipping bucket" regenmeter. Deze gegevens zijn met een interval van 5 minuten opgeslagen.

In de eikenopstand van de Edesebos locatie is in plaats van een eddy-correlatiesysteem een Bowen ratio systeem gebruikt. De Bowen ratio is gemeten met behulp van een "Thermometer Interchange System". De meeste van de andere metingen zijn op dezelfde manier opgezet als bij de andere locaties.

In 1997 zijn twee speciale meetcampagnes uitgevoerd voor de duur van een paar maanden. Hierbij zijn additionele metingen onder de kruin gedaan bij de populierenopstand en bij de dennenopstand. Voor deze meetcampagnes is een eddy-correlatie systeem gebruikt, identiek aan het systeem boven de kruin, samen met metingen van de luchttemperatuur, -vochtigheid en netto straling.

De gegevens die voor dit proefschrift zijn gebruikt betreffen de jaren 1988, 1989 voor de eikenopstand van de Edesebos locatie en de jaren 1995, 1996, 1997 en 1998 voor de andere plaatsen. De langste gegevensreeks die gebruikt is betreffen de gegevens vanaf 1995 tot 2009 van de dennenopstand van de Loobos locatie.

Kwaliteitscontrole van de flux metingen

Aangezien de terreincondities van het aanstroomgebied bovenwinds van de meetsensor de plaats en de sterkte van de bijdrage van de bronnen bepalen, is een schatting gemaakt van de lengte van het aanstroomgebied. Deze aanstroomlengte wordt samen met de kwaliteitsbeoordeling van de metingen besproken in Hoofdstuk 5.

Na het opslaan van alle gegevens in een database, is een kwaliteitscontrole uitgevoerd (zie Fig. 6.1). Om onderscheid te kunnen maken tussen records met ontbrekende gegevens, gegevens van goede kwaliteit en gegevens van twijfelachtige kwaliteit, zijn vlaggen gebruikt. De goedgekeurde gegevens zijn daarna gebruikt om empirische relaties tussen verschillende variabelen af te leiden. Op basis van deze relaties zijn synthetische gegevens geproduceerd.

De bestanden met gegevens waarvan de kwaliteit als twijfelachtig gevlagd was, zijn vervolgens vergeleken met de synthetische gegevens, gecontroleerd op consistentie in de tijd en gecontroleerd op de oorzaak van het vlaggen van de gegevens. De originele meting is daarna goedgekeurd indien die aan drie condities voldeed:

- Ten eerste, de gemeten gegevens veroorzaakt geen inconsistentie in de tijdreeks.
- Ten tweede, de synthetische en gemeten gegevens verschilden weinig.
- Ten derde, de reden dat de vlag werd geplaatst kon als waarschuwing in plaats van als een fout worden beschouwd.

Indien de gegevens niet aan deze voorwaarden voldeden, werd de meting als onbetrouwbaar gekwalificeerd en zijn de gegevens niet in de verdere analyse meegenomen.

De analyse van de aanstroomcondities (zie Table 5.1) laat zien dat voor de belangrijkste windrichting bij alle locaties de oorsprong van de maximumstroomdichtheid ruim binnen het gebied van de voetafdruk van de meettorens ligt. De Loobos locatie en de Fleditebos locatie kunnen voor alle windrichtingen als het meest homogeen worden beschouwd.

Op basis van de vergelijking met de volledige rotatiecorrecties is geconcludeerd dat de invloed van het niet toepassen van de rotaties op λE te verwaarlozen is, namelijk minder dan 5%.

De relatief goede sluiting van de energiebalans, gebaseerd op dagelijkse totalen (zie Fig. 5.3), evenals de goede gelijkenis van de gemeten en gemodelleerde co-spectra van $\overline{w'\varkappa'}$ (zie Fig. 5.2) geeft vertrouwen in de kwaliteit van λE. Het feit dat de sluiting van de energiebalans voor 30 minuten gegevens minder goed is, te weten $> 80\%$, wijst erop dat een groot deel van de onzekerheid in de ramingen van de hitteopslag in zowel de bodem als de biomassa zit.

Indien de sluiting van de energiebalans als schatting van de onzekerheid van de meting wordt gebruikt, is λE, in deze studie bepaald met behulp van een eddy-correlatie systeem, in de zomertijd beter dan 5% en in wintertijd beter dan 15% voor de locaties Bankenbos, Fleditebos en Loobos. Voor de Kampina locatie is de energiebalanssluiting in de zomertijd minder goed, d.w.z. de onzekerheid is beter dan 15%.

Bij het gebruik van een Bowen ratio systeem wordt voor overdag de onzekerheid in λE op een heldere dag in de zomer op 10% geschat, en voor een droge dag in de lente met kleine veranderingen in luchtvochtigheid op 20%.

De analyse van de windcomponenten gemeten met de sonische anemometer toonde het kleine effect van regen op de prestaties van deze sensor. Ook het beperkte aantal beschikbare gegevens onder natte omstandigheden van de open pad Krypton hygrometer op de Fleditebos locatie, toonde een redelijk goede sluiting van de energiebalans, d.w.z. beter dan 80% (zie Fig. 5.6), en eveneens een redelijk goede overeenkomst met de gemodelleerde spectra (zie Fig. 5.5).

Deze bevindingen tonen de goede prestaties van de sonische anemometer onder natte omstandigheden aan en geven derhalve vertrouwen in de relatief goede schattingen van H. De bijbehorende onzekerheid in λE, gebaseerd op het percentage van de energiebalanssluiting, is beter dan 20%.

Gaten vullen voor het genereren van continue datasets

Lange termijn metingen produceren zelden ononderbroken gegevensreeksen. De gaten in de gegevensreeksen kunnen veroorzaakt worden door bijvoorbeeld het uitvallen van instrumenten door stroomstoringen, of doordat de kwaliteit van de meetgegevens onvoldoende is. Nochtans zijn ononderbroken gegevensreeksen van kapitaal belang in de modellering van studies en in het interpreteren van metingen, afkomstig van verschillende locaties. Soms zijn de gaten in de gegevensreeksen in deze studie beïnvloed door meteorologische condities. Bijvoorbeeld, een aantal sensoren werkten minder goed onder natte omstandigheden. Natte omstandigheden zijn in Nederland in zomer en winter meestal gekoppeld aan een specifieke windrichting. Als deze bias niet in acht wordt genomen en de relaties die voor droge periodes zijn afgeleid, gebruikt worden om ontbrekende gegevens tijdens natte periodes te vervangen, kunnen grote afwijkingen worden verkregen.

Om een objectieve methode te gebruiken om ontbrekende gegevens aan te vullen, werden in Hoofdstuk 6 de mogelijkheden onderzocht van een neuraal netwerk. De resultaten toonden aan dat voor gegevens, zoals temperatuur of specifieke luchtvochtigheid, het aanvullen van ontbrekende gegevens veel zou kunnen worden verbeterd door knopen te introduceren die de seizoens- en dag-cyclus weergeven, of door metingen van de zelfde variabele te gebruiken, die door een verschillend instrument op dezelfde, of op een andere locatie is gemeten. Een ander voordeel van het gebruik van een neuraal netwerk is, dat het niet noodzakelijk is om op voorhand aannames te maken over een fysische relatie tussen de variabelen. Bij korte tijdstappen, zoals in deze studie, dient zorgvuldigheid te worden betracht wanneer slechts de variabelen van verschillende locaties worden gebruikt om het netwerk te voeden. Aangezien een neuraal netwerk geen aannames over fysische relaties tussen de variabelen maakt, zijn

de resultaten zo goed (of slecht) als de gegevens die worden gebruikt om het netwerk te trainen.

Droge kruin verdamping

Hoofdstuk 7 beschrijft de variatie in parameterwaarden die de transpiratiesnelheid bepalen voor vijf typisch Nederlandse bossen en tevens de bijdrage hieraan van de ondergroei voor twee van deze bosopstanden. De belangrijkste doelstelling is om de processen die de transpiratiesnelheid van een bos bepalen beter te leren begrijpen. Dit met speciale aandacht voor de verschillen in transpiratie tussen bosopstanden met verschillende boomsoorten, en voor de bijdrage van ondergroei. Gezien de verwachte toename van het aantal en de duur van periodes met droogte, is speciale aandacht besteed aan het begrijpen van de wateropname door de wortels en de modellering van waterstress. Voor de twee plaatsen met overvloediger ondergroei is een poging gedaan om de verdampingsnelheid van de ondergroei en die van de bomen te scheiden. Om de variatie in verdamping tussen jaren en tussen locaties te verklaren, is het Jarvis-Stewart model met een enkele open kruin en met een dubbele vegetatielaag geoptimaliseerd voor verschillende periodes.

Op alle locaties was het dampspanningstekort e_D de belangrijkste sturende variabele voor het oppervlaktegeleidingsvermogen g_s. Alhoewel een parabolische functie is gebruikt voor de relatie tussen luchttemperatuur T_a en g_s was deze relatie voor lagere temperaturen T_a niet goed gedefinieerd. Bij temperaturen onder de optimale luchttemperatuur, is voor deze locaties in een gematigd klimaat geen duidelijke verlaging van g_s gevonden. Dit gedrag wordt vooral veroorzaakt doordat op deze locaties bij lagere T_a de dauw op de ondergroei bijna nooit helemaal verdwijnt.

Deze onduidelijke relatie van g_s bij lagere T_a en de sterke correlatie tussen T_a en e_D voor hogere T_a maakt de temperatuurafhankelijkheid van g_s overbodig.

Op basis hiervan en in het licht van de beperkte variatie tussen de locaties, kan de parameterwaarde voor de relatie g_s =f(T_a) op een vaste waarde worden gezet. Op basis van de hogere R^2 die voor bijna alle jaren op de verschillende locaties werd gevonden bij het gebruik van f(T_a) = 1, wordt aanbevolen om voor alle bossen in Nederland f(T_a) = 1 te gebruiken.

De lage gevoeligheid van de bossen voor θ_D, toont aan dat deze bossen niet erg gevoelig zijn voor veranderingen in de hoeveelheid bodemvocht zoals die zijn opgetreden tijdens deze studie. Of deze bossen gevoelig zijn voor drogere omstandigheden kan niet uit de huidige gegevens worden geconcludeerd. De voorgestelde model voor bodemvochttekorten inclusief een aparte feedback voor het bodemvocht in diepere bodemlagen, werkt goed voor de omstandigheden van deze studie, maar dient verder getest te worden voor meer extreem droge omstandigheden.

Het belang van de bijdrage van de ondergroei aan de totale verdamping E_{Tot} is

voor twee boslocaties in Nederland aangetoond: de *dennenbos* opstand van de Loobos locatie met een ondergroei die voornamelijk uit gras bestaat en de *populieren* opstand van de Fleditebos locatie met een ondergroei van een mengsel van gras, kleefkruid en brandnetels (zie Fig. 7.12). De bijdrage van de verdamping van de ondergroei aan de totale verdamping varieerde bij het populierenbos van de Fleditebos locatie tussen 0.25 en 1.0, en voor het dennenbos van de Loobos locatie tussen 0.10 en 0.20.

De boomverdamping als resultaat van het "dual source"-model (twee-bronnen-model) laat een goede vergelijking zien met de sapstroommetingen van de Loobos locatie (zie Tabel 7.9). De overschatting van de gesimuleerde ondergroeiverdamping E_{Low} is waarschijnlijk het gevolg van de beperkte hoeveelheid gegevens die is gebruikt voor de afleiding van de parameterwaarden in Tabel 7.8. Dergelijke data zijn nog steeds beperkt beschikbaar. Meer en langere datasets zullen helpen de onzekerheid te verminderen in de gemodelleerde verdampingssnelheid van de ondergroei.

Natte kruin verdamping

In Hoofdstuk 8 worden de belangrijkste parameters, die de hoeveelheid neerslag dat door het blad wordt vastgehouden en daarna verdampt, besproken. Pogingen zijn gedaan om de schattingen van de interceptie verdamping E_i en de kruinberging C, twee van de belangrijkste parameters om het interceptieverlies te simuleren.

Metingen tonen aan dat zowel de ruwheidslengte voor warmte z_{0H} als die voor momentum z_{0M} onder natte omstandigheden anders zijn dan onder droge omstandigheden. Het gebruik van een waarde voor $kB^{-1} = 1.0$ voor de verhouding tussen de aerodynamische weerstand voor warmte en momentum (Zie Eq. 2.67) lijkt goed geschikt voor de dennenopstand van deze studie. De grootte van kB^{-1} verschilt per locatie, is in het algemeen hoger voor de winterperiode en is verschillend voor natte en droge omstandigheden. Onder natte omstandigheden benaderde $kB^{-}1$ slechts zelden nul. Dit laatste gebeurde vooral bij grote buien. Op basis van de beschikbare gegevens van deze studie kan als vuistregel worden gehanteerd: $kB^{-1} = 1.0-1.5$ voor naaldbossen en voor loofbossen $kB^{-1} = 3.0 - 4.0$ in de zomer en $kB^{-1} = 5.0 - 6.0$ in de winter (Zie Tabel 8.1).

Schattingen van de verdampingssnelheid E onder natte omstandigheden gebaseerd op regressieanalyse van de gemeten doorval T_f, de stemflow S_f en de neerslag P zijn ongeveer twee keer zo groot als E afgeleid van de energiebalanssluiting tijdens buien. Mogelijke oorzaken hiervoor zijn: de systematische onderschatting van de gemeten P, maar ook doordat bij uur gegevens geen rekening wordt gehouden met de neerslag die na de betreffende tijdstap nog van het blad valt. Bij gegevens die gebaseerd zijn op totalen van neerslagbuien wordt bij het gebruik van de gemeten T_f impliciet de hoeveelheid water meegenomen die aan het eind van de bui op het blad achterblijft en omvat dus ook de relatief hoge E die, nadat de bui is gestopt, plaatsvindt (zie

Fig. 8.4).

Het feit dat neerslaggebeurtenissen waarbij geen verdamping E optreedt bijna niet voorkomen, is de belangrijkste oorzaak voor de vaak lage waarden van de interceptieberging C bij het gebruik van technieken gebaseerd op de methode van Leyton et al. (1967). Het gebruik van het niet gesloten kronendak-model van Gash et al. (1995) in combinatie met de verdamping E afgeleid uit de energiebalanssluiting om C te berekenen, geeft waarden die 3 keer zo hoog zijn dan wanneer de methode van Leyton wordt gebruikt. Vooral tijdens de wintermaanden treden grote verschillen op. De relatief goede modelresultaten verkregen met het Gash-model met behulp van verschillende parameterssets voor dezelfde locatie, tonen de compenserende werking aan tussen C en E.

Het gebruik van vaste parameterwaarden kan de dagelijkse modelresultaten aanzienlijk verslechteren. Voor de Edesebos locatie werd dit hoofdzakelijk veroorzaakt door verschillen in C.

Het gebruik van lokatie en boom specifieke waarden voor kB^{-1} in combinatie met C per eenheid kruinbedekking, zal in bijna alle gevallen de toepasbaarheid van de interceptiemodellen verbeteren. De hier gpresenteerde waarden voor kB^{-1} en C kunnen goed gebruikt worden voor vergelijkbare bossen met ongeveer dezelfde meteorologische omstandigheden. Additionele experientele data zullen echter nodig zijn om de verschillen tussen sites voldoende accuraat te kunnen parameteriseren, voordat de huidige resultaten algemeen toepasbaarzijn voor gebieden met andere klimatalogische omstandigheden.

Epiloog

Om de schattingen van de waterbalans te verbeteren is in Hoofdstuk 9 een vijfstappen plan voorgesteld. Een belangrijk onderdeel van deze aanpak is de inzet van rechtstreekse metingen van de actuele verdamping op strategisch gekozen locaties. Deze metingen kunnen gebruikt worden voor het verbeteren van onze proceskennis en voor verificatie doeleinden. In het bijzonder wordt het gebruik aanbevolen voor verificatie gedurende extreme condities, zoals droogte. Voor het toekomstig onderzoek gerelateerd aan het watergebruik van bossen, zijn er twee belangrijke uitdagingen. De eerste is gerelateerd aan de toegenomen risico's van droogtes en het effect van dalende grondwaterstanden op de fysiologie en het waterverbruik van bossen. De tweede onderzoeksuitdaging is gerelateerd aan de nog steeds vaak verwaarloosde bijdrage van de ondergroei aan de totale bosverdamping. Om onderzoek in deze richtingen mogelijk te maken zijn additionele datasets nodig. Deze datasets zouden speciaal gericht moeten zijn op het goed weergeven van de verschillende fysiologische stadia van de vegetatie en dienen in ieder geval de volgende elementen te bevatten:

- datasets van de verdamping van de ondergroei,

- datasets van de verdamping en van de hoeveelheid bodemvocht van bossen die watertekort hebben.

Vanwege het sterke verband tussen de transpiratie en de fotosynthese zijn de bovenstaande onderwerpen ook van belang voor het onderzoek naar de koolstofuitwisseling van bossen.

Curriculum Vitae

Eddy Moors was born in Dakar (Senegal) on 19 July 1958. After living in Bamako, Kuala Lumpur and Singapore he and his family moved to the Netherlands. Here he finished his high school at the Emmaus College in Rotterdam.

He did his MSc at Wageningen University in the Netherlands. During his practical period he worked for IWACO as an consultant in Ouagadougou, Burkina Faso. He graduated "Cum Laude (met lof)"in 1985 at Wageningen University on the topics meteorology, catchment hydrology, agro-hydrology and computer science.

Moors spend his military service as an officer in The Hague working among others on computer aided training and war games for command posts. Before returning to Africa, he worked for a short while at Wageningen University.

From 1987 to 1991 he worked as an hydrologist for the World Meteorological Organization First he was stationed at the Agrhymet Center in Niamey and later at the Caribbean Meteorologic Institute on Barbados.

In 1992 Moors returned to the Netherlands and started working at the Chair group Hydrology and Water Management of Wageningen University.

In 1993 he transferred to the Winand Staring Center, that is now integrated in Alterra Wageningen UR. Here his main occupation at that time was the project "Forest hydrology in the Netherlands". The data collected for this project became the basis for his PhD thesis. Later the Loobos site of this project was combined with the research on carbon exchange of the EU funded EuroFlux project that came into place in 1996 with the Kyoto agreement. At present the Loobos site is one of the longest running flux stations in the World (see e.g. www.climateXchange.nl).

In 1999 he became team leader, first of the Team Water Atmosphere and Constituents, later of the Team Land Atmosphere Interactions.

Since 2006 he is heading, together with Pavel Kabat, the group Earth System Science and Climate Change, which is a merger of an Alterra Team and a Chair Group of Wageningen University (see www.alterra.wur.nl/UK/research/ Specialisation+water+and+climate/ESSCC/).

List of selected publications

Ashby, M., Dolman, A.J., Kabat, P., **Moors, E. J.** and Ogink-Hendriks, M.J., 1996. *SWAPS version 1.0; technical reference manual*. Tech. rep.

Beer, C., Ciais, P., Reichstein, M., Baldocchi, D., Law, B.E., Papale, D., Soussana, J.F., Ammann, C., Buchmann, N., Frank, D., Gianelle, D., Janssens, I.A., Knohl, A., Köstner, B., **Moors, E.**, Roupsard, O., Verbeeck, H., Vesala, T., Williams, C.A. and Wohlfahrt, G., 2009. Temporal and among-site variability of inherent water use efficiency at the ecosystem level. *Global Biogeochemical Cycles*, 23.

Beniston, M., Stoffel, M., Harding, R., Kernan, M., Ludwig, R., **Moors, E.**, Samuels, P., Tockner, K., 2012. Obstacles to data access for research related to climate and water: Implications for science and EU policy-making. *Environmental Science and Policy*, 17(3): 41–48.

Davi, H., Dufrêne, E., Francois, C., Le Maire, G., Loustau, D., Bosc, A., Rambal, S., Granier, A. and **Moors, E. J.**, 2006. Sensitivity of water and carbon fluxes to climate changes from 1960 to 2100 in european forest ecosystems. *Agricultural and Forest Meteorology*, 141(1): 35–56.

Dolman, A.J., **Moors, E. J.** and Elbers, J.A., 2002. The carbon uptake of a mid latitude pine forest growing on sandy soil. *Agricultural and Forest Meteorology*, 111(3): 157–170.

Dolman, A.J., **Moors, E. J.**, Elbers, J.A. and Snijders, W., 1998. Evaporation and surface conductance of three temperate forests in the Netherlands. *Annales Des Sciences Forestieres*, 55(1-2): 255–270.

Elbers, J.A., Dolman, A.J., **Moors, E. J.** and Snijders, W., 1996. *Hydrologie en waterhuishouding van bosgebieden in Nederland; fase 2: meetopzet en eerste resultaten*. Tech. rep., Wageningen, SC-DLO, 1996. Rapport 333.2, 65 blz.

Elbers, J.A., **Moors, E. J.** and Jacobs, C.M.J., 2010. *Gemeten actuele verdamping voor twaalf locaties in Nederland*. Tech. rep., Alterra Wageningen UR, Alterra - Rapport / STOWA rapport : 1920 / 2010-36 rapport nummer: Alterra Rapport 1920.

Falge, E., Baldocchi, D., Olson, R., Anthoni, P., Aubinet, M., Bernhofer, C., Burba, G., Ceulemans, G., Clement, R., Dolman, H., Granier, A., Gross, P., Grünwald, T., Hollinger, D., Jensen, N.O., Katul, G., Keronen, P., Kowalski, A., Lai, C.T., Law, B.E., Meyers, T., Moncrieff, J., **Moors, E.**, Munger, J.W., Pilegaard, K., Rannik, U., Rebmann, C., Suyker, A., Tenhunen, J., Tu, K., Verma, S., Vesala, T., Wilson, K. and Wofsy, S., 2001. Gap filling strategies for long term energy flux data sets. *Agricultural and Forest Meteorology*, 107(1): 71–77.

Gockede, M., Foken, T., Aubinet, M., Aurela, M., Banza, J., Bernhofer, C., Bonnefond, J.M., Brunet, Y., Carrara, A., Clement, R., Dellwik, E., Elbers, J., Eugster, W., Fuhrer, J., Granier, A., Grünwald, T., Heinesch, B., Janssens, I.A., Knohl, A., Koeble, R., Laurila, T., Longdoz, B., Manca, G., Marek, M., Markkanen, T., Mateus, J., Matteucci, G., Mauder, M., Migliavacca, M., Minerbi, S., Moncrieff, J., Montagnani, L., **Moors, E.**, Ourcival, J.M., Papale, D., Pereira, J., Pilegaard, K., Pita, G., Rambal, S., Rebmann, C., Rodrigues, A., Rotenberg, E., Sanz, M.J., Sedlak, P., Seufert, G., Siebicke, L., Soussana, J.F., Valentini, R., Vesala, T., Verbeeck, H. and Yakir, D., 2008. Quality control of carboeurope flux data - part 1: Coupling footprint analyses with flux data quality assessment to evaluate sites in forest ecosystems. *Biogeosciences*, 5(2): 433–450.

Granier, A., Reichstein, M., Bréda, N., Janssens, I.A., Falge, E., Ciais, P., Grünwald, T., Aubinet, M., Berbigier, P., Bernhofer, C., Buchmann, N., Facini, O., Grassi, G., Heinesch, B., Ilvesniemi, H., Keronen, P., Knohl, A., Köstner, B., Lagergren, F., Lindroth, A., Longdoz, B., Loustau, D., Mateus, J., Montagnani, L., Nys, C., **Moors, E. J.**, Papale, D., Peiffer, M., Pilegaard, K., Pita, G., Pumpanen, J., Rambal, S., Rebmann, C., Rodrigues, A., Seufert, G., Tenhunen, J., Vesala, T. and Wang, Q., 2007. Evidence for soil water control on carbon and water dynamics in European forests during the extremely dry year: 2003. *Agricultural and Forest Meteorology*, 143(1-2): 123–145.

Hamaker, P., Beets, C.P., **Moors, E. J.** and Dolman, A.J., 2002. *De waterhuishouding van een loofbosaanplant in de droogmakerij De Purmer; resultaten van onderzoek gedurende de periode 1990-2000*. Tech. rep., Utrecht, STOWA, 2002. STOWA Rapp. 2002-30, 172 blz.

Jacobs, C.M.J., **Moors, E. J.**, ter Maat, H.W., Teuling, A.J., Balsamo, G., Bergaoui, K., Ettema, J., Lange, M., van den Hurk, B.J.J.M., Viterbo, P. and Wergen, W., 2008. Evaluation of European Land Data Assimilation System (ELDAS) products using in site observations. *Tellus Series A: Dynamic Meteorology and Oceanography*, 60(5): 1023–1037.

Klaassen, W., van Breugel, P.B., **Moors, E. J.** and Nieveen, J.P., 2002. Increased heat fluxes near a forest edge. *Theoretical and Applied Climatology*, 72(3-4): 231–243.

Kruijt, B., Elbers, J.A., von Randow, C., Araújo, A.C., Oliveira, P.J., Culf, A., Manzi, A.O., Nobre, A.D., Kabat, P. and **Moors, E. J.**, 2004. The robustness of eddy correlation fluxes for amazon rain forest conditions. *Ecological Applications*, 14(4): S101–S113, suppl. S.

Le Maire, G., Delpierre, N., Jung, M., Ciais, P., Reichstein, M., Viovy, N., Granier, A., Ibrom, A., Kolari, P., Longdoz, B., **Moors, E.J.**, Pilegaard, K., Rambal, S., Richardson, A. and Vesala, T., 2010. Detecting the critical periods that underpin interannual fluctuations in the carbon balance of European forests. *Journal of Geophysical Research G: Biogeosciences*, 115(4), G00H03.

Mahecha, M.D., Reichstein, M., Jung, M., Seneviratne, S.I., Zaehle, S., Beer, C., Braakhekke, M.C., Carvalhais, N., Lange, H., Le Maire, G. and **Moors, E.**, 2010. Comparing observations and process-based simulations of biosphere-atmosphere exchanges on multiple timescales. *Journal of Geophysical Research-Biogeosciences*, 115.

Maximov, T.C., Dolman, A.J., **Moors, E. J.**, Ohta, T., Sugimoto, A. and Ivanov, B.I., 2005. Parameters of carbon and water cycles in the forest ecosystems of the cryolithozone. *Doklady Earth Sciences*, 405(8): 1199–1201.

Moors, E. J., 2008. *Evaporation*. IAHS Special Publication : 8, IAHS Press, Centre for Ecology and Hydrology, Wallingford, Oxfordshire, UK, pp. 23–41.

Moors, E. J., Dolman, A.J., Bouten, W. and Veen, A.W.L., 1996. De verdamping van bossen. *H2O*, (29)16: 462–466.

Moors, E. J. and Dolman, H., 2003. *Land-use change, climate and hydrology*. Kluwer, Dordrecht, pp. 139–165.

Moors, E.J., Groot, A., Biemans, H., van Scheltinga, C., Siderius, C., Stoffel, M., Huggel, C., Wiltshire, A., Mathison, C., Ridley, J., Jacob, D., Kumar, P., Bhadwal, S., Gosain, A. and Collins, D., 2011. Adaptation to changing water resources in the Ganges basin, northern India. *Environmental Science and Policy*, 14: 758-769.

Moors, E.J., Jacobs, C., Jans, W., Supit, I., Kutsch, W., Bernhofer, C., Bziat, P., Buchmann, N., Carrara, A., Ceschia, E., Elbers, J., Eugster, W., Kruijt, B., Loubet, B., Magliulo, E., Moureaux, C., Olioso, A., Saunders, M. and Sogaard, H., 2010. Variability in carbon exchange of European croplands. *Agriculture, Ecosystems and Environment*, 139(3): 325–335.

Ohta, T., Maximov, T.C., Dolman, A.J., Nakai, T., Molen, van de M.K., Kononov, A.V., Maximov, T., Hiyama, T., Iijima, Y., **Moors, E. J.** and Tanaka, H., 2008. Interannual variation of water balance and summer evapotranspiration in an eastern Siberian larch forest over a 7-year period (1998-2006). *Agricultural and Forest Meteorology*, 148(12): 1941–1953.

Rebmann, C., Göckede, M., Foken, T., Aubinet, M., Aurela, M., Berbigier, P., Bernhofer, C., Buchmann, N., Carrara, A., Cescatti, A., Ceulemans, R., Clement, R., Elbers, J.A., Granier, A., Grünwald, T., Guyon, D., Havránková, K., Heinesch, B., Knohl, A., Laurila, T., Longdoz, B., Marcolla, B., Markkanen, T., Miglietta, F., Moncrieff, J., Montagnani, L., **Moors, E. J.**, Nardino, M., Ourcival, J.M., Rambal, S., Rannik, Ü., Rotenberg, E., Sedlak, P., Unterhuber, G., Vesala, T. and Yakir, D., 2005. Quality analysis applied on eddy covariance measurements at complex forest sites using footprint modelling. *Theoretical and Applied Climatology*, 80: 121–141.

Richardson, A.D., Black, T.A., Ciais, P., Delbart, N., Friedl, M.A., Gobron, N., Hollinger, D.Y., Kutsch, W.L., Longdoz, B., Luyssaert, S., Migliavacca, M., Montagnani, L., Munger, J.W., **Moors, E.**, Piao, S.L., Rebmann, C., Reichstein, M., Saigusa, N., Tomelleri, E., Vargas, R. and Varlagin, A., 2010. Influence of spring and autumn phenological transitions on forest ecosystem productivity. *Philosophical Transactions of the Royal Society B-Biological Sciences*, 365(1555): 3227–3246.

Su, Z., Timmermans, W.J., van der Tol, C., Dost, R.J.J., Bianchi, R., Gomez, J.A., House, A., Hajnsek, I., Menenti, M., Magliulo, V., Esposito, M., Haarbrink, R., Bosveld, F.C., Rothe, R., Baltink, H.K., Vekerdy, Z., Sobrino, J.A., Timmermans, J., van Laake, P., Salama, S., van der Kwast, H., Claassen, E., Stolk, A., Jia, L., **Moors, E.**, Hartogensis, O. and Gillespie, A., 2009. Eagle 2006 - multi-purpose, multi-angle and multi-sensor in-situ, airborne and space borne campaigns over grassland and forest. *Hydrol. Earth Syst. Sci.*, 13: 833–845.

Teuling, A.J., Seneviratne, S.I., Stockli, R., Reichstein, M., **Moors, E.**, Ciais, P., Luyssaert, S., van den Hurk, B., Ammann, C., Bernhofer, C., Dellwik, E., Gianelle, D., Gielen, B., Grünwald, T., Klumpp, K., Montagnani, L., Moureaux, C., Sottocornola, M. and Wohlfahrt, G., 2010. Contrasting response of European forest and grassland energy exchange to heatwaves. *Nature Geoscience*, 3(10): 722–727.

Valentini, R., Matteucci, G., Dolman, A.J., Schulze, E.D., Rebmann, C., **Moors, E. J.**, Granier, A., Gross, P., Jensen, N.O., Pilegaard, K., Lindroth, A., Grelle, A., Bernhofer, C., Grünwald, T., Aubinet, M., Ceulemans, R., Kowalski, A.S., Vesala, T., Rannik, Ü., Berbigier, P., Loustau, D., Gudmundsson, J., Thorgeirsson, H.,

Ibrom, A., Morgenstern, K., Clement, R., Moncrieff, J., Montagnani, L., Minerbi, S. and Jarvis, P.G., 2000. Respiration as the main determinant of carbon balance in European forests. *Nature 404 (2000), 20 April: 861-865.*

van Breugel, P.B., Klaassen, W. and **Moors, E. J.**, 1999. The spatial variability of turbulence above a forest. *Theoretical and Applied Climatology*, 62(1-2): 43–50.

van Loon, W.K.P., Bastings, H.M.H. and **Moors, E. J.**, 1998. Calibration of soil heat flux sensors. *Agricultural and Forest Meteorology*, 92(1): 1–8.

List of main symbols used

The list of main symbols contains those symbols that are used regularly in the text. Symbols not often used and specific for one chapter are defined at the first location where they are being used in that chapter.

Symbol	Description	Units	Dimensions
A	Available energy flux density	W m^{-2}	M T^{-3}
A_T	Amplitude of the soil temperature	K	Θ
a	Maximum interception loss	mm	L
b	Reciprocal value of a	mm^{-1}	L^{-1}
$C, C_{\max}$	Actual and maximum water storage on the vegetation or litter layer on an areal basis	m	L
C_{soil}	Volumetric heat capacity of the soil	J m^{-3} K^{-1}	M L $^{-1}$ T^{-2} Θ^{-1}
c_c, c_{veg}	Fraction of cloud cover, fraction of canopy cover	-	1
c_x	Specific heat ($x = p$ for air at constant pressure, v for dry air at constant volume, c for clay, o for organic matter, q for quartz, w for water, veg for vegetation)	J kg^{-1} K^{-1}	L^2 T^{-2} Θ^{-1}

Symbol	Description	Units	Dimensions
D	Canopy drip	m s^{-1}	L T^{-1}
D_{BH}	(Tree) Diameter at Breast Height	cm	L
$D_T{}'$	Apparent diffusivity	m ^{2} s^{-1}	L^2 T^{-1}
d	Displacement height	m	L
e, e_D	Vapour pressure of water, Deficit of e	hPa	M L^{-1} T^{-2}
E	Evaporation flux density	kg m^{-2} s^{-1}	M L^{-2} T^{-1}
E_i	Evaporation flux density of intercepted water	kg m^{-2} s^{-1}	M L^{-2} T^{-1}
F_{lat}	Lateral advective energy flux density	W m^{-2}	M T^{-3}
F_A	Photosynthesis flux density	μmol CO_2 m^{-2} s^{-1}	mol L^{-2} T^{-1}
G	Soil heat flux density	W m^{-2}	M T^{-3}
g	Acceleration of gravity	ms^{-2}	L T^{-2}
H	Sensible heat flux density	W m^{-2}	M T^{-3}
h	Height	m	L
J	Change in energy storage of the vegetation and air per unit area	W m^{-2}	M T^{-3}
J_X	Change in storage ($X = H$ of sensible heat in the air, E of latent heat in the air, veg of the vegetation)	W m^{-2}	M T^{-3}
K_X	Turbulent exchange coefficient or eddy diffusivities ($X = E$ for moisture, H for heat and M for momentum)	m^2 s^{-1}	L^2 T^{-1}
k, k_s	Hydraulic conductivity, saturated hydraulic conductivity	m s^{-1}	L T^{-1}
k_T	Thermal conductivity	W m^{-1} K^{-1}	M L T^{-3} Θ^{-1}
L	Monin-Obukhov scaling length	m	L
L_{AI}	Leaf Area Index	m^2 m^{-2}	1
l	Parameter Van Genuchten function	-	1

Symbol	Description	Units	Dimensions
m	Parameter Van Genuchten function	-	1
N_{tree}	Tree density	ha^{-1}	L^{-2}
n	Parameter Van Genuchten function	-	1
P, P_{net}	Precipitation rate, net precipitation rate	$m\ s^{-1}$	$L\ T^{-1}$
p	Atmospheric pressure	hPa	$M\ L^{-1}\ T^{-2}$
p_f	Free throughfall coefficient	-	1
p_{stem}	Stem flow coefficient	-	1
Q	Discharge	$m^3\ s^{-1}$	L^3T^{-1}
q_{lat}	Lateral soil water flow rate	$m\ s^{-1}$	$L\ T^{-1}$
$q_{b,net}$	Net flow rate at the bottom of the soil profile	$m\ s^{-1}$	$L\ T^{-1}$
q_r, $q_{r,net}$	Surface run-off, net surface run-off	$m\ s^{-1}$	$L\ T^{-1}$
R_s^{atm}	Solar radiation at the top of the atmosphere	$W\ m^{-2}$	$M\ T^{-3}$
R_s^{down}, R_s^{up}	Downward, upward short-wave (0.3-3 μm) radiation flux density	$W\ m^{-2}$	$M\ T^{-3}$
R_l^{down}, R_l^{up}	Downward, upward long-wave (3-100 μm) radiation flux density	$W\ m^{-2}$	$M\ T^{-3}$
R_{net}	Net radiation flux density	$W\ m^{-2}$	$M\ T^{-3}$
r_a, r_{aX}	Aerodynamic resistance, Aerodynamic resistance ($X = M$ momentum, $X = E$ vapour and $X = H$ heat)	$s\ m^{-1}$	$T\ L^{-1}$
r_s	Surface resistance	$s\ m^{-1}$	$T\ L^{-1}$
S_f	Stemflow (rate)	$m\ s^{-1}$	$L\ T^{-1}$
S_E	Sink term for the deep soil latent heat flux	$cm^3\ cm^{-3}\ s^{-1}$	T^{-1}
S_{roots}	Sink term for root water uptake	$cm^3\ cm^{-3}\ s^{-1}$	T^{-1}
T, T_x	Temperature, temperature ($x =$ *a* air -, *d* dry bulb -, *s* of surface -, *soil* soil -, *son* sonic -, *v* virtual -, *veg* vegetation -, *w* wet bulb temperature)	K	Θ

Symbol	Description	Units	Dimensions
T_{AI}	Tree Area Index	-	1
T_f	Throughfall rate	m s^{-1}	L T^{-1}
t	Time	s	T
u	Wind speed in the x-direction	m s^{-1}	L T^{-1}
u_*	Friction velocity	m s^{-1}	L T^{-1}
u_{cup}	Scalar wind speed as measured by a cup anemometer	m s^{-1}	L T^{-1}
u_{dir}	Wind direction	∘	1
u_{hor}, u_{tot}	Horizontal wind vector, total wind vector	m s^{-1}	L T^{-1}
v	Wind speed in the y-direction	m s^{-1}	L T^{-1}
V_{AI}	Vegetation Area Index	m^2 m^{-2}	1
w	Wind speed in the z-direction	m s^{-1}	L T^{-1}
W	Water holding capacity	mm	L
W_{AI}	Wood Area Index	m^2 m^{-2}	1
X_x	Volume fraction ($x = a$ of air, c clay, o organic matter, q quartz, w water)	m^3 m^{-3}	1
x, $x_{\max}$	Distance upwind of sensor, distance upwind of sensor where the flux source is maximal	m	L
x_p	Path length	m	L
z	Elevation head, depth, height (positive upwards)	m	L
z_{0H}, z_{0M}	roughness length for heat, momentum	m	L
z_b, z_{ref}	Bottom boundary depth, height of the reference level	m	L
z_g, z_{sw}	Groundwater level depth, surface water level	m	L
z_i	Boundary layer height	m	L
z_s	Soil surface	m	L
z_{tree}, z_{can}, z_{root}	Tree height, canopy base height, rooting depth	m	L

Greek symbols

Symbol	Description	Units	Dimensions
α	Parameter Van Genuchten function	m^{-1}	L^{-1}
α_l	Reflectivity of the surface for the long-wave radiation	-	1
α_s	Albedo of the surface	-	1
β	Bowen ratio	-	1
γ	Psychrometer constant	hPa K^{-1}	M L^{-1} T^{-2} Θ^{-1}
Δ_e	Gradient of the saturated vapour pressure versus the temperature curve	hPa K^{-1}	M L^{-1} T^{-2} Θ^{-1}
$\Delta_\varkappa$	Gradient of the saturated specific humidity versus the temperature curve	K^{-1}	Θ^{-1}
ϵ	Dielectric permittivity	J V^2 m^{-1}	M^{-1} L^{-3} Θ^{-2} Q^2
ξ_l	Absorptivity of the surface for the long-wave radiation	-	1
ζ	Stability parameter	m m^{-1}	L^{-1} L^{-1}
κ	Von Karman constant (= 0.40)	-	1
λ	Latent heat of vaporization of water per unit mass	J kg^{-1}	L^2 T^{-2}
η	Eddy-decay coefficient	-	1
ρ_x	Density (for $x = a$ of air, c clay, o organic matter, q quartz, w water, veg vegetation)	kg m^{-3}	M L^{-3}
σ	Stefan Boltzmann constant (= $5.67 \cdot 10^{-8}$ W m^{-2} K^{-4})	W m^{-2} K^{-4}	M T^{-3} Θ^{-4}
Θ, Θ_s	Potential temperature, potential temperature at the surface	K	Θ
θ, θ_D	Volumetric soil water content, Deficit of θ	m^3 m^{-3}	1

Symbol	Description	Units	Dimensions
θ_r	Residual volumetric soil water content	$m^3\ m^{-3}$	1
θ_s	Saturated volumetric soil water content	$m^3\ m^{-3}$	1
θ_{stem}	Moisture content of the stem	$m^3\ m^{-3}$	1
$\varkappa$, $\varkappa_D$, $\varkappa_s$	Specific humidity, Deficit of $\varkappa$, saturated specific humidity	$kg\ kg^{-1}$	1
$\varkappa_{abs}$	Absolute humidity	$kg\ m^{-3}$	$M\ L^{-3}$
$\varkappa_r$	Relative humidity	-	1
τ	Momentum flux density or shear stress	$kg\ m^{-1}\ s^{-2}$	$M\ L^{-1}\ T^{-2}$
μ	Solar energy ($\approx$ 0.422 J μmol$(CO_2)^{-1}$)	Jμmol $(CO_2)^{-1}$	$M\ L^2\ T^{-2}$
ϕ_T	Phase angle of the diurnal cycle of the temperature	$\circ$	1
ϕ_X	Similarity function ($X = E$ for moisture, H for heat and M for momentum)	-	1
ψ	Soil water pressure	Pa	$M\ L^{-1}\ T^{-2}$
ω	Diurnal angular frequency	$rad\ h^{-1}$	T^{-1}

Operators

Symbol	Description
$\overline{x}$	Average of x
x'	Turbulent component of x
S_{xx}	Spectra and co-spectra of x and x
T_x, T_{xx}	Transfer functions of x and composite transfer functions of xx

List of Figures

List of Tables

Bibliography

Allen, R.G., Pereira, L.S., Howell, T.A. and Jensen, M.E., 2011. Evapotranspiration information reporting: I. Factors governing measurement accuracy. *Agricultural Water Management*, 98(6): 899–920.

Anderson, A.R. and Pyatt, D.G., 1986. Interception of precipitation by pole-stage Sitka spruce and Lodgepole pine and mature Sitka spruce at Kielder forest, Northumberland. *Forestry*, 59(1): 29–38.

Ashby, M., Dolman, A.J., Kabat, P., Moors, E. and Ogink-Hendriks, M.J., 1996. *SWAPS version 1.0. Technical reference manual.* Technical Document Technical Document 42, DLO-Staring Centrum.

Aston, A.R., 1979. Rainfall interception by eight small trees. *Journal of Hydrology*, 42(3-4): 383–396.

Aubinet, M., Grelle, A., Ibrom, A., Rannik, U., Moncrieff, J., Foken, T., Kowalski, A.S., Martin, P.H., Berbigier, P., Bernhofer, C., Clement, R., Elbers, J., Granier, A., Grunwald, T., Morgenstern, K., Pilegaard, K., Rebmann, C., Snijders, W., Valentini, R. and Vesala, T., 2000. Estimates of the annual net carbon and water exchange of forests: The EUROFLUX methodology. *Advances in Ecological Research, Vol 30*, 30: 113–175.

Bakker, M.R., Augusto, L. and Achat, D.L., 2006. Fine root distribution of trees and understory in mature stands of maritime pine (Pinus pinaster) on dry and humid sites. *Plant and Soil*, 286(1-2): 37–51.

Baldocchi, D.D. and Xu, L.K., 2007. What limits evaporation from Mediterranean oak woodlands - The supply of moisture in the soil, physiological control by plants

or the demand by the atmosphere? *Advances in Water Resources*, 30(10): 2113–2122.

Ball, J., 1987. Calculations related to gas exchange. In: E.Z.G.F.I. Cowan (Ed.), *Stomatal Function*, Stanford University Press, Stanford, CA, pp. 446–476.

Bartelink, H.H., 1998. Radiation interception by forest trees: a simulation study on effects of stand density and foliage clustering on absorption and transmission. *Ecological Modelling*, 105(2-3): 213–225.

Begue, A., Prince, S.D., Hanan, N.P. and Roujean, J.L., 1996. Shortwave radiation budget of Sahelian vegetation. 2. Radiative transfer models. *Agricultural and Forest Meteorology*, 79(1-2): 97–112.

Black, T.A., Tan, C.S. and Nnyamah, J.U., 1980. Transpiration rate of Douglas-fir trees in thinned and un-thinned stands. *Canadian Journal of Soil Science*, 60(4): 625–631.

Blyth, E.M. and Dolman, A.J., 1995. The roughness length for heat of sparse vegetation. *Journal of Applied Meteorology*, 34(2): 583–585.

Boels, D., Van Gils, J., Veerman, G.J. and Wit, K.E., 1978. Theory and system of automatic-determination of soil-moisture characteristics and unsaturated hydraulic conductivities. *Soil Science*, 126(4): 191–199.

Bosveld, F.C., 1997. Derivation of fluxes from profiles over a moderately homogeneous forest. *Boundary-Layer Meteorology*, 84(2): 289–327.

Bosveld, F.C., 1999. *Exchange processes between a coniferous forest and the atmosphere*. Ph.D. thesis, Wageningen Agricultural University, Wageningen, The Netherlands.

Bosveld, F.C. and Bouten, W., 2003. Evaluating a model of evaporation and transpiration with observations in a partially wet Douglas-fir forest. *Boundary-Layer Meteorology*, 108(3): 365–396.

Bouten, W., Swart, P.J.F. and Dewater, E., 1991. Microwave transmission, a new tool in forest hydrological research. *Journal of Hydrology*, 124(1-2): 119–130.

Breuer, L., Eckhardt, K. and Frede, H.G., 2003. Plant parameter values for models in temperate climates. *Ecological Modelling*, 169(2-3): 237–293.

Brunner, I. and Godbold, D.L., 2007. Tree roots in a changing world. *Journal of Forest Research*, 12(2): 78–82.

Brutsaert, W., 1982. *Evaporation into the atmosphere.* Reidel, Dordrecht, The Netherlands.

Bryant, M.L., Bhat, S. and Jacobs, J.M., 2005. Measurements and modeling of throughfall variability for five forest communities in the southeastern US. *Journal of Hydrology*, 312(1-4): 95–108.

Buckley, T.N., 2005. The control of stomata by water balance. *New Phytologist*, 168(2): 275–291.

Butler, D.R., 1985. The energy-balance of water drops on a leaf surface. *Boundary-Layer Meteorology*, 32(4): 337–349.

Butler, D.R., 1986. Evaporation from rain drops on leaves in a cereal canopy - a simulation-model. *Boundary-Layer Meteorology*, 36(1-2): 39–51.

Calder, I.R., 1986. A stochastic model of rainfall interception. *Journal of Hydrology*, 89(1-2): 65–71.

Calder, I.R., Hall, R.L., Rosier, P.T.W., Bastable, H.G. and Prasanna, K.T., 1996. Dependence of rainfall interception on drop size. 2. Experimental determination of the wetting functions and two-layer stochastic model parameters for five tropical tree species. *Journal of Hydrology*, 185(1-4): 379–388.

Calder, I., 1990. *Evaporation in the Uplands.* Wiley, Chichester, UK.

Caldwell, M.M., Dawson, T.E. and Richards, J.H., 1998. Hydraulic lift: Consequences of water efflux from the roots of plants. *Oecologia*, 113(2): 151–161.

Calfapietra, C., Ainsworth, E.A., Beier, C., De Angelis, P., Ellsworth, D.S., Godbold, D.L., Hendrey, G.R., Hickler, T., Hoosbeek, M.R., Karnosky, D.F., King, J., Korner, C., Leakey, A.D.B., Lewin, K.F., Liberloo, M., Long, S.P., Lukac, M., Matyssek, R., Miglietta, F., Nagy, J., Norby, R.J., Oren, R., Percy, K.E., Rogers, A., Mugnozza, G.S., Stitt, M., Taylor, G. and Ceulemans, R., 2010. Challenges in elevated co_2 experiments on forests. *Trends in Plant Science*, 15(1): 5–10.

Canadell, J.G., Pitelka, L.F. and Ingram, J.S.I., 1996. The effects of elevated co_2 on plant-soil carbon below-ground: A summary and synthesis. *Plant and Soil*, 187(2): 391–400.

Cannell, M.G.R., 1982. Crop and isolation ideotypes - evidence for progeny differences in nursery-grown Picea Sitchensis. *Silvae Genetica*, 31(2-3): 60–66.

Carlyle-Moses, D.E., 2004. A reply to R. Keim's Comment on "Measurement and modelling of growing-season canopy water fluxes in a mature mixed deciduous forest stand, southern Ontario, Canada". *Agricultural and Forest Meteorology*, 124(3-4): 281–284.

Chapin, F., Matson, P. and Mooney, H., 2002. *Principles of terrestrial ecosystem ecology*. Springer, New York.

Chason, J.W., Baldocchi, D.D. and Huston, M.A., 1991. A comparison of direct and indirect methods for estimating forest canopy leaf-area. *Agricultural and Forest Meteorology*, 57(1-3): 107–128.

Christensen, J.H., Hewitson, B., Busuioc, A., Chen, X., Gao, I., Held, R., Kolli, R.K., Kwon, W.T., Laprise, R., Magana Rueda, L., Mearns, L.O., Menendez, C.G., Risnen, J., Rinke, A., Sarr, A. and Whetton, P., 2007. *Regional climate projections. Climate Change 2007: The physical science basis. Contribution of the working group I to the fourth assessment report of the intergovernmental panel on climate change*. Cambridge and New York.

Cochard, H., Coll, L., Le Roux, X. and Ameglio, T., 2002. Unraveling the effects of plant hydraulics on stomatal closure during water stress in walnut. *Plant Physiology*, 128(1): 282–290.

Corrsin, S., 1974. Second 25 years of statistical-theory of turbulent-diffusion. *Transactions-American Geophysical Union*, 55(3): 135–135.

Cowan, I., 1977. Stomatal behavior and environment. *Adv. Bot. Res.*, 4: 117–228.

Crockford, R.H. and Richardson, D.P., 2000. Partitioning of rainfall into throughfall, stemflow and interception: effect of forest type, ground cover and climate. *Hydrological Processes*, 14(16-17): 2903–2920.

Davi, H., Dufrne, E., Francois, C., Le Maire, G., Loustau, D., Bosc, A., Rambal, S., Granier, A. and Moors, E.J., 2006. Sensitivity of water and carbon fluxes to climate changes from 1960 to 2100 in European forest ecosystems. *Agricultural and Forest Meteorology*, 141(1): 35–56.

Dawson, T.E., 1996. Determining water use by trees and forests from isotopic, energy balance and transpiration analyses: The roles of tree size and hydraulic lift. *Tree Physiology*, 16(1-2): 263–272.

De Vries, D., 1963. Thermal properties of soils. In: W.v. Wijk (Ed.), *Physics of plant environment*, North-Holland Publishing Company, Amsterdam., pp. 210–235.

Deguchi, A., Hattori, S. and Park, H.T., 2006. The influence of seasonal changes in canopy structure on interception loss: Application of the revised Gash model. *Journal of Hydrology*, 318(1-4): 80–102.

Denmead, O. and Bradley, E., 1985. Flux-gradient relationships in a forest canopy. In: B. Hutchison and B. Hicks (Eds.), *The forest-atmosphere interaction*, Reidel, Dordrecht, p. 421.

Desai, A.R., Bolstad, P.V., Cook, B.D., Davis, K.J. and Carey, E.V., 2005. Comparing net ecosystem exchange of carbon dioxide between an old-growth and mature forest in the upper Midwest, USA. *Agricultural and Forest Meteorology*, 128(1-2): 33–55.

Dewar, R.C., 2002. The Ball-Berry-Leuning and Tardieu-Davies stomatal models: synthesis and extension within a spatially aggregated picture of guard cell function. *Plant Cell and Environment*, 25(11): 1383–1398.

Dik, E., 1990. *Estimating volumes and timber heights of poplars (in Dutch).* Tech. Rep. Report nr. 590, De Dorschkamp - Instituut voor Bosbouw en Groenbeheer.

Dik, E., 1996. *Revised stem-volume functions of some tree species: Tables, conversion to trade volume, bark percentages and taper of the stem (in Dutch).* Tech. Rep. Report nr. 223, Instituut voor Bos- en Natuuronderzoek (IBN-DLO).

Dirkse, G., Daamen, W., Schoonderwoerd, H., Japink, M., van Jole, M., van Moorsel, R., Schnitger, P., Stouthamer, W. and Vocks, M., 2006. *Meetnet Functievervulling bos 2001-2005. Vijfde Nederlandse Bosstatistiek.* Tech. Rep. Report dk065-O, Directie Kennis, LNV.

Dolman, A.J., 1986. Estimates of roughness length and zero plane displacement for a foliated and non-foliated oak canopy. *Agricultural and Forest Meteorology*, 36(3): 241–248.

Dolman, A.J., 1987. Summer and winter rainfall interception in an oak forest - predictions with an analytical and a numerical-simulation model. *Journal of Hydrology*, 90(1-2): 1–9.

Dolman, A.J., 1988. Transpiration of an oak forest as predicted from porometer and weather data. *Journal of Hydrology*, 97(3-4): 225–234.

Dolman, A.J., 1993. A multiple-source land-surface energy-balance model for use in general-circulation models. *Agricultural and Forest Meteorology*, 65(1-2): 21–45.

Dolman, A.J. and de Jeu, R.A.M., 2010. Evaporation in focus. *Nature Geoscience*, 3(5): 296–296.

Dolman, A.J. and Wallace, J.S., 1991. Lagrangian and K-theory approaches in modeling evaporation from sparse canopies. *Quarterly Journal of the Royal Meteorological Society*, 117(502): 1325–1340.

Domec, J.C., Noormets, A., King, J.S., Sun, G., McNulty, S.G., Gavazzi, M.J., Boggs, J.L. and Treasure, E.A., 2009. Decoupling the influence of leaf and root hydraulic conductances on stomatal conductance and its sensitivity to vapour pressure deficit as soil dries in a drained loblolly pine plantation. *Plant Cell and Environment*, 32(8): 980–991.

Droogers, P., 2009. *Verbetering bepaling actuele verdamping voor het strategisch waterbeheer: definitiestudie (In Dutch).* Tech. Rep. STOWA rapport 2009-11, STOWA, Future Water, Wageningen, The Netherlands.

Dufour, F., 2000. *Groundwater in the Netherlands - Facts and figures.* Netherlands Institute of Applied Geoscience TNO - National Geological Survey, Delft/Utrecht.

Dyer, A.J., Garratt, J.R., Francey, R.J., McIlroy, I.C., Bacon, N.E., Hyson, P., Bradley, E.F., Denmead, O.T., Tsvang, L.R., Volkov, Y.A., Koprov, B.M., Elagina, L.G., Sahashi, K., Monji, N., Hanafusa, T., Tsukamoto, O., Frenzen, P., Hicks, B.B., Wesely, M., Miyake, M. and Shaw, W., 1982. An international turbulence comparison experiment (ITCE 1976). *Boundary-Layer Meteorology*, 24(2): 181–209.

Dyer, A., 1974. A review of flux-profile relationships. *Boundary-Layer Meteorology*, 7: 363–372.

Evers, P., Bouten, W., van Grinsven, J. and Steingrver, E., 1991. *CORRELACI: Identification of traditional and air pollution related stress factors in a Douglas fir ecosystem: the ACIFORN stands.* Tech. Rep. Report 626, De Dorschkamp.

Falge, E., Baldocchi, D., Olson, R., Anthoni, P., Aubinet, M., Bernhofer, C., Burba, G., Ceulemans, G., Clement, R., Dolman, H., Granier, A., Gross, P., Grunwald, T., Hollinger, D., Jensen, N.O., Katul, G., Keronen, P., Kowalski, A., Lai, C.T., Law, B.E., Meyers, T., Moncrieff, J., Moors, E., Munger, J.W., Pilegaard, K., Rannik, U., Rebmann, C., Suyker, A., Tenhunen, J., Tu, K., Verma, S., Vesala, T., Wilson, K. and Wofsy, S., 2001. Gap filling strategies for long term energy flux data sets. *Agricultural and Forest Meteorology*, 107(1): 71–77.

Farquhar, G.D., Schulze, E.D. and Kuppers, M., 1980. Responses to humidity by stomata of Nicotiana-Glauca L and Corylus-Avellana L are consistent with the optimization of carbon-dioxide uptake with respect to water-loss. *Australian Journal of Plant Physiology*, 7(3): 315–327.

Feddes, R.A..and Zaradny, H., 1978. Model for simulating soil-water content considering evapotranspiration - comments. *Journal of Hydrology*, 37(3-4): 393–397.

Feddes, R.A., Hoff, H., Bruen, M., Dawson, T., de Rosnay, P., Dirmeyer, O., Jackson, R.B., Kabat, P., Kleidon, A., Lilly, A. and Pitman, A.J., 2001. Modeling root water uptake in hydrological and climate models. *Bulletin of the American Meteorological Society*, 82(12): 2797–2809.

Feddes, R.A. and Raats, P.A.C., 2004. Parameterizing the soil - water - plant root system. In: R.A. Feddes, G. de Rooij and J.C. van Dam (Eds.), *Unsaturated-zone Modeling: Progress, Challenges and Applications*, Wageningen UR Frontis Series, Kluwer Academic Publishers, Dordrecht, p. 95:141.

Filius, A. and Roosenschoon, O., 1993. *Verloofing van de Veluwe (in Dutch).* Tech. Rep. Hinkeloord Reports 7, Department of Forestry, Wageningen Agricultural University.

Finnigan, J.J., 2002. personal communication.

Fleischbein, K., Wilcke, W., Goller, R., Boy, J., Valarezo, C., Zech, W. and Knoblich, K., 2005. Rainfall interception in a lower montane forest in Ecuador: effects of canopy properties. *Hydrological Processes*, 19(7): 1355–1371.

Ford, E.D., 1976. Canopy of a Scots pine forest - description of a surface of complex roughness. *Agricultural Meteorology*, 17(1): 9–32.

Franks, P.J., 2004. Stomatal control and hydraulic conductance, with special reference to tall trees. *Tree Physiology*, 24(8): 865–878.

Franks, P.J., Drake, P.L. and Froend, R.H., 2007. Anisohydric but isohydrodynamic: seasonally constant plant water potential gradient explained by a stomatal control mechanism incorporating variable plant hydraulic conductance. *Plant Cell and Environment*, 30(1): 19–30.

Fuchs, M. and Tanner, C.B., 1970. Error analysis of bowen ratios measured by differential psychrometry. *Agricultural Meteorology*, 7(4): 329–&.

Gardner, M.W. and Dorling, S.R., 1998. Artificial neural networks (the multilayer perceptron) - a review of applications in the atmospheric sciences. *Atmospheric Environment*, 32(14-15): 2627–2636.

Garratt, J.R. and Hicks, B.B., 1973. Momentum, heat and water-vapor transfer to and from natural and artificial surfaces. *Quarterly Journal of the Royal Meteorological Society*, 99(422): 680–687.

Gash, J.H.C., 1979. Analytical model of rainfall interception by forests. *Quarterly Journal of the Royal Meteorological Society*, 105(443): 43–55.

Gash, J.H.C. and Dolman, A.J., 2003. Sonic anemometer (co)sine response and flux measurement I. the potential for (co)sine error to affect sonic anemometer-based flux measurements. *Agricultural and Forest Meteorology*, 119(3-4): 195–207.

Gash, J.H.C., Lloyd, C.R. and Lachaud, G., 1995. Estimating sparse forest rainfall interception with an analytical model. *Journal of Hydrology*, 170(1-4): 79–86.

Gash, J.H.C., Valente, F. and David, J.S., 1999. Estimates and measurements of evaporation from wet, sparse pine forest in Portugal. *Agricultural and Forest Meteorology*, 94(2): 149–158.

Gerrits, A.M.J., Pfister, L. and Savenije, H.H.G., 2010. Spatial and temporal variability of canopy and forest floor interception in a beech forest. *Hydrological Processes*, 24(21): 3011–3025, gerrits, A. M. J. Pfister, L. Savenije, H. H. G.

Giacomin, A. and Trucchi, P., 1992. Rainfall interception in a beech coppice (Acquerino, Italy). *Journal of Hydrology*, 137(1-4): 141–147.

Goulden, M.L., Munger, J.W., Fan, S.M., Daube, B.C. and Wofsy, S.C., 1996. Measurements of carbon sequestration by long-term eddy covariance: Methods and a critical evaluation of accuracy. *Global Change Biology*, 2(3): 169–182.

Granier, A., Loustau, D. and Breda, N., 2000. A generic model of forest canopy conductance dependent on climate, soil water availability and leaf area index. *Annals of Forest Science*, 57(8): 755–765.

Granier, A., Reichstein, M., Bréda, N., Janssens, I.A., Falge, E., Ciais, P., Grünwald, T., Aubinet, M., Berbigier, P., Bernhofer, C., Buchmann, N., Facini, O., Grassi, G., Heinesch, B., Ilvesniemi, H., Keronen, P., Knohl, A., Küstner, B., Lagergren, F., Lindroth, A., Longdoz, B., Loustau, D., Mateus, J., Montagnani, L., Nys, C., Moors, E.J., Papale, D., Peiffer, M., Pilegaard, K., Pita, G., Pumpanen, J., Rambal, S., Rebmann, C., Rodrigues, A., Seufert, G., Tenhunen, J., Vesala, T. and Wang, Q., 2007. Evidence for soil water control on carbon and water dynamics in european forests during the extremely dry year: 2003. *Agricultural and Forest Meteorology*, 143(1-2): 123–145.

Green, R., 1979. *Sampling design and statistical methods for environmental biologist.* John Wiley & Sons, New York, USA.

Grelle, A., Lundberg, A., Lindroth, A., Moren, A.S. and Cienciala, E., 1997. Evaporation components of a boreal forest: Variations during the growing season. *Journal of Hydrology*, 197(1-4): 70–87.

Groen, K., 1997. *Pestice leaching in polders: Field and model studies on cracked clays and loamy sand.* Tech. Rep. Van Zee tot Land 62, Ministerie van Verkeer en Waterstaat, Directoraat-Generaal Rijskwaterstaat, Directie IJsselmeergebied.

Haan, C., 1977. *Statistical methods in hydrology.* Iowa State University Press, Ames, Iowa.

Hall, R.L. and Harding, R.J., 1993. The water-use of the Balquhidder catchments - a processes approach. *Journal of Hydrology*, 145(3-4): 285–314.

Hall, R., 2002. Aerodynamic resistance of coppiced poplar. *Agricultural and Forest Meteorology*, 114: 83–102.

Hanan, N.P., 2001. Enhanced two-layer radiative transfer scheme for a land surface model with a discontinuous upper canopy. *Agricultural and Forest Meteorology*, 109(4): 265–281.

Helvey, J.D. and Patric, J.H., 1965. Canopy and litter interception of rainfall by hardwoods of eastern united states. *Water Resources Research*, 1(2): 193–&.

Hendriks, M., Kabat, P., Homma, F. and Postma, J., 1990. *Onderzoek naar de verdamping van een loofbos: meetresultaten en enkele modelberekeningen.* Tech. rep., Studiecommissie Waterbeheer Natuur, Bos en Landschap (in Dutch). Staring Center.

Hilhorst, M., 1984. A sensor for the determination of the complex permittivity of materials as a measure for the moisture content. In: P. Bergveld (Ed.), *Sensors and Activators*, Kluwer Technical Books, Deventer, The Netherlands, pp. 79–84.

Hojstrup, J., 1981. A simple model for the adjustment of velocity spectra in unstable conditions downstream of an abrubt change in roughness and heat flux. *Boundary-Layer Meteorology*, 21: 341 – 356.

Hormann, G., Branding, A., Clemen, T., Herbst, M., Hinrichs, A. and Thamm, F., 1996. Calculation and simulation of wind controlled canopy interception of a beech forest in northern Germany. *Agricultural and Forest Meteorology*, 79(3): 131–148.

Horton, R., 1919. Rainfall interception. *Mon. Weather Rev.*, 47: 603 – 623.

Huntingford, C. and Cox, P.M., 1997. Use of statistical and neural network techniques to detect how stomatal conductance responds to changes in the local environment. *Ecological Modelling*, 97(3): 217–246.

Ibrom, A., Dellwik, E., Flyvbjerg, H., Jensen, N.O. and Pilegaard, K., 2007. Strong low-pass filtering effects on water vapour flux measurements with closed-path eddy correlation systems. *Agricultural and Forest Meteorology*, 147(3-4): 140–156, doi: 10.1016/j.agrformet.2007.07.007.

Ishii, H.T., Jennings, G.M., Sillett, S.C. and Koch, G.W., 2008. Hydrostatic constraints on morphological exploitation of light in tall sequoia sempervirens trees. *Oecologia*, 156(4): 751–763.

Jackson, R.B., Schenk, H.J., Jobbagy, E.G., Canadell, J., Colello, G.D., Dickinson, R.E., Field, C.B., Friedlingstein, P., Heimann, M., Hibbard, K., Kicklighter, D.W., Kleidon, A., Neilson, R.P., Parton, W.J., Sala, O.E. and Sykes, M.T., 2000. Belowground consequences of vegetation change and their treatment in models. *Ecological Applications*, 10(2): 470–483.

Jacobs, C.M.J., Moors, E.J., Ter Maat, H.W., Teuling, A.J., Balsamo, G., Bergaoui, K., Ettema, J., Lange, M., Van den Hurk, B., Viterbo, P. and Wergen, W., 2008. Evaluation of European Land Data Assimilation System (ELDAS) products using in situ observations. *Tellus Series a-Dynamic Meteorology and Oceanography*, 60(5): 1023–1037.

Jarvis, P.G., 1976. Interpretation of variations in leaf water potential and stomatal conductance found in canopies in the field. *Philosophical Transactions of the Royal Society of London Series B-Biological Sciences*, 273(927): 593–610.

Jarvis, P.G., 1980. Stomatal conductance, gaseous exchange and transpiration. In: P.G.J. J. Grace E. D. Ford (Ed.), *Plants and their atmospheric environment*, Blackwell Scientific Publications, Oxford, pp. 175–204.

Jonkheer, R., 1989. *Vegetatiekartering Kampina 1988*. Tech. Rep. Report 2870, Natuurmonumenten.

Kabat, P., Hutjes, R.W.A. and Feddes, R.A., 1997. The scaling characteristics of soil parameters: From plot scale heterogeneity to subgrid parameterization. *Journal of Hydrology*, 190(3-4): 363–396.

Kaimal, J.C. and Finnigan, J.J., 1994. *Atmospheric boundary layer flows*. Oxford-University-Press, New-York-(State).

Kaimal, J.C., Izumi, Y., Wyngaard, J.C. and Cote, R., 1972. Spectral characteristics of surface-layer turbulence. *Quarterly Journal of the Royal Meteorological Society*, 98(417): 563–589.

Kaimal, J.C. and Kristensen, L., 1991. Time-series tapering for short data samples. *Boundary-Layer Meteorology*, 57(1-2): 187–194.

Katul, G., Oren, R., Ellsworth, D., Hsieh, C.I., Phillips, N. and Lewin, K., 1997. A Lagrangian dispersion model for predicting co_2 sources, sinks, and fluxes in a uniform loblolly pine (Pinus taeda L) stand. *Journal of Geophysical Research-Atmospheres*, 102(D8): 9309–9321.

Keim, R.F., 2004. Comment on "Measurement and modeling of growing-season canopy water fluxes in a mature mixed deciduous forest stand, southern Ontario, Canada". *Agricultural and Forest Meteorology*, 124(3-4): 277–279.

Kelliher, F.M., Black, T.A. and Price, D.T., 1986. Estimating the effects of understory removal from a Douglas-fir forest using a 2-layer canopy evapotranspiration model. *Water Resources Research*, 22(13): 1891–1899.

Klaassen, W., Bosveld, F. and de Water, E., 1998. Water storage and evaporation as constituents of rainfall interception. *Journal of Hydrology*, 213(1-4): 36–50.

Koop, T., Kapilashrami, A., Molina, L.T. and Molina, M.J., 2000. Phase transitions of sea-salt/water mixtures at low temperatures: Implications for ozone chemistry in the polar marine boundary layer. *Journal of Geophysical Research-Atmospheres*, 105(D21): 26393–26402.

Körner, C., 1985. Humidity responses in forest trees - precautions in thermal scanning surveys. *Archives for Meteorology Geophysics and Bioclimatology Series B-Theoretical and Applied Climatology*, 36(1): 83–98.

Kouwenberg, L., McElwain, J., Kurschner, W., Wagner, F., Beerling, D., Mayle, F. and Visscher, H., 2003. Stomatal frequency adjustment of four conifer species to historical changes in atmospheric co_2. *American Journal of Botany*, 90(4): 610–619, doi:10.3732/ajb.90.4.610.

Kruijt, B., Witte, J.P., Jacobs, C. and Kroon, T., 2008. Effects of rising atmospheric co_2 on evapotranspiration and soil moisture: A practical approach for the Netherlands. *Journal of Hydrology*, 349(3-4): 257–267.

Kume, T., Kuraji, K., Yoshifuji, N., Morooka, T., Sawano, S., Chong, L. and Suzuki, M., 2006. Estimation of canopy drying time after rainfall using sap flow measurements in an emergent tree in a lowland mixed-dipterocarp forest in Sarawak, Malaysia. *Hydrological Processes*, 20(3): 565–578.

Laming, P., Rijsdijk, J. and Verwijs, J., 1978. *Timber types, information for practical applications (in Dutch).* Houtinstituut TNO, Delft.

Lankreijer, H., Lundberg, A., Grelle, A., Lindroth, A. and Seibert, J., 1999. Evaporation and storage of intercepted rain analysed by comparing two models applied to a boreal forest. *Agricultural and Forest Meteorology*, 98-9: 595–604.

Lankreijer, H.J.M., Hendriks, M.J. and Klaassen, W., 1993. A comparison of models simulating rainfall interception of forests. *Agricultural and Forest Meteorology*, 64(3-4): 187–199.

Laubach, J., Raschendorfer, M., Kreilein, H. and Gravenhorst, G., 1994. Determination of heat and water-vapor fluxes above a spruce forest by eddy-correlation. *Agricultural and Forest Meteorology*, 71(3-4): 373–401.

Leuning, R. and Moncrieff, J., 1990. Eddy-covariance co_2 flux measurements using open-path and closed-path co_2 analyzers - Corrections for analyzer water-vapor sensitivity and damping of fluctuations in air sampling tubes. *Boundary-Layer Meteorology*, 53(1-2): 63–76.

Leuning, R., Zhang, Y.Q., Rajaud, A., Cleugh, H. and Tu, K., 2008. A simple surface conductance model to estimate regional evaporation using MODIS leaf area index and the Penman-Monteith equation. *Water Resources Research*, 44(10): W10419, doi:10.1029/2007WR006562.

Leyton, L., Reynolds, E.R.C. and Thompson, F.B., 1967. Rainfall interception in forest and moorland. In: W. Sopper and H. Lull (Eds.), *Forest Hydrology*, Pergamon Press, Oxford, UK, pp. 163 – 178.

Lindroth, A., 1984. Gradient distributions and flux profile relations above a rough forest. *Quarterly Journal of the Royal Meteorological Society*, 110(464): 553–563.

Linsley, R., Kohler;, M. and Paulhus;, J., 1982. *Hydrology for Engineers*. 3rd edn., McGraw-Hill international book company, Tokyo, Japan.

Lloyd, C.R., 1995. The effect of heterogeneous terrain on micrometeorological flux measurements - a case-study from Hapex-Sahel. *Agricultural and Forest Meteorology*, 73(3-4): 209–216.

Lloyd, C.R. and Marques, A.D., 1988. Spatial variability of throughfall and stemflow measurements in Amazonian rainforest. *Agricultural and Forest Meteorology*, 42(1): 63–73.

Lloyd, J. and Taylor, J.A., 1994. On the temperature-dependence of soil respiration. *Functional Ecology*, 8(3): 315–323.

Loescher, H.W., Gholz, H.L., Jacobs, J.M. and Oberbauer, S.F., 2005. Energy dynamics and modeled evapotranspiration from a wet tropical forest in Costa Rica. *Journal of Hydrology*, 315(1-4): 274–294.

Lösch, R. and Schulze, E.D., 1994. Internal coordination of plant responses to drought and evaporative demand. In: E.D.S.M. Caldwell (Ed.), *Ecophysiology of Photosynthesis, Ecological Studies*, vol. 100, Springer, Heidelberg, p. 185204.

Loustau, D., Berbigier, P., Granier, A. and Moussa, F.E., 1992. Interception loss, throughfall and stemflow in a maritime pine stand. I. variability of throughfall and stemflow beneath the pine canopy. *Journal of Hydrology*, 138(3-4): 449–467.

Ludwig, F., Dawson, T.E., de Kroon, H., Berendse, F. and Prins, H.H.T., 2003. Hydraulic lift in Acacia tortilis trees on an East African savanna. *Oecologia*, 134(3): 293–300.

Luxmoore, R.J., 1983. Water-budget of an eastern deciduous forest stand. *Soil Science Society of America Journal*, 47(4): 785–791.

Makkink, G., 1959. Testing the Penman formula by means of lysimeters. *J. Int. Water Eng.*, 11: 277–288.

Marin, C.T., Bouten, I.W. and Dekker, S., 2000. Forest floor water dynamics and root water uptake in four forest ecosystems in northwest Amazonia. *Journal of Hydrology*, 237(3-4): 169–183.

McLaren, J.D., Arain, M.A., Khomik, M., Peichl, M. and Brodeur, J., 2008. Water flux components and soil water-atmospheric controls in a temperate pine forest growing in a well-drained sandy soil. *Journal of Geophysical Research-Biogeosciences*, 113(G4): G04031, doi:10.1029/2007JG000653.

McMillen, R.T., 1988. An eddy-correlation technique with extended applicability to non-simple terrain. *Boundary-Layer Meteorology*, 43(3): 231–245.

McNaughton, K.G. and Van den Hurk, B., 1995. A Lagrangian revision of the resistors in the 2-layer model for calculating the energy budget of a plant canopy. *Boundary-Layer Meteorology*, 74(3): 261–288.

Medlyn, B.E., Barton, C.V.M., Broadmeadow, M.S.J., Ceulemans, R., De Angelis, P., Forstreuter, M., Freeman, M., Jackson, S.B., Kellomaki, S., Laitat, E., Rey, A., Roberntz, P., Sigurdsson, B.D., Strassemeyer, J., Wang, K., Curtis, P.S. and Jarvis, P.G., 2001. Stomatal conductance of forest species after long-term exposure to elevated co_2 concentration: a synthesis. *New Phytologist*, 149(2): 247–264.

MFV-Bos, 2006. *Meetnet Functievervulling Bos 2001-2005. Vijfde Nederlandse Bosstatistiek.* Tech. rep., Ministerie van Landbouw, Natuur en Voedselkwliteit. Directie Kennis, The Hague, The Netherlands.

Milly, P.C.D. and Dunne, K.A., 2011. On the hydrologic adjustment of climate-model projections: The potential pitfall of potential evapotranspiration. *Earth Interactions*, 15: 1–14.

Mizutani, K. and Ikeda, T., 1994. Evaporation of intercepted rainfall from a Castanopsis cuspidata Schottky forest using various micrometeorological methods. In: *International Symposium Forest Hydrology 1994*, Tokyo, Japan, pp. 69–76.

Moffat, A.M., Papale, D., Reichstein, M., Hollinger, D.Y., Richardson, A.D., Barr, A.G., Beckstein, C., Braswell, B.H., Churkina, G., Desai, A.R., Falge, E., Gove, J.H., Heimann, M., Hui, D.F., Jarvis, A.J., Kattge, J., Noormets, A. and Stauch, V.J., 2007. Comprehensive comparison of gap-filling techniques for eddy covariance net carbon fluxes. *Agricultural and Forest Meteorology*, 147(3-4): 209–232.

Mölder, M. and Kellner, E., 2002. Excess resistance of bog surfaces in central Sweden. *Agricultural and Forest Meteorology*, 112(1): 23–30.

Mölder, M. and Lindroth, A., 1999. Thermal roughness length of a boreal forest. *Agricultural and Forest Meteorology*, 98-99: 659–670.

Mölder, M. and Lindroth, A., 2001. Dependence of kB^{-1} factor on roughness Reynolds number for barley and pasture. *Agricultural and Forest Meteorology*, 106(2): 147–152.

Moncrieff, J., Valentini, R., Greco, S., Seufert, G. and Ciccioli, P., 1997. Trace gas exchange over terrestrial ecosystems: Methods and perspectives in micrometeorology. *Journal of Experimental Botany*, 48(310): 1133–1142.

Moncrieff, J.B., Malhi, Y. and Leuning, R., 1996. The propagation of errors in long-term measurements of land-atmosphere fluxes of carbon and water. *Global Change Biology*, 2(3): 231–240.

Monteith, J.L., 1965. Light distribution and photosynthesis in field crops. *Annals of Botany*, 29(113): 17–37.

Monteith, J. and Unsworth, M., 1990. *Principles of Environmental Physics, second edition*. Edward Arnold, London.

Moore, C.J., 1986. Frequency-response corrections for eddy-correlation systems. *Boundary-Layer Meteorology*, 37(1-2): 17–35.

Moors, E.J., 2008. Evaporation. In: P.T. M. Bierkens H. Dolman (Ed.), *Climate and the Hydrological Cycle*, IAHS Special Publication : 8, IAHS Press, Centre for Ecology and Hydrology, Wallingford, Oxfordshire, UK, pp. 23–41.

Moors, E. and Dolman, A., 2001. Long term measurements of weather and fluxes of co_2: treatment of discontinuous data. In: *Phuket Proceedings of the international workshop on GAME-AAN/Radiation, Phuket, Thailand 2001*, Bulletin of the Terrestrial Environment Research Center. University of Tsukuba, pp. 75–78.

Musters, P., 1998. *Temporal and spatial patterns of root water uptake in an Austrian pine stand on sandy soil*. Ph.D. thesis, Thesis University of Amsterdam, The Netherlands.

Nadezhdina, N., Cermak, J., Meiresonne, L. and Ceulemans, R., 2007. Transpiration of Scots pine in Flanders growing on soil with irregular substratum. *Forest Ecology and Management*, 243(1): 1–9.

Nadezhdina, N., Tatarinov, F. and Ceulemans, R., 2004. Leaf area and biomass of Rhododendron understory in a stand of Scots pine. *Forest Ecology and Management*, 187(2-3): 235–246.

Ogink-Hendriks, M.J., 1995. Modeling surface conductance and transpiration of an oak forest in the Netherlands. *Agricultural and Forest Meteorology*, 74(1-2): 99–118.

Ohta, T., Maximov, T.C., Dolman, A.J., Nakai, T., Molen, M.K.v.d., Kononov, A.V., Maximov, T., Hiyama, T., Iijima, Y., Moors, E.J. and Tanaka, H., 2008. Interannual variation of water balance and summer evapotranspiration in an eastern Siberian larch forest over a 7-year period (1998-2006). *Agricultural and Forest Meteorology*, 148(12): 1941–1953.

Olsthoorn, A.F.M., 1998. *Soil acidification effects on fine root growth of Douglas-fir on sandy soils*. Ph.D. thesis, Wageningen University, Wageningen, The Netherlands.

Paulson, C., 1970. The mathematical representation of wind speed and temperature profiles in the unstable atmospheric surface layer. *J. appl. Met.*, 9: 857861.

Penman, H.L., 1948. Natural evaporation from open water, bare soil and grass. *Proceedings of the Royal Society of London Series a-Mathematical and Physical Sciences*, 193(1032): 120.

Pierce, L.L. and Running, S.W., 1988. Rapid estimation of coniferous forest leaf-area index using a portable integrating radiometer. *Ecology*, 69(6): 1762–1767.

Pook, E.W., Moore, P.H.R. and Hall, T., 1991. Rainfall interception by trees of Pinus-Radiata and Eucalyptus-Viminalis in a 1300 mm rainfall area of southeastern New-South-Wales. I. gross losses and their variability. *Hydrological Processes*, 5(2): 127–141.

Press, W., Flannery, B., Teukosky, S. and Vetterling, W., 1989. *Numerical recipes. The Art of Scientific Computing. "Fortran version".* Cambridge University Press, USA.

Price, A.G. and Carlyle-Moses, D.E., 2003. Measurement and modelling of growing-season canopy water fluxes in a mature mixed deciduous forest stand, southern Ontario, Canada. *Agricultural and Forest Meteorology*, 119(1-2): 69–85.

Pypker, T.G., Bond, B.J., Link, T.E., Marks, D. and Unsworth, M.H., 2005. The importance of canopy structure in controlling the interception loss of rainfall: Examples from a young and an old-growth Douglas-fir forest. *Agricultural and Forest Meteorology*, 130(1-2): 113–129.

Qu, W., Henderson-Sellers, A., Pitman, A. and Chen, T., 1996. *Cabauw Sensitivity Experimental Results from PILPS.* Tech. Rep. 24, IGPO Publication Series.

Rambal, S., 1984. Water balance and pattern of root water uptake by a Quercus coccifera L. evergreen srub. *Oecologia*, 62(1): 18–25.

Raupach, M.R., 1989. Applying Lagrangian fluid-mechanics to infer scalar source distributions from concentration profiles in plant canopies. *Agricultural and Forest Meteorology*, 47(2-4): 85–108.

Roberts, J., Pymar, C.F., Wallace, J.S. and Pitman, R.M., 1980. Seasonal-changes in leaf-area, stomatal and canopy conductances and transpiration from bracken below a forest canopy. *Journal of Applied Ecology*, 17(2): 409–422.

Rolf, H., 1989. *Verlaging van de grondwaterstanden in Nederland: analyse periode 1950-1986.* Tech. rep., Ministerie van Verkeer en Waterstaat.

Rutter, A.J., Morton, A.J. and Robins, P.C., 1975. Predictive model of rainfall interception in forests. 2. Generalization of model and comparison with observations in some coniferous and hardwood stands. *Journal of Applied Ecology*, 12(1): 367–380.

Rutter, A., Kershaw, K., Robins, P. and Morton, A., 1971. A predictive model of rainfall interception in forests. I. Derivation of the model from observations in a plantation of Corsican pine. *Agricultural Meteorology*, 9: 367–384.

Saxén, B. and Saxén, H., 1995. *NNDT - a neural network development tool. Version 1.2.* Tech. rep., A bo Akademi University, A bo, Finland, pp 19.

Schotanus, P., Nieuwstadt, F.T.M. and De Bruin, H.A.R., 1983. Temperature-measurement with a sonic anemometer and its application to heat and moisture fluxes. *Boundary-Layer Meteorology*, 26(1): 81–93.

Schuepp, P.H., Leclerc, M.Y., Macpherson, J.I. and Desjardins, R.L., 1990. Footprint prediction of scalar fluxes from analytical solutions of the diffusion equation. *Boundary-Layer Meteorology*, 50(1-4): 353–373.

Schymanski, S.J., Sivapalan, M., Roderick, M.L., Beringer, J. and Hutley, L.B., 2008. An optimality-based model of the coupled soil moisture and root dynamics. *Hydrology and Earth System Sciences*, 12(3): 913–932.

Sellers, P.J. and Lockwood, J.G., 1981. A computer-simulation of the effects of differing crop types on the water-balance of small catchments over long-time periods. *Quarterly Journal of the Royal Meteorological Society*, 107(452): 395–414.

Shalhevet, J., Maas, E.V., Hoffman, G.J. and Ogata, G., 1976. Salinity and hydraulic conductance of roots. *Physiologia Plantarum*, 38(3): 224–232.

Shuttleworth, W.J., 1978. A simplified one-dimensional theoretical description of the vegetation-atmosphere interaction. *Boundary-Layer Meteorol.*, 14: 3–27.

Shuttleworth, W.J., 2007. Putting the 'vap' into evaporation. *Hydrology and Earth System Sciences*, 11(1, Part 2): 210–244.

Shuttleworth, W., 1976. A one-dimensional theoretical description of the vegetation-atmosphere interaction. *Boundary-Layer Meteorology*, 10: 273–302.

Shuttleworth, W. and Wallace, J.S., 1985. Evaporation from sparse crops - an energy combination theory. *Quarterly Journal of the Royal Meteorological Society*, 111(469): 839–855, doi:10.1256/smsqj.46909.

Siau, J.F., 1971. *Flow in wood.* Syracuse University Press, Syracuse, USA.

Sinclair, T., 2005. Theoretical analysis of soil and plant traits influencing daily plant water flux on drying soils. *Agronomy Journal*, 97: 1148 – 1152.

Sinclair, T., Holbrook, N. and Zwieniecki, M., 2005. Daily transpiration rates of woody species on drying soil. *Tree Physiology*, 25: 1469 1472.

Skaar, C., 1972. *Water in wood*. Syracuse University Press, Syracuse, USA.

Stenberg, P., Linder, S., Smolander, H. and Flowerellis, J., 1994. Performance of the LAI-2000 plant canopy analyzer in estimating leaf-area index of some Scots pine stands. *Tree Physiology*, 14(7-9): 981–995.

Stewart, J.B., 1977. Evaporation from wet canopy of a pine forest. *Water Resources Research*, 13(6): 915–921.

Stuurgroep-Grondwaterbeheer-Midden-Nederland, 1992. *Een nieuw evenwicht (in Dutch)*. Tech. rep., Provincie Gelderlands.

Swanson, R.H., 1994. Significant historical developments in thermal methods for measuring sap flow in trees. *Agricultural and Forest Meteorology*, 72(1-2): 113–132.

Talsma, T. and Gardner, E., 1986. Soil water extraction by a mixed eucalypt forest during a drought period. *Australian Journal of Soil Research*, 24(1): 25–32.

Tanner, B., Swiatek, E. and Greene, J., 1993. Density fluctuations and use of krypton hygrometer in surface flux measurements. In: *Conf. on Management of Irrigation and Drainage Systems*, ASCE, Park City, UT, p. 945952.

Teklehaimanot, Z. and Jarvis, P.G., 1991. Modeling of rainfall interception loss in agro-forestry systems. *Agroforestry Systems*, 14(1): 65–80.

Teklehaimanot, Z., Jarvis, P.G. and Ledger, D.C., 1991. Rainfall interception and boundary-layer conductance in relation to tree spacing. *Journal of Hydrology*, 123(3-4): 261–278.

Thom, A., Stewart, J., Oliver, H. and Gash, J., 1975. Comparison of aerodynamic and energy budget estimates of fluxes over a pine forest. *Quarterly Journal of the Royal Meteorological Society*, 101(427): 93–105, doi:10.1002/qj.49710142708.

Trimble, G. and Weitzman, S., 1954. Effect of hardwood forest canopy on rainfall intensities. *Transactions-American Geophysical Union*, 35: 226–234.

Turner, J. and Lambert, M.J., 1987. Forest water usage and interactions with nutrition of Pinus-Radiata. *Acta Oecologica-Oecologia Plantarum*, 8(1): 37–43.

Valente, F., David, J.S. and Gash, J.H.C., 1997. Modelling interception loss for two sparse eucalypt and pine forests in central Portugal using reformulated Rutter and Gash analytical models. *Journal of Hydrology*, 190(1-2): 141–162.

Van Dam, J.C., 2000. Simulation of field-scale water flow and bromide transport in a cracked clay soil. *Hydrological Processes*, 14(6): 1101–1117.

van den Burg, J., 1996. *De betekenis van bodem en klimaat voor het Nederlandse bos*. Ph.D. thesis, Wageningen University, Wageningen, The Netherlands.

Van den Hurk, B. and McNaughton, K.G., 1995. Implementation of near-field dispersion in a simple 2-layer surface-resistance model. *Journal of Hydrology*, 166(3-4): 293–311.

Van der Tol, C., Gash, J.H.C., Grant, S.J., McNeil, D.D. and Robinson, M., 2003. Average wet canopy evaporation for a sitka spruce forest derived using the eddy correlation-energy balance technique. *Journal of Hydrology*, 276(1-4): 12–19.

van Dijk, A. and Bruijnzeel, L.A., 2001a. Modelling rainfall interception by vegetation of variable density using an adapted analytical model. Part 1. Model description. *Journal of Hydrology*, 247(3-4): 230–238.

van Dijk, A. and Bruijnzeel, L.A., 2001b. Modelling rainfall interception by vegetation of variable density using an adapted analytical model. Part 2. Model validation for a tropical upland mixed cropping system. *Journal of Hydrology*, 247(3-4): 239–262.

Van Genuchten, M.T., 1980. A closed-form equation for predicting the hydraulic conductivity of unsaturated soils. *Soil Science Society of America Journal*, 44(5): 892–898.

van Loon, W.K.P., Bastings, H.M.H. and Moors, E.J., 1998. Calibration of soil heat flux sensors. *Agricultural and Forest Meteorology*, 92(1): 1–8.

Van Ulden, A.P. and Holtslag, A.A.M., 1985. Estimation of atmospheric boundary-layer parameters for diffusion applications. *Journal of Climate and Applied Meteorology*, 24(11): 1196–1207.

van Wijk, M.T. and Bouten, W., 2001. Towards understanding tree root profiles: simulating hydrologically optimal strategies for root distribution. *Hydrology and Earth System Sciences*, 5(4): 629–644.

Van Wijk, W. and Vries, D.D., 1963. Periodic temperature variations in a homogenous soil. In: W. Van Wijk (Ed.), *Physics of plant environment*, North Holland Publ. Co., Amsterdam, pp. 103 – 143.

Veerman, G., 1998. personal communication.

Verhoef, A. and Allen, S.J., 2000. A SVAT scheme describing energy and co_2 fluxes for multi-component vegetation: calibration and test for a Sahelian savannah. *Ecological Modelling*, 127(2-3): 245–267.

Verma, S.B., Baldocchi, D.D., Anderson, D.E., Matt, D.R. and Clement, R.J., 1986. Eddy fluxes of co_2, water-vapor, and sensible heat over a deciduous forest. *Boundary-Layer Meteorology*, 36(1-2): 71–91.

Vincke, C. and Thiry, Y., 2008. Water table is a relevant source for water uptake by a Scots pine (Pinus sylvestris L.) stand: Evidences from continuous evapotranspiration and water table monitoring. *Agricultural and Forest Meteorology*, 148(10): 1419–1432.

Watanabe, T. and Mizutani, K., 1994. Multilayer canopy model for estimation of rainfall interception. In: *Proceedings International Symposium Forest Hydrology, 1994*, Tokyo, Japan, pp. 55–61.

Waterloo, M., 1994. *Water and nutrient dynamics of Pinus caribaea plantation forests on former grassland soils in Southwest Viti Levu, Fiji*. Ph.D. thesis, Vrije Universiteit, Amsterdam, The Netherlands.

Webb, E.K., Pearman, G.I. and Leuning, R., 1980. Correction of flux measurements for density effects due to heat and water-vapor transfer. *Quarterly Journal of the Royal Meteorological Society*, 106(447): 85–100.

Wendroth, O., Ehlers, W., Hopmans, J.W., Kage, H., Halbertsma, J. and Wosten, J.H.M., 1993. Reevaluation of the evaporation method for determining hydraulic functions in unsaturated soils. *Soil Science Society of America Journal*, 57(6): 1436–1443.

Whitehead, D. and Kelliher, F.M., 1991. A canopy water balance model for a *pinus radiata* stand before and after thinning. *Agricultural and Forest Meteorology*, 55: 109–126.

Wilson, K.B., Hanson, P.J., Mulholland, P.J., Baldocchi, D.D. and Wullschleger, S.D., 2001. A comparison of methods for determining forest evapotranspiration and its components: sap-flow, soil water budget, eddy covariance and catchment water balance. *Agricultural and Forest Meteorology*, 106(2): 153–168.

Wind, G., 1968. Capillary conductivity data estimated by a simple method. In: P. Rijtema and H. Wassink (Eds.), *Proceedings of the Wageningen symposium: Water*

in the unsaturated zone, June 1966, vol. 1, IAHS Gentbrugge/ Unesco Paris, pp. 181–191.

Woodruff, D.R., McCulloh, K.A., Warren, J.M., Meinzer, F.C. and Lachenbruch, B., 2007. Impacts of tree height on leaf hydraulic architecture and stomatal control in Douglas-fir. *Plant Cell and Environment*, 30(5): 559–569.

Wösten, J.H.M., Lilly, A., Nemes, A. and Le Bas, C., 1999. Development and use of a database of hydraulic properties of European soils. *Geoderma*, 90(3-4): 169–185.

Wright, S., 1996. Phenological responses to seasonality in tropical forest plants. In: R.C. Mulkey S.S. and A. Smith (Eds.), *Tropical Forest Plant Ecophysiology*, Chapman and Hall, New York, pp. 440–460.

Xia, Y.L., Fabian, P., Stohl, A. and Winterhalter, M., 1999. Forest climatology: estimation of missing values for Bavaria, Germany. *Agricultural and Forest Meteorology*, 96(1-3): 131–144.